Organisation of, and ligand-independent signalling by the TCR, with a special emphasis on the pre-TCR

Elizabeth Chi-Fang Huang

The Queen's College

Thesis submitted for the degree of Doctor of Philosophy

Trinity Term, 2017

The work described in this thesis was supported by Nuffield Department of Medicine Prize Studentship.

Abstract

Organisation of, and ligand-independent signalling by the TCR, with a special emphasis on the pre-TCR

Elizabeth Chi-Fang Huang, The Queen's College
Thesis submitted for the degree of Doctor of Philosophy
Trinity Term, 2017

Understanding how immune signalling is initiated and regulated spatiotemporally is likely to be helped by investigations of receptor stoichiometry. The pre-TCR expressed by thymocytes shares similarities in structure and signalling components with the mature TCR but, in contrast to the TCR, it has no known ligands. This thesis has therefore analysed the stoichiometry of the pre-TCR using mutagenesis- and imaging-based approaches, and explored how ligand-independent signalling might be initiated by both the TCR and pre-TCR. The mutational analysis, which required considerable optimisation because the pre-TCR is very weakly expressed in transfected cells, suggested that only one contiguous surface on pre-Tα needs to be buried in the pre-TCR complex in order for it to reach the cell surface. This comprised the surface buried at the interface with the constant region of TCRβ and therefore was incompatible with previous suggestions that the pre-TCR assembles into a 'head-to-tail' dimer. Unexpectedly, super-resolution imaging experiments combined with cluster analysis, and the method of single-molecule cross-colour coincidence detection were suggestive that, rather than dimers, the pre-TCR forms higher-order oligomers in transfected cells and possibly also in thymocytes. Similar analyses showed that the organisation of the TCR was heterogeneous, depending on the level of expression of the receptor. Overall, technical limitations that emerged in the course of the study highlighted some of the difficulties in studying native receptor stoichiometry on resting cells generally. The final part of the thesis investigated ligand-independent signalling by the TCR, using a novel assay based on the binding of a superagonistic antibody to a non-signalling form of the receptor CD28. Using CRISPR/Cas-mediated gene editing, it was shown that ligand-independent signalling by the mature TCR and pre-TCR was dependent on Lck and Zap70, indicating that it is reliant on the triggering of conventional signalling pathways. Ways in which the pre-TCR might initiate signalling, that could be tolerant of complexes exhibiting a range of stabilities, are also discussed.

Acknowledgements

First and foremost, I would like to thank my supervisor, Prof. Simon Davis, for guiding and inspiring me at every stage throughout my PhD study. My immediate thanks also need to go to all of the members of the Davis laboratory, past and present, and special thanks need to go to Susan Yu, Dr. Yuan Lui, Dr. Veronica Chang and Janet Fennelly for their unwavering support (inside and outside of the laboratory) and friendship over the past years.

In addition, my grateful thanks also go to my collaborators in the Klenerman laboratory in Cambridge, especially to Dr. James McColl, Anna Lippert, Dr. Steven Lee and Dr. Matthieu Palayret, for their respective contributions to this project and for insightful discussions and many great hours spent on the microscopes in the dark basement.

I also wish to express my gratitude to Dr. Yu-Fen Chang, Zuzana Kalivodova, Xiaoxiao, for their invaluable help and friendship.

Finally, I owe a great debt of gratitude to my parents for their devotion and love which made me who I am today. The PhD journey is not easy as I am aware now, and I cannot imagine how my father managed to do his PhD with two naughty children (*i.e.* my brother and me) messing around. I am eternally thankful to my brother Po-Ting, Dr. Shih-Jung Fan, grandparents, nanny, aunties and cousins – thanks for your enormous love and thanks for raising me up to more than I can be.

This is all my own work except where it is indicated. It needs also to be acknowledged that I obtained substantial help with my English from Prof. Simon Davis and Dr.Yuan Lui.

Abbreviations

APC	Antigen-presenting cell
BCR	B-cell receptor
CD	Cluster of differentiation
CDR	Complementarity-determining region
c-SMAC	Central supramolecular activation cluster
cTEC	Cortical thymic epithelial cell
CTLA-4	Cytotoxic T-lymphocyte-associated protein 4
DAM	Donkey anti mouse Fc antibody
d-SMAC	Distal supramolecular activation cluster
DySCo	Dynamic single-molecule co-localisation
EGFR	Epidermal growth factor receptors
ELISA	Enzyme-linked immunosorbent assay
Fab	Fragment antigen-binding
FACS	Fluorescence-activated cell sorting
Fc	Fragment crystallisable
FCCS	Fluorescence cross-correlation spectroscopy
FCS	Fluorescence correlation spectroscopy
FcR	Fragment crystallisable receptor
FRAP	Fluorescence recovery after photobleaching
FRET	Förster resonance energy transfer
GPCR	G-protein coupled receptor
GPI	Glycosylphosphatidylinositol
GTP	Guanosine triphosphate
HA	Haemagglutinin

hPALM	High-speed photoactivated localisation microscopy
IFN	Interferon
Ig	Immunoglobulin
IgSF	Immunoglobulin superfamily
IL	Interleukin
ITAM	Immunoreceptor tyrosine-based activation motif
LAT	Linker for activation of T cells
Lck	Lymphocyte-specific protein tyrosine kinase
MHC	Major histocompatibility complex
mTEC	Medullary thymic epithelial cell
NFAT	Nuclear factor of activated T-cells
NFκB	Nuclear factor kappa-light-chain-enhancer of activated B cells
NMR	Nuclear magnetic resonance
PALM	Photoactivated localisation microscopy
pHR	pHR-SIN-CSGWdNotI/dEcoRI
PKC	Protein kinase C
PSF	Point-spread function
p-SMAC	Peripheral supramolecular activation cluster
Q	Association quotient
SA	Superagonistic antibody
SDS-PAGE	Sodium dodecyl sulphate polyacrylamide gel electrophoresis
SH1	Src homology domain 1
SH2	Src homology domain 2
SH3	Src homology domain 3
SH4	Src homology domain 4

SMAC	Supramolecular activation cluster
SMCCCD	Single-molecule cross-colour coincidence detection
SLP-76	SH2 domain-containing Leukocyte Protein, 76kDa
STORM	Stochastic optical reconstruction microscopy
TCCD	Two-colour coincidence detection
TCR	T cell antigen receptor
TEC	Thymic epithelial cell
TEM	Transmission electron microscopy
TIRF	Total internal reflection fluorescence
TNF	Tumour necrosis factor
ZAP-70	Zeta-chain associated protein of 70 kDa

Contents

Chapter 1

Introduction

I. Overview of the immune system

Immunity, originating from a Latin term immunis which means exemption, stands for the protection of self from pathogenic challenges. In the immune system, organisms protect themselves against diseases by recognising non-self-antigens and then invoking suitable responses. This involves the innate immunity, the first line of defence, in all organisms and the adaptive immunity, mediated by lymphocytes including T cells and B cells, in higher organisms in the phylum Vertebrata. Foreign antigens are detected by T cells and B cells through receptors known as the T cell receptor (TCR) and B cell receptor (BCR), respectively. When the TCR, for example, engages with a peptide-major histocompatibility complex (MHC) complex on an antigen presenting cell, such as a dendritic cell or a B cell, T cell signalling initiates, leading to T cell activation and the generation of specific responses.

T cell activation needs to be well-controlled and regulated spatially and temporally in response to specific pathogens, but not self-antigens, in organisms. Then this allows effective immune responses to occur. However, it still remains unclear how TCRs and other proteins behave prior to activation and how signalling is initiated. In addition, TCRs share similar structures with the receptors on precursor T cells (pre-T cells), known as pre-TCRs. However, in contrast to the TCR, there is likely no known cognate ligand for the pre-TCR and therefore it seems possible that pre-TCR signalling is initiated in a ligand-independent way. The structure and organisation of the pre-TCR is therefore of interest and it might allow us to further understand the requirements for

signal-initiation generally.

This thesis explores receptor stoichiometry and signalling initiation in T cells, with a special emphasis on pre-T cells. In this introductory chapter, overviews of innate and adaptive immunity are given, followed by a discussion of the structure and function of T cells, receptor stoichiometry and super-resolution imaging techniques.

II. Immune responses

A. Innate immunity

Innate immunity provides the first line of defence, with discrimination between self- and non-self antigens achieved by recognition of certain small structural motifs, or pathogen-associated molecular patterns (PAMPs), for example, lipopolysaccharide, peptidoglycan and lipoteichoic acids in bacteria, β-glucan in fungi and viral nucleic acids in viruses [1]. As the PAMPs play essential roles in microbial physiology and are often conserved among many microbes, the recognition of PAMPs is a very efficient basis for self and non-self discrimination [2].

There are many different forms of pattern recognition receptors (PRRs), either in soluble or transmembrane forms, allowing innate immunity to respond to many different PAMPs [2]. Soluble circulating PRRs, *e.g.* mannose-binding lectin, C-reactive protein and lipopolysaccharide-binding protein, are able to bind to the microbial surface and are capable of opsonisation of microbes for phagocytosis as well as initiating complement-mediated responses [3]. On the other hand, scavenger receptors, toll-like receptors and dectin-1 are transmembrane PRRs. The scavenger receptors, expressed on macrophages and dendritic cells, are able to recognise and phagocytose bacteria and apoptotic cells [4]. The toll-like receptors (TLRs), expressed on cell or endosomal membranes, recognise a variety of PAMPs including bacterial

lipoproteins (TLR2 and TLR6), viral dsRNA (TLR3), lipopolysaccharide (TLR4), flagellin (TLR5) and unmethylated cytosine linked to guanine (CpG) sequence (TLR9) [5]. Dectin-1, mainly expressed on macrophages and dendritic cells, is able to bind to β-glucan and invoke tyrosine kinase-triggered mitogen-activated protein kinase (MAPK) signalling, thus activating antifungal defence such as NADPH oxidase and cytokine production [6].

Innate immunity, however, does not function independently of adaptive immunity, but instead, they are highly interconnected. The potency of adaptive immunity is based on the prior innate responses, *i.e.* inflammatory responses, and adaptive immunity in turn regulates or activates innate responses [7]. Some phagocytic cells involved in innate immunity activate specific responses in the adaptive immunity. For example, dendritic cells, which phagocytose antigens in the infection site after PAMP recognition using PRRs, are able to present processed antigen to the adaptive immune cells in the lymph node and stimulate adaptive immune responses [2, 8]. Moreover, those effector T helper cells in turn produce cytokines which specifically activate more innate cells such as macrophages or neutrophils [2].

In addition, there are some lymphocytes which play roles in both innate and adaptive immune responses, for example, natural killer cells (NKs) and γδ T cells (discussed in III.C.(c)). NKs are able to provide fast host defence against virus infection, especially herpesvirus infection, and a wide range of tumour cells, in the absence of previous immunisation [9, 10]. In addition, NKs express MHC-I-specific inhibitory receptors, *i.e.* killer cell immunoglobulin-like receptors (KIRs) or CD94/NKG2A [11], thus producing cytokines or directly killing those cells ‘in distress’ which downregulate self-MHC molecules or upregulate stress-induced self molecules such as NKG2D ligand [12, 13]. In addition, NKs are found to enhance their cytokine production and cytolytic efficiency after the repeated exposure to

immune challenges, for example, in the hapten-specific contact hypersensitivity response, the anti-mouse cytomegalovirus (MCMV) response is enhanced by the immunological memory of the NK cells [14, 15] .

B. Adaptive immunity

In contrast to innate immunity, which serves as the first line of defence and is characterised by limited specificity, the hallmarks of adaptive immunity are antigen specificity, diversity and immunological memory. Distinguishing antigens with subtle degrees of structural difference can be achieved by lymphocytes exhibiting a broad variety of specificities. In addition to its high degree of specificity, the wide diversity in antigen recognition and immunological memory allow for very comprehensive and efficient protection for organisms.

(a) Cells involved in the adaptive immune system

Two important types of lymphocytes, T cells and B cells, are involved in adaptive immunity. T cells and B cells are derived from multi-potential haematopoietic stem cells from the bone marrow [16-18]. Multi-potential haematopoietic stem cells first differentiate into common lymphoid progenitors and common myeloid progenitors. Those cells that migrate from the bone marrow to the thymus develop and differentiate into different subsets of T cells (details discussed in III.C), while those that stay in the bone marrow develop into B cells [19, 20]. T cells and B cells are responsible for cellular immunity and humoral immunity, respectively.

(b) Diversity in antigen recognition achieved by gene rearrangement

The potency of the adaptive immunity is its capability to recognise a variety of potential antigens with membrane-bound receptors, or antibodies secreted by

lymphocytes. The diverse repertoire of the TCRs and BCRs for antigen recognition arises from combinatorial and junctional diversity. Firstly, combinational diversity is achieved by genetic recombination. Variable (V), diversity (D) and joining (J) gene segments of the receptor genes, which undergo recombination during lymphocyte development mediated by lymphoid specific recombinases, *i.e.* recombination-activating genes (RAG-1 and RAG-2) [21, 22] and terminal deoxynucleotidyl transferase (TdT) [23, 24]. In addition, diversity is further enhanced by adding or deleting nucleotides at the junctions, creating what is called junctional diversity [25]. These mechanisms give rise to the hypervariable regions which correspond to the complementarity determining regions (CDRs) of the immunoglobulin superfamily (IgSF) domains of the TCR and BCR in responsible for antigen recognition [26-28]. The gene arrangement occurs sequentially in the course of development, first in the TCRβ chain and the heavy chain of the BCR, respectively [29]. Thus, in early developmental stages of T cells and B cells, the rearranged TCRβ chains and the rearranged heavy chains of BCR are expressed on the cell membrane in association with an invariant pre-T cell antigen receptor alpha (pre-Tα) and a surrogate light chain (Vpre-B and λ5), respectively. Only cells that successfully undergo gene arrangement, wherein the rearranged gene produces a subunit that can pair and be expressed at the cell surface with the invariant counterparts, can survive and proliferate before entering the next phase of gene rearrangement of the other receptor chains, *i.e.* the α chain of the TCR and light chain of the BCR. This step-wise progress linked to development in this way introduces regulatory check points for successful gene rearrangement as well as a mechanism to increase the diversity of the receptor and antibody repertoire [29, 30].

(c) Interactions of T cells and antigens with the MHC restriction

The TCR only recognises those antigens which have been processed into small peptides and loaded into the cleft of the MHC [31-33]. The extraordinarily large number of different alleles at each genetic locus of MHC makes the MHC highly polymorphic, which allows MHCs to capture a variety of antigen peptides and present to T cells via their TCRs, leading to activation of the T cells [34]. In addition to the polymorphic peptide binding regions of MHC for diverse antigen recognition, there is considerable variation in the contributions, in aspects of binding affinities and binding energies (termed as energetic footprints), of different TCRs to peptide recognition [35].

There are two main types of MHCs: Class I MHC (MHC-I) and Class II MHC (MHC-II) which are able to present processed antigens to cytotoxic T cells ($CD8^+$ cells) and T helper cells ($CD4^+$ T cells), respectively. MHC-I molecules are expressed on all nucleated cells of vertebrate species whereas MHC-II molecules are expressed only on antigen-presenting cells (APCs), *i.e.* macrophages, B cells and dendritic cells, and these present antigen peptides from extracellular pathogens [34]. MHC-I comprises one heavy chain (α chain) in association with a light chain (β2-microglobulin). The α chain consists of three extracellular domains, *i.e.* α1, α2 and α3 domains (about 90 amino acids in each domain), a transmembrane domain (about 25 amino acids) and a short cytoplasmic domain (about 30 amino acids). The β2-microglobulin, with a similar size to the α3 domain, needs to associate with α3 via non-covalent bonding in order for correct folding to occur. The β2-microglobulin and the α3 domains are highly conserved [36]. X-ray crystallographic analysis confirmed that MHC-II is similar in structure to MHC-I [37]. MHC-II consists of two non-identical glycoprotein chains, α and β chains, with each chain having two extracellular domains (membrane-distal domains, *i.e.* α1 and β1 domains, and

membrane-proximal domains, *i.e.* α2 and β2 domains), a transmembrane domain and a short cytoplasmic domain [36].

Processing of the antigen into small antigen peptides is required in order for the antigen to be bound to the peptide-binding cleft in either MHC-I or MHC-II and to be eventually recognised by T cells. The different chains of MHC-I and MHC-II are first synthesised and assembled in the endoplasmic reticulum (ER) with the assistance of chaperones and invariant chains. For example, MHC-I associates with the chaperones calnexin, calreticulin and tapasin, sequentially, and MHC-II associates with the invariant chain *i.e.* CD74, which is gradually degraded until a short fragment remains in the peptide-binding cleft. This short fragment is called class II-associated invariant chain peptide (CLIP) [38, 39]. These chaperones are bound to the MHC molecules in order to promote folding, stabilise complex formation or prevent premature binding of peptide [40]. In the end, only those MHCs that are no longer reliant on their chaperones because they have been, *e.g.* replaced with the processed antigenic peptides, are able to be transported to the membrane and present processed antigens to T cells.

Antigens presented by MHC-I and MHC-II are processed in different intracellular compartments before antigen presentation. Endogenous antigens are processed via a cytosolic pathway. The endogenous antigens are first degraded in the cytosol and then transported into the lumen of the rough endoplasmic reticulum via the ATP-binding cassette transporter proteins, transporter associated with antigen processing (TAP)s [41, 42]. This processed endogenous antigen, with length of 8 to 10 amino acids, is then loaded into the peptide-binding cleft of the MHC-I. The peptide-binding cleft locates in the two membrane-distal polymorphic domains, α1 and α2 domains of MHC-I [34]. On the other hand, exogenous antigens are processed via a clathrin-mediated endocytic pathway. The antigens are internalised and degraded

by a range of endopeptidases and exopeptidases in the gradually decreasing-pH compartments from early to late endosomes and further to lysosomes, into 13-18 amino acids [36, 43, 44]. The peptide-binding cleft of MHC-II locates in the two membrane-distal polymorphic domains of each chain, *i.e.* α1 and β1 domains of MHC-II. In comparison with the pocket-shaped peptide-binding cleft in the MHC-I, the cleft in MHC-II forms a somewhat open-ended groove with the capability to bind 13-18 amino peptides [34].

(d) Interactions of B cells and antigens

The diverse BCRs for antigen recognition are generated in the bone marrow where gene rearrangement occurs. Those B cells which react to self-antigens are eliminated by negative selection (clone deletion) or undergone light chain editing in the course of maturation in the bone marrow [45, 46]. These regulatory mechanisms ensure that only the immunocompetent, non-self-reactive B cells can exit the bone marrow and enter the peripheral lymphoid organs [47, 48].

The BCR complex expressed on mature B cells consists of membrane immunoglobulin for antigen-binding, and the heterodimer Ig-α/Ig-β (CD79a and CD79b) for signalling transduction with the immunoreceptor tyrosine-based activation motifs (ITAMs; two repeats of the conserved amino acids YxxL/I where x is any random amino acid). In addition, there are three co-receptors associated with signal amplification including TAPA-1 (CD81), CR2 (CD21) and CD19, which contains a long cytoplasmic tail with two YxxM (where x is any random amino acid) motifs as docking sites for downstream signalling molecules [49-52].

Unlike the TCR, the BCR and other antibodies secreted by B cells are capable of recognising antigens alone. Interactions of B cells with multivalent antigens which crosslink BCRs drive B cells to begin cell cycling (clonal expansion), activation and

differentiation. The progression signals drive B cells from the G_0 into the G_1 stage and from G_1 into S stage, respectively [53, 54]. Some antigens, *i.e.* type 1 thymus-independent antigens, are capable of generating competence signals after crosslinking BCRs, while others, *i.e.* thymus-dependent antigens, require competence signals to be delivered as signals from CD40 and B7 on B cells, associating with CD40L and CD28 on T helper cells, in addition to a first signal generated by antigen-BCR crosslinking [55-57]. The progression signals, or cytokines generated by T helper cells such as IL-2, IL-4 and IL-5, support B cell activation and differentiation [54]. For example, the antigens bound by BCRs are internalised, processed and presented on the MHC-II on B cells to T helper cells [58]. The T helper cells then stimulate the B cells via CD40L-CD40 engagement and cytokine secretion [54].

When activated, B cells are able to secret antibodies, or undergo affinity maturation and class switching in the germinal centre [59]. Affinity maturation involves both somatic hypermutation in the CDRs of BCRs and the clonal selection of those B cells with highest affinity for antigens [60, 61]. In contrast to affinity maturation, class switching involves the constant regions of the BCRs in order to produce $IgG_{1\text{-}4}$, $IgA_{1\text{-}2}$ or IgE antibodies, in addition to the IgM and IgD produced by naïve mature B cells, allowing different responses towards different pathogens. In addition, cytokines from T helper cells or regulatory T cells such as IL-4, IL-5, interferon-γ (IFN-γ), TGFβ or IL-10, are able to promote or suppress production of certain isotypes or subtypes of antibodies [62, 63]. B cells in the end are differentiated into plasma cells for antibody secretion or memory cells for long-term protection and faster, more effective secondary response to previously encountered antigens [64-66].

III. T cell receptor and T cell development

A. T cell receptor complex

TCR complexes were first identified as disulphide-linked hetero-dimeric glycoproteins using immunoprecipitation mediated by monoclonal antibodies [67, 68]. The cDNA sequences of TCRα and TCRβ were later isolated using DNA subtractive hybridisation techniques, and gene rearrangement confirmed by Southern-blot analysis of different T cell clones [69-72].

The majority of T cells expresses αβ TCR complexes and the remainder (up to 15%) expresses γδ TCR complexes on the cell surface in general [73]. However, the ratios of T cells expressing αβ TCR to those expressing γδ TCR vary significantly among different organs, individuals and species. For example, αβ TCR-expressing and γδ TCR-expressing intraepithelial lymphocytes are at a 50:50 ratio in mice [74]. The domain structure of the TCR, both αβ TCR heterodimer and γδ TCR heterodimer, are classified as belonging to the IgSF based on their structure similarities with other family members. Each TCR chain contains two IgSF domains, a variable and a constant domain. The membrane-distal variable domain exhibits diversity in sequence resulting from V(D)J gene recombination (discussed in I.B.(b)), and this domain contains three CDRs, *i.e.* CDR1, CDR2 and CDR3, and one additional hypervariable region, HV4, for peptide-MHC recognition or superantigen binding [26-28]. In contrast to the variable domain, the membrane-proximal constant domain has a much more conserved sequence. In addition to the variable and constant domains, there are also a connecting peptide sequence, a transmembrane region and a short cytoplasmic tail for each chain [75, 76].

The TCR does not exist as a simple heterodimer on the membrane. An entire TCR complex comprises a TCR heterodimer in association with three dimeric CD3

subunits, *i.e.* CD3δε, CD3γε, and either CD3ζζ or CD3ζη, and these have to correctly assemble in the ER in order for well-folded intact TCR complex to reach the cell surface [77-79]. The association of the TCR heterodimer with CD3 subunits allows signalling to be transduced across the membrane following ligand binding. In contrast to the very short cytoplasmic domains of TCR heterodimer, therefore, the CD3 subunits have long cytoplasmic domains containing ITAMs [80].

B. T cell development

T cell development occurs in the thymus. T cells are derived from committed lymphoid progenitors in bone marrow and that migrate to the thymus for further development. In the thymus, thymocytes undergo β-selection, positive selection and negative selection and eventually become mature T cells. Mature T cells leave the thymus and are responsible for adaptive immune responses in the periphery.

(a) Double negative stage

Thymocytes initially lacking expression of TCR, CD4 and CD8 are known as double negative (DN) thymocytes. Based on CD25 and CD44 expression, these pre-T cells can be further subdivided into four developmental stages: DN1 ($CD25^-CD44^+$), DN2 ($CD25^+CD44^+$), DN3 ($CD25^+CD44^-$) and DN4 ($CD25^-CD44^-$) [81]. The regulation of thymocyte development relies heavily on the thymic microenvironment and signalling, which initiates the course of development [82].

DN1 thymocytes are early T lineage progenitor (ETP) cells, which differentiate from thymus-settling precursors in the thymic cortex. Engagement of Notch receptors on thymocytes with Notch ligands on thymic stromal cells initiates Notch signalling at this stage [83]. Thus, DN1 cells are able to proliferate and start to lose B cell lineage potential. Notch signalling not only assists in T lineage commitment but also allows

for pre-Tα gene activation as thymocytes migrate towards the thymus capsule at the DN2 stage [84].

At the DN3 stage, thymocytes further migrate to the thymus subcapsular zone and the T lineage becomes fully committed. At this stage, the TCRβ gene undergoes gene rearrangement mediated mainly by the RAG-1 and RAG-2 proteins [21, 22, 25, 85]. A rearranged TCRβ chain then pairs with a non-rearranged invariant pre-Tα chain and CD3 subunits, thus forming a pre-TCR complex that expresses on the cell surface [86]. Only those thymocytes expressing functional pre-TCR on the cell surface at this stage are able to further develop, while those which fail to rearrange the TCRβ gene, or those which fail to produce a functional pre-TCR at the cell surface, are eliminated by apoptosis. This check point for pre-TCR cell surface expression and for receptor assembly is referred to as β-selection [81, 87].

Those thymocytes which pass β-selection require pre-TCR and other signalling for allelic exclusion (inhibition of further rearrangement of the TCRβ gene), further differentiation and survival [88]. The extra signalling required is initiated by receptor/ligand interactions involving, for example, c-kit, Flt3, IL-7 receptor [89], Notch receptor [90] and CXCR4 [91] on thymocytes and their cognate ligands on the thymic cortex. Pre-TCR signalling, on the other hand, is initiated in a ligand-independent manner as there is no clear cognate ligand for this receptor [92, 93]. Indeed, β-selection is proposed not to even require the extracellular domains of the pre-TCR. Pre-TCR signalling likely involves ITAM and tyrosine kinases, similar to those involved in TCR signalling. In the course of signalling initiation, tyrosines in the ITAMs are phosphorylated by Src-family tyrosine kinases, thus forming docking sites for further signalling molecules involved in downstream signalling pathways [80]. The strength of the signals at this stage is involved in determining T lineages. For example, weaker signalling from the pre-TCR or from the γδTCR commits to the

αβ T lineage while stronger signalling from the γδTCR produces commitment to the γδ T lineage [93-95]. The majority (~80%) of the thymocytes at this stage are in this way directed to the αβ T lineage and start to express co-receptors CD4 and CD8, thus progressing into the double positive stage [96].

(b) Double positive stage

At the double positive stage, cells with a rearranged TCRβ and an invariant non-rearranged pre-Tα proliferate, and during this phase the recombinase RAG-2 is rapidly degraded [29]. This expansion before TCRα gene rearrangement allows greater diversity of TCR repertoire in antigen recognition to be achieved. When proliferation ceases, rearrangement of the TCRα gene resumes, resulting in the expression of the mature TCR containing rearranged TCRα and TCRβ, and the CD3 subunits [30, 97].

Double positive (DP) cells then undergo positive selection. While β-selection ensures gene rearrangement of the β chain and pre-TCR surface expression, positive selection is viewed as a check point for the rearrangement of the α chain and for functional self-MHC restriction [98]. DP cells encounter MHC-expressing cortical thymic epithelial cells (cTECs) [99]. Only those DP cells which can successfully engage with MHC receive survival signals for further differentiation while the majority of DP cells which fail to interact with MHC undergo apoptosis [100]. The self-MHC restricted DP cells consequently develop into either $CD4^+$ or $CD8^+$ single positive (SP) cells, depending on whether they engage with MHC-II or MHC-I expressed on the thymic cortex, respectively.

(c) Single positive stage

After β- and positive selection, SP cells migrate to the thymus medulla, whereupon

negative selection occurs in order to eliminate those self-reactive TCRs, thus minimising the potential for autoimmunity [101]. Medullary epithelial cells (mTECs) express MHC molecules bearing a self-peptide (self-peptide-MHC) [99]. SP cells which bind to the self-peptide-MHC strongly are eliminated. In general, most thymocytes fail selection and undergo apoptosis in the thymus. The surviving small fraction (~5%) establishes the repertoire of mature T cells, either $CD4^+$ or $CD8^+$, that leaves the thymus [98].

C. Subsets of T cells

T cells are lymphocytes and undergo a series of differentiation steps in the thymus as discussed above. Based on their surface markers, cytokine secretion activity, transcription factors and functions, T cells are further categorised into different subsets including T helper cells, cytotoxic T cells, memory T cells, regulatory T cells and natural killer T cells.

(a) T helper cells

T helper cells express the CD4 glycoprotein on their surface. T helper cells play an essential role in adaptive immunity since they assist and regulate immune responses including activation of B cells, cytotoxic T cells and macrophages. Therefore, the depletion of T helper cells, for example in human immunodeficiency virus (HIV)-infected patients, results in immunodeficiency or susceptibility to opportunistic infections [102-104]. Engagement of T helper cells with antigenic peptide-MHC-II on antigen presenting cells is required for clonal expansion and the differentiation of naïve T helper cells into different lineages [105]. As a result of different net signals from antigen presenting cells, activation of co-stimulatory molecules and cytokine signalling, naïve T helper cells differentiate into Th1, Th2, Th17 or induced regulatory T cells

(iTreg), which have different effector functions [106-108] .

i. Th1 and Th2 cells

Th1 cells are required for immune responses against intracellular bacteria and protozoa [109]. With IL-12 secreted by dendritic cells and other transcriptional factors, *i.e.* T-bet and STAT4, T helper cells are induced to become Th1 cells. Effector Th1 cells produce IFN-γ, which then activates macrophages and cytotoxic T cells, and the inducible form of nitric oxide synthase (iNOS), which helps eliminate intracellular bacteria and protozoa [110, 111].

On the other hand, when organisms encounter extracellular parasites or helminths, naïve T helper cells are exposed to the cytokines IL-2 and IL-4 which activate transcription factors STAT6 and GATA3 and induce Th2 cell differentiation [109, 112]. Effector Th2 cells are then able to produce IL-4, IL-5, IL-9, IL-10 or IL-13. Among these cytokines, IL-4 is also involved in a positive feedback loop which makes more naïve T helper cells differentiate into effector Th2 cells [113, 114]. In contrast to cell-mediated Th1 responses, Th2 responses are involved in humoral immunity. The cytokines produced by Th2 cells consequently activate B cells, eosinophils, basophils and mast cells [115]. Accordingly, the combination of IgE antibodies, histamine, serotonin and leukotriene results in helminth expulsion from respiratory or gastrointestinal systems [116, 117]. However, overexpression of IgE can cause IgE-mediated allergies and hypersensitivity, such as allergic rhinitis or asthma [105].

Th1 and Th2 cells appear to be mutually exclusive in terms of their differentiation and effector functions [118]. Cytokines produced by Th1 and Th2 cells promote their own lineages to differentiate and function and in the meantime block differentiation into cells of the other lineage. For example, IFN-γ antagonises IL-4, and vice versa. IFN-γ secreted from Th1 cells promotes more Th1 development, and it also inhibits

Th2 development. Similarly, IL-10 secreted by Th2 cells inhibits IL-12 production and therefore prevents Th1 lineage development [119].

ii. Th17 and iTreg cells

In addition to Th1 and Th2 cells, another reciprocal subset of T helper cells comprises Th17 and induced regulatory T cells (iTreg) [120]. Th17 cells are pro-inflammatory. The transcription factor, *i.e.* ROR-γt, and cytokines, *i.e.* TGF-β, IL-6, IL-21 and IL-23, are required for Th17 differentiation from naïve T helper cells [121]. Effector Th17 cells produce IL-17, IL-21 and IL-22 which are mainly involved in mucosal immunity by eliminating pathogens at mucosal surfaces. Loss of Th17 cells very often results in microbial translocations from mucosal surfaces [122]. However, dysregulation of Th17 cells is also a common cause of autoimmunity or tissue damage, for example, rheumatoid arthritis or symptoms observed in experimental autoimmune encephalomyelitis (EAE) in animal models [123].

The counterpart of Th17 cells is iTreg cells. IL-17 secreted from Th17 inhibits iTreg cell differentiation. iTreg cells, in contrast to Th17 cells, downregulate effector T cells, increasing tolerance to self-antigens and alleviating autoimmunity [124]. Without IL-6, TGF-β *per se* induces the transcription factor Forkhead box P3 (FOXP3) which is required for iTreg differentiation [125]. In addition, retinoic acid from intestinal $CD103^+$ dendritic cells enhances TGF-β-driven iTreg cell differentiation from naïve T helper cells in order to maintain intestinal immune tolerance for dietary antigens and resident microflora while suppressing Th17 cell differentiation [126, 127].

(b) Cytotoxic T cells

Cytotoxic T cells or "killer" T cells, express CD8. Cytotoxic T cells are generated in the thymus and express TCR on their surfaces [128]. However, in contrast to T helper cells

which recognise peptide-MHC-II, cytotoxic T cells recognise peptides presented by MHC-I on antigen presenting cells. This TCR-peptide-MHC interaction is further stablised by the co-receptor CD8 glycoprotein [129]. In addition to aiding stablisation, CD8 increases antigen sensitivity. Followed by the second signal from co-stimulatory receptors, such as engagement of CD28 on cytotoxic T cells with CD80/CD86 on antigen presenting cells, naïve cytotoxic T cells become effector cells [130, 131]. However, T helper cells are indispensable for this activation process, and for clonal expansion and survival of cytotoxic T cells.

Cytotoxic T cells are responsible for elimination of intracellular pathogens including viruses and bacteria and for tumour surveillance based on three mechanisms. Firstly, effector cytotoxic T cells secrete effector cytokines, such as anti-microbial IFN-γ and tumour necrosis factor-α (TNF-α) [132]. Secondly, effector cytotoxic T cells directly kill infected or cancer cells by releasing perforins and granzymes. Thirdly, activated cytotoxic T cells may also express FAS ligands (FASL) on their cell surface, which are able to bind to FAS on target cells and also induce apoptosis [133]. FASL/FAS signalling is also involved in cytotoxic T cell homeostasis at the end of immune responses [134].

(c) γδ T cells

There is another subset of T cells, γδ T cells, which express γδ TCR complexes rather than αβ TCRs on the cell surface [73, 135]. The γδ TCR complex consists of a γδ TCR heterodimer and CD3 subunits, but unlike αβ TCRs, γδ TCRs are not conventionally MHC-restricted. Complementing αβ T cells, γδ T cells have the ability to recognise bacterial patterns or stress-inducible MHC-related molecules (MICA/B) [136]. The diversity of γδ TCRs in antigen recognition is achieved by gene rearrangement including genetic recombination, similar to the VDJ gene segments

used in the αβ TCR. In addition to the VDJ gene segments, δ gene consists of an additional D segment [137, 138]. Although these VDDJ gene segments are able to provide greater potential for diversity, physical constraints in the association of the γδ chains however limits diversity in γδ TCR [139]. The proinflammatory cytokines, *i.e.* IL-17 or IFN-γ, secreted by γδ T cells provide protection from some bacterial infections, such as Mycobacterium tuberculosis, Staphylococcus aureus or Listeria monocytogenes [122, 140, 141]. However, the γδ T cells are also found to worsen some inflammatory or autoimmune diseases, such as psoriasis, colitis or autoimmune encephalomyelitis [142-144]. Thus, several studies suggested that γδ T cells have properties that link both innate and adaptive immune responses [145-147].

(d) Memory T cells

Immunological memory is one of the key features of adaptive immunity. At the end of immune responses, the majority of effector T cells undergo apoptosis, but a small fraction develops into memory T cells [148, 149]. Upon re-exposure to their cognate antigens, these antigen-experienced memory cells are able to rapidly expand into a large quantity of effector cells and thus help eliminate pathogens much more efficiently [150]. Therefore, memory T cells can give rise to faster, stronger immune responses, which is also the basis for immunisation and vaccination [151]. Based on cell markers and functions, memory T cells can be further sub-divided into stem memory T cells, central memory T cells and effector memory T cells [152, 153].

Stem memory T cells are found at the earliest development stage of memory T cells and retain an enormous capacity for self-renewal. Stem memory T cells are capable of generating central memory T cells and further effector memory T cells while maintaining their own population. These cells are characterised by surface expression of both naïve and memory T cell markers, *i.e.* chemokine receptors CCR7 and CXCR3,

CD45RA, lymph node homing receptor CD62L (L-selectin), CD95, IL-2Rβ and CD58, as well as stem cell antigen-1 (Sca-1) [153, 154]. Central and effector memory T cells express CD45RO and lose CD45RA. Central memory T cells also express CCR7 and CD62L but effector memory T cells do not [155]. Unlike stem memory T cells and central memory T cells with CCR7 and CD62L which home to secondary lymphoid organs, $CCR7^{-}CD62L^{-}$ effector memory T cells accumulate in the periphery and produce effector cytokines [156].

(e) Regulatory T cells

If the adaptive immune system is not well-regulated, it can cause autoimmunity or allergy. In this case, highly specific adaptive immune responses target self-antigens or non-pathogenic immunogens, rather than foreign pathogens. These can consequently cause damage to tissues or organs. Regulatory T cells which provide self-tolerance and prevent damage to tissues or organs are characterised by expression of FOXP3 and CD25 (the α chain of IL-2) [157]. It has been shown that FOXP3 deficiency leads to immune dysregulation, polyendocrinopathy and enteropathy X-linked syndrome [158]. Regulatory T cells downregulate immune responses by directly producing or promoting production of immunosuppressive cytokines such as TGF-β and IL-10, or by inducing apoptosis of effector immune cells [159, 160]. There are two types of regulatory T cells. Those which develop from T helper cells in the periphery are iTreg (discussed in III.C.(a).ii.) and those developing in the thymus are called natural regulatory T cells (nTreg). In contrast to iTreg in which FOXP3 expression is induced by TGF-β, FOXP3 expression on these thymus-derived nTreg cells is not subject to external regulation [161, 162] but regulated by the conserved non-coding sequences on its gene locus [163].

(f) Natural Killer T cells

Natural killer T cells are a special subset of T cells that express natural killer cell-associated marker NK1.1 (also known as CD161). Natural killer T cells recognise glycolipids and lipids presented by CD1d receptors, which are non-polymorphic MHC-I related glycoproteins, on antigen presenting cells. Natural killer T cells can be further grouped into two types.

Type 1 natural killer T cells are invariant natural killer T cells (iNKT). Their TCR diversity is very limited, comprising the Vα14Jα18 chain paired with a limited Vβ chain repertoire (Vβ2, Vβ7, Vβ8.1, Vβ8.2 or Vβ8.3) in the mouse or Vα24Jα18 chain paired with a Vβ11 chain in humans. These TCRs recognise lipid antigens, *i.e.* α-galactosylceramide (αGalCer), loaded in the CD1d complex and promote IFN-γ production [164, 165]. On the other hand, type 2 non-invariant natural killer T cells (non-iNKT), or diverse natural killer T cells (dNKT) have a more diverse TCR repertoire [165]. Effector natural killer T cells are capable of eliminating glycolipid- or lipid-expressing pathogens by producing cytokines including IFN-γ, granulocyte macrophage colony-stimulating factor (GM-CSF), IL-2, IL-4, IL-13, IL-17, IL-21 and TNF-α. Thus, natural killer T cells play a critical role in mycobacterium defence and tuberculosis prevention [166-168].

IV. T cell activation

A. Src kinases and tyrosine phosphatases in the early events of TCR signalling

In order for specific immune responses to occur, after TCR-peptide-MHC engagement (as discussed above), the CD3 subunits in the TCR complex, which carry ten conserved ITAMs for tyrosine kinase phosphorylation in their long intracellular tails, convert the recognition information to signal transduction [80, 169]. This is achieved

when multiple sites for phosphorylation in the CD3s are phosphorylated in a non-sequential, random process [170]. The ITAMs are phosphorylated by Lck tyrosine kinase [171, 172], which is a Src family kinase [173]. Lck and other Src family kinases, *i.e.* Blk, Fgr, Fyn, Hck, Lyn, Src, Yes and Yrk, consist of six consecutive domains from N- to C- terminus, including the N terminal myristoylated SH4 domain which in Lck is unique for CD4/CD8 interactions, the conserved SH3 domain for proline-motif recognition, the conserved SH2 domain for phosphotyrosine recognition, the linker region, the conserved SH1 kinase domain for tyrosine phosphorylation and the C-terminal tail [174, 175].

In addition to kinases that activate signalling, there are also negative regulators such as Csk, which phosphorylates and inhibits Lck, and the phosphotyrosine phosphatase (PTP) CD45, which dephosphorylates both Lck and the TCR. The fine regulation mechanisms of Lck involve tyrosine phosphorylation and internal SH2-/SH3-domain interactions [173, 174]. Trans auto-phosphorylation of Y394 of Lck promotes Lck's kinase activity by stabilising the catalytic site, promoting ATP binding and enzyme-substrate interactions. Phosphorylation of Y505 of Lck by Csk, on the other hand, inhibits Lck's kinase activity by 'closing' the Lck structure via association of the SH2 domain and C-terminal tail. This phosphorylation also stabilises the binding of the SH3 domain to the PxxP motif (where x is a random amino acid) in the linker region between the SH2 and SH1 domains. This further restricts Y394 phosphorylation and Lck-substrate interactions [176, 177]. In general, Lck kinase regulation is more affected by Y394 than Y505 phosphorylation [175, 178].

CD45 comprises 10% of the T cell surface proteins and exists largely in the form of monomers on the membrane [179, 180]. CD45 is capable of protein dephosphorylation with a broad specificity and high catalytic rate using the highly

conserved catalytic domain (D1) in its cytoplasmic tail [181]. In comparison with the conserved cytoplasmic tail of CD45, the extracellular region is composed of more diverse sequences and exons resulting from alternative splicing [182]. Although the extracellular region of CD45 does not provide catalytic activity, this extracellular region is critical for TCR signalling initiation. For example, truncating the extracellular region of CD45 (and also CD148) [183, 184], or elongating the complex formed by the TCR with an MHC-I ligand, reduces T cell signalling and cytokine production [185]. Structural and imaging studies also suggest that the extracellular region of CD45 is relatively large and rigid, which is likely to prevent the CD45 from diffusing into the close-contact zone created by engagement of the TCR with peptide-MHC (discussed below) [183].

B. Signalling pathways leading to T cell activation

Following phosphorylation of the ITAMs of the CD3 subunits, the tandem SH2 domains of ZAP70 bind to the ITAMs resulting in an increase in the activity of the ZAP70 kinase and its localisation at the cell surface. The active form of ZAP70 is then able to phosphorylate adaptor proteins such as the cytosolic adapter SLP76 and membrane tethered LAT [186]. The phosphorylated tyrosines on LAT serve as docking sites that in turn recruit a series of downstream signalling molecules, for example, PLCγ1, p85 (the regulatory subunit of phosphoinositide 3-kinase, PI3K), GEF, GRB2, GADS and GADS-mediated SLP76 [173, 187]. As a consequence, PLCγ1, PKC, Ca^{2+} and small G protein-mediated pathways (Ras/MAP kinase pathway) become activated. These signalling pathways lead to changes in gene expression mediated by NFκB, NFAT and AP-1, and to increased cell mobility, cytoskeleton rearrangements and activation responses [173, 188].

C. Costimulatory signals

A second signal, in addition to the first signal initiated by TCR engagement with the peptide-MHC, is required for T cell activation [189]. In the absence of the second signal, T cells become anergic, *i.e.* incapable of clonal expansion [190]. The antigen-nonspecific costimulatory second signal results from the engagement of dimeric CD28 on T cells with B7 receptors, *i.e.* B7-1 (CD80) or B7-2 (CD86), on the APC. The cytoplasmic domain of CD28 contains tyrosine motifs (YMNM and PYAP), and phosphorylation of these motifs by Lck, the same kinase involved in generating the first signal by TCR engagement, allows further signalling molecules to be recruited, for example PI3K, ITK and TEC. This second signal activates PI3K and other pathways, thus increasing the NFκB, NFAT and AP-1 mediated transcriptional activity of genes for cytokine production and for cell mobility [131, 191].

In addition to CD28, the structurally similar receptors, CTLA-4 (CD152) and PD-L1 (CD274), which share significant homology with CD28, are also ligands for B7. But in contrast to CD28, these inhibit and downregulate T cell activation [192, 193]. These molecules play important roles in signalling regulation. They are undetectable on resting or naïve T cells, but their expression levels on the cell surface are increased following T-cell activation. The level of CTLA-4 on the cell surface is also increased by the costimulatory signal generated by CD28 [194]. In addition, the affinity of CTLA-4 to B7 is higher than that of CD28 to B7 [195]. These regulatory mechanisms attenuate T cell activation and maintain lymphocyte homeostasis [196].

D. Immunological synapse formation

TCR engagement with peptide-MHC leads to changes in the actin cytoskeleton, the large-scale rearrangement of membrane proteins and polarisation of T cells, producing

an immunological synapse, a structure that in some respects is analogous to the classical neuronal synapse, between the T cell and the APC [197]. The immunological synapse, also known as the supramolecular activation cluster (SMAC), is composed of different concentric rings of membrane proteins forming a bull's eye pattern [198, 199]. The three concentric regions are the central SMAC (c-SMAC), peripheral SMAC (p-SMAC) and the distal SMAC (d-SMAC). The TCR, the co-receptors, *i.e.* CD4 or CD8, and the costimulatory receptor, *i.e.* CD28, are found in the c-SMAC [200]. The adhesion molecule, *i.e.* LFA-1 (CD11a/CD18), is enriched in the p-SMAC, which surrounds the c-SMAC. These molecules are indispensable for cell-cell interactions and signalling. For example, the interactions formed by integrin LFA-1 with its ligand ICAM-1 on the APC are much more stable than those formed by the TCR and the peptide-MHC [201], and the CD2-family proteins are especially important in T cell-B cell interactions [202]. Although structurally different, both the integrins and the CD2 family proteins are claimed to use Fyn, instead of Lck, for signalling [203]. In addition to the integrins, there are also cytoskeletal proteins, *i.e.* talin, in the p-SMAC [198]. Finally the phosphatases, *i.e.* CD45 and other large proteins, *e.g.* CD43, are located in the d-SMAC [204, 205].

The immunological synapse was first proposed to be the structure that allows TCR engagement with the peptide-MHC to sustain signalling and to promote T cell proliferation [206-208]. However, it was later found out that TCR signalling is required for the formation of the immunological synapse, and that, in addition, formation of the immunological synapse is not strictly required for T cell activation [209, 210]. Upon TCR triggering, TCR microclusters are generated at the periphery of the immunological synapse and move centripetally to the c-SMAC. In the c-SMAC, signalling through the TCR is terminated and signalling receptors are internalised for degradation [211, 212]. Secretion of granzymes and other cytotoxic agents by

cytotoxic T cells also occurs in the c-SMAC [213]. Retaining these soluble products between the membranes of the immune and target cells in close proximity likely maximises the efficacy of the delivery of effector functions while also reducing bystander effects [199, 209].

V. Models of T cell activation

The mechanism of how the TCR engages peptide-MHC is well-understood and the subsequent signalling leading to changes in gene expression and activation responses are well-studied. However, how signalling is initiated across the membrane after this initial engagement remains unclear and controversial. The problem is complicated by the recognition of peptide-MHC being able to mediate efficient discrimination between self and non-self ligands, with the non-self-peptide-MHC often being in very small proportion of total peptide-MHC. Different non-self-peptides loaded in the MHC produce ligands with different binding strengths for TCRs. Finally, the binding interfaces of TCR and peptide-MHC are very diverse as well. Thus, any signal initiation theory would need to incorporate these special properties of the TCR-peptide-MHC recognition process, *i.e.* its discrimination ability, sensitivity and diversity [214].

Three principal models for T cell activation have been proposed: the aggregation model, the conformational change model and the kinetic-segregation (KS) model [214, 215]. In the aggregation model, the formation of dimeric or high-order multimeric TCRs is a prerequisite for signalling, whereas in the conformational change model, binding-induced changes in the structure of the TCR are claimed to occur. The kinetic-segregation model is based on the physical segregation of antagonistic signalling proteins.

A. Aggregation model

Aggregation, including dimerisation or oligomerisation, of receptors is one of the most popular models to explain signal initiation and the induction of downstream responses. The classical example is the dimerisation of the epidermal growth factor receptors (EGFRs) and other members in the ErbB family, which initiates mostly proliferative responses. Upon ligand binding, EGFRs form active homodimers, or heterodimers (when EGFR pairs with another ErbB family member) [216]. The ligand-induced dimerisation favours trans-autophosphorylation of tyrosine residues in the cytoplasmic tails of the receptors, which then serve as the docking sites for the SH2 domains of signalling molecules, thus initiating downstream signalling cascades [217]. This type of mechanism has been considered even relatively recently for TCR signal initiation. According to this idea, the aggregation of TCR might contribute to increased levels of Src kinases and substrates locally for phosphorylation [218]. There is also evidence that TCR signalling can be triggered directly by aggregation of the TCR induced by crosslinked antibodies or multimeric peptide-MHC [219, 220].

There are other aggregation models, which heavily rely on the binding of co-receptors, such as CD4 or CD8. The two major versions are the heterodimerisation model and pseudodimerisation model. The heterodimerisation model suggests that the TCR-CD3 complex and a co-receptor, either CD4 or CD8, engage the same peptide-MHC protein simultaneously. As a result, the co-receptor associated tyrosine kinase, Lck, is brought to the TCR, thus allowing signalling to be initiated. However, it has been shown in the co-receptor knock-out mice that mouse TCRs can still be triggered in the absence of co-receptors, and the alloreactive cytotoxity of mouse TCRs has been shown to be induced in the absence of CD8 [221-223]. The pseudodimerisation model, on the other hand, postulates that signalling is initiated by

self-peptide-MHC and agonist-peptide-MHC being “crosslinked” by co-receptor proteins, to create pseudo-dimers of TCRs. This model is claimed to be supported by T cell activation being induced by the soluble peptide-MHC dimers. However, the heterodimerisation and pseudodimerisation models have been questioned since, as discussed above, in the absence of co-receptors, TCR signalling could still occur [223, 224].

Some other studies have posed challenges to aggregation as an explanation for T cell activation. For example, it has been shown that a single agonist peptide-MHC is able to trigger T cells [225-227]. In addition, the affinity of co-receptors, especially CD4, to MHC is very weak [228]. Also, the binding of co-receptor, *i.e.* CD8, to MHC was found to require the SH2 domain of Lck after TCR engagement with peptide-MHC and phosphorylation of ITAMs [229]. The surface densities of agonist- and self-peptide MHC are much lower than the surface density of TCRs in the contact zone (surface densities: agonist-peptide MHC << self-peptide MHC < TCR), so that the pseudodimerisation model is challenged by the low probability of association of self- and agonist-peptide-MHCs and how these self- and agonist-peptide-MHCs at low surface densities could drive TCR dimerisation [230]. Taken together, aggregation might be a process that leads to signalling amplification after signal initiation, rather than for TCR triggering *per se* [230].

Nevertheless, several studies have emerged suggesting that the TCR [231] and some proximal signalling molecules, such as LAT [231] and Lck [232] or the pre-TCR in early T cell development [233, 234], aggregate or form (nano-) clusters in resting cells, *i.e.* prior to activation. Yet other studies showed that the receptors are monomeric and that structural regions that could form oligomers do not exist or are not necessary for signalling [93, 235-237]. A possible resolution of this, which is supported by work in this thesis, is that aggregation is an artefact of the non-resting

status of the T cells used in the above studies, or the result of some other technical limitation of the techniques used for investigation, such as the blinking of fluorophores in the case of super-resolution imaging techniques [238].

B. Conformational change model

In the conformational change model, it is proposed that TCR signal initiation results from conformational changes of receptors, analogous to the mechanism utilised by, *e.g.* G-protein coupled receptors. The model allows TCR signalling to occur even at the low densities of the peptide-MHC on the APC. For example, Janeway *et al.* proposed this mechanism of TCR triggering based on the observation that different anti-TCR antibodies give different levels of signalling [239]. However, no direct linkage of TCR signalling with induced structural rearrangements of the TCR induced by these antibodies has been obtained, and generally antibodies do not radically alter the structures of the proteins they bind to [240]. Nevertheless, intra- or inter-subunit changes in the TCR complex resulting from engagement of the TCR and agonist peptide-MHC have been claimed to initiate TCR signalling. These have focussed on the TCR itself, the CD3 cytoplasmic domain or the CD3 extracellular domain.

(a) Conformational change in TCR

Crystallographic studies of the LC13 TCR in the free form and as TCR-peptide-MHC complexes were suggested to reveal a conformational change in the constant region of the TCRα chain upon ligand binding [241]. Another study using both crystal- and fluorescence-based techniques also showed a peptide-MHC binding-induced conformational change in the constant regions of the α chain of this TCR, and mutagenesis of the residues impaired T cell signalling [242]. However, the resolution of the constant region of TCRα in the TCR-peptide-MHC complex is often poor in

crystal structures, and it has yet to be convincingly shown that other TCRs undergo a similar structural change [214]. In addition, it is sometimes difficult to distinguish between effects on TCR structural assembly and effects on signal initiation. For example, mutations of the constant region of TCRα could lead to imperfect assembly or instability of the TCR complex.

(b) Conformational change in CD3 cytoplasmic domain

In other studies, conformational changes in the cytoplasmic domains of the CD3 subunits have been proposed. After engagement of the TCR with self- or agonist-peptide-MHC, the TCR-CD3 complex is proposed to undergo a substantial conformational change which allows the proline-rich motif of the CD3ε cytoplasmic tail to be exposed. This was proposed to allow the Nck adaptor protein to then be recruited to these proline residues [243, 244]. However, normal T cell responses can still be induced during immune responses and by antibodies in mice lacking the proline rich motif of CD3ε [245]. This suggests that TCR signalling is not dependent on the interaction between the CD3ε proline-rich motif and Nck [245], regardless of whether the conformational change occurs.

Another proposed conformational change-based mechanism is claimed on the basis of Förster resonance energy transfer (FRET) and nuclear magnetic resonance (NMR) experiments [246, 247]. The authors of this study argued that the cytoplasmic domain of CD3ε was sequestered in the membrane, and that this acts as a protective mechanism for avoiding unnecessary triggering (*i.e.* as a 'safety-catch'). After peptide-MHC binding, it was proposed that the cytoplasmic domain of CD3ε dissociates from the membrane so that the ITAMs are accessible to Src kinases that drive downstream signalling [246, 247]. However, even without TCR engagement with the peptide-MHC, it was shown by others that the ITAMs are still accessible to

kinases following treatment of the cells with the tyrosine phosphatase inhibitor, pervanadate, arguing against membrane squestration [248, 249].

(c) Conformational change in CD3 extracellular domain

Yet more studies have proposed that, after TCR engagement with peptide-MHC, large inter- and intra-subunit conformational changes and the formation of new interfaces involving the CD3 subunits can drive TCR signalling [250, 251]. However, a mutagenesis-based analysis of CD3ε surface residues utilising the method of 'drastic mutagenesis' has shown that there are no new inter-CD3 subunit contacts formed during signalling induced with antibodies. This suggests that substantial conformational rearrangements are not always required for TCR signalling [252].

C. Kinetic-segregation model

The aggregation and conformational change models are two distinct ways of addressing the triggering question. Apart from these ideas, the kinetic-segregation model proposed by Davis and van der Merwe offers a third way to explain how TCR signalling initiates [215, 253].

First of all, Springer *et al.* proposed that bulky glycocalyx elements such as CD45, CD43 and CD148 are excluded from the close-contact zone where TCR and peptide-MHC proteins interact [201]. They suggested that this could have signalling implications, because CD45 acts on the Lck [201]. It was later proposed that receptor signalling would be initiated by phosphatase exclusion if there was constitutive phosphorylation of the TCR by Lck [253, 254]. This idea later became known as the kinetic-segregation model [215, 255] (Figure 1.1).

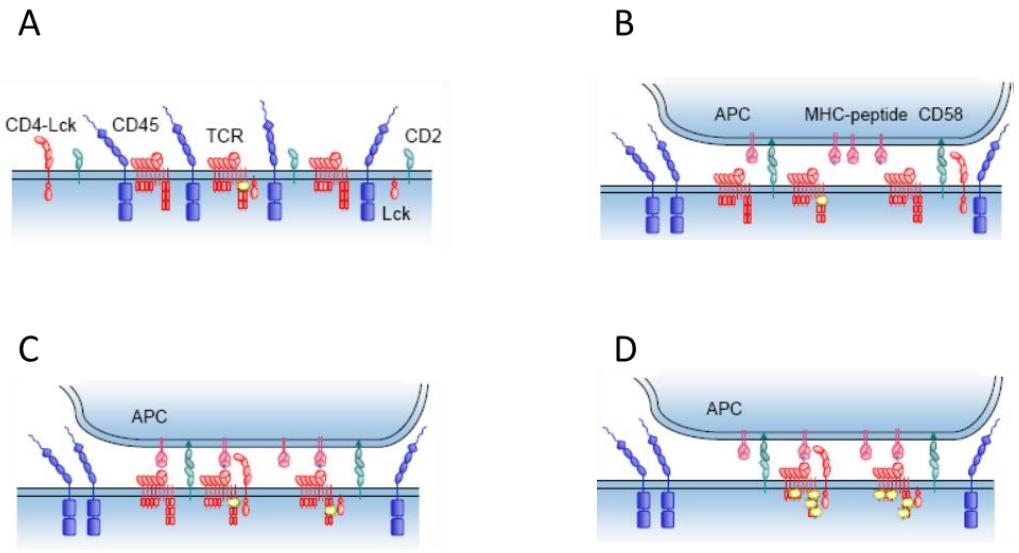

Figure 1.1: The kinetic-segregation model (adapted from [215]). (A) Random molecule interactions result in a zero (or very low) net balance of phosphorylation of the TCR by tyrosine kinases and its dephosphorylation by tyrosine phosphatases. (B-D) After the bulky phosphatase CD45 is excluded, the formation of the close-contact zone by the TCR-peptide-MHC or small adhesion molecules such as CD2 alters the balance and leads to a phosphorylation-favoured tendency for triggering. TCRs temporarily engaged to non-specific peptide-MHC due to lower affinity binding would diffuse out of the contact zone in order to maintain the specificity of TCR signalling.

In more detail, in the kinetic-segregation model, on resting T cells, surface proteins interact by random diffusion. Thus, TCR-CD3 complexes are phosphorylated by kinases and de-phosphorylated by phosphatases randomly. Therefore, the net phosphorylation level is too low to initiate signalling. However, upon TCR-peptide-MHC engagement, the distance in the contact zone spanned by TCR-peptide-MHC as well as small adhesion molecules such as CD2 and LFA3 is only 140 Å [256]. By contrast, CD45 phosphatase is at least three-fold longer in length versus the TCR and it has been shown to be very rigid in the extracellular domain [183]. Therefore, size-dependent phosphatase exclusion alters the balance between kinases and phosphatases. This results in phosphatase exclusion increasing the half-lives of phosphorylated proteins in the contact zone [201, 257]. In addition, in the kinetic-segregation model, not only the phosphatases and kinases but also the quality of engagement between the TCR and peptide-MHC plays an important role. This is because TCRs which fail to bind MHC or which have lower affinity to MHC might thereafter diffuse out of the contact zone before signalling is initiated [215].

The kinetic-segregation model was partly prompted by studies using phosphatase inhibitor, pervanadate [248]. These experiments showed that phosphatases were constraining signalling in resting cells, and that signalling would be spontaneously initiated if the effects of the phosphatases could be reduced, *e.g.* by their exclusion from contacts. Subsequently, as has been discussed, it was shown that either truncated phosphatases or elongated TCR-peptide-MHC complexes lower the level of net phosphorylation since receptors presumably are more easily dephosphorylated in the contact zone [184, 185, 254, 258]. Therefore, TCR triggering is reduced while TCR-peptide-MHC ligation is not affected. More recently, the segregation of CD45 and kinases has been visualised at the submicron-scale on model surfaces and this has provided further support for the importance of segregation for signalling to occur

[183]. At present the kinetic-segregation model is perhaps the best supported by experiments, although close-contact zones have yet to be shown to form during the early seconds of cell-cell contact when signalling is initiated.

D. Integrated model

The T cell activation models discussed above show the difficulties in studying structures of multi-subunit membrane proteins and the intricacies of TCR signalling initiation from the resting state. Although each of these models is supported by respective empirical evidence in certain conditions, it remains controversial which model can fully present T cell signalling initiation. In addition, it has been proposed by van der Merwe and colleagues that more than one model might be involved in a single initiation event [214, 230]. For example, engagement of TCR-peptide-MHC might create a close-contact zone and exclude phosphatases, thus favouring kinase phosphorylation and signalling initiation, as proposed in the kinetic-segregation model. This engagement, might also induce aggregation of more TCR/CD3 receptors and conformational changes of TCR/CD3s. As a consequence, more kinases and substrates could be recruited to the contact zone for further phosphorylation. Further studies, however, are required to explore this hypothesis to better understand T cell signalling initiation. It is worth stressing also, however, that conformational changes and oligomerisation are not requirements of signaling, and that, in principle, the kinetic-segregation model offers a complete explanation for signalling initiation.

VI. Untangling receptor stoichiometry

A. Controversy over TCR stoichiometry

Whatever signalling theory is eventually found to be the correct one, it will have had to

explain the signalling activities of both the mature TCR and the pre-TCR. Since different TCR organisations in the resting state could have a bearing on the different triggering models, an important initial goal is to understand how the TCR and pre-TCR are organised at the surface. Several single-molecule imaging techniques have been used to try to understand TCR stoichiometry, principally two-colour coincidence detection (TCCD), dynamic single-molecule colocalisation (DySCo), high-speed photoactivated localisation microscopy (hsPALM), transmission electron microscopy (TEM) and fluorescence recovery after photobleaching (FRAP). In addition to imaging-based approaches, mutagenesis has been done on CD3 subunits to investigate the organisation of the TCR complex.

(a) Identification of monomeric TCRs using TCCD

As an extension of fluorescence correlation spectroscopy (FCS) and fluorescence cross-correlation spectroscopy (FCCS), TCCD offers additional advantages in sensitivity and reduced background [235, 259, 260]. The principle is based on detection of coincident bursts from two fluorescence labels diffusing through a small confocal volume. The molecule of interest is bound by the antigen-binding fragment (Fab) of a specific antibody tagged with either of two fluorescence labels. Dimeric molecules diffuse at the same time through the beam and give rise to coincident bursts of fluorescence. By contrast, the non-simultaneous movements of monomeric molecules give individual bursts of fluorescence at each time point. Subject to quantification by a statistic comprising the "association quotient" (Q), which is proportional to the numbers of coincident fluorescence-bursts, molecules can either be categorised as a monomer or a dimer [235, 261].

In TCCD analyses of the mouse TCR expressed by a T cell hybridoma (DO11.10), the association quotient (Q) of the TCRβ chain resembled that of

monomeric protein CD86, and was significantly different from that of positive control dimeric proteins CD28 and CD3ε. Importantly, the molecules analysed in TCCD are randomly diffusing at the apical membrane of the cell, away from any surfaces [235].

(b) Identification of monomeric TCRs using DySCo

In DySCo experiments, labelled molecules are tracked at the interface between cells and glass slides using total internal reflection fluorescence (TIRF) microscopy [262, 263]. Because the method relies on low expression of target proteins (in order to identify single molecules), in the case of analysing the TCR, the surface of the slide is not expected to induce activation and complicate the analysis. Extending the TCCD concept, less mobile or slowly diffusing molecules, which are difficult to be detected by TCCD, can be imaged by DySCo [236]. By being tracked with a Bayesian-based algorithm for a defined series of frames after excitation with two overlapped 488 nm- and 568 nm-laser beams, non-associated molecules can be distinguished from associated molecules [236, 264]. Complementing the analyses using TCCD, the DySCo experiments showed that most TCRs behaved in the same way as the monomeric control CD86, rather than the dimeric protein CD28. This suggested once again that the TCR complex is monovalent. However, experiments with latrunculin, which is used to disrupt the actin cytoskeleton, showed that there is a certain degree of confinement or "corralling" of receptors by actins, making CD86 and TCR exhibit a degree of partial self association. For example, after latrunculin treatment, the coincident levels of CD86 and TCR decrease from 10.2% and 4.8%, respectively, to 3.3% and 2.3%.

(c) Detection of 'TCR protein islands' using super-resolution imaging techniques

The visualisation and understanding of membrane protein organisation as well as the

very early events of membrane signalling initiation might be well-suited to analyses using super-resolution imaging techniques which allow the bypassing of the optical diffraction limit.

The major far-field super-resolution techniques used in biology are based on two major types of techniques: the deterministic super-resolution techniques, such as stimulated emission depletion microscopy (STED) and the stochastic super-resolution techniques, such as photoactivated localisation microscopy (PALM) [265] and stochastic optical reconstruction microscopy (STORM) [266]. In STED, the fluorophores are firstly excited by one laser beam and some of them are then instantaneously returned to the ground state by the other red-shifted stimulation beam, termed the STED beam. The STED beam is able to deplete the fluorophores surrounding the excitation spot and hence higher resolution can be achieved [266].

In PALM and STORM, image resolution can be achieved at distance scales as low as 2 to 25 nm. This resolution is about ten-fold higher than diffraction-limited fluorescence imaging (250 nm). The principle is that target molecules are tagged with photo-switchable fluorescent labels in a dark state. Only a subset of the fluorescent labels are then activated at a given time before being photobleached irreversibly. This, in principle, rules out the chances of a single fluorescent label being tracked more than once. This photo-activation process is then repeated sequentially [265]. At the end, the position of each individual fluorescent object is identified using a Gaussian fit of the point-spread function (PSF) [267]. All events are then summed and compiled and therefore the final image is presented at super-resolution. A new variant of PALM, hsPALM could process 100-250 frames per second in a stream-acquisition mode [231, 265, 268]. In addition to PALM, a related imaging technique, STORM, which shares the same fundamental principle, is also widely used in the field [266], and also in this thesis.

Contrary to the findings obtained with TCCD and DySCo [235, 236], using hsPALM, Lillemeier *et al.* found that TCR and LAT were each pre-clustered into "protein islands" on the resting T cell surface when the cells were imaged on non-specific poly-L-lysine surfaces [231]. These observations were supported by studies of two-sized labelled gold particles using TEM [269]. The spatiotemporal relationship between TCR and LAT pre-clusters was further investigated using dual-colour fluorescence cross-correlation spectroscopy (dcFCCS) [270], which suggested that TCR and LAT moved independently within their own protein islands and there was little correlated movement between distinct TCR- and LAT-islands [231].

One way in which these observations could be reconciled is if the cells analysed by Lillemeier *et al.* were not fully resting and were partially activated. Their experiments were done at normal levels of expression of TCR on coated surfaces. The TCCD experiments were interrogating the apical surface of T cells and the DySCo experiments were done at low expression levels of TCR. Another confounding factor was that the Lillemeier experiments were done on poly-L-lysine coated surfaces whereas the DySCo experiments were done on non-specific IgG coated surfaces.

(d) Analysis of 'TCR protein islands' by FRAP

FRAP analysis has suggested that the glass surfaces where cells were placed and observed over time may trigger TCR signalling to some extent and affect the mobility of TCRs [180]. In these experiments, the fraction of mobile molecules was measured. It was found that a substantial fraction of those molecules at the cell-glass interface become immobile, but not those at the distal surface, where the TCCD analysis had been done. On the contrary, using Lck-deficient cells which cannot trigger kinase signalling, it was shown that mobility increased at the cell-glass interface when there was no signalling. This suggested that clusters form as a result of signalling induced by

the glass surface in the TIRF experiments. This study clearly indicated that the approaches to understanding TCR organisation might be affected by the use of surfaces [180].

B. Question of pre-TCR stoichiometry and signalling

While exactly how TCR signalling is initiated remains controversial, how the pre-TCR signals, such that the successful expression on the surface of correctly folded TCRβ chains can be detected by the cell, is even less clear. In addition, although pre-TCRs and TCRs are similar in structure and both involve tyrosine kinase signalling, pre-TCRs likely have no known cognate ligand in the thymus (Figure 1.2A). Therefore, better insights into pre-TCR signalling may give us new insights into the general features of TCR triggering. Autonomous 'head-to-tail' dimerisation or oligomerisation of pre-TCRs, driven by the extracellular domains of the pre-Tα and TCRβ subunits, has been used to explain ligand-independent pre-TCR signalling in previous studies (Figure 1.2B and C) [233, 234, 271, 272]. When 'dimerising' or 'oligomerising' pre-Tα residues in the extracellular domains of the receptor were mutated, it was shown that the mutant proteins were incapable of signalling and driving thymocyte development. It was suggested by Yamasaki *et al.* that four charged mouse pre-Tα residues (D22, R24, R102 and R117), where the first three are in the extracellular domain and R117 is in the connecting peptide near the transmembrane region, were especially indispensable for pre-TCR oligomerisation, signalling and thymocyte development [234]. This general notion was supported by the X-ray crystallographic analysis and small-angle X-ray scattering studies of Pang *et al.*, wherein an autonomous head-to-tail dimeric structure was observed to form by human pre-TCRs [233].

In subsequent *in silico* gene synteny-based analysis, the four charged pre-Tα

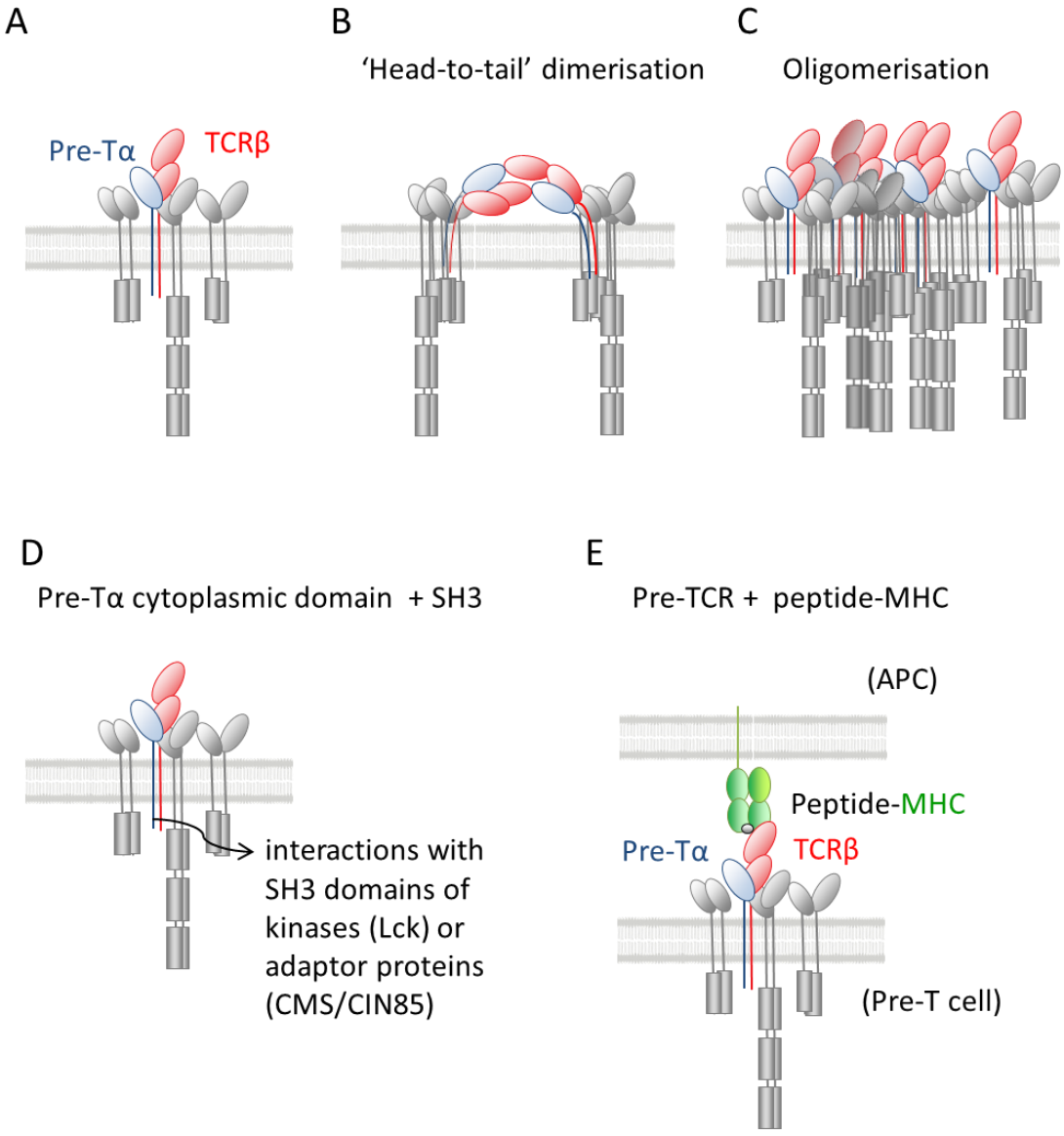

Figure 1.2: Different models for pre-TCR signalling initiation. (A) Single pre-TCR expression on the cell surface. (B) Autonomous 'head-to-tail' dimerisation of pre-TCRs [233]. (C) Oligomerisation of pre-TCRs [234]. (D) Interactions of pre-Tα cytoplasmic domain with SH3 domains of Lck kinase or CMS/CIN85 adaptor proteins [273, 274], or (E) engagement of pre-TCR and peptide-MHC [275].

mouse residues were found not to be conserved among several Sauropsids and Mammals [276]. In some sauropsidian and mammalian pre-Tαs, these residues were missing or had opposite charges. In addition, the claimed role for mouse pre-TCR oligomerisation mediated by these four residues for signalling was also questioned. A truncated form of the mouse pre-TCR lacking the pre-Tα extracellular domain was capable of pre-TCR signalling and thymocyte development [93]. Similar work had been done earlier, by Irving *et al.* showing that a pre-TCR entirely lacking extracellular domains could still initiate pre-TCR signalling [237]. These studies suggested that dimerisation of the pre-TCR might not be necessary for pre-TCR signalling to occur. However, the possibility that the truncated pre-TCR was oligomerising was not formally ruled out; indeed, truncations of the extracellular domains might be expected to increase oligomerisation (*i.e.* aggregation).

It has been proposed that autonomous signalling could arise if the proline-rich motif in the cytoplasmic domain of the pre-Tα, once it got to the T cell surface, interacted with the SH3 domains of intracellular kinases, allowing signalling (Figure 1.2D) [273, 274]. However, recent evolutionary analysis questions this since in Sauropsids and lower Mammalia, such as monotremes, marsupials and lagomorphs, the cytoplasmic domains of the pre-Tα are shorter and lack these proline-rich motifs, and therefore they are unlikely to be involved in signalling [276].

In addition, Mallis *et al.* claimed that the pre-TCR, like the TCR, was able to engage with a peptide-MHC for signalling initiation [275] (Figure 1.2E). Using nuclear magnetic resonance and biomembrane force probe analysis, the pre-TCR was found to bind to the vesicular stomatitis octapeptide loaded onto the MHC class I (VSV8/K^b) via the complementarity-determining regions (CDRs) and the hydrophobic patch in the Vβ chain of the pre-TCR. The engagement and subsequent conformational changes in the Cβ chain of the pre-TCR were found to trigger calcium

flux and grant further pre-T cell proliferation and development [275, 277-280]. However, Mallis *et al.* did not fully exclude the possibility of ligand-independent pre-TCR signalling. Indeed, they claimed that pre-TCR signalling initiation might not solely depend on the engagement of the pre-TCR and peptide-MHC. This engagement might be able to generate stronger pre-TCR signalling and more readily facilitate proliferation at the DN3 stage, in comparison with ligand-independent pre-TCR signalling initiation [275]. However, this pre-TCR-peptide-MHC engagement lacks direct evidence *in vivo*. Furthermore, this engagement model cannot easily be incorporated into the context of different thymic compartments in association with different functions in order for T cell development to occur at different stages. For example, MHC-presenting thymic epithelial cells are dominant in the cortex and medulla regions in the thymus for positive and negative selection, respectively [281, 282]. No direct evidence was shown that abundant MHC-presenting cells are present in the subcapsular region when pre-TCR signalling is initiated at the DN3 stage. In addition, the requirement for MHC engagement for early T cell development is also challenged in γδ T cells which do not bind to conventional MHCs. Instead, it has been shown that the γδ T lineage is determined by signalling strength at the β-selection checkpoint in early T cell development [93, 283]. Thus, how pre-TCR signalling is initiated still remains unknown and, overall, the evidence for ligand engagement is relatively weak. .

VII. Aims of the thesis

Understanding signalling initiation will likely require a detailed understanding of receptor organisation and stoichiometry. The aim of the thesis is to further our understanding of the stoichiometry and signalling of the TCR, with a special emphasis

on the pre-TCR.

The hypothesis about surface expression of monomeric, non-oligomeric receptors, *i.e.* TCR or pre-TCR, prior to signalling is tested using mutagenesis- and imaging-based approaches, avoiding artefacts inherent in different technical approaches that may have influenced the interpretation of previous TCR and pre-TCR studies. First of all, the stoichiometry of the pre-TCR is investigated using mutagenesis. This involves an *in silico* analysis of the surfaces of the pre-TCR and drastic mutation of the pre-Tα residues, including those possibly involved in the dimerisation [233]. Each of the mutant forms of the receptor are then tested for surface expression. The rationale for this is that, if constitutive dimerisation of the pre-TCR is necessary for its assembly, then drastic mutation should disrupt pre-TCR expression at the cell surface. Secondly, a stoichiometric analysis of the TCR and pre-TCR is undertaken using super-resolution imaging techniques including PALM and direct STORM (dSTORM). This involves the development of a labelling strategy, and an investigation of the relationship between heterogeneity of TCR organisation and its expression levels on a cell-to-cell basis. Both *in vitro* and *ex vivo* imaging experiments are undertaken.

Since, unlike the TCR, there is likely no known cognate ligand for the pre-TCR in the thymus. If pre-TCR is monomeric as hypothesised, how a pre-T cell recognises that successful pre-TCR expression on the cell surface has occurred at the β-selection stage is addressed. Given the structural similarities in TCR and pre-TCR, it seems reasonable to hypothesise that the mechanisms for their triggering will be related. Thus, the requirements for ligand-independent signalling are investigated in an assay in which ligand-independent mature TCR signalling is triggered using an antibody binding to a non-signalling form of CD28. Using CRISPR/Cas-mediated gene deletion of the signalling molecules and receptors, *i.e.* ZAP70, Lck and TCR, an attempt is made to understand if ligand-independent mature TCR triggering, used in the first instance as

a proxy for pre-TCR signalling, is any different in broad outline versus conventional TCR signalling [284].

Chapter 2

General materials and methods

I. Molecular cloning

A. General molecular cloning

(a) Polymerase chain reaction (PCR)

Genes of interest were amplified from complementary DNAs (cDNAs) or plasmid DNAs. Oligonucleotide primers with appropriate restriction sites were designed at both the 5'- and 3'-ends. In addition, the Kozak consensus sequence, and sequences encoding signal peptides or HA-tags were also included at the 5'- end, if required. PCR was optimised for each primer and gene of interest. The PCR was performed as follows:

General PCR for one reaction (40 μL)

Template DNA (50 ng)	1 μL
10 mM dNTP (NEB)	2 μL
5x Phusion-HF buffer* (NEB)	8 μL
Phusion high fidelity polymerase (NEB)	1 μL
10 μM 5'-forward primer (Sigma-Aldrich)	0.4 μL
10 μM 3'-reverse primer (Sigma-Aldrich)	0.4 μL
MilliQ water	27.2 μL

(*5x Phusion GC-buffer and 3% DMSO were optimised and used for the GC-rich primers)

PCR programme

95 degrees Celsius for initial denaturation	2 min
95 degrees Celsius for denaturation	30 sec
55 degrees Celsius for annealing	30 sec
72 degrees Celsius for extension	30 sec per kb
(repeat steps of denaturation, annealing and extension)	24 cycles
72 degrees Celsius for final extension	10 min

For site-directed mutagenesis (Chapter 3), chimeric PCR was utilised, in which three general PCR reactions were sequentially involved. The first two PCR reactions amplified two adjacent fragments, with a small degree of overlap, in a template sequence. The first fragment was amplified using a forward primer at the very 5'-end of the template sequence and a reverse primer containing nucleotide(s) for mutation, and the other one used a forward primer containing the same nucleotide(s) for mutation and a reverse primer at the very 3'-end of the template sequence.

These two fragments were then added into a PCR reaction mixture for a final overlap-extension PCR reaction with the forward and the reverse primers at the very 5'- and 3-end of the original template sequence. All PCR reactions were set up as above.

(b) Agarose gel separation

The PCR products or DNAs were separated on an 1% (for general PCR products) or 2% (for those <200 bp) agarose gel in 0.1M Tris/ 0.1 M borate/ 2 mM EDTA buffer with ethidium bromide. The PCR products were electrophoresed at 70 mA and detected using an UV irradiation. The bands were excised and DNAs were purified using QIAquick gel extraction kit (Qiagen).

(c) Restriction enzyme digestion

PCR products and vectors were digested with appropriate restriction enzymes for 1 hour at 37 or 55 degrees Celsius as required by restriction enzymes. A reaction mixture for restriction enzyme digestion was as follows. Digested DNAs were separated on agarose gels, excised and purified as in I.A.(b)

Restriction enzyme digestion (20 μL)

PCR product, insert or vector (1 μg)	5 μL
10x appropriate restriction enzyme buffer (NEB)	2 μL
Restriction enzyme(s) (NEB)	2 μL in total
MilliQ water	11 μL

(d) Ligation

Digested PCR products or inserts were ligated at different ratios with the vectors. Ligation mixtures were prepared as follows and incubated for 1 hour at 16 degrees Celsius or overnight at 16 degrees Celsius.

Ligation (20 μL)

Vectors (100 ng)	5 μL
Inserts	0, 1 or 10 μL
10x T4 DNA ligase buffer (NEB)	2 μL
T4 DNA ligase (NEB)	1 μL
MilliQ water	up to 20 μL

(e) Transformation

20 μL of one ligation mixture was added to 35 μL TOP10 competent cells on ice for 10

minutes. Cells were heat-shocked for 45 seconds at 42 degrees Celsius in a PCR machine and were immediately placed back on ice. Cells were supplied with 150 μL S.O.C. medium (Thermo Fisher Scientific) before being incubated for 1 hour at 37 degrees Celsius in an incubator shaker. Under sterile conditions, 150 μL mixture was plated out on a 90mm petri dishes (Sterilin) coated with the LB agar (Sigma-Aldrich) containing an appropriate antibiotic, such as Ampicillin at 100 μg/mL (Sigma-Aldrich) for pHRsin [285], pHRIsin or lentiCRISPRv2 vectors [286]. Plates were incubated overnight at 37 degrees Celsius. Colonies were screened using PCR to detect the presence of inserted genes of interest as follows before amplification.

Colony PCR for one reaction (40 μL)

Individual transformant	single colony
10 mM dNTP (NEB)	2 μL
10x Thermo buffer (NEB)	4 μL
Taq DNA polymerase (NEB)	1 μL
10 μM 5'-forward primer (Sigma-Aldrich)	0.4 μL
10 μM 3'-reverse primer (Sigma-Aldrich)	0.4 μL
MilliQ water	32.2 μL

PCR programme

95 degrees Celsius for initial denaturation and bacteria lyse	7 min
95 degrees Celsius for denaturation	30 sec
55 degrees Celsius for annealing	30 sec
72 degrees Celsius for extension	70 sec per kb
(repeat steps of denaturation, annealing and extension)	24 cycles
72 degrees Celsius for final extension	10 min

(f) Plasmid preparation

10 mL LB broth (Sigma-Aldrich) with bacteria and an appropriate antibiotic, such as Ampicillin at 100 μg/mL (Sigma-Aldrich), were cultured overnight at 37 degrees Celsius in an incubator shaker and the bacteria pellet was obtained after 4,000 rcf for 10 minutes at 37 degrees Celsius. Plasmids were purified using PureLink HiPure Miniprep or Maxiprep kit (Invitrogen). DNA concentrations were determined using NanoDrop (Thermo Fisher Scientific).

B. Gene editing

(a) shRNA

As for the design of mouse shLck and mouse shZap70, the pattern of oligonucleotide primers, N2[GC]N[A]N6[UT]N2[ATUC]N5[A]N2 (in which N was any base pair; any single letter in the bracket could be selected), was used in order to enhance effectiveness and reduce potential off-target effects for genes knocked down by shRNA [287, 288]. Using this pattern as the first criterion, the candidate sequences for targeting mouse Lck or mouse Zap70 were selected by the siRNA Selection Program developed by the Whitehead Institute for Biomedical Research. In addition, since the thermodynamic values were inversely correlated to degrees of sequence stability, candidate sequences with low or negative thermodynamic values predicted by the siRNA Selection Program were further selected. Moreover, those with negative thermodynamic values were analysed for the best knock-down efficiency via a web tool called siRNA scales [289]. Then, the most stable, efficient sequences for knocking down mouse Lck (5'-gcatcaagttgaatgtcaa-3') and mouse Zap70 (5'-gcaatgttctactggtcaa-3') were determined. In addition, a sequence targeting GFP was designed as for the non-targeting control. In the end, each of these sequences was

cloned respectively into the pHR-sin vector [285] with the RNA polymerase III promoter, U6 promotor, for lentiviral infection.

(b) CRISPR/Cas9 system

The CRIPSPR/Cas9 system used in this thesis was composed of a lentiCRISPRv2 vector with two expression cassettes of sequences including the Cas9 and the guide RNA [286]. The guide RNA was 20 base pairs of the target sequence (for example, mouse Lck, mouse Zap70 or mouse TCRα) designed by a web tool (crispr.mit.edu) and flanked on the 3'-end by a 3 base-pair NGG PAM sequence (in which N represented any base pair). In terms of selecting target sequences, the candidate target sequences were ranked in the inverse likelihood of off-targeting binding on the web tool. The top five ranked candidate sequences for each gene were selected for cloning into the lentiCRISPRv2 vector respectively and were listed as follows:

Selected target sequences

Mouse Lck (1)	5'-atctcgctgcccatccggaa-3'
Mouse Lck (2)	5'-gattgcacgatctagtccgc-3'
Mouse Lck (3)	5'-tgcagcacccgcggctagtc-3'
Mouse Lck (4)	5'-gccttgataggcctttcggt-3'
Mouse Lck (5)	5'-ataccgttccatttcctgaa-3'
Mouse Zap70 (1)	5'-gccgagcgcaaactctattc-3'
Mouse Zap70 (2)	5'-ctcgtggcggacatcgagct-3'
Mouse Zap70 (3)	5'-gccgatgagccgcacgatgt-3'
Mouse Zap70 (4)	5'-tctggcgcgtaccacttcag-3'
Mouse Zap70 (5)	5'-tgtgattcgccccgccccat-3'
Mouse TCRα (1)	5'-tctaggccttcacctagctg-3'

Mouse TCRα (2)	5’-ttctaggccttcacctagct-3’
Mouse TCRα (3)	5’-tcacctagctggggtgagtg-3’
Mouse TCRα (4)	5’-ggggaaggtcccgctctcct-3’
Mouse TCRα (5)	5’-gctgagcctggcagagattc-3’

C. Vectors used in the thesis

The vectors used in the thesis were pHR-sin [285], pHRI-sin and lentiCRISPRv2 [286]. The pHR-sin vector carries the strong spleen focus forming virus (SFFV) promoter while the pHRI-sin carries the ecdysone-inducible promoter instead, which only drives gene expression at very low levels in the absence of ecdysone or analogues. The cloning sites for the insertion of genes of interest in the pHR-sin and pHRI-sin vectors are between the restrict enzymes MluI and BamHI and between BamHI and NotI. The lentiCRISPRv2 vector, with two expression cassettes of sequences including a Cas9 and a 20 base-pair of a guide RNA of interest, was used for gene knock-out in this thesis.

II. Cell culture

A. General techniques

Cell culture work was performed in the HEPA-filter cabinets and cells lines were grown at 37 degrees Celsius with 5% CO_2.

(a) Cell counting

Cell density and viability were assessed and counted using the trypan blue solution (0.4%, Sigma-Aldrich) and hemocytometers. Trypan blue, when mixed at 1:1 ratio (v/v) with cells, penetrates damaged cell membranes, thus distinguishing viable from

nonviable cells.

(b) Subculturing of cells

All cells were kept at density between 2×10^5 to 1×10^6 cells per mL. For suspension cell lines including Jurkat [290], DO11.10 [68] and their derivatives, cells were cultured in the RPMI-1640 medium (Sigma-Aldrich). For the adherent HEK-293T cell line [291, 292], cells were cultured in the DMEM medium (Sigma-Aldrich) instead. Both RPMI-1640 and DMEM were supplemented with 10% (v/v) foetal calf serum (Sigma-Aldrich), 1 mM sodium pyruvate (Sigma-Aldrich), 10 mM HEPE (Sigma-Aldrich) and antibiotics including penicillin, streptomycin and neomycin (50 units per mL, 50 μg per mL and 100 μg per mL, respectively; Sigma-Aldrich). Additionally, in order to minimise the background fluorescence and any possible fluorescence interference, these cells were cultured with the phenol red-free RPMI-1640 medium (Sigma-Aldrich) instead, with the same supplements applied as described above, for at least 2 passages before being imaged.

Cells were split when the density reached or nearly reached 1×10^6 cells per mL for the suspension cells, or when the confluency was 70% to 90% for the adherent HEK-293T cells. For the adherent HEK-293 T cells, the medium was removed and the cells were washed with phosphate-buffered saline (PBS) solution and then disassociated from tissue culture flasks using trypsin for 3 minutes at 37 degrees Celsius. Tissue culture flaks containing trypsinised HEK-293T cells were then gently shook in order to completely disassociate the cells. The activity of trypsin was inhibited when 2 times the volume of fresh supplemented DMEM was added. The cells were then harvested and spun at 1,300 rcf for 3 minutes. In the end, the pellets were resuspended and split 1:4 into a new flask with fresh supplemented DMEM.

(c) Freezing and thawing cells

Cells were kept at -80 degrees Celsius or in liquid nitrogen tanks for short-term or long-term storage, respectively. About 10^7 cells were first spun down, resuspended in 1 mL of freezing buffer containing 10% v/v dimethyl sulfoxide (DMSO, Sigma-Aldrich) in the foetal calf serum and then transferred to the freezing cryovials (Nunc). Cryovials were transferred to isopropanol-filled freezing chambers (Thermo Fisher Scientific). The isopropanol-filled freezing chambers allow gradual decrease in temperature at 1 degree per minute until -80 degrees Celsius in order to achieve better cell viability when in use in the future. For the long-term storage, the cryovials were further transferred to liquid nitrogen tanks for the long-term storage on the next day.

Cells in the cryovials from the liquid nitrogen storage were thawed in the water baths at 37 degrees Celsius and immediately diluted in 30 mL of supplemented RPMI-1640 or DMEM medium in order to inhibit the activity of DMSO as well as minimise the DMSO effects. Then, cells were spun at 1,300 rcf for 3 minutes and the pellets were resuspended in the fresh supplemented medium. Cells were cultured at 37 degrees Celsius with 5% CO_2 and cell viability was tracked every day.

B. Transfection of cells lines

(a) Electroporation

DNA electroporation was performed using Neon® Transfection system (Thermo Fisher Scientific). 2×10^6 cells were resuspended in 100 μL of the Resuspension Buffer R (Thermo Fisher Scientific) to a final concentration of 2×10^7 cells per mL. 10 μg of constructs (v-ras in pHRsin or in pHRIsin vectors) were added into the cell-containing Resuspension Buffer R. Cells were electroporated in the Neon® pipette tip according to manufacturer's instructions (3 pulses at 1600V pulse voltage with 10ms pulse width)

before being transferred into a 6-well cell culture plate containing 2 mL pre-warmed antibiotics-free supplemented RPMI-1640 medium. Cell viability and cell numbers were monitored after 24 hours.

(b) Lentiviral transfection

Cells were stably transfected with genes of interest in the constructs (pHRsin or pHRIsin) using a human immunodeficiency virus (HIV)-derived system. The HIV genome has been divided into three individual vectors including pMD-G, p8.91 and pHRsin/pHRIsin [285] in this system. pMD-G encodes VSV-G envelope proteins, p8.91 encodes gag, pop, rev and tat proteins for integration, and pHRsin/pHRIsin carries viral cis-elements for infection and genes of interest under control of SFFV promoter. Virus were produced in HEK-293T cells.

i. Normal lentiviral transfection

6×10^5 HEK-293T cells were seeded in a 6-well cell culture with 2 mL supplemented RPMI-1640 24 hours prior to infection. The following day when the cells reached about 80% confluence, a mixture of 150 µL non-supplemented DMEM, 4.5 µL Genejuice transfection reagent (Merck), 0.5 µg pMD-G, 0.5 µg pQ8.91 and 0.5 µg target construct including the gene of interest was incubated for 20 minutes at room temperature and then drop-wise added into the HEK-293T cells. After 48-hour incubation, 2 mL supernatant of HEK-293T cells was harvested by centrifugation at 2,000 rcf for 5 minutes. This 2 mL virus-containing supernatant was further filtered using 0.45 µm filter (Sartorius) and infected 10^6 target cells. 5 ml fresh supplemented RPMI-1640 medium was added on the following day. Cell viability and cell numbers were monitored after 24 hours.

ii. Maxi lentiviral transfection

The very high density of lentivirus was used to enhance the expression levels of pHRsin-encoding proteins, for example, pre-TCR expression levels in Chapter 3.

HEK-293T cells were culture in a T175 flask with 20 mL supplemented DMEM until 80% confluency was achieved (about 24 hours after HEK-293T cells were split at 1:2.5 ratio from the full confluency in a T175 flask). A mixture of 2 mL non-supplemented DMEM, 45 μL Genejuice transfection reagent (Merck), 5 μg pMD-G, 5 μg pQ8.91 and 5 μg target construct including the gene of interest was incubated for 20 minutes at room temperature and then drop-wise added into the HEK-293T cells in each T175 flask. The virus-containing supernatant was collected at 48 hours and 72 hours post-transfection by centrifugation at 2,000 rcf for 5 minutes. 20 mL fresh supplemented DMEM was refilled into T175 flasks after removal of supernatant each time. 40 mL supernatant in total was filtered using 0.45 μm filter (Sartorius) and then layered up very slowly over the 10% sucrose solution in a 50 mL falcon. Virus precipitate was obtained by centrifugation at 15,000 rcf for 3 hours at 4 degrees Celsius. The pellet was resuspended in 100 μL RPMI-1640 and infected 10^6 cells in 2 mL supplemented RPMI-1640. 5 ml fresh supplemented RPMI-1640 medium was added on the following day. Cell viability and cell numbers were monitored after 24 hours.

III. Protein and phenotypic analysis

A. Sodium Dodecyl Sulphate – Polyacrylamide Gel Electrophoresis (SDS-PAGE)

Proteins are allowed to be separated using the polyacrylamide gel electrophoresis (PAGE) in proportional to their electrophoretic mobility, determined by molecular mass, conformation and charge of the proteins. The sodium dodecyl sulphate (SDS), an

amphipathic detergent, binds to proteins non-covalently so that it denatures proteins and confers negative charges to proteins. Thus, electrophoretic mobility of SDS-treated proteins mainly depends on their molecular mass-to-charge ratios. Protein bands on the gel are visualised after application of staining dyes, such as Coomassie Brilliant Blue or Instant Blue® (Expedeon), and the position of the bands are compared to protein markers of known sizes.

A mix of 10 µL protein sample and 10 µL reducing or non-reducing 2x loading buffer was boiled for 5 minutes at 95 degrees Celsius. 15 µL boiled mix was loaded into a well in a 12% SDS-PAGE gel, consisting of a stacking and a seperating gel. Electrophoresis was performed at 150 V with a Tris/glycine/SDS-PAGE running buffer (National diagnostics).

The 2x loading buffer, 12% stacking gel, 12% seperating gel were prepared as follows:

<u>2x loading buffer</u>

0.5 M Tris-HCL (pH 6.8)	1 mL
Glycerol	0.8 mL
10% SDS	1.6 mL
Bromophenol blue	0.2 mL
β-mercaptoethanol (for reducing loading buffer)	0.4 mL

<u>12% stacking gel</u>

MilliQ water	1.55 mL
Stacking buffer (Tris-HCl/pH 6.8/ SDS; ProtoGel)	625 µL
Acrylamide	325 µL

10% ammonium persulphate	12 µL
TEMED	5 µL

12% separating gel

MilliQ water	1.75 mL
Resolving buffer (Tris-HCl/pH 8.8/ SDS; ProtoGel)	1.25 mL
Acrylamide	2 mL
10% ammonium persulphate	25 µL
TEMED	5 µL

B. Fab fragments production from antibodies

(a) Antibody purification

Before papain or ficin digestion of antibodies into Fabs, all antibodies were first purified using size-exclusion chromatography by the Superdex® 200 HR column in the ÄKTA fast protein liquid chromatography (FPLC) system. The whole system including the pumps, sample loops and column was first washed using HBS (150 mM sodium chloride, 10 mM HEPES and 0.05% sodium azide; pH 7.4).

Antibodies were centrifuged at 13,000 rcf for 5 minutes in order to remove aggregated ones. The antibodies injected into the system per round was less than 10 mg and 40 mg/mL (maximum capacity of the Superdex® 200 HR column). The antibodies were in the end eluted with HBS in 500 µL fractions. Each fraction was measured for absorption at 280 nm using spectrophotometry (NanoDrop, Thermo Fisher Scientific) and checked on a SDS page for purity as described above.

(b) Digestion of antibody with papain or ficin for Fab production

Antibodies were digested into Fabs using papain or ficin. Papain, isolated from

papaya latex, is a widely-used cysteine protease in fragmentation of proteins or digestions of antibodies into Fabs [293]. However, efficiency of papain is limited in some species of antibodies/IgG [294-296]. On the other hand, ficin, a sulfhydryl protease isolated from fig latex with a similar active site with papain, showed more efficient than papain in antibody digestion into Fabs [297, 298].

i. Papain digestion

For papain digestion, 500 µL immobilised papain resin slurry (50% glycerol, 100 mM sodium acetate and 0.05% sodium azide; pH 4.4; Thermo Fisher Scientific) was mixed well, equilibrated twice with 4 mL digestion buffer (20 mM sodium phosphate, 10 mM EDTA and 20 mM cysteine-HCl; pH 7) by centrifugation at 3,000 rcf for 5 minutes and resuspended in 500 µL digestion buffer. Purified antibodies were then buffer-exchanged to the sample buffer (20 mM sodium phosphate and 10 mM EDTA; pH 7) using the ÄKTA FPLC system. The fractions containing antibodies were collected and concentrated to 2-20 mg/mL in 500 µL. Same volume of the digestion buffer were added into the antibodies and mixed well. Then, this 1 mL mixture (antibodies/sample buffer/digestion buffer) was added to the vial containing 500 µL immobilised papain in digestion buffer (as above) for 4-hour incubation or overnight-incubation at 37 degrees Celsius in an incubator shaker.

ii. Ficin digestion

3 mL immobilised ficin resin slurry (Thermo Fisher Scientific) was first equilibrated with 20 mL of ficin equilibration buffer (5 mM EDTA and 25 mM cysteine in 100 mM citrate buffer; pH 6) by centrifugation at 1,000 rcf for 1 minute and the ficin equilibration buffer was then removed. The purified antibodies were buffer-exchanged into 100 mM citrate buffer (pH 6) using the ÄKTA FPLC system as described above

and then added with 1/10 volume of ficin digestion buffer (50 mM EDTA and 250 mM cysteine; pH 6). Then, the antibody mixture was added into the immobilised ficin and incubated for 4 hours or overnight at 37 degrees Celsius in an incubator shaker.

(c) Separation of antibodies and Fabs using Protein G columns

The slurry mixture was pelleted at 3,000 rcf for 5 minutes and the supernatant was loaded into a Protein G column (containing Protein G Sepharose® beads). The first flow-through was collected and then re-loaded twice before the final flow-through was collected. The mixture/Protein G column was washed using 10x column volume of cold PBS with 0.5 m sodium chloride at pH 7.4 and the fractions, expectedly containing Fabs, were collected. Then, elution was with 5 mL of 100 mM glycine at pH 2.5. The fractions, expectedly containing undigested antibodies or Fc were collected at 0.5 mL each and neutralised with 2.75 M Tris at pH 8.5. All fractions from flow-through, wash and elution were measured for absorption at 280 nm using spectrophotometry (NanoDrop, Thermo Fisher Scientific) and separated by SDS-PAGE as described above. Fabs were purified using the size-exclusion chromatography by the Superdex® 75 HR column in the ÄKTA FPLC system as described in III.B.(a).

C. Labelling strategy (HaloTag system)

HaloTag Ligand labelling was performed under manufacturer's instructions, except for the concentrations of HaloLigands. Serial concentrations were tested for the best signal-to-noise ratios, *i.e.* 100 nM (manufacturer's recommended concentrations), 50 nM, 25 nM and 12.5 nM. The signal-to-noise ratios were determined based on fluorescence geometric means by FACS as well as confocal images. Labelling for different requirements of HaloTag Ligands is detailed in III.C.(a) and III.C.(b).

As for fixation, after HaloTag Ligand labelling cell were centrifuged and resuspended in the 4% PFA for 10 minutes at room temperature, followed by another spin-down and PBS-Triton (0.1% Triton X-100) incubation for 10 minutes at room temperature. In the end, the cells were centrifuged and resuspended in 500 μL or 200 μL PBS for FACS analysis or for microscope slide mounting, respectively.

(a) Oregon Green and TMR labelling

10^6 cells stably expressing the HaloTag-fusion proteins of interest were incubated with 1 mL phenol red-free RPMI-1640 medium containing the HaloLigand (Oregon Green, TMR or both) at one of serial concentrations (100, 50, 25 or 12.5 nM) for 15 or 30 minutes at 37 degrees Celsius with 5% CO_2. HaloLigand-containing medium was washed out twice with PBS by centrifuge at 1,300 rcf for 3 minutes. Then, cells were incubated with the phenol red-free RPMI-1640 medium at 37 degrees Celsius with 5% CO_2 for 30 minutes. Fixation and image preparation steps were followed as described in IV.B. and IV.C.

(b) R110Direct and TMRDirect Labelling

10^6 cells stably expressing the HaloTag-fusion proteins of interest were incubated with 1 mL phenol red-free RPMI-1640 medium containing the HaloLigand (Oregon Green, R110Direct, TMRDirect or both) at one of serial concentrations (100, 50, 25 or 12.5 nM) overnight at 37 degrees Celsius with 5% CO_2. HaloLigand-containing medium was washed out with PBS twice by centrifuge at 1,300 rcf for 3 minutes. Fixation and image preparation steps were followed as described in IV.B. and IV.C.

D. Labelling of antibodies and Fabs with fluorescent dyes

Antibodies and Fabs were labelled with the fluorescent dyes Alexa Fluor® 488, Alexa

Fluor® 647 and Atto 655 according to manufacturer's instructions. After labelling, the antibodies or Fabs were measured using spectrophotometry (NanoDrop, Thermo Fisher Scientific) for protein concentration and for labelling efficiency.

Protein concentration (M) was determined by: $[A_{280}–(A_{dye}*CF_{dye})]/ \varepsilon_{(protein)}$, where CF_{dye} is the correction factor for absorption readings at 280 nm, *i.e.* $CF_{(Alexa\ Fluor®\ 488)}$=0.11, $CF_{(Alexa\ Fluor®\ 647)}$= 0.03, $CF_{(Atto\ 655)}$=0.08, and the $\varepsilon_{(antibody)}$ = 203,000 and $\varepsilon_{(Fab)}$ = 70,000 [299].

Degrees of labelling (moles of dye per mole of protein) was determined by: $A_{dye}/[\varepsilon_{(dye)}*$protein concentration (M)], in which $\varepsilon_{(dye)}$ is the molar extinction coefficient of the dye. For example, $\varepsilon_{(Alexa\ Fluor®\ 488)}$ is 71,000 $cm^{-1}M^{-1}$, $\varepsilon_{(Alexa\ Fluor®\ 647)}$ is 239,000 $cm^{-1}M^{-1}$ and $\varepsilon_{(Atto\ 655)}$ is 125,000 $cm^{-1}M^{-1}$ [299]. All degrees of labelling in this thesis were achieved at 3 to 4 moles of dye per mole of protein.

(a) Alexa Fluor® labelling

Antibodies or Fabs were labelled with Alexa Fluor® 488 or with Alexa Fluor® 647 using Molecular Probes® Antibody Labeling Kits (Thermo Fisher scientific) according to manufacturer's instructions. The labelling was based on formation of a stable covalent bond between an amine-reactive N-hydroxysuccinimide ester (Alexa Fluor®) and a primary amine such as the lysine side chain of antibodies or Fabs.

100 µL antibodies or Fabs at 1 mg/mL was first mixed with 10 µL 1 M sodium bicarbonate (Sigma-Aldrich). The mixture was then added to the vial containing the Alexa Fluor® dye and incubated in the dark for 1 to 1.5 hours at room temperature. In order to separate free unbound dyes from labelled ones, purification columns bedded with 1.5 mL of resin were used. For example, 1.5 mL resin was applied into a purification column by centrifugation at 1,100 rcf for 3 minutes. The mixture was added to a resin-bedded column and centrifuged at 1,100 rcf for 5 minutes. The free

and labelled dyes were separated using the columns (provided in the kit); the free dyes were captured in columns and the labelled antibodies or Fabs were collected from the flow-through.

(b) Atto 655 labelling

Antibodies or Fabs were labelled with Atto 655 using the Atto 655 Protein Labeling Kit (Sigma-Aldrich) according to manufacturer's instructions. A vial of 0.25 mg Atto 655 dye was dissolved in 10 µL DMSO or in PBS and then immediately added with 100 µL antibodies or Fabs at 1 mg/mL in sodium bicarbonate solution (provided in the kit; pH 9.5; Sigma-Aldrich). The mixture was incubated in the dark for 2 hours, with few times of gentle stirring applied in between, at room temperature. The free and labelled dyes were separated and the degrees of labelling were determined as described in III.D.

E. Fluorescence-activated cell sorting (FACS)

The expression levels of proteins of interest in cells were measured by quantifying fluorescence intensities, either from fluorochromes in fusion with proteins of interest or from fluorophore-labelled antibodies/Fabs bound to proteins of interest using FACS. The latter was used to determine the expression levels of membrane proteins of interest on the cell surface in this thesis.

10^6 cells from tissue culture were first centrifuged at 1,300 rcf for 3 minutes and the cell pellet was resuspended in 3 mL FACS wash buffer (PBS with 0.05% sodium azide) in polypropylene or polystyrene tubes (depending on FACS machine models). Appropriate staining was applied if required. For general FACS analyses, the controls contained the non-staining control (cells only), the negative staining control (cells that did not express proteins of interest), the isotype control (cells that were stained with

another antibody with the same isotype as the first antibody but did not recognise proteins of interest) or the non-specific binding control (cells stained with the fluorophore-labelled secondary antibody only). For multiple-colour FACS analyses or multiple-colour FACS sorting, the single-colour staining control, the fluorescence-minus-one control and fluorescence compensation were applied.

(a) Membrane proteins of interest

For fluorochromes in fusion with membrane proteins of interest, cells were directly analysed by FACS after fixation. For fluorophore-labelled antibodies/Fabs bound to membrane proteins of interest, cells were incubated with the fluorophore-labelled antibodies/Fabs at 10 ng/mL on ice for an hour. In addition, if fluorophores were labelled on the secondary antibodies, cells were then first incubated with the first antibodies on ice for an hour and sequentially incubated with the secondary antibodies on ice for another hour. The unbound or unspecific antibodies were washed out with 3 mL FACS wash buffer and centrifuged at 1,300 rcf for 3 minutes at 4 degrees Celsius after the first and the second incubations.

(b) Intracellular proteins of interest

In order to measure the expression levels of intracellular proteins of interest in the cell, for example, the remaining levels of Lck or Zap70 after gene knock-down or gene knock-out, cells were first fixed and permeabilised in order for the fluorophore-labelled antibodies to pass through the cell membrane.

Cells were first washed in the FACS buffer (FACS wash buffer with 5% foetal calf serum and 1% bovine serum albumin) at 1,300 rcf for 3 minutes at 4 degrees Celsius before being incubated with 1% formaldehyde/PBS for fixation for 15 minutes at room temperature. Then, the permeabilisation was performed at every wash step

using ICS buffer (FACS buffer with 0.5% saponin). Cells were stained with the first and the second antibodies for 1 hour respectively at 4 degrees Celsius. The unbound or unspecific antibodies were washed out with 3 mL ICS buffer and centrifuged at 1,300 rcf for 3 minutes at 4 degrees Celsius after the first and the second incubations.

(c) Fixation and FACS analysis

All cells were centrifuged at 1,300 rcf for 3 minutes at 4 degrees Celsius and resuspended with 2% PFA/FACS wash buffer for fixation. FACS was performed using a CyAn Advanced Digital Processing High-Performance Flow Cytometer (DakoCytomation), LSR Fortessa (BD Biosciences) or Attune NxT Flow Cytometer (Thermo Fisher scientific). FACS data analysis was performed using FlowJo software (FlowJo LLC).

IV. Imaging

A. Microscopy set-up

For the super-resolution imaging set-up, two laser beams including 561 nm (Cobolt, Jive 500) and 405 nm (Cobolt, MLD 405) were first aligned. Each excitation beam was first finely tuned and polarised by optical density filterwheels and quarter-wave plates, respectively. The size of each beam was adjusted by Galilean beam expanders and each beam can be promptly switched on and off via a quick automated shutter. Beams were then aligned by mirrors and irises and combined by dichroic mirrors. Fluorescence signal from samples was collected by the Olympus 1.49 NA 60x oil objective and then projected on an EMCCD camera (Photometrics, Evolve Delta).

For single-molecule cross-colour coincidence detection (SMCCCD), single-molecule resolution was reached using total internal reflection fluorescence

(TIRF) microscopy by limiting the evanescence surface to about 100 nm. Overlapped Kr/Ar laser beam at 488 and 568 nm (353-LDL-840-240, Melles Griot) excited the surface through an objective (60x Plan Apo TIRF, NA 1.45, Nikon) in Nikon TE2000-U microscope. Returning emission beam was collected and split by Dual-View (Optical Insights) filters and these split colours were recorded by EMCCD (Cascade II: 512 Princeton instruments).

B. Slide surface preparation

Coverslips (20 mm^2) were first cleaned using argon plasma for 15 minutes. Slides were either treated with antibodies (*i.e.* IgG or Gap8.3) overnight at 37 degrees Celsius, or with 2 % melted agarose gel pad (Sigma-Aldrich) at room temperature.

C. Cell fixation and fluorescence labelling

For HaloTag Ligand (TMR) labelling for dSTORM imaging, cells were first fixed with 4% PFA for 30 minutes at 37 degrees Celsius and labelled with HaloTag Ligands (TMR) at room temperature in the dark for 30 minutes. After being washed three times, cells were mounted on agarose-coated microscopic slides for super-resolution imaging.

In the course of imaging experiments, several experiments for optimisation were performed, for example, for the best fixation effect and largest contact area between cells and slides for PALM imaging. Cells were fixed in PBS with either 0.2% (v/v) with 4% (v/v) paraformaldehyde or 0.4% (v/v) glutaraldehyde with 4% (v/v) paraformaldehyde for 1 hour at 37 degrees Celsius. Then, the fixed cells were washed and either settled by gravity or spun by the Cytospin Centrifuge onto slide surfaces, which had been previously coated with non-activating Gap8.3 (anti-hCD45) antibody overnight, or agarose gel pad.

For the experiments using super-resolution imaging techniques in Chapter 4 and

single-molecule cross colour coincidence detection (SMCCCD) in Chapter 5, cells, if not tagged with fluorescence-fusion proteins, were first labelled with Fabs for 30 minutes at 4 degrees Celsius and then fixed with 4% (v/v) paraformaldehyde and 0.2% (v/v) glutaraldehyde for 1 hour at room temperature before being imaged on slides with agarose gel pads.

V. Signalling analysis

A. IL-2 production

B. The bioluminescence of IL-2 production using the enzyme-linked immunosorbent assay (ELISA)

The mouse T-cell lines (DO11.10), or other derivative cell lines with stable expression of exogenous rat CD28 or with certain gene knock-out, were triggered for ligand-independent signalling using the anti-rat CD28 superagonist JJ316 antibodies (BD Biosciences) at serial concentrations. The anti-Thy1 OX7 antibody (Human Immunology Unit, Oxford) and the anti-mouse CD3 KT3 antibody (Bio-Rad AbD Serotec) were used as an isotype control and a positive control, respectively, at one or serial concentrations. The level of ligand-independent signalling was determined by IL-2 production from cells measured using ELISA with technical triplicates for each cell line and antibody condition.

(a) IL-2 production

Costar® flat-bottomed 96-well EIA-RIA plates were first coated with filtered coating buffer (50 mM sodium carbonate buffer with 0.02% sodium azide at pH 9.6) containing the donkey-anti-mouse antibody (Stratech Scientific) at 500 μg/mL

overnight at 4 degrees Celsius. As for the positive control, plates were coated with the same coating buffer containing the donkey-anti-mouse antibody at 500 μg/mL as well as KT3 at concentrations of 0.08, 0.4, 2, 10 and 50 μg/mL overnight at 4 degrees Celsius. All wells were washed three times with 200 μL sterile PBS on the following day.

5×10^5 cells for each well were centrifuged at 1,300 rcf for 5 minutes and then resuspended in 100 μL RPMI-1640 medium containing the JJ316 antibody at one of serial concentrations (*i.e.* at 0.08, 0.4, 2, 10 and 50 μg/mL) for 20 minutes at room temperature, which allowed the antibody to bind to the cells. As for the positive control, the same amount of cells were centrifuged and resuspended in the RPMI-1640 medium only. Then, this cell/JJ316 or cell/medium mixtures were added into each well and incubated for 48 hours at 37 degrees Celsius with 5% CO_2.

(b) IL-2 ELISA

ELISA is a solid phase- (plate-) based enzyme immune assay for quantification of the amount of proteins of interest, for example IL-2. Proteins of interests are sandwiched between the pre-immobilised capture antibodies, which are able to specifically bind to proteins of interest, and the detection antibodies, which are subsequently added and able to specifically bind to proteins of interest. The detection antibodies are either directly conjugated with enzymes or attached with a moiety which can be further recognised by other enzyme-conjugated secondary antibodies. In the end, the amount of proteins of interest is determined by an ELISA microplate spectrophotometer. For example, the detection antibody for the IL-2 protein used in this thesis was attached with a biotin and the HRP (horseradish peroxidase)-conjugated avidin was used to measure the amount of IL-2 by a linear amplification of the signal after the enzyme-substrate reaction, *i.e.* HRP and its chromogenic substrate, TMB

(Tetramethylbenzidine).

The cell supernatant from V.B.(a) was analysed for the level of IL-2 production using the mouse IL-2 ELISA Ready-SET-Go!® kit (eBioscience; Thermo Fisher Scientific) according to manufacturer's instructions. The wells in the EIA plastic plates were pre-coated with the IL-2 capture antibody in coating buffer overnight at 4 degrees Celsius. On the following day, wells were washed 5 times with 200 μL PBS-Tween (0.05%) and incubated in blocking buffer (1x assay diluent) for an hour. After another 5 times of wash with 200 μL PBS-Tween (0.05%), the supernatant from V.B.(a) was transferred to the wells as well as a serial dilution of mouse IL-2 standards (800, 400, 200, 100, 50, 24, 12.5 and 0 pg/mL) and all were incubated overnight at 4 degrees Celsius. Followed by 5 times of wash, 100 μL of the detection antibody attached with a biotin was incubated for an hour at room temperature on the following day. After another 5 times of wash in between, 100 μL avidin-HRP was incubated for 30 minutes at room temperature and 100 μL TMB-substrate was applied and incubated until colour developed. The HRP-TMB reaction was terminated using 50 μL sulphuric acid. The colourimetric reaction results were read at the absorbance of 450 nm using an ELISA microplate spectrophotometer, thus allowing the amount of IL-2 in the wells to be quantitatively determined.

Chapter 3

Mutational analysis of human pre-TCR assembly

I. Introduction

Since the TCR and its developmental precursor, the pre-TCR, share similar structures and signalling components, it seems reasonable to assume that both the TCR and pre-TCR share similar stoichiometries and signalling mechanisms. This expectation is challenged, however, by a study in which the pre-TCR was found to form an autonomous head-to-tail dimer, using interfaces formed between the pre-Tα subunit and both the TCRβ constant and variable domains, based on X-ray crystallographic analysis and small-angle X-ray scattering. Although the authors of this study went to considerable effort to independently confirm their findings using mutagenesis, they relied heavily on just three mutant proteins [233]. Because of the unexpected nature of their findings, it seemed worthwhile to subject the pre-TCR to a more systematic mutational analysis, as reported in this thesis, in order to test the dimerisation hypothesis.

Previously, this laboratory used a “drastic” mutagenesis approach to identify the ligand binding sites of the receptors CD2 and CD48. More relevantly, the method was also used to investigate the interfaces that are required to form in order for receptor assembly, and to further our understanding of receptor stoichiometry at the cell surface [252, 300, 301]. The investigation of receptor stoichiometry on T cells using the mutagenesis-based approach as employed in these previous studies is indispensably

based on the idea that only successfully-assembled, well-folded intact complexes are likely to reach the cell surface [78, 79]. For example, in the study of mature TCR assembly, drastic mutations of subunit interface residues in the TCR/CD3 complex were used to investigate whether the complex formed dimers, or whether there were any changes in the organisation of the TCR/CD3 complex after the receptor was triggered with an antibody.

This was done by monitoring the effects of mutations of surface residues on TCR/CD3 complex expression at the cell surface, and subsequently on antibody-mediated receptor triggering. The principle used was: if there was a new subunit interface that needed to form for assembly and dimerisation or during conformational changes in the receptor after ligand binding, then drastic mutations of residues that were initially exposed on the surface of the complex but later become buried in the newly-formed dimer or the conformationally-altered receptor, would prevent assembly (*i.e.* dimerisation) and antibody-induced signalling, respectively. It was found that there was no evidence of extra interfaces being needed for complex assembly, or for newly-formed interfaces when the TCR was triggered with antibodies, as would have been expected if conformational changes in the TCR/CD3 complex were involved as part of the receptor triggering mechanism [252]. The method relies heavily on the existence of a crystal or nuclear magnetic resonance-based structure, so that surface residues can be easily identified for mutation, and in-pointing residues likely to be important for folding can be avoided.

The pre-TCR crystal structure suggested that there was one contiguous interface between the extracellular domain of the pre-Tα subunit and TCRβ. In this chapter we used the mutagenesis approach to probe pre-TCR stoichiometry and indeed to determine if there were other contiguous interfaces required for dimerisation or higher-order organisation. As described below, residues of the pre-Tα subunit in the

pre-TCR complex were first thoroughly analysed *in silico* using the Naccess programme to identify surface-exposed residues, and a set of seventy-four residues including residues for folding and assembly controls was selected for drastic mutation. Successful surface expression was then tested for using FACS, revealing the effects of individual mutant pre-Tα residues on pre-TCR complex assembly. The analysis showed that there was only one contiguous interface formed between the pre-Tα subunit and TCRβ, and this involved the Cβ, rather than the Vβ domain of the pre-TCR.

II. Results

A. Naccess

Naccess (Naccess version 2.1.1; S.J. Hubbard; 1996, an implementation of Lee and Richard's method [302]) is a programme that calculates the atomic and residue accessibilities for both proteins and nucleic acids using coordinates deposited at the Protein Data Bank (http://www.rcsb.org). Naccess rolls a probe with a pre-set value for radius on the van der Waal surface, taking successive thin slices in the z-axis through the 3D molecular volume, in this way identifying the atomic surface area. If a 1.4 Å probe (the radius of water) is used as the radius of the probe, then the defined surface comprises the solvent accessible surface, or solvent-exposed surface. Only those atoms with more than 5 $Å^2$ of solvent-exposed area are considered to be solvent-exposed. Amino acid residues consisting of more than half solvent-exposed atoms are considered to be solvent-exposed residues.

B. Naccess calculation

The pre-TCR crystal structure was first obtained from the protein data bank (PDB ID:

3OF6). Naccess calculations were run using a 'probe' of 1.4 Å, on each side-chain atom of pre-Tα either alone, in the pre-TCR monomer complex, or in the pre-TCR dimer complex, in order to identify solvent-exposed pre-Tα residues forming interfaces in the pre-TCR monomer and dimer complexes. Naccess identifies a side-chain atom as solvent-exposed if >5 $Å^2$ of the surface area of the atom is exposed to the probe. The fractional changes in the number of side-chain atoms buried when pre-Tα forms monomer and dimer pre-TCR complexes are shown in Figure 3.1

Based on these results, pre-Tα residues meeting any one of the following criteria were considered for mutagenesis (Table 3.1).

(i) Solvent-exposed residues with >50% solvent-exposed atoms both in pre-Tα in isolation and in the pre-TCR monomer (Table 3.1; (i)).

(ii) 'Contact' residues, which had >50% solvent-exposed atoms in the pre-Tα in isolation but had lower fractions of solvent-exposed atoms in the pre-TCR monomer complex (Figure 3.1; cyan bars), and additional 'contact' residues (L13, A14, V28 and T66) previously proposed in [233]. These 'contact' residues were further confirmed by visual inspection of the crystal structures. Pre-Tα residues falling in this category were considered to be in association with the constant region of TCRβ (Table 3.1; (ii)).

(iii) 'Dimerising' pre-Tα residues, which had >40% solvent-exposed atoms in the pre-TCR monomer complex but had a smaller fraction of solvent-exposed atoms in the pre-TCR dimer (Figure 3.1; purple bars), and additional 'dimerising' residues (S53, A54, P64, R102 and S103) previously proposed [233] as dimerisation sites involving the interaction of pre-Tα with the variable region of TCRβ or between the two pre-Tαs, according to the crystal structure (Table 3.1; (iii)). The two sets of 'contact' and 'dimerising' residues are different because a smaller surface probe volume was used by Pang *et al.* [233].

(iv) Glycine residues, which had α carbons pointing outwards without further

Figure 3.1: Fractional differences in numbers of solvent-exposed side-chain atoms of pre-Tα residues in monomeric and dimeric pre-TCR complexes. 1.4 Å was used as the Naccess probe radius and 5 $Å^2$ was used as the threshold for identifying solvent-exposed atoms. Only residues with at least one solvent-exposed atom are shown. Cyan, fractional differences in numbers of solvent-exposed side-chain atoms following pre-Tα association with TCRβ in the pre-TCR monomer complex; purple, fractional differences in numbers of pre-Tα solvent-exposed side-chain atoms following assembly of the pre-TCR dimer complex from the monomer complex. Residues are numbered in order from N- to C-terminus as in the pre-Tα crystal structure (PDB ID:3OF6). Naccess analyses were done in collaboration with Dr. Yuan Lui.

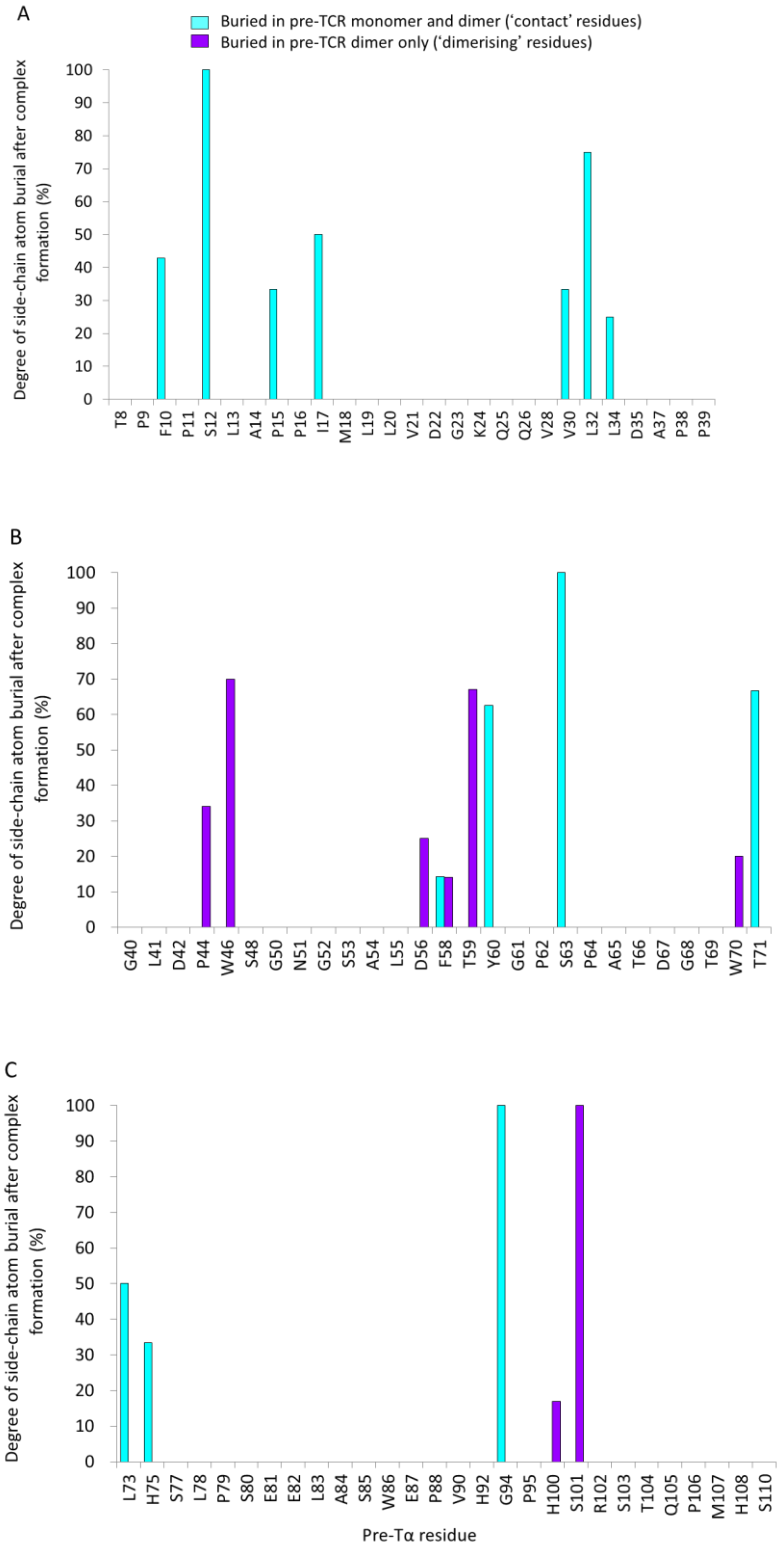
A
Buried in pre-TCR monomer and dimer ('contact' residues)
Buried in pre-TCR dimer only ('dimerising' residues)
Degree of side-chain atom burial after complex formation (%)
T8 P9 F10 P11 S12 L13 A14 P15 P16 I17 M18 L19 L20 V21 D22 G23 K24 Q25 Q26 V28 V30 L32 L34 D35 A37 P38 P39
B
Degree of side-chain atom burial after complex formation (%)
G40 L41 D42 P44 W46 S48 G50 N51 G52 S53 A54 L55 D56 F58 T59 Y60 G61 P62 S63 P64 A65 T66 D67 G68 T69 W70 T71
C
Degree of side-chain atom burial after complex formation (%)
L73 H75 S77 L78 P79 S80 E81 E82 L83 A84 S85 W86 E87 P88 V90 H92 G94 P95 H100 S101 R102 S103 T104 Q105 P106 M107 H108 S110
Pre-Tα residue

Table 3.1: Pre-Tα residues analysed and mutated, based on the calculations from Naccess, the previous study [233] and the preTα structure from the Protein Data Bank. Mutating nucleotides are capitalised as shown in the forward primers.

	(i) Solvent-exposed ?	(ii) 'Contact' ?	(iii) 'Dimerising' ?	Forward primer for cloning
T8R	Yes[1]			ggtgtgggcggcaGacccttccttct
P9R	Yes[1]			gtgggcggcacacGctttccttctctg
F10R		Yes[1,2]		ggcggcacacccAGAccttctctggcc
S12R		Yes[1,2]		acacccttcctAGActggccccacca
L13R		Yes[2]		ccctttccttctcGggccccaccaatc
A14R		Yes[2]		tttccttctctgCGcccaccaatcatg
P15R		Yes[1,2]		ccttctctggcccGGccaatcatgctg
P16R	Yes[1]			tctctggccccacGGatcatgctgctg
I17R		Yes[1,2]		ctggccccaccaaGGatgctgctggtg
M18R	Yes[1]			gccccaccaatcaGgctgctggtggat
L19R	Yes[1]			ccaccaatcatgcGgctggtggatgga
L20R	Yes[1]			ccaatcatgctgcGggtggatggaaag
V21R	Yes[1]			atcatgctgctgCGggatggaaagcag
D22R	Yes[1]			atgctgctggtgCGGggaaagcagcag
G23R	Yes[1]			ctgctggtggatAgaaagcagcagatg
K24E	Yes[1]			ctggtggatggaGagcagcagatggtg
Q25R	Yes[1]			gtggatggaaagcGgcagatggtggtg
V28R		Yes[2]		aagcagcagatgCGggtggtctgcctg
V30R		Yes[1,2]		cagatggtggtgGGctgcctggtcctt
L32R		Yes[1,2]		gtggtggtctgccGggtccttgatgtt
L34R		Yes[1,2]		gtctgcctggtccGGgatgttgcaccc
D35R	Yes[1]			tgcctggtccttCGGgttgcaccccct
A37R	Yes[1]			gtccttgatgttAGacccccctggcctt
P38R	Yes[1]			cttgatgttgcacGccctggccttgac
P39R	Yes[1]			gatgttgcaccccGGggccttgacagc
G40R	Yes[1]			gttgcacccccctCgccttgacagcccc
L41R	Yes[1]			gcacccccctggccGGgacagccccatc
D42R	Yes[1]			ccccctggccttCGcagccccatctgg
P44R	Yes[1]		Yes[1,2]	ggccttgacagccGcatctggttctca
W46R	Yes[1]		Yes[1,2]	gacagccccatcCggttctcagccggc
S48R	Yes[1]			cccatctggttcAGagccggcaatggc
G50R	Yes[1]			tggttctcagccCgcaatggcagtgca
N51R	Yes[1]			ttctcagccggcaGGggcagtgcactg
G52R	Yes[1]			tcagccggcaatCgcagtgcactggat
S53R	Yes[1]		Yes[2]	gccggcaatggcagAgcactggatgcc
A54R	Yes[1]		Yes[2]	ggcaatggcagtAGactggatgccttc
D56R	Yes[1]		Yes[1,2]	ggcagtgcactgCGGgccttcacctat

F58R		Yes[1,2]	Yes[1,2]	gcactggatgccAGGacctatggccct
T59R	Yes[1]		Yes[1,2]	ctggatgccttcaGGtatggcccttcc
Y60R		Yes[1,2]		gatgccttcaccAGAggcccttcccca
G61R	Yes[1]			gccttcacctatCgcccttccccagca
S63R		Yes[1,2]		acctatggccctCGcccagcaacggat
P64R	Yes[1]		Yes[2]	tatggcccttcccGGgcaacggatggc
A65R	Yes[1]			ggcccttccccaAGaacggatggcacc
T66R		Yes[2]		ccttccccagcaaGggatggcacctgg
D67R	Yes[1]			tccccagcaacgCGGggcacctggacc
G68R	Yes[1]			ccagcaacggatCgcacctggaccaac
W70R			Yes[1,2]	acggatggcaccCggaccaacttggcc
T71R		Yes[1]		gatggcacctggaGGaacttggcccat
L73R		Yes[1,2]		acctggaccaacAGggcccatctctcc
H75E		Yes[1,2]		accaacttggccGaActctccctgcct
S77R	Yes[1]			ttggcccatctcCGcctgccttctgag
P79R	Yes[1]			catctctccctgcGCtctgaggagctg
S80R	Yes[1]			ctctccctgcctAGAgaggagctggca
E81R	Yes[1]			ctgccttctAGggagctggcatcc
E82R	Yes[1]			ccttctgagAGgctggcatcctgg
L83R	Yes[1]			ccttctgaggagcGggcatcctgggag
A84R	Yes[1]			tctgaggagctgAGatcctgggagcct
S85R	Yes[1]			gaggagctggcaCGctgggagcctttg
P88R	Yes[1]			gcatcctgggagcGGttggtctgccac
V90R	Yes[1]			tgggagcctttgCGctgccacactggg
G94R	Yes[1]	Yes[1]		gtctgccacactCggcctggggctgag
P95R	Yes[1]			tgccacactgggcGcggggctgagggt
H100E	Yes[1]		Yes[1,2]	ggggctgagggtGaGagcaggagtaca
S101R	Yes[1]		Yes[1,2]	gctgagggtcacagAaggagtacacag
R102E	Yes[1]		Yes[2]	gagggtcacagcGAgagtacacagccc
S103R	Yes[1]		Yes[2]	ggtcacagcaggagAacacagcccatg
T104R	Yes[1]			cacagcaggagtaGacagcccatgcat
Q105R	Yes[1]			agcaggagtacacGgcccatgcatctg
P106R	Yes[1]			aggagtacacagcGcatgcatctgtca
M107R	Yes[1]			agtacacagcccaGgcatctgtcagga
H108E	Yes[1]			acacagcccatgGaActgtcaggagag
S110R	Yes[1]			cccatgcatctgAGaggagaggcttct

[1] predicted by Naccess, [2] predicted as interface residue in [233]

interactions with other atoms by visual inspection of the crystal structures of both of the pre-Tα and pre-TCR.

(v) The cysteine residue involved in the disulfide bond responsible for pre-Tα domain folding based on the structural information from UniProt (UniProt ID: Q6ISU1). Mutation of this cysteine (C31R) functioned as an internal folding control for pre-TCR complex assembly [233] as it was expected to prevent pre-TCR complex assembly and expression at the cell surface.

C. Expression of the pre-TCR

(a) Drastic mutation

For drastic mutagenesis, each of the chosen residues except basic residues were mutated to arginine, and the basic residues were mutated to glutamic acid. The drastic mutation principle is based on the fact that the introduction of bulky, charged side chains in place of smaller uncharged side chains, or of side chains that had the opposite charge is likely to be highly disruptive of binding or of the formation of subunit interfaces. The highest-frequency codons used in humans for encoding arginine and glutamic acid were also used. The drastic mutations of the pre-Tα subunit of the pre-TCR are listed in Table 3.1.

(b) Expression strategy

After identification of solvent-exposed pre-Tα residues, 'contact' residues (mediating pre-Tα association with the constant region of TCRβ), 'dimerising' residues (mediating pre-Tα association with the variable region of TCRβ or between the pre-Tα subunits) and pre-Tα structure/folding controls, a set of seventy-four mutant forms of pre-Tα cDNA were made and transduced into the E6.1-57 cell line, along with TCRβ. The E6.1-57 cell line, a kind gift of Dr Takamasa Ueno, Kumamoto University, does not

express αβ TCRs. To detect expression of pre-Tα, a haemagglutinin (HA) tag-encoding sequence was introduced immediately downstream of the sequence encoding the signal peptide. To allow confirmation of comparable levels of lentiviral transduction for the wild-type and mutant proteins, sequence encoding Emerald-Green Fluorescent Protein (GFP) was introduced downstream of an internal ribosome entry site (IRES) sequence, in addition to the wild-type or mutant pre-Tα coding sequences (Figure 3.2).

(c) Low expression of pre-Tα at the cell surface

Surface expression levels of pre-TCR/CD3 complexes were measured by FACS using anti-HA antibody for HA-tagged pre-Tα or anti-CD3ε UCHT1 antibody for CD3ε. Pre-TCRs with either a wild-type pre-Tα or one of five different mutant forms of pre-Tα were firstly expressed in E6.1-57 cells with TCRβ in a pilot experiment. These five mutant forms comprised mutations of two solvent-exposed residues (A37R and D42R), two 'contact' residues (L32R and L34R) and mutation of a residue (P64R) proposed to mediate reciprocal van der Waal's contact between the two pre-Tα subunits of the proposed pre-TCR dimer [1] (although this residue was in fact predicted to be solvent-exposed in both the pre-TCR monomer and pre-TCR dimer by Naccess).

FACS analysis revealed that the fluorescence signals for anti-HA staining (*i.e.* of HA-tagged pre-Tα) were only just above background, presumably due to low surface expression levels of the pre-TCR/CD3 complex at the cell surface (Figure 3.3). Staining with the anti-CD3ε UCHT1 antibody to monitor surface expression gave higher levels of fluorescence (Figure 3.4), but the results were, however, somewhat inconsistent (as discussed below and in II.C.(d).i).

As shown in Figure 3.4, the mutations of the surface-exposed residues (A37R and D42R) had little effect on the expression levels versus the wild-type pre-Tα protein, as expected. However, the mutations of the pre-Tα residues contacting the constant

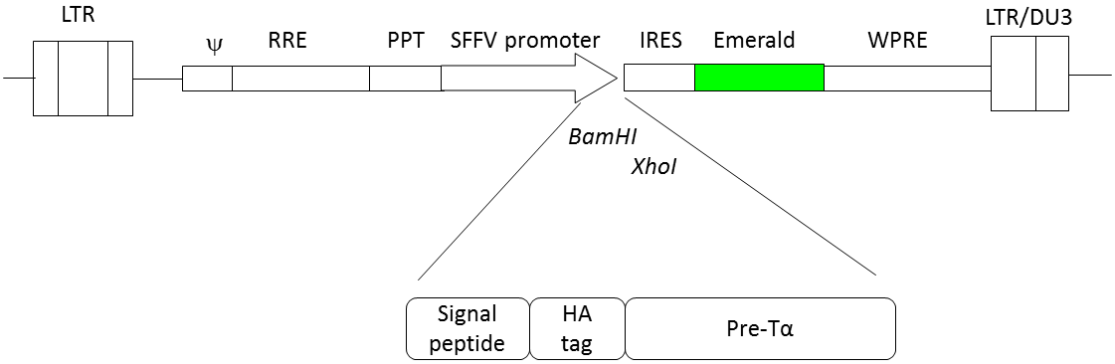

Figure 3.2: Schematic view of pre-Tα construct design. Wild-type and mutant forms of pre-Tα-encoding sequence lacking its original signal peptide sequence were inserted downstream of both a new signal peptide-encoding sequence and the haemagglutinin (HA) tag-encoding sequence in the pHRsin vector. The internal ribosome entry site sequence driving expression of Emerald-GFP is also shown.

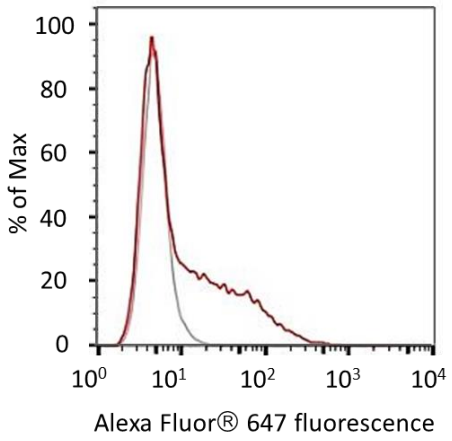

Figure 3.3: Surface expression level of pre-TCR/CD3 on E6.1-57 cells transduced with wild-type HA-pre-Tα and TCRβ. Expression was measured using anti-HA antibody staining and FACS analysis. Red, cells stained with the mouse anti-HA antibody and the secondary antibody (anti-mouse IgG conjugated with Alexa Fluor® 647); grey, cells stained with the secondary antibody only.

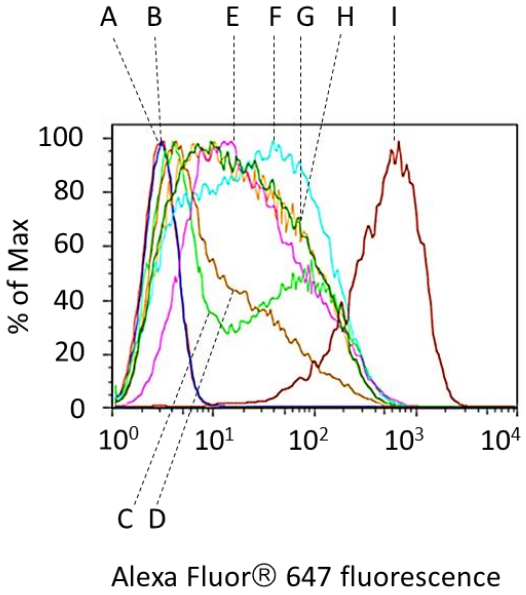

Figure 3.4: The expression levels of pre-TCR/CD3 comprising different forms of pre-Tα and experimental controls measured using FACS. Expression levels were measured in the APC channel using the primary antibody UCHT1 (anti-CD3ε antibody) and a secondary antibody (anti-mouse IgG conjugated with Alexa Fluor® 647). The curves correspond to the following E6.1-57 cell transductants: (A, red) TCRβ unstained. (B, blue) TCRβ stained with the second antibody only. (C, bright green) L32R pre-Tα and TCRβ stained with UCHT1 and the secondary antibody. (D, brown) P64R pre-Tα and TCRβ. (E, magenta) D42R and TCRβ. (F, cyan) A37R pre-Tα and TCRβ. (G, orange) L34R pre-Tα and TCRβ. (H, green) wild-type pre-Tα and TCRβ. (I, maroon) Wild-type Jurkat T-cells were stained with the primary and secondary antibodies.

regions of TCRβ (L32R and L34R), were discordant in this first trial: the L34R mutant was highly expressed, whereas expression of the L32R mutant was severely reduced.

This implied that pre-Tα did not contact TCRβ in the way proposed in the crystal structure, or that there were some issues with the assay. Finally, the expression levels of the pre-Tα subunit mutated at residue P64, which had been claimed to form part of the dimerisation interface with another pre-Tα subunit in the 'head-to-tail' dimer, significantly decreased. The significance of this was unclear, however, as a mutation of a proline residue, which are often involved in determining secondary structure, might have affected the folding of the pre-Tα domain [303].

However, above all, the main issue with this experiment lay in the very low expression levels of HA-tagged pre-Tα on the cell surface giving very low fluorescence signals in FACS. As a result, comparing subtle differences in low expression levels among the wild-type and the mutant forms was very difficult. The low expression levels of pre-TCR/CD3 on the cell surface might be due to inefficient pre-Tα transduction or high endoplasmic reticulum retention of the pre-TCR in the enoplasmic reticulum as noted elsewhere [304]. Therefore, optimisation of the assay was undertaken.

(d) Optimisation of the assay

To increase the surface expression of wild-type or mutant forms of pre-TCR/CD3 complexes, the following approaches were used: multiple lentiviral infections of pre-Tα and TCRβ, alterations to the pre-Tα cytoplasmic domain, and 'maxi-lentiviral' infections (high titres of lentiviral infections) of pre-Tα and TCRβ followed by comparisons of individual internal negative controls. It was finally found that the expression levels of the wild-type or mutant forms of pre-TCR complexes could be boosted by 'maxi-lentiviral' infections of pre-Tα and TCRβ and, together with the comparisons of the internal negative controls, the effects of mutated residues could be

reliably determined.

i. Multiple lentiviral infections

An attempt was made to enhance the expression of the pre-TCR/CD3 complex at the cell surface using multiple (i.e. serial) lentiviral infections of E6.1-57 cells. Alongside the wild-type pre-Tα the L32R mutant pre-Tα was tested because the mutation gave rise to two sub-populations of cells with different surface expression levels in the initial experiment (Figure 3.4C, bright green plot). The levels of expression of the pre-TCR/CD3 complex from different transduction repeat-series were then measured and compared based on the geometric means of anti-CD3ε UCHT1 antibody staining using FACS normalised versus positive control cells (*i.e.* Jurkat cells) after subtraction of background staining levels. As shown in Figure 3.5, there were no signs of consistent increases in expression levels following multiple infections with lentiviruses expressing pre-Tα or TCRβ. In addition, curiously, expression of the L32R mutant was completely lost following re-transduction.

ii. Alterations in the pre-Tα cytoplasmic domain

Alterations including truncations or replacement of the pre-Tα cytoplasmic domains were also tested for increasing expression levels. Previously [304], low pre-TCR surface expression was found to be pre-Tα dependent. In particular, the last 48 residues at the C-terminus of pre-Tα were shown to be very critical for its endoplasmic reticulum retention, which resulted in low pre-TCR surface expression. In another study, the pre-Tα sequences from several vertebrates including mammals and sauropsids were aligned and analysed [276] (Figure 3.6), and it was found that some pre-Tα regions, such as the extracellular Ig-like domain and transmembrane domain, were very highly conserved, but not the cytoplasmic domain. For example, several vertebrates had

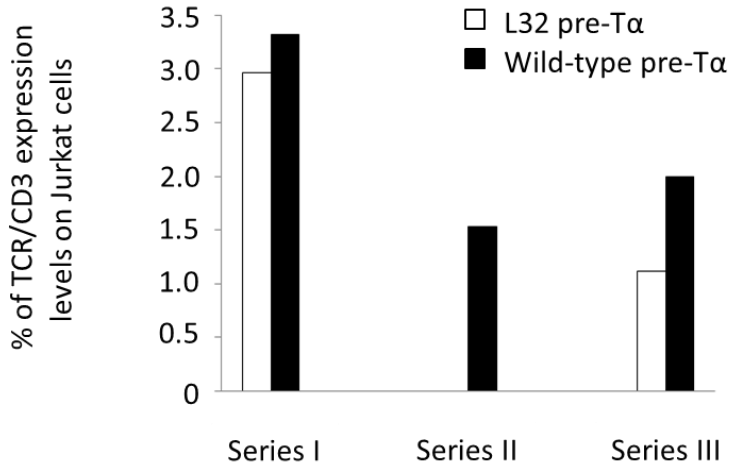

Figure 3.5: Pre-TCR/CD3 expression by lentivirally-infected E6.1-57 cells as a fraction of TCR/CD3 expression Jurkat cells in a series of multiple infections with pre-Tα-encoding lentiviruses. In series I, E6.1-57 cells expressing TCRβ were infected with pre-Tα. In series II, the series I cells were re-infected with pre-Tα. In series III, the series II cells were infected again with TCRβ. White, L32R mutant pre-Tα-expressing cells. Black, wild-type pre-Tα-expressing cells. FACS analysis was as described in Figure 3.4.

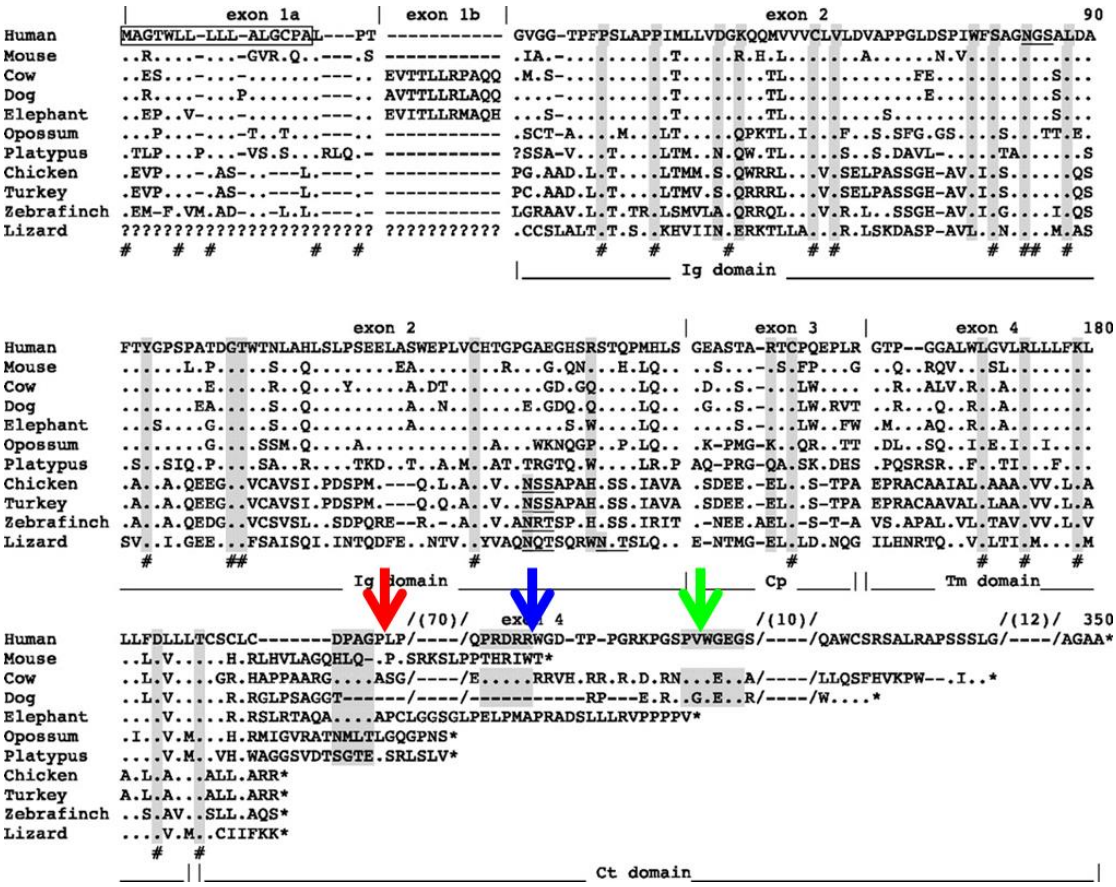

Figure 3.6: The alignment of pre-Tα sequences among amniotes and the truncation sites in the cytoplasmic domain for the pre-Tα chimeras I (red arrow), II (blue arrow) and III (green arrow). Residues identified as important in the mouse pre-Tα sequence are indicated by grey columns; ‖, indicates limits of exons; . indicates residue identical to the human pre-Tα residue; - (exon 1-3), indicates indel; - with numbers within parentheses above (exon 4), indicates numbers of non-converved residues; #, indicates unchanged residue; ?, indicates unknown residue; and * indicates stop codon. Potential N-glycosylation sites are underlined. Cp, connecting peptide; Ct, cytoplasmic tail; Tm, transmembrane. The figure is taken from [276].

extremely short cytoplasmic domains. This implied that truncation of the pre-Tα cytoplasmic domain might allow for an increase in expression levels with little effect on function.

Four different chimeric pre-Tαs were generated with four different truncations of the cytoplamsic domains:

(i) A construct lacking the majority of residues in the cytoplamic domain, except the eleven charged, conserved residues right after the Tm domain (Figure 3.6; red arrow).

(ii) A construct retaining some conserved residues in the cytoplasmic domain (blue arrow).

(iii) A construct lacking the last 48 residues at the C-terminus (green arrow).

(iv) A pre-Tα chimera in which the cytoplasmic domain was replaced with the very short mature TCRα cytoplasmic domain.

As shown in Figure 3.7, almost-complete removal of the cytoplasmic domain (chimera I) significantly reduced expression versus the wild-type protein. Among all of the chimeras, only the pre-Tα chimera iv significantly increased pre-TCR surface expression. However, the small increase (about 30%) was not expected to be enough in order to allow for easy differentiation between the subtle differences in pre-TCR levels for all the mutant forms of pre-Tα that had to be tested.

iii. Increasing virus titre and inclusion of internal negative controls

The previous two approaches, failed to significantly enhance pre-TCR surface expression levels. A final approach involved 'maxi-lentiviral' infections and comparisons with individual internal negative controls, was used. To maximise expression, cells were also infected with very high densities of lentivirus (see Chapter 2 Materials and Methods). 'Maxi-lentiviral' infections (with very high densities of

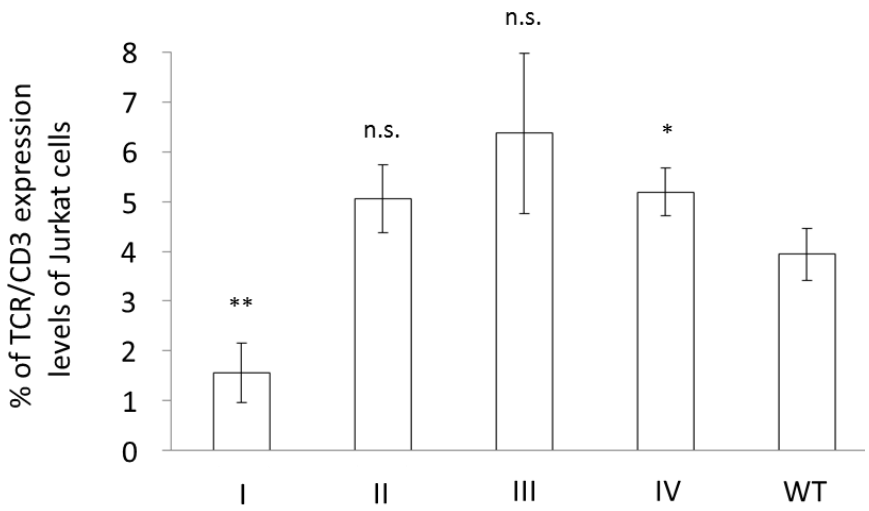

Figure 3.7: The effects of different pre-Tα cytoplasmic domain truncations on pre-TCR/CD3 expression levels, as a fraction of TCR/CD3 expression levels on Jurkat cells. Chimera I lacked the majority of the cytoplasmic domain; chimera II retained conserved residues in the cytoplasmic domain; chimera III lacked the last forty eight residues at the C-terminus; and chimera IV contained the very short mature TCRα cytoplasmic domain instead; WT, is the wild-type pre-Tα. The averages of four individual replicates are shown. Error bar, standard deviations. Statistical comparisons of the chimeras and the wild-type pre-Tα were performed using student's two-tailed t-test: *, $0.01<p\leq0.05$; **, $p \leq 0.01$; n.s., non-significant or $p>0.05$.

lentivirus) improved pre-TCR surface expression by about 3.5-fold, compared to the standard lentiviral infection (Figure 3.8A and Figure 3.3). For these experiments the TCRβ subunit of the pre-TCR complex was tagged with three mCherry fluorescent proteins in tandem to ease detection in the PE-channel of the flow cytometer. As an additional refinement, TCRβ expressing and non-expressing cells were transduced with pre-Tα-expressing viruses and mixed at a 50:50 ratio (Figure 3.8B). The TCRβ negative cells served as the internal negative controls, insofar as the assay tested the ability of pre-Tα mutants to get to the cell surface by forming a complex with TCRβ. The surface expression levels of the pre-TCRs were determined by FACS with anti-HA primary antibody and Alexa Fluor® 647-conjugated secondary antibody.

The chief advantage of the new approach was that surface expression levels of pre-TCR resconstituted with the wild-type or the mutant pre-Tα proteins (Figure 3.8C-E, right boxes) could be normalised against those of the cells lacking TCRβ in the internal negative controls (Figure 3.8C-E, left boxes), using the geometric means of fluorescence. Cells transfected with both wild-type pre-Tα and TCRβ gave rise to a marked increase in fluorescence intensity (Figure 3.8C). On the other hand, the pre-Tα subunit mutated at residue C31R (the folding control; Figure 3.8D) or L32R (fully buried in the contact surface formed with the constant region of TCRβ; Figure 3.8E) gave fluorescence levels indistinguishable from those for the TCRβ-only expressing cells. This complete abrogation of the pre-TCR surface expression indicated that the assay would detect mutations affecting folding/assymbly. The new assays was then used to screen the entire set of seventy-four mutant forms of pre-Tα. The mutational screen was repeated four times; an example set of FACS data from one of the experiments is shown in Figure 3.9.

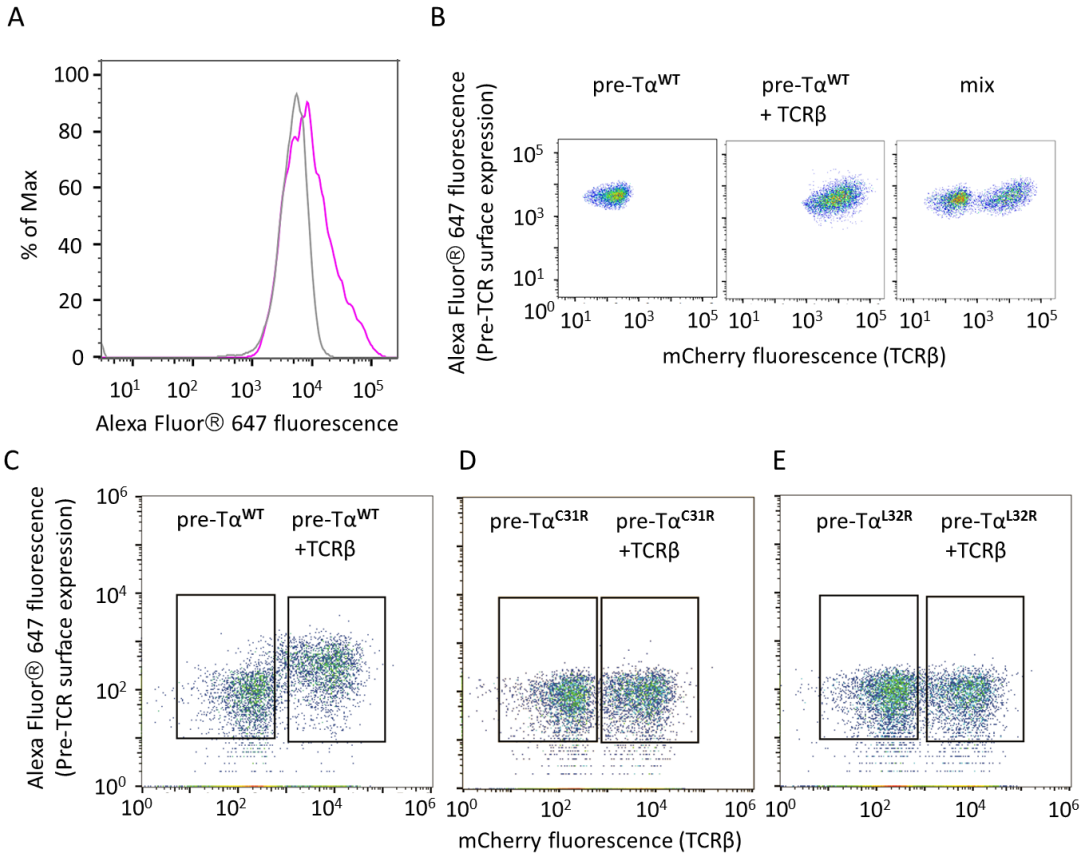

Figure 3.8: The assay for pre-TCR assembly. (A) Surface expression of the pre-TCR on E6.1-57 cells, after 'maxi lentiviral' infections with viruses encoding wild-type HA-pre-Tα and TCRβ. Cells were stained with the mouse anti-HA antibody and a secondary antibody (anti-mouse IgG conjugated with Alexa Fluor® 647, red). The cells were also stained with the secondary antibody only (grey). (B) Cells 'maxi lentivirally' infected with wild-type HA-pre-Tα alone (left), or together with TCRβ (middle). In the right panel these two groups of cells were mixed prior to FACS analysis. (C) Cells expressing wild-type pre-Tα with (right box) or without (left box) TCRβ. (D) Cells expressing C31R-mutated pre-Tα with (right box) or without (left box) TCRβ. (E) Cells expressing L32R-mutated pre-Tα with (right box) or without (left box) TCRβ. Data in panels A and C-E were obtained at different times on different FACS equipment, than the data in panel B.

Figure 3.9: A representative set of FACS data showing levels of pre-TCR surface detection on cells expressing both a mutant form of pre-Tα and TCRβ (right box), or a mutant form of pre-Tα only (left box).

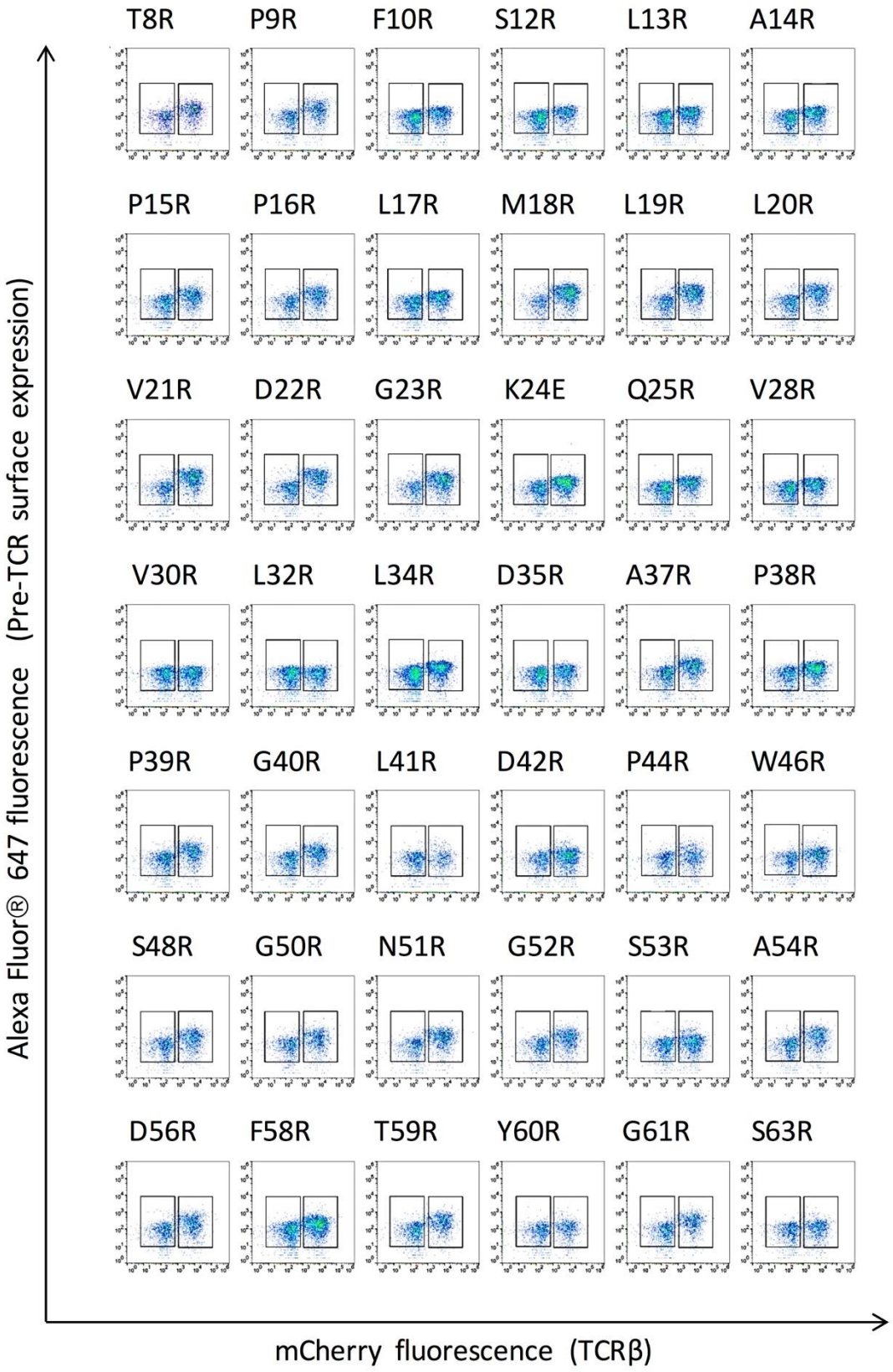
T8R
P9R
F10R
S12R
L13R
A14R
P15R
P16R
L17R
M18R
L19R
L20R
V21R
D22R
G23R
K24E
Q25R
V28R
V30R
L32R
L34R
D35R
A37R
P38R
P39R
G40R
L41R
D42R
P44R
W46R
S48R
G50R
N51R
G52R
S53R
A54R
D56R
F58R
T59R
Y60R
G61R
S63R
Alexa Fluor® 647 fluorescence (Pre-TCR surface expression)
mCherry fluorescence (TCRβ)

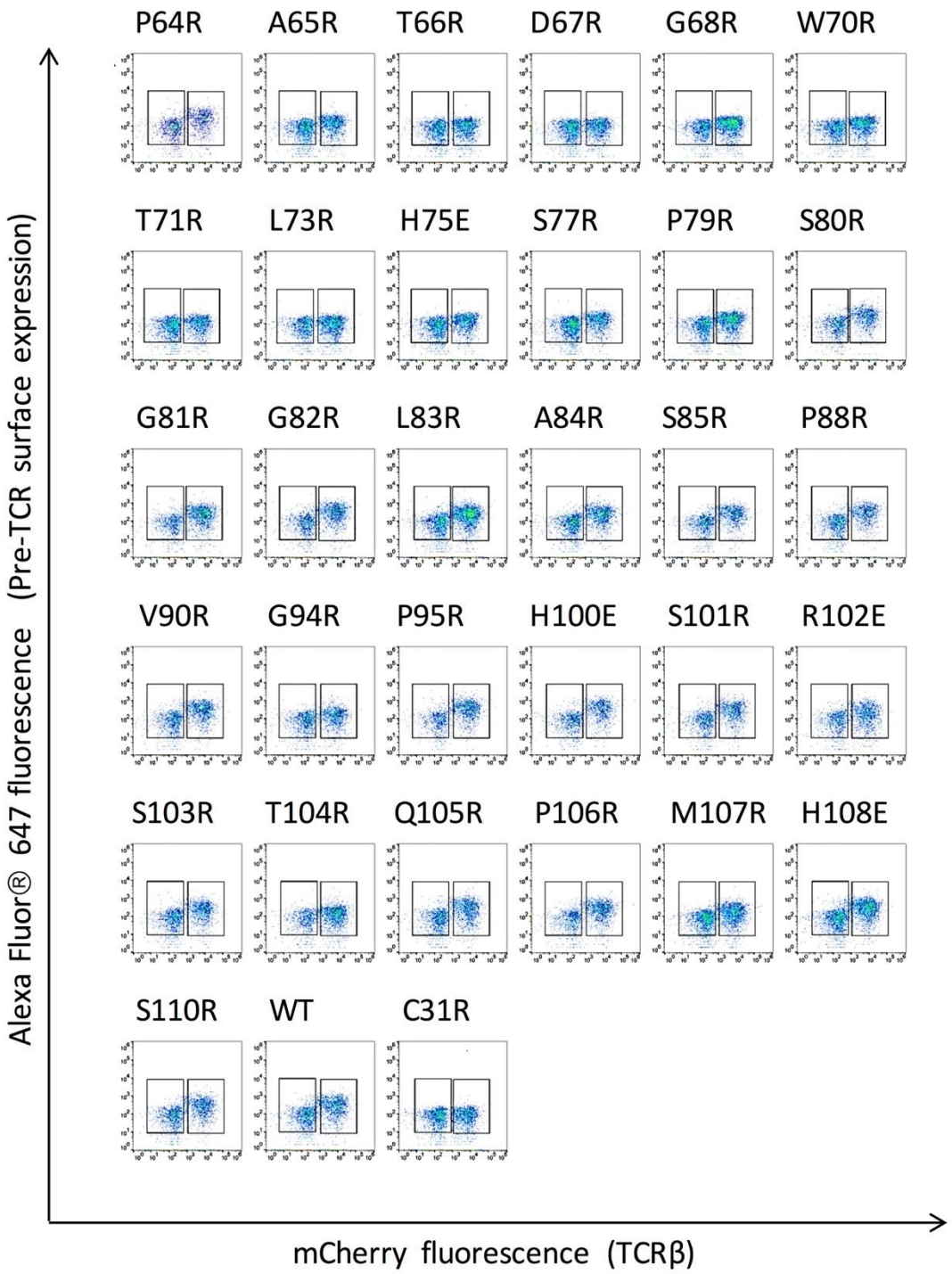
P64R
A65R
T66R
D67R
G68R
W70R
T71R
L73R
H75E
S77R
P79R
S80R
G81R
G82R
L83R
A84R
S85R
P88R
V90R
G94R
P95R
H100E
S101R
R102E
S103R
T104R
Q105R
P106R
M107R
H108E
S110R
WT
C31R
Alexa Fluor® 647 fluorescence (Pre-TCR surface expression)
mCherry fluorescence (TCRβ)

D. Mapping the interfaces formed by pre-Tα subunits in the pre-TCR

The levels of pre-TCR surface expression were determined for each of the mutants and the wild-type pre-Tα subunit, in the absence and in the presence of TCRβ. The increases in expression versus the internal negative controls were then determined and expressed as a fraction of the increase observed versus the negative control for the wild-type subunit (Figure 3.10). The effects of the mutations were further categorised as no or little inhibition (more than 66% pre-TCR surface expression versus the wild-type), moderate inhibition (33%-66% surface expression versus the wild-type) and severe reduction (less than 33% surface expression versus the wild-type). These categories are colour coded green, yellow and red in the following figures in this chapter.

The mutagenesis results shown in Figure 3.10 indicate that 15 and 24 mutations had severe and moderate effects on pre-TCR surface expression, respectively, implying that these pre-Tα residues are likely to be involved in forming interface(s) needed for pre-TCR surface expression, or that these pre-Tα residues play important roles in structural folding or stability. These residues map onto the pre-Tα crystal structure (Figure 3.11A), producing both a large contiguous surface and a set of residues scattered across the surface of the subunit (Figure 3.11B). The contiguous surface closely matches the 'contact' interface predicted by Naccess, *i.e.* the region buried by the pre-Tα in association with the constant region of TCRβ (Figure 3.11C).

Accordingly, all of the mutations of the 'contact' residues predicted by Naccess inhibited pre-TCR surface expression. Indeed, 9 out of 14 mutant 'contact' residues (F10R, S12R, P15R, I17R, L34R, F58R, L73R, H75E and G94R) had moderate inhibitory effects and the remainder (V30R, L32R, Y60R, S63R and T71R) severely reduced expression. Drastic mutations of the four additional residues (L13R, A14R,

Figure 3.10: Effects of mutations of pre-Tα residues on pre-TCR expression levels at the cell surface, shown as the ratio of mutant to wild-type complex levels, expressed as a percent. Surface expression levels were measured as geometric means of fluorescence intensity for anti-HA antibody binding detected by FACS. The geometric mean values for the TCRβ low population in each experiment were subtracted, and the change in geometric mean expressed as a percentage of that for wild-type complexes (as discussed in II.D). Data are presented in sequence order. Means are shown for four individial repeat experiments; error bars are standard errors. Colour key: less than 33% reduction of expression versus wild-type, green; 33% to 66% reduction of expression, yellow; and greater than 66% reduction, red.

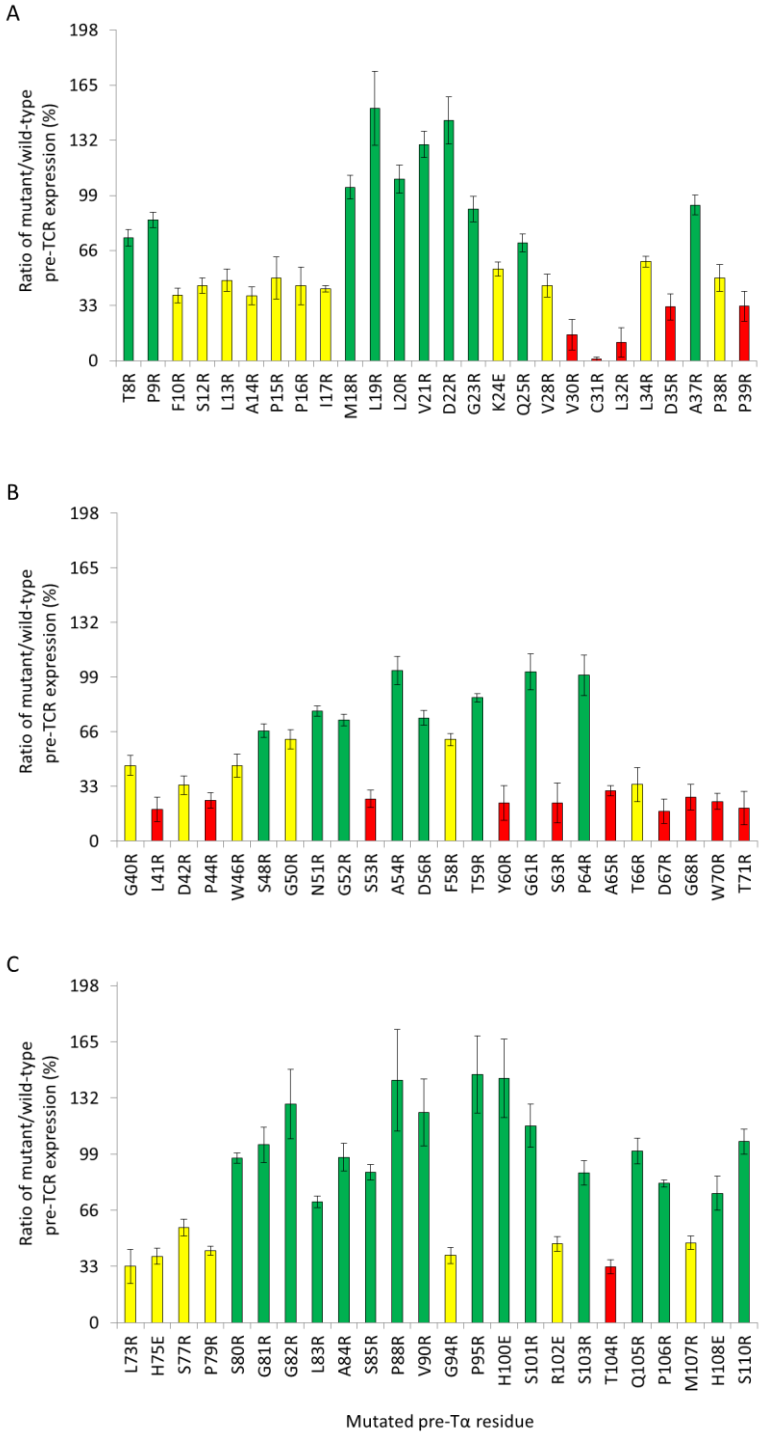
A
Ratio of mutant/wild-type pre-TCR expression (%)
198
165
132
99
66
33
0
T8R
P9R
F10R
S12R
L13R
A14R
P15R
P16R
I17R
M18R
L19R
L20R
V21R
D22R
G23R
K24E
Q25R
V28R
V30R
C31R
L32R
L34R
D35R
A37R
P38R
P39R
B
Ratio of mutant/wild-type pre-TCR expression (%)
198
165
132
99
66
33
0
G40R
L41R
D42R
P44R
W46R
S48R
G50R
N51R
G52R
S53R
A54R
D56R
F58R
T59R
Y60R
G61R
S63R
P64R
A65R
T66R
D67R
G68R
W70R
T71R
C
Ratio of mutant/wild-type pre-TCR expression (%)
198
165
132
99
66
33
0
L73R
H75E
S77R
P79R
S80R
G81R
G82R
L83R
A84R
S85R
P88R
V90R
G94R
P95R
H100E
S101R
R102E
S103R
T104R
Q105R
P106R
M107R
H108E
S110R
Mutated pre-Tα residue

Figure 3.11: Mapping the interfaces formed by pre-Tα based on the crystal structure of the proposed pre-TCR dimer [233]. The structural views are displayed using Pymol. The views shown on the left and right panels are rotated 220° around the vertical and 20° around the horizontal axes. (A) Pre-TCR structural views [233]: white, the pre-Tα subunit; orange, the TCRβ subunit. (B) The effects of mutations of pre-Tα subunit residues on pre-TCR surface expression levels. The residues giving severe, moderate and little/no reductions in expression are labelled with red, yellow and green, respectively, in the pre-Tα subunit. In the bottom panel, the entire set of 'dimerising' residues, *i.e.* comprising the set identified here with Naccess, and the additional dimerising residues identified in [233] are labelled. (C) The 'contact' residues of the pre-Tα subunit involved in forming the interface between the pre-Tα and the constant region of TCRβ, coloured in cyan. (D) The 'dimerising' residues of the pre-Tα subunit involved in forming the 'head-to-tail' pre-TCR dimers in the crystal structure work [233], coloured in purple.

A. Pre-TCR structure

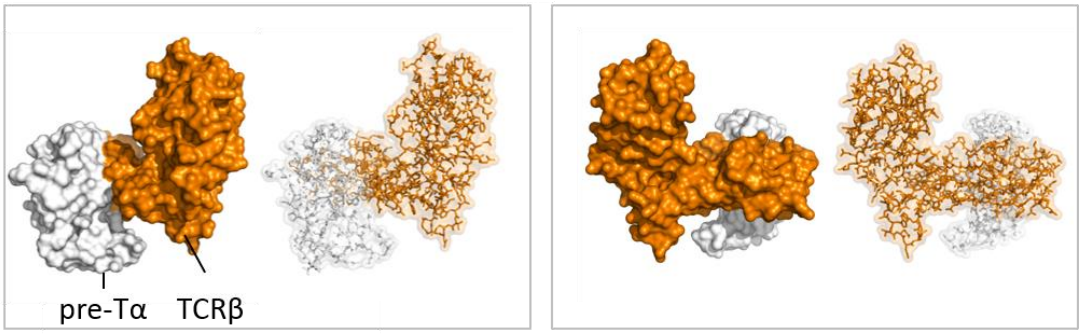

B. Mutagenesis of pre-Tα

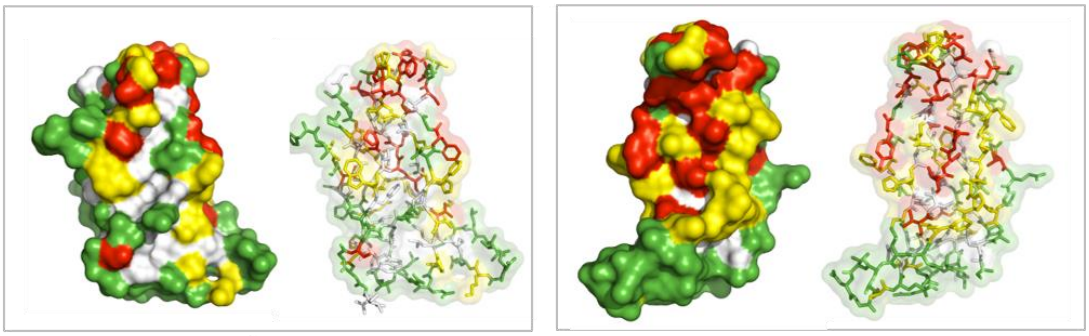

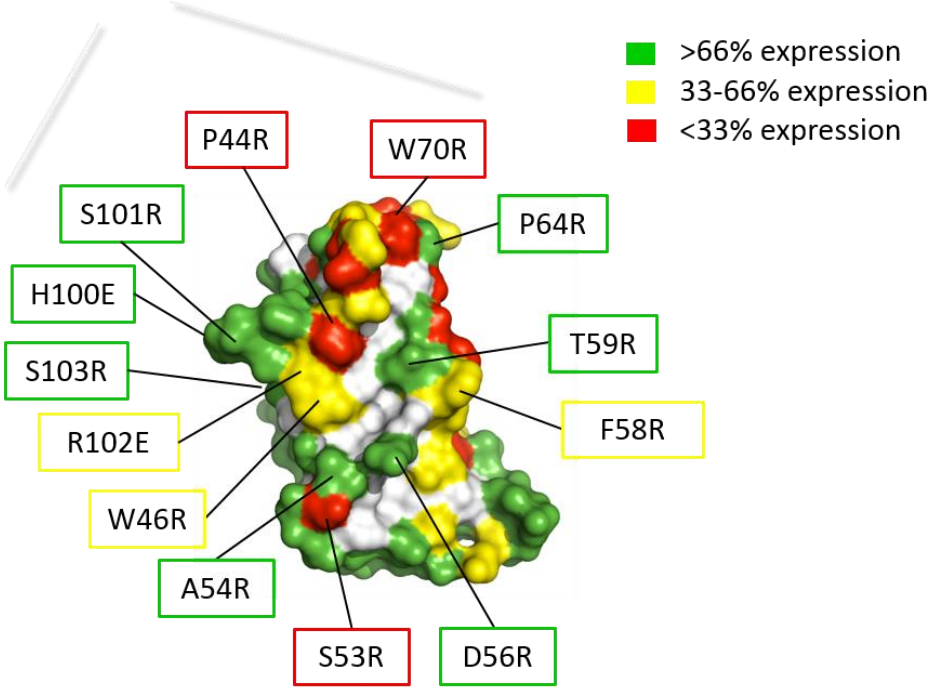

C. ‘Contact’ interface

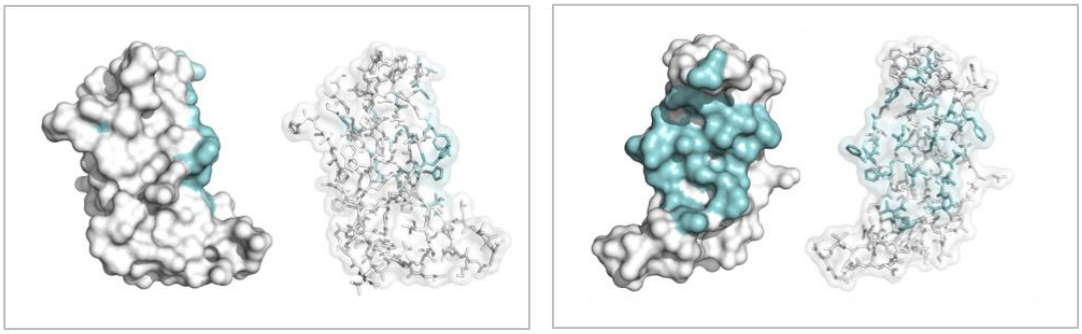

D. ‘Dimerising’ interface

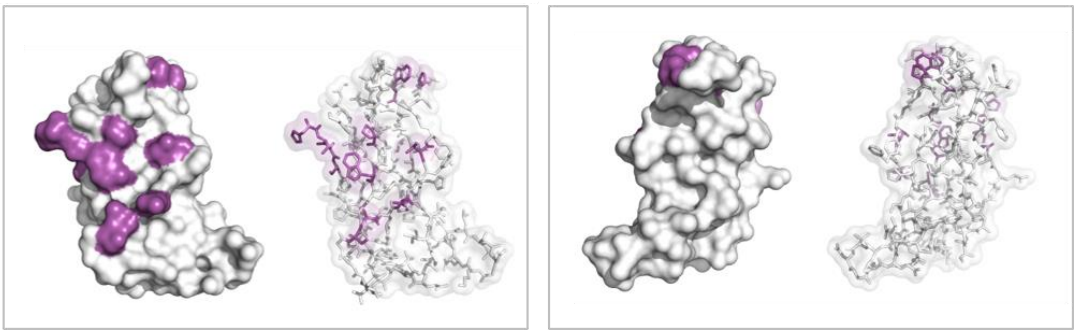

V28R andT66R) predicted as ‘contact’ residues in [233], also had moderate effects.

In contrast, 62% of the mutations of solvent-exposed residues had little or no effect. Although an additional 20% and 18% of mutations of residues had moderate or severe effects on expression, respectively, these did not form a large contiguous interface (Figure 3.10 and Figure 3.11B). This suggests, consistent with previous studies [252], that the drastic mutation approach is capable of identifying large interfaces that need to form within complexes in order to reach the cell surface. The results reveal only one such large contiguous surface, *i.e.* matching the ‘contact’ interface, for which mutations were capable of disrupting pre-TCR expression.

Only 46% of the mutations of ‘dimerising’ residues interfered with pre-TCR complex assembly, *i.e.* A54R, D56R, T59R, P64R, H100E, S101R and S103R. This fraction of disruptive mutant residues in the surface forming the ‘dimerising’ interface is comparable to the fraction of total surface residues whose mutation affected expression (38%). There were three mutant ‘dimerising’ residues with moderate effects (W46R, F58R and R102E) and three mutants of ‘dimerising’ residues with severe effects (P44R, S53R and W70R). However, these residues were relatively dispersed in the structure, and the two that were in close proximity (P44R and W46R) were proline and tryptophans, with bulky side chains or likely to be of structural importance. As a result, it was concluded, based on this mutational study, that the assembled pre-TCR is comprised of only a single pre-Tα and a single TCRβ subunit, alongside the CD3 subunits. Overall, these results suggested that the dimerisation of pre-TCRs might be dispensable for their assembly and expression at the cell surface.

III. Discussion

The stoichiometry of the pre-TCR and the structural requirements for pre-TCR

complex assembly and surface expression were investigated using a mutagenesis-based strategy, as described in this chapter. Several optimisation routes were used to try to improve pre-TCR surface expression levels in order to better distinguish differences of these levels among the wild-type and mutant constructs. These approaches included multiple infections, alterations in the pre-Tα cytoplasmic domain, increasing virus titre, and the use of internal negative controls.

Multiple infections did not improve the pre-TCR surface expression levels on the cell surface. This suggests that the gene transduction capacity and pre-TCR surface expression levels were "saturated" using this standard lentiviral infection approach. The second approach considered was intended to prevent any subunits of the pre-TCR complex from being retained in the endoplasmic reticulum by the pre-Tα cytoplasmic domain [304]. Four pre-Tα chimeras, including three truncations with different lengths of the pre-Tα cytoplasmic domain and one replacement of this entire region with the mature TCRα cytoplasmic domain, were made. Severe truncations of the pre-Tα cytoplasmic domain did not improve pre-TCR surface expression levels. Partial truncations of the last 48 pre-Tα residues in the cytoplasmic domain increased the expression by about 60% on average, but the effect was not statistically significant. This, however, was unlike the results of a previous study showing that partial truncation of the last 48 pre-Tα residues in the cytoplasmic domain could rescue surface receptor expression, by preventing an endoplasmic reticulum retention effect of the pre-Tα cytoplasmic domain [304]. Replacement of the mature Tα cytoplasmic domain increased pre-TCR expression by about 30%, but this seemed unlikely to be enough to allow the subtle effects of the mutations to be easily distinguished.

Finally, the mutagenesis-based strategy was optimised with an approach based on both including internal negative controls for basing comparison and increasing virus titre. Comparisons with the internal negative control, *i.e.* cells transduced with the

pre-Tα gene only, allowed changes in pre-TCR surface expression levels due to complex assembly for the cells transduced with both pre-Tα and TCRβ to be identified and compared across all mutants. These comparisons might have also been done between the internal negative control and the pre-TCR at native, low expression levels using the standard virus titre in the transductions; however, these were not explored in this study. Instead, the high virus titre used in this study allowed ten times larger amounts of pre-Tα and TCRβ genes to be transduced so that surface expression levels of the pre-TCR were boosted by about 3.5 fold. Thus, the pre-TCR at the cell surface could be more easily directly detected using anti-HA antibody-mediated FACS to detect HA-tagged pre-Tα. In addition, This increment in expression levels of pre-TCR gave rise to greater differences in expression levels between the internal negative control and pre-TCR, thus allowing better comparisons across all mutants. Using this optimised approach, the mutation effects could be identified and categorised as: no/limited inhibition, moderate inhibition and severe inhibition of expression.

Based on the use of this assay, only one large contiguous surface in which residues were very sensitive to mutation could be identified. This contiguous interface corresponded closely to the contact interface known to be the site of interaction of pre-Tα with the constant domain of TCRβ. However, there were also small patches containing residues whose mutation affected expression, especially tryptophans and prolines. Several studies have shown that these residues and their surrounding residues provide critical steric configuration and stability in protein structures [303, 305, 306]. Importantly, the mutation-sensitive small patches were dispersed and did not correspond well to the set of ‘dimerising’ residues revealed by Naccess based on the structure of Pang *et al.* [233], or the additional ‘dimerising’ residues proposed in [233]. In sum, although the roles of the dispersed mutations with effects on expression

are yet to be fully explained, the results in this chapter strongly suggest that the pre-TCR complex does not need to form dimers to appear at the cell surface. However, whether individual pre-TCRs are sufficient to initiate pre-TCR signalling and mediate β-selection during thymocyte development would need further investigation.

Chapter 4

Stoichiometric analysis of the TCR and pre-TCR using super-resolution imaging

I. Introduction

In addition to biochemical and cellular approaches, microscopy-based techniques provide a way to further our understanding of biological structure and organisation. Among these techniques, electron microscopy and optical microscopy are very widely used. Electron microscopy has higher resolution than optical microscopy because the wavelength of electrons is several orders of magnitude shorter than that of visible-light photons. The stoichiometry of T-cell membrane proteins or TCRs on fixed membranes has been investigated using gold-labelled bivalent antibodies and transmission electron microscopy, and clusters of molecules were found. However, using electron microscopy, disruptive processes in sample preparation which might lead to artefacts are sometimes unavoidable [269, 307, 308].

TCR organisation before signal initiation has been extensively studied in our laboratory using the optical microscopy-based approaches of TCCD, DySCo and FRAP [180, 235, 236]. Using TCCD, the diffusion through a confocal volume of fluorescently-labelled TCRs and other proteins present on the apical surface of a cell is characterised. Associated molecules, such as dimers, give rise to coincident bursts of fluorescence while non-associated molecules, *i.e.* monomers, do not [235]. In the case of DySCo experiments, TCRs weakly expressed at the surface of T cells are imaged using TIRF video microscopy. The localisations of the TCRs are tracked with a

Bayesian-based algorithm over time, and paired tracks are indicative of co-localisation. The results of both TCCD and DySCo experiments showed that both TCR organisation and diffusional behaviour was comparable to that of the monomeric control protein CD86 and suggested that the TCR is functionally monovalent [235, 236].

In contrast to these results, other imaging techniques such as hsPALM in addition to transmission electron microscopy have suggested that the TCR as well as LAT form clusters at the basal surface of T cells interacting with poly-L-lysine coated glass surfaces [231]. Further study from our group using FRAP has attempted to reconcile these disparate findings for TCR organisation. FRAP showed that the mobility of the TCRs on the basal surface was reduced in comparison to the mobility of TCRs on the apical surface. This reduction in mobility could only be detected for TCRs expressed by wild-type cells and not for mutant, non-signalling cells [180]. It was concluded that the TCRs with less mobility were likely to have been triggered to a certain degree so that higher oligomeric forms were generated and detected in, *e.g.* the hsPALM-based study.

Building on these studies, here the TCR and pre-TCR were analysed using advanced optical microscopy, *i.e.* super-resolution techniques (in this chapter) and two-colour co-localisation analysis (in Chapter 5). Because TCRs appear to be very sensitive to triggering, which might lead to misleading conclusions about the "resting" state, several approaches to sample preparation, and the use of varying TCR expression levels and contact surfaces were tested and optimised. Comparison were made between the mature TCR and pre-TCR.

A. Methodological considerations

Resolution, which in the context of imaging defines the shortest distance over which two point sources can be distinguished, is very limited in the optical microscope. It does not depend on the lens but is highly dependent on the inherent properties of light.

Specifically, Ernst Abbe showed resolution to be “diffraction limited”, insofar as the minimum resolvable feature size, d, is approximated as $\lambda/2n\sin\theta$ (where λ is the wavelength of light; n is the index of refraction; and θ is the half-angle subtended by the optical objective lens) [309]. In practice, resolution refers to the ability to distinguish two adjacent airy disks, which are the projected images with the surrounding diffraction rings from single point objects in the microscope.

Due to diffraction, the resolution of modern fluorescence microscopy is generally limited to about 200-250 nm, which is much larger than most biological molecules of interest. Far-field optical super-resolution techniques have been developed to image cellular molecules or structures well below the diffraction limit (~20 nm). The two approaches in current widespread use are deterministic and stochastic super-resolution imaging.

(a) Deterministic super-resolution microscopy

Deterministic super-resolution microscopy limits fluorescence emissions to spatial scales smaller than the diffraction limit [310]. This involves the photo-switching of fluorophores among at least two or more electronic states by an excitation laser beam and depletion laser beam. One of the main methods is Stimulated Emission Depletion (STED) microscopy [311]. In STED, the fluorophores are initially excited by one laser beam and a subset are then instantaneously returned to the ground state by the other red-shifted stimulation beam, called the STED depletion beam. The STED beam, which has donut-shaped intensity is able to deplete the fluorophores surrounding the excitation spot, thereby increasing resolution (Figure 4.1A).

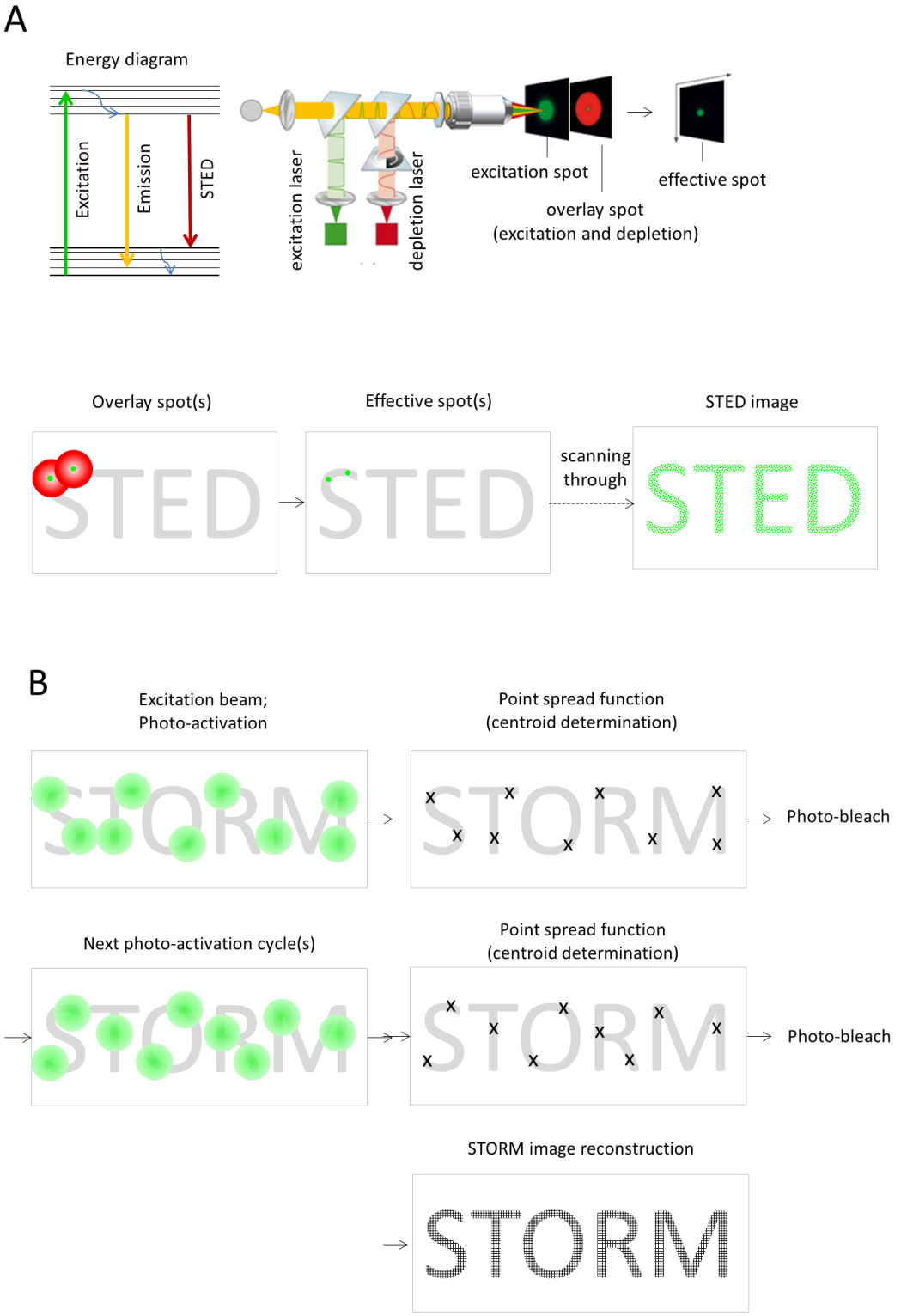

Figure 4.1: The principles of the main super-resolution imaging techniques. (A) The principle of deterministic super-resolution microscopy, STED. Diagram edited from [312]. (B) The principle of the stochastic super-resolution imaging method, STORM.

(b) Stochastic super-resolution technique

In stochastic approaches to super-resolution imaging, subsets of fluorophores are activated individually and complete images are re-constructed at the end. The two most widely used examples of the approach are STORM [266] and PALM [265] (Figure 4.1B). In these methods only an optically resolvable fraction of the photo-switchable or photo-convertible fluorophores are activated at any single time, and different fractions are activated in separate cycles. The localisations of fluorophores can be determined to high accuracy by using the point-spread function (PSF) to obtain the centroid localisation through a Gaussian fit to the PSF. The approach initially required specialised fluorophores, but now conventional carbocyanine fluorophores placed in a reducing thiol compound-containing buffer can be used in a modification of STORM, called dSTORM [313, 314].

(c) Labelling strategy

To better track and analyse single membrane proteins such as pre-TCRs using imaging, a labelling system utilising bright, specific dyes is required. Labelling can be approached by using labelled antibodies or fluorescent proteins genetically fused to the proteins of interest. In this chapter, the HaloTag® labelling system, which had only just been developed commercially when the project started, was first optimised. In other experiments, in order to overcome the lack of photo-stability of the HaloTag in some instances, mEos fusion proteins, or mEos fusion proteins combined with other fluorescently labelled Fabs, were used to establish the stoichiometry of our receptors of interest.

i. HaloTag and HaloTag Ligand

Previously, tagging of fluorescent proteins, such as with three repeats of mCherry, was used for single-molecule imaging in our laboratory. However, even three mCherry molecules were often not bright enough for some experiments. To overcome this, the HaloTag labelling system was tested owing to its claimed brightness, high signal-to-noise ratio and great flexibility. The HaloTag protein is modified from the prokaryotic haloalkane dehalogenase and is designed to form a covalent bond with the chloroalkane linker of a HaloTag Ligand (*e.g.* fluorescent dye). The nucleophilic displacement of the terminal chloride by an aspartate residue leads to the formation of a covalent product, *i.e.* HaloTag Ligand. The formation of the covalent bond between the HaloTag and the Ligand is site-specific as well as irreversible since the histidine which catalyzes hydrolysis of the intermediate is modified in the conjugation process [315].

ii. Eos fluorescent protein

The Eos fluorescent protein is an irreversibly photoactivatable fluorescent protein producing green-to-red photo-conversion that is useful in super-resolution imaging. Eos fluorescent protein is derived from the scleractinian coral, Lobophyllia hemprichii, and contains a chromophore with the green-emission peak of 516 nm. Upon irradiation with low-level near UV light of ~390 nm, cleavage of the peptide backbone near the chromophore leads to changes in electron conjugation, giving rise to a characteristic red emission peak at 581 nm. After the photo-conversion, Eos fluorescent protein is very bright and allows long-term imaging [316, 317].

Beginning with the Eos fluorescent protein, several variants with more advanced imaging compatibilities have been developed. Derived from the wild-type tetramer, a monomeric form of the Eos fluorescent protein, *i.e.* mEos, has been generated by mutagenesis of the amino acids involved in the oligomerisation of the molecule. This

monomeric form is not only bright and photo-stable but also well suited to single-molecule, super-resolution imaging. However, formation of its chromophore requires temperatures below 30℃. The mEos2 fluorescent protein overcomes this temperature sensitivity, allowing it to be very compatible with live-cell imaging of mammalian cells. In addition, the tendency for mEos2 to form dimers or oligomers at high concentrations has been further reduced in the commonly used photoactivatable fluorescent proteins, mEos 3.1 and mEos 3.2 [318-320].

B. Ascorbic acid and T-cell activation

As discussed, in super-resolution imaging sub-diffraction resolution relies on only a few of the photo-activated fluorophores being activated at any one time. All fluorophores except a few are photo-switched off (the off-state) at the beginning of imaging acquisition, and the remainder are kept in the on-state through constant weak illumination. In order to have better localisation, very short but bright on-states and long off-states are favourable and oxygen-radical scavengers such as ascorbic acid are commonly used to extend off-state times [321-324]. The effects of ascorbic acid on live cells, including T cells, have been studied, and it was found in the majority of studies that short exposure to ascorbic acid does not affect T-cell proliferation and cytokine production at low concentrations, for example, at the levels of 40 to 50 μM used in the present study. According to proteome analysis, however, expression of phosphatidylinositol transfer protein (PITP) together with a number of other proteins (comprising 1.3% of the total proteome) are affected by ascorbic acid treatment [325]. The function of PITP is to transport phosphatidylcholine and phosphatidylinositol between inner and outer membranes and is likely only to indirectly affect signal transduction [325, 326]. Nevertheless, here T cells for imaging were fixed to minimise any potential effects of ascorbic acid on PITP and signalling.

II. Results

A. Overview

In this chapter, the organisation of the pre-TCR and TCR, and the control proteins CD86 and CD28 were investigated in cell lines using the single-molecule imaging techniques, PALM and dSTORM. The experiments were undertaken in collaboration with Dr James McColl, Anna Lippert, Dr Steven Lee and Dr Matthieu Palayret in Prof. David Klenerman's group at the University of Cambridge.

First, HaloTag labelling of pre-Tα and TCRβ had to be optimised as this labelling strategy was new to the laboratory. Then, using dSTORM, the numbers of photo-bleaching steps for individual HaloTag fluorescent spots were analysed to investigate the stoichiometry of the pre-TCR. However, there were no significant differences between the numbers of photo-bleaching steps measurable for the monomeric and dimeric controls owing at least in part to the photo-physics of the HaloTag Ligands.

mEos2 fluorescent protein fused to pre-Tα or TCRβ, and direct dSTORM-based localisation, helped improve the analysis with regard to brightness and photo-stability. We found, interestingly, that there was a great deal of heterogeneity in the organisation of the mature TCR among cells taken straight from tissue culture. We speculated that there is weak activation in culture and that this results in TCR re-organisation.

To confirm the stoichiometry of the mature TCR prior to any, even very weak, activation in culture, cells were sorted based on their TCR expression levels and those with low expression levels were examined. However, there was the possibility that not every TCR would be fluorescent in the form of TCR-mEos2, leading to a possible monomer bias. Therefore, in a second approach, anti-TCR Fabs labelled with fluorescent dyes were used to maximise the possibility of visualising all the TCRs on

the membrane using PALM and dSTORM. However, even this was problematic due to the kinetics and optical properties of the fluorescent dyes themselves, as discussed below. Finally, preliminary cluster analysis of the dSTORM data did suggest that the pre-TCR might not be clustered in T-cell transfectants.

B. dSTORM and photo-bleaching analysis in the HaloTag-based system

Using the HaloTag-based labelling system, genes of interest were genetically fused upstream of the HaloTag sequence including CD86, CD28 and TCRβ, or downstream of the HaloTag sequence including pre-Tα (Figure 4.2 and Chapter 2). The constructs were cloned into the pHR-sin vector and transfected into Jurkat-derived cells, *i.e.* J.RT3-T3.5 (TCRβ-negative) or E6.1-57 (TCRα- and TCRβ-negative) cells, using lentiviruses. Then, HaloTag Ligands were conjugated to the HaloTag fusion protein and optimised for labelling efficiency and signal-to-noise ratio. An advantage of the HaloTag-based system is that a variety of HaloTag Ligand fluorescent dyes with distinct wavelengths and the properties of cell-permeability or cell-impermeability, are available (Table 4.1).

(a) Optimisation of labelling efficiency

HaloTag labelling efficiency was first compared with a fluorescence labelling system commonly used in our laboratory: *i.e.* proteins/membrane receptors of interest fused to tandem repeats of citrine fluorescent proteins. Among the HaloTag Ligands available, only those with wavelengths compatible with laser channels in the microscopes in the Klenerman laboratory were considered for optimisation: TMR and TMRDirect ($555_{Ex}/585_{Em}$) for the 561-nm laser, and Oregon Green ($494_{Ex}/516_{Em}$), diAcFAM ($494_{Ex}/526_{Em}$), Alexa Fluor® 488 ($494_{Ex}/517_{Em}$) and R110Direct ($502_{Ex}/527_{Em}$) for the 488-nm laser. However, diAcFAM and the Alexa Fluor® 488 Ligands were

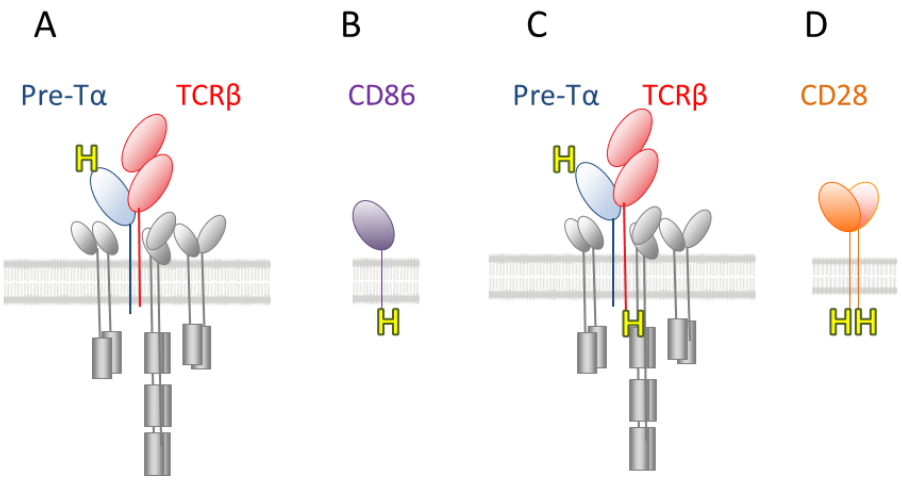

Figure 4.2: Schematic view of the design of HaloTag fusion proteins for expression in E6.1-57 cells. (A) Construct for determining pre-TCR stoichiometry. (B) The CD86 monomeric control. In (C) and (D), two dimeric controls are shown. H, stands for HaloTag.

Table 4.1: Properties of different HaloTag Ligands and usable laser wavelengths.

HaloTag Ligand	Cell-Permeability	Ex/Em (nm)	Laser used in the microscopy (nm)
TMR	Cell-Permeable	555/585	561
TMRDirect	Cell-Permeable	555/585	561
R110Direct	Cell-Permeable	502/527	488
diAcFAM	Cell-Permeable	494/526	488
Alexa Fluor® 488	Cell-Impermeable	494/517	488
Oregon Green	Cell-Permeable	494/516	488

immediately excluded because the former is the least stable for tracking molecules over time and the latter exhibited a poor signal-to-noise ratio in initial trials. The first experiments indicated that receptors labelled via HaloTags were better localised to the membrane, evidenced as thin, bright fluorescent rings, than the citrine fusions (Figure 4.3).

(b) Optimisation of concentration and signal-to-noise ratio

To optimise HaloTag-based labelling, HaloTagged CD28 homodimers were labelled with Oregon Green, TMR, R110Direct or TMRDirect at several dilutions. J.RT3-T3.5 cells not transfected with HaloTag-fusion proteins served as negative controls. Labelling efficiencies and signal-to-noise ratios were analysed using FACS. The signal-to-noise ratios, measured as geometric means of fluorescence for CD28-HaloTag expressing versus non-expressing J.RT3-T3.5 cells (Figure 4.4), revealed that, overall, Oregon Green and R110Direct would be more useful than TMR and TMRDirect. The results also suggested that generally lower concentrations (*i.e.* 12.5 nM and 25 nM) of HaloTag Ligands gave better signal-to-noise ratios.

Two-colour HaloTag Ligand labelling was optimised using the confocal microscope. Anticipating different labelling requirements, Oregon Green and TMR, and R110Direct and TMRDirect, were used as pairs, respectively. Similar to the FACS results, R110Direct and TMRDirect at a concentration of 12.5 nM gave the best contrast in the confocal images. In addition, when dual-labelling with both R110Direct and TMRDirect, the concentration of 12.5 nM consistently gave the best results and was used for all subsequent experiments (Figure 4.5).

(c) Photo-bleaching step analysis

To visualise and to understand its stoichiometry on the resting T-cell, pre-Tα-HaloTag

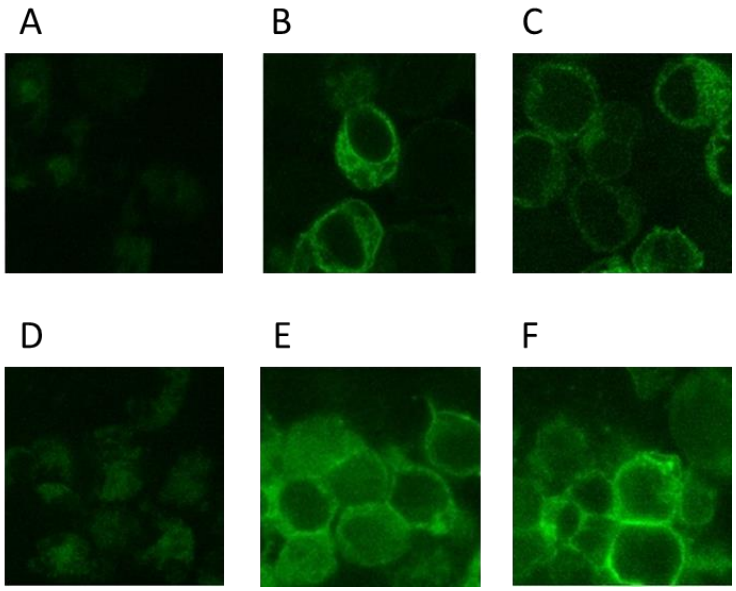

Figure 4.3: HaloTag labelling versus the use of three tandem repeats of citrine fluorescent protein. In the top panels, J.RT3-T3.5 cells (A), and two examples (B,C) of J.RT3-T3.5 cells expressing a TCRβ chain fused to three citrine fluorescent proteins are shown. In the bottom panels, J.RT3-T3.5 cells (D), and two examples (E,F) of J.RT3-T3.5 cells expressing a TCRβ chain fused to HaloTag and labelled with a HaloTag Ligand (Oregon Green) are shown. In (D) and (F) the cells were labelled for 30 minutes and in (E) for 15 minutes.

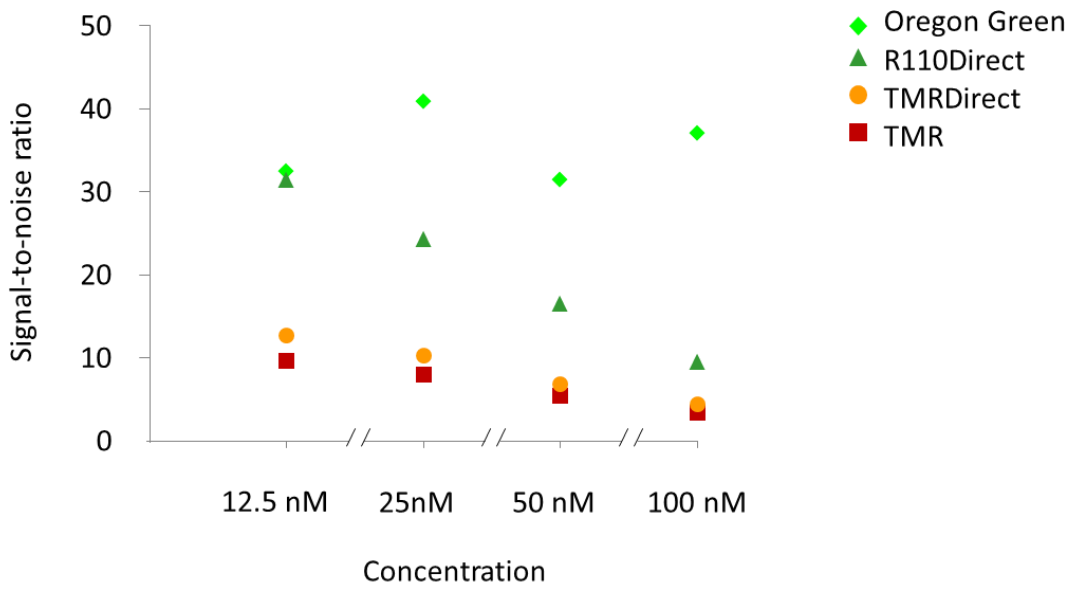

Figure 4.4: Signal-to-noise ratios for CD28-HaloTag expressing J.RT3-T3.5 cells labelled with different concentrations of HaloTag Ligands. The Ligands used were: Oregon Green (diamonds); R110Direct (triangles); TMRDirect (circles); and TMR (squares). The signal-to-noise ratios, measured as the ratio of the geometric means of fluorescence for CD28-HaloTag expressing versus non-expressing J.RT3-T3.5 cells, were determined at the indicated concentrations of HaloTag Ligands. The revised manufacturing protocols for labelling are described in Chapter 2.

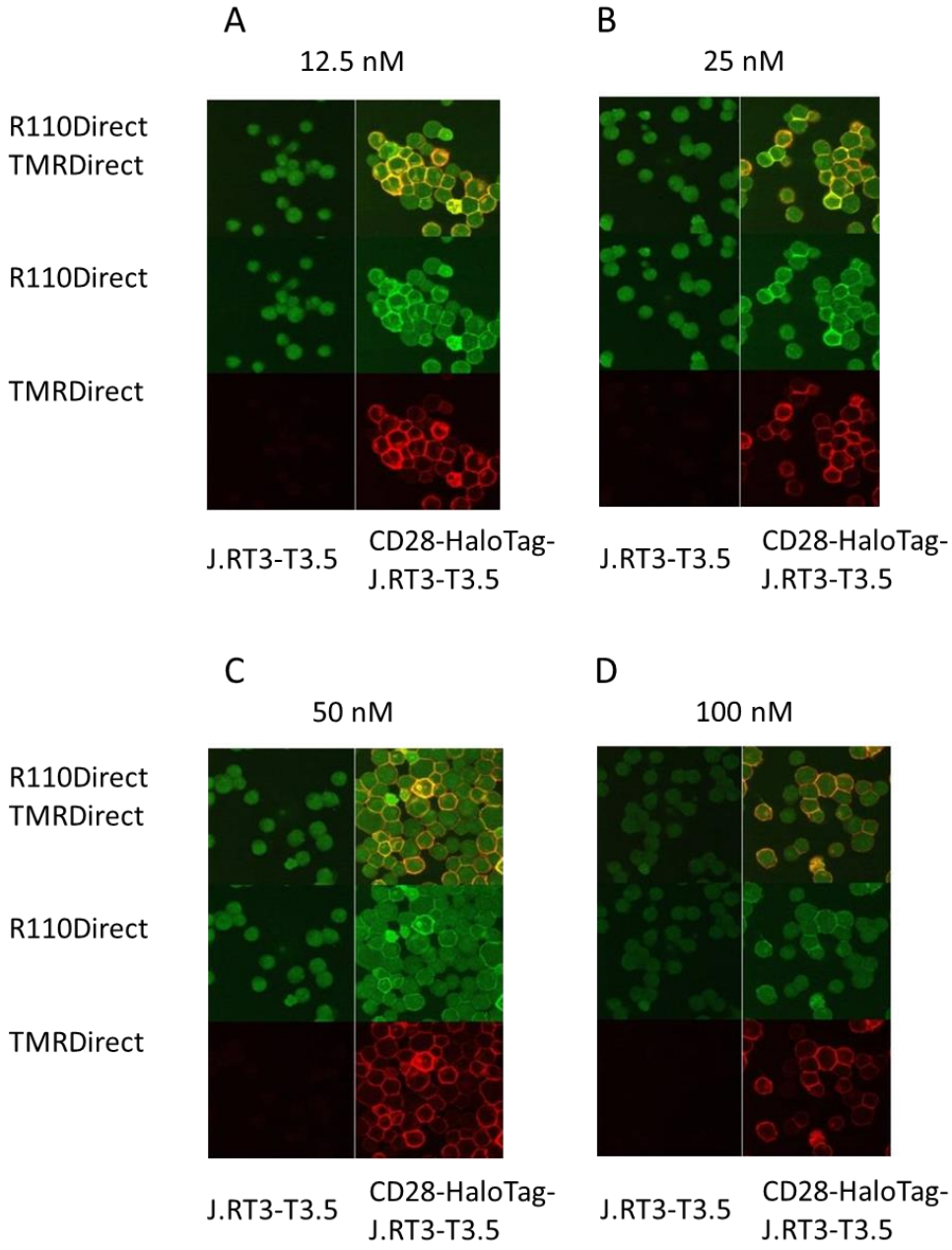

Figure 4.5: HaloTag labelling with R110Direct and TMRDirect used as a pair or individually. The HaloTag Ligands were used at concentrations of (A) 12.5 nM, (B) 25 nM, (C) 50 nM and (D) 100 nM, and the fluorescence measured by confocal microscopy. In the upper panels, merged images are shown. In the middle and lower panels, labelling in the R110Direct and TMRDirect channels is shown.

fusion proteins were expressed alongside exogenous TCRβ in E6.1-57 cells. The numbers of photo-bleaching steps of the HaloTag Ligands in each complex were measured using a dSTORM-based strategy, allowing single receptors to be examined. Monomers were expected to give single photo-bleaching steps whereas dimers or oligomers were expected to produce two or more steps. As a monomer control, CD86 fused with HaloTag at the C-terminus expressed in E6.1-57 cells was used. For dimeric controls, CD28-HaloTag or pre-Tα-HaloTag/TCRβ-HaloTag expressed together in E6.1-57 cells were used. HaloTags were cloned ahead of pre-Tα and at the C-terminus of TCRβ to avoid steric hindrance or interaction of the HaloTag proteins (Figure 4.2).

The cells were labelled with TMR Ligand and fixed in PFA and, following dSTORM imaging, fluorescent spots were analysed to determine the number of photo-bleaching steps using a bespoke algorithm (M. Palayret, unpublished). Examples of single, double and multiple photo-bleaching steps are shown in (Figure 4.6). However, for the E6.1-57 cells expressing pre-Tα-HaloTag and TCRβ-HaloTag, *i.e.* the dimeric control, similar numbers of single versus multiple photo-bleaching steps were observed. This implied that relatively few of the dimers were being dually labelled, despite optimisation of the labelling, or that HaloLigands exhibited a non-single decay process. An additional confounding factor, perhaps, is that HaloTag Ligands, such as TMR used in this work, without being chemically modified or caged, are not notable for being extremely photo-stable [327, 328], thus adding to the difficulties of determining receptor stoichiometry using photo-bleaching step analysis.

C. PALM and mEos2 fluorescent protein

(a) Developing the methodology

To avoid the disadvantages of the photo-bleaching step analysis, a stoichiometric

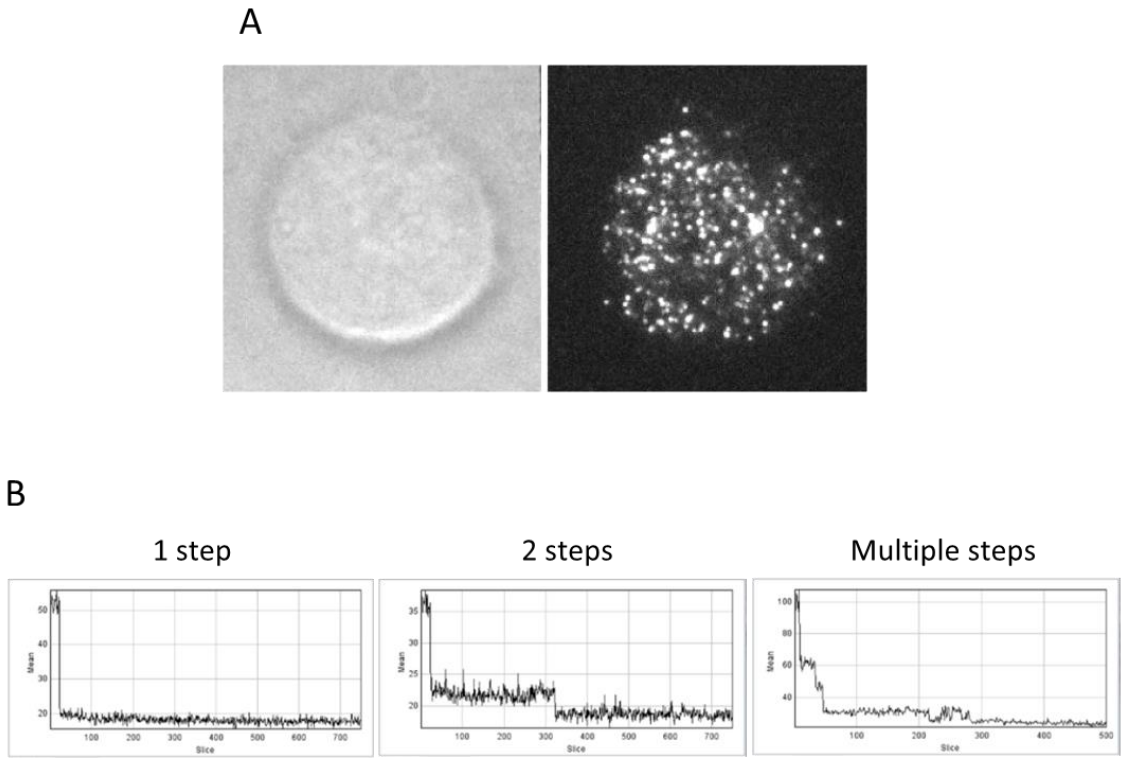

Figure 4.6: Pre-TCR imaging and examples of photo-bleaching decay curves. (A) Imaging of the pre-TCR (in E6.1-57 cells expressing pre-Tα-HaloTag and TCRβ) including white-field (left) and TIRF (right) images. In (B), examples of one, two and multiple photo-bleaching steps are shown. Data collection in collaboration with Dr Matthieu Palayret.

analysis was undertaken utilising PALM and receptors expressed as fusions with the photoactivatable fluorescent protein, mEos. It was of special interest to first investigate TCR stoichiometry using PALM since this was the approach Lillemeier *et al.* used to propose that TCR and LAT are clustered at contacts of T cells with poly L-lysine coated glass coverslips. Their results contrasted with observations from this laboratory that only monomeric TCRs were detected on the apical surface of T cells using TCCD, and TCR weakly-expressing cells examined using DySCo (as discussed above and in Chapter 1).

TCRβ-mEos2 fusion protein that was intended to pair with native TCRα in J.RT3-T3.5 cells, and cells expressing either CD86-mEos2 or CD28-mEos2 control fusion proteins were prepared. In pilot experiments, clusters of TCR/mEos2 fusion proteins were detected if the live cells were directly placed on IgG-coated coverslips (Figure 4.7). To image receptors on truly resting cells, non-triggering surfaces would be required. Because it was expected that such surfaces might be difficult to obtain, we chose to fix the cells in suspension and then to analyse the cells with PALM. Different fixation solutions, including glutaraldehyde and/or paraformaldehyde, were first compared for their effects on reducing the mobility of receptors. In addition, different slide surfaces including non-activating Gap8.3 (anti-hCD45 antibody) coated surfaces and agarose gel pads, both used to trap the fixed cells on a surface for imaging were tested. Surfaces on which cells formed larger contact areas were preferred since more receptor-mEos proteins could be imaged in the same visual field. Allowing cells to settle under gravity or spinning cells onto slide surfaces using a Cytospin Centrifuge were also tested. Cells fixed in PBS with glutaraldehyde and paraformaldehyde and then centrifuged onto slide surfaces coated with Gap8.3 antibody overnight gave the best results (Figure 4.8).

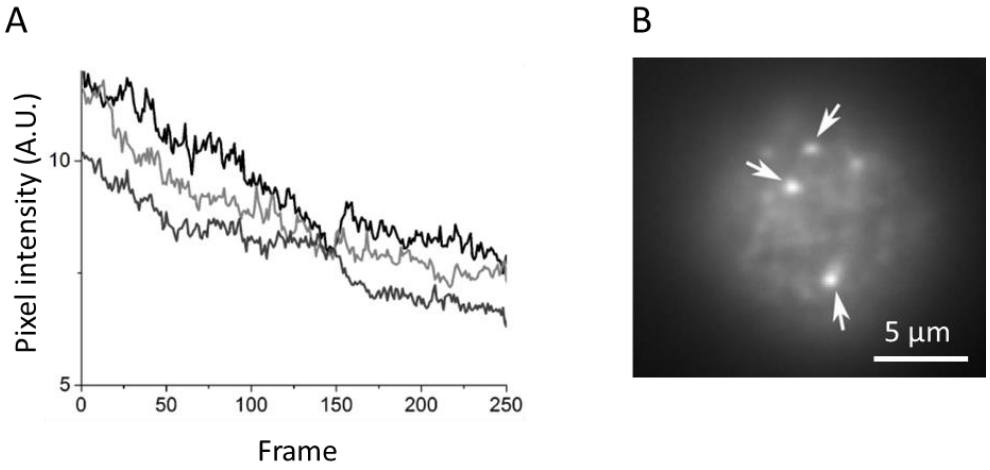

Figure 4.7: Clustering of TCRs expressing TCRβ-mEos2 fusion protein placed onto IgG-coated coverslips. The cells were imaged using both 561 nm TIRF illumination and low-level, continuous 405 nm activation. (A) The pixel intensity traces of three bright and immobile objects identified with the white arrows in (B). The complex photo-bleaching curves indicate that the bright objects are likely clusters of TCRs. A.U., arbitrary units. The figures present from Dr Matthieu Palayret.

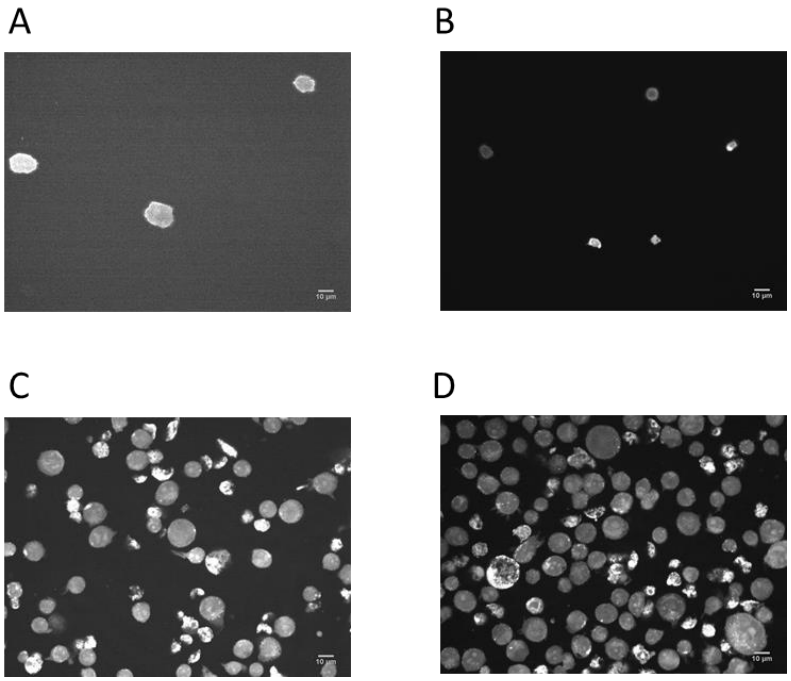

Figure 4.8: Generation of large contact areas for PALM imaging. (A) After fixation with 0.2 % glutaraldehyde and 4% paraformaldehyde but no centrifugation, the average contact area was 204.73 μm^2 but relatively few cells attached to the Gap8.3 anti-CD45 antibody-coated surface. (B) Following fixation in 0.4% glutaraldehyde and 4% paraformaldehyde and no centrifugation the average contact area was 77.88 μm^2. Following Cytospin deposition of the cells onto the antibody-coated surface and fixation in 0.2 % glutaraldehyde and 4% paraformaldehyde (C), or 0.4 % glutaraldehyde and 4% paraformaldehyde (D), the average contact areas were 142.56 and 160.10 μm^2, respectively.

(b) PALM imaging of the TCR on fixed cells

Unexpectedly, PALM imaging showed that TCRβ-mEos2 distributions exhibited a great deal of heterogeneity among cells taken straight from tissue culture, with some cells exhibiting high levels of apparent TCRβ-mEos2 clustering; other cells showed much less clustering. Representative cells are shown in Figure 4.9. The mean numbers of localisations per cluster for the TCR and the monomeric and dimeric control proteins were determined. The mean numbers of spots per cluster were 1.4 for untransfected J.RT3-T3.5 cells, 2.1 for cells expressing the CD86-mEos2 monomeric control, 3.2 for cells expressing TCRβ-mEos2 fusion protein, and 4.5 for cells expressing the CD28-mEos2 dimeric control (Figure 4.10A). The numbers of clusters with more than three spots was also determined, and here the TCR behaved similarly to the CD86 monomer control rather than the CD28 dimer control, in that as most cells had 100 or fewer clusters containing more than three localisations. However, a small fraction of cells exhibited very large numbers of TCR clusters, exceeding even the number formed by CD28-expressing cells (Figure 4.10B). These observations suggested that the apparent TCR organisation varied significantly between cells and that for some cells TCRs could be induced to form clusters or high-order structures. One possibility is that the cells might be so sensitive to signalling effects, that interactions between cells and flask surfaces or between cells could lead to weak receptor triggering and re-organisation.

D. Dual super-resolution based strategy: PALM and STORM/dSTORM

These findings suggested that cells with lower TCR expression levels, which might be less prone to tonic signalling and might better reflect the “ground-state” TCR stoichiometry, might be preferable for imaging and analysis. To get homogeneous expression and to achieve lower overall expression levels, the cells were FACS-sorted

Figure 4.9: Super-resolution PALM imaging of TCRs on T cells fixed immediately from culture. (A) J.RT3-T3.5 cells expressing CD86-, CD28- and TCRβ-mEos2 fusion proteins were imaged using dSTORM. Each mEos localisation is shown and coloured according to its acquisition time, from purple (t=0) to red (end of acquisition time). Likely cell outlines are indicated with dotted lines. In (B) the regions marked with squares in panel A are shown magnified. The post-hoc data process was undertaken by Dr Matthieu Palayret and Dr James McColl.

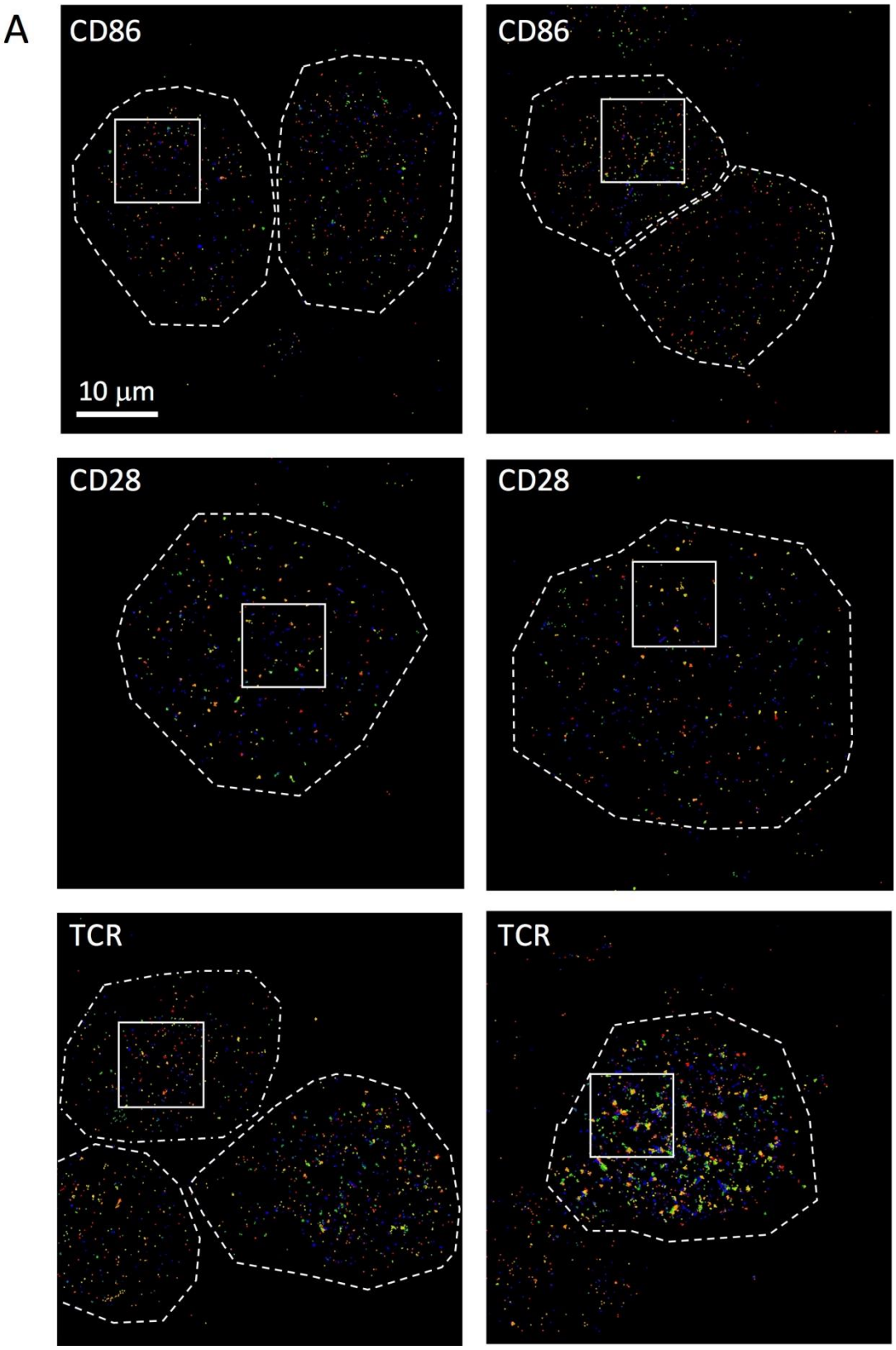
A
CD86
CD86
10 µm
CD28
CD28
TCR
TCR

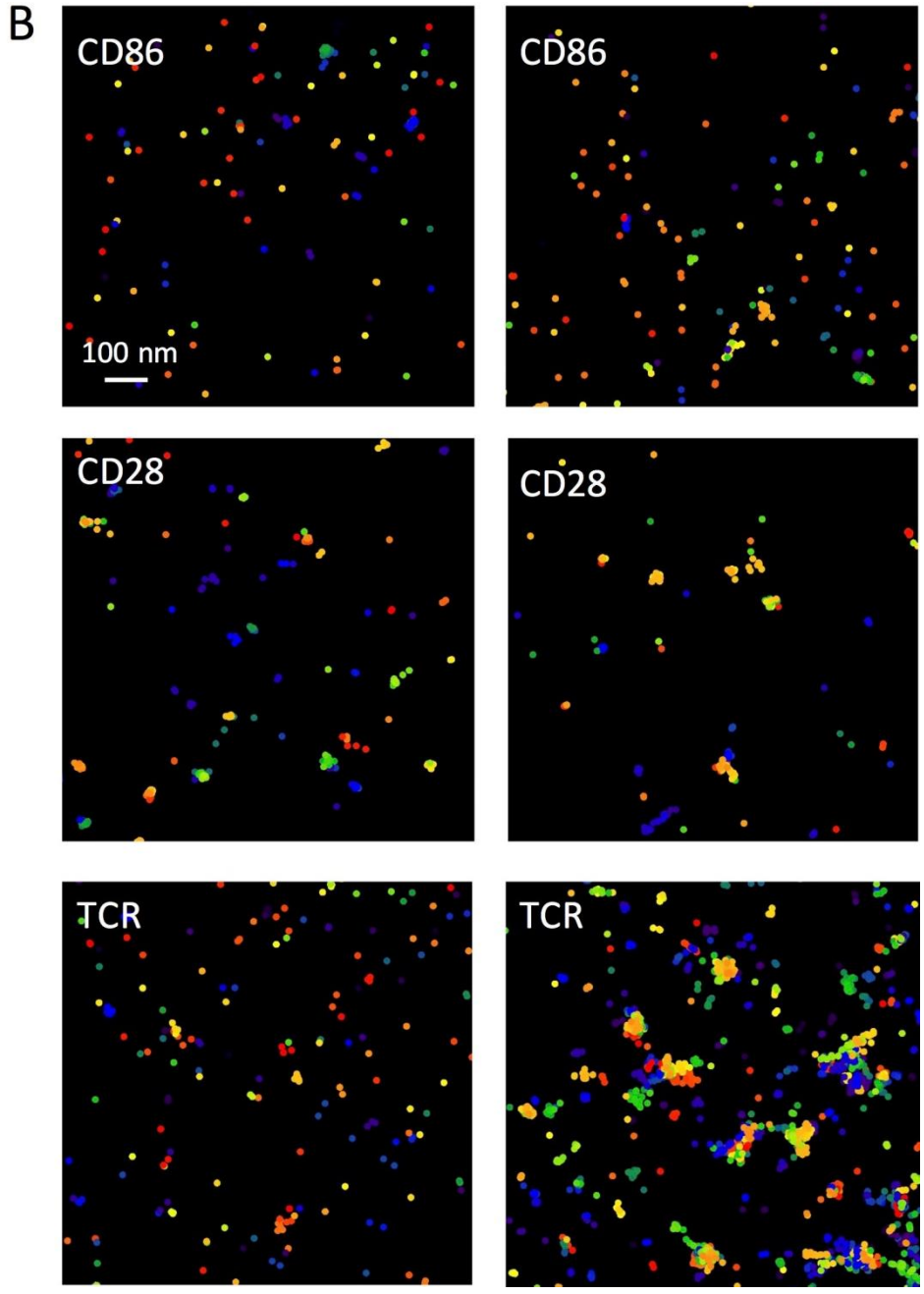
B
CD86
100 nm
CD86
CD28
CD28
TCR
TCR

Figure 4.10: Analysis of localisations per cluster. (A) Mean number of localisations (spots) per cluster for the untransfected J.RT3-T3.5 cells, and for J.RT3-T3.5 cells expressing the CD86-, CD28- and TCRβ-mEos2 fusion proteins. (B) Numbers of clusters per cell containing more than three localisations. The figures present the results of a single analysis of the PALM data undertaken by Dr Matthieu Palayret.

A

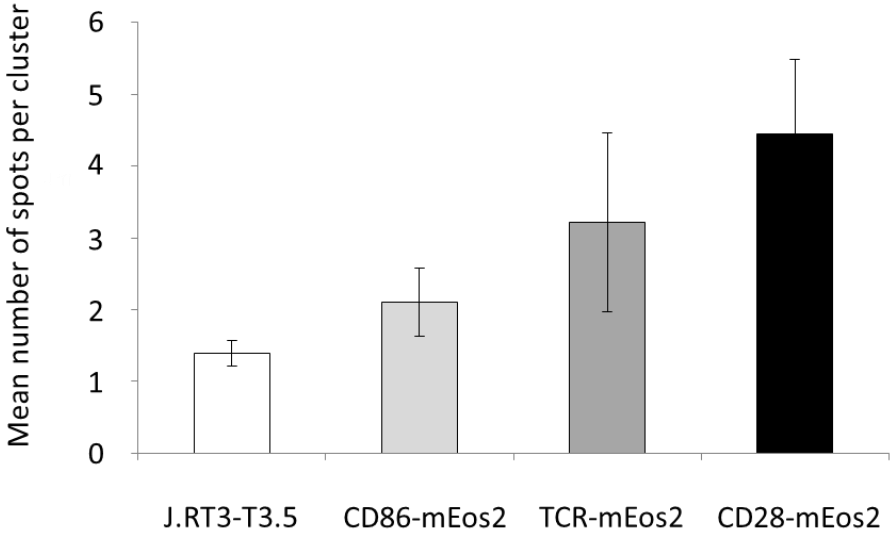
Mean number of spots per cluster
6
5
4
3
2
1
0
J.RT3-T3.5
CD86-mEos2
TCR-mEos2
CD28-mEos2

B

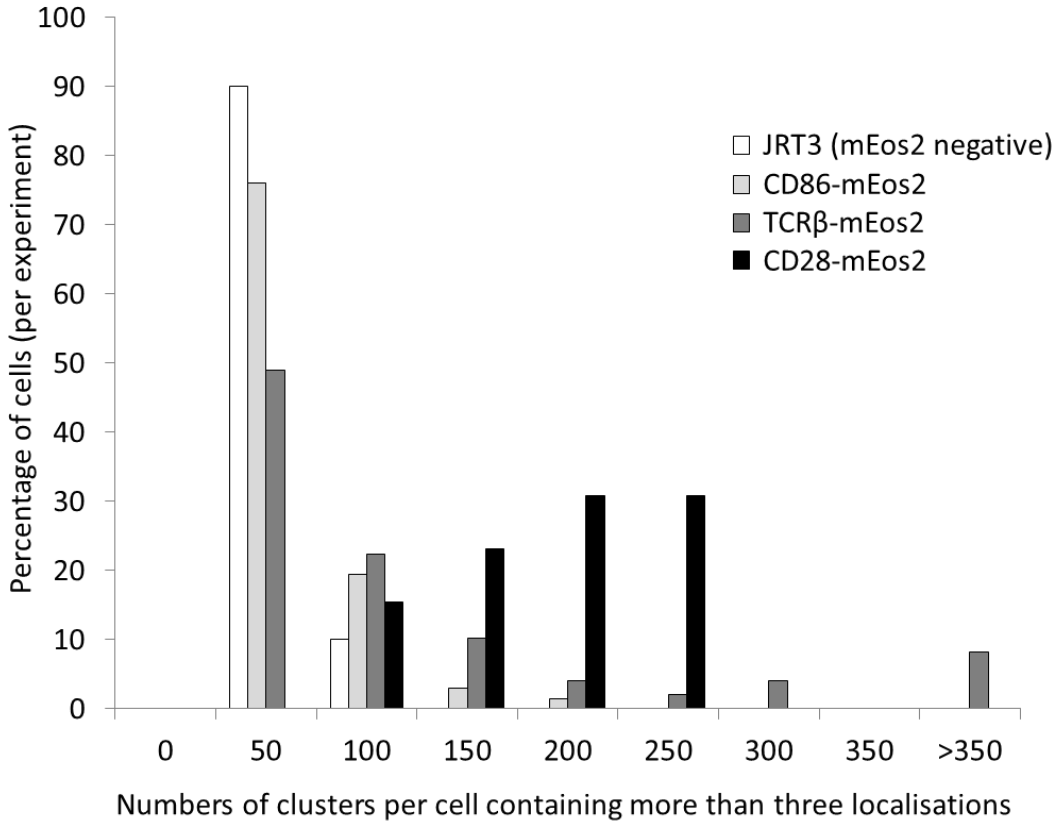
Percentage of cells (per experiment)
100
90
80
70
60
50
40
30
20
10
0
JRT3 (mEos2 negative)
CD86-mEos2
TCRβ-mEos2
CD28-mEos2
0
50
100
150
200
250
300
350
>350
Numbers of clusters per cell containing more than three localisations

into three or four sub-populations according to the intensity of mEos fluorescence which was then matched with those for CD86 and CD28 (Figure 4.11). Cells with CD86-mEos2 proteins were sorted into three populations while those with CD28-mEos2 were sorted into four. This was because the cells in general expressed fewer CD86-mEos2 proteins and had a narrower range of CD86-mEos2 fluorescence intensity than those expressing CD28. Cells with TCR-mEos2 proteins were sorted into three sub-populations since an additional set of cells were generated that expressed TCRβ-mEos2 proteins transcribed from the inducible promotor of the pHRI vector, which gives low expression.

However, in the sub-populations expressing low levels of protein it was very difficult to distinguish signals from background fluorescence. In addition, since <100% of single-colour fluorescence signals will be detected and localised in any single super-resolution experiment, the probability of monomers would normally be over-estimated. In an attempt to circumvent these limitations, PALM and dSTORM were combined to allow imaging signals to be distinguished from the background by only considering spots with signals from both mEos and fluorescently labelled Fabs, and to help reduce the monomer bias. In the new strategy, receptors fused with intracellular mEos fluorescence imaged with PALM were stained with fluorescently-labelled Fabs extracellularly and also imaged using STORM. Initially, it was intended that mEos2 be paired with Atto 655 for PALM and STORM, since mEos and Atto 655 have well-separated absorbance and emission spectra as well as comparable imaging solvent compatibilities for photo-conversion in the dual super-resolution based imaging strategy [329, 330]. However, unexpectedly, it was impossible to make functional anti-CD3ε UCHT1 Fabs labelled with Atto 655 dyes for dSTORM. Although efficient Fab labelling could be achieved, cells expressing TCR/CD3 complexes could not be labelled with the Fabs, even at high concentrations

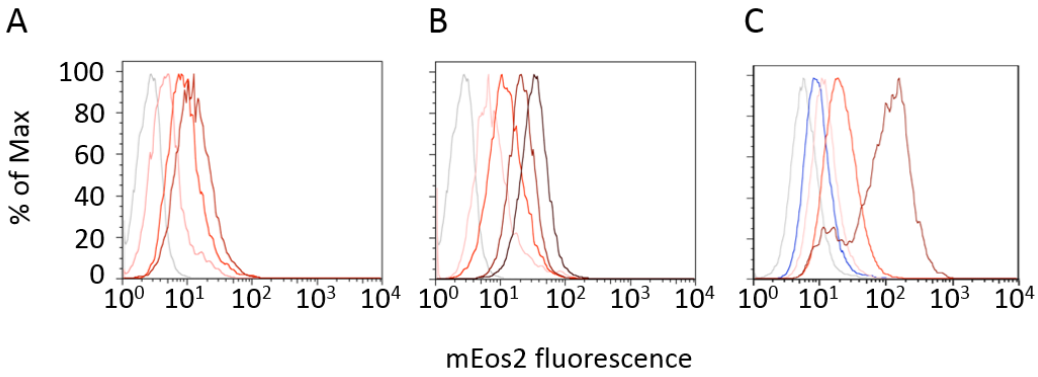

Figure 4.11: Analysis of expression levels of receptors using FACS. The J.RT3-T3.5 cells analysed express CD86- (A), CD28- (B) and TCRβ-mEos2 (C) fusion proteins. The grey curve corresponds to untransfected J.RT3-T3.5 cells.

(data not shown). This implied that labelling with Atto655 had some effect on binding of UCHT1 Fab to CD3ε in the TCR complex, for example via steric hindrance, or destruction of the paratope of UCHT1. However, UCHT1 Fabs could be readily labelled with Alexa Fluor® 488 or with Alexa Fluor® 647 and these Fabs gave good TCR staining (data not shown). Unfortunately, however, dual PALM/dSTORM super-resolution imaging proved to be impossible due to the photo-physics of these dyes. If 561 nm and 405 nm illumination were first used for PALM imaging of mEos, the Alexa Fluor® 647 dyes would be too heavily bleached by the 561 nm illumination to be useful for dSTORM imaging. If, on the other hand, 640 nm illumination and constant 405 nm illumination were first applied for imaging Alexa Fluor® 647 in dSTORM experiments, the TCRβ-mEos2 proteins would be pre-activated by the 405 nm illumination, preventing PALM imaging.

E. Cluster analysis

In a final set of super-resolution experiments, dSTORM analysis of the pre-TCR expressed by transfected DO11.10 cells was returned to. The problem of receptor over-expression and weak-signalling induced clustering was less of an issue because the pre-TCR was expressed weakly in these cells [233, 331, 332] (Figure 4.12). In the course of these experiments Baumgart *et al.* published a study showing that dSTORM/PALM analysis is prone to a "cluster-bias" since blinking receptors can be over-counted resulting in the incorrect identification of clusters [238]. Their approach involved the deliberate variation of labelling density, *e.g.* titration of fluorescent antibody, combined with quantitative cluster analysis. This required the analysis of the average densities of fluorophores detected (ρ) over areas covered by a mask (η). In the case of non-clustered molecules, or molecules in random diffusion, a largely constant value for ρ would be observed when the amounts of labelling with fluorescent

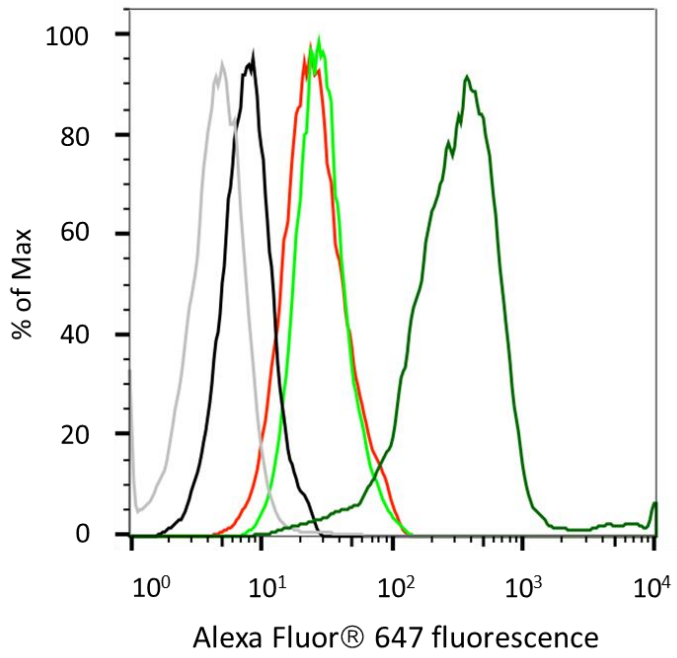

Figure 4.12: The expression levels of the pre-TCR and TCR on DO11.10 cells. Expression levels were measured using F23.1 (anti-mouse TCRβ) Fab conjugated with Alexa Fluor® 647 in the APC channel using FACS. Grey, DO11.10 cells without any staining. Black, DO11.10 cells stained with donkey-anti-mouse IgG conjugated with Alexa Fluor® 647 as a negative control. Red, pre-TCR expressing DO11.10 cells stained with the fluorescent F23.1 Fab. Bright green, FACS-sorted wild-type DO11.10 with TCR expression matched to the level of the pre-TCR, stained with the F23.1 Fab. Dark green, wild-type DO11.10 cells stained with the F23.1 Fab.

antibodies increased. On the other hand, for clustered molecules, ρ would increase proportionally with η. An analysis of the pre-TCR dSTORM data in this context was undertaken by Dr James McColl in Prof. David Klenerman's group at the University of Cambridge.

In preliminary experiments, control monomeric glycosylphosphatidylinositol (GPI)-linked GFP data was obtained from Dr Baumgart in Vienna, and processed using the code to give the characteristic "monomer" signal (*i.e.* no change in the ρ/ρ_0 ratio with η; Figure 4.13A). This required optimisation of some parameters used in Dr Baumgart's code. When CD86 dSTORM data collected with Dr McColl was analysed using the same code, this also gave the monomer signature (Figure 4.13B). In addition, preliminary dSTORM data for the pre-TCR expressed in DO11.10 cells was suggestive of the existence of pre-TCR non-clusters in Figure 4.13C.

In a second experiment, the pre-TCR and clathrin (used as a cluster control) were labelled with serial dilutions of Alexa Fluor® 647-labelled Fabs, and the numbers of total fluorophores detected per μm^2 counted using dSTORM at each concentration. Using the same parameters in the programme as those used in the pilot experiment, the pre-TCR exhibited behaviour that was clearly distinct from that of clustered clathrin (Figure 4.14), and was compatible with the low numbers of pre-TCRs on the DO11.10 T-cell surface exhibiting a random distribution.

III. Discussion

The work described in this chapter attempted to use and/or develop several super-resolution imaging-based techniques for analysing the stoichiometry of receptors, especially the pre-TCR and TCR, in situ. With regard to methodology, different imaging techniques were explored and several fluorescent labelling systems were

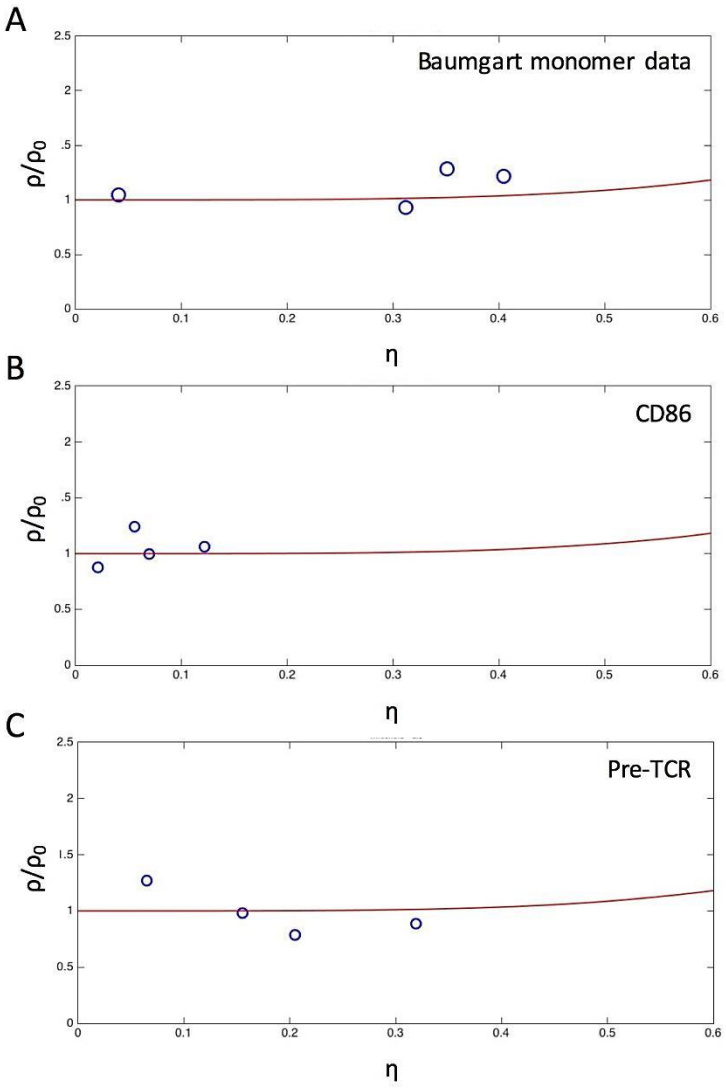

Figure 4.13: Preliminary analysis of dSTORM data using the approach of Baumgart *et al.* [238]. From dSTORM localisation maps, ρ and η values were calculated to generate normalised ρ/η plots. 10 or more images were recorded per titration step; each data point represents a single image. The red lines indicate the reference curve for a random distribution. In (A) sample monomer data was obtained from Dr Baumgart in which mGFP-GPI expressing CHO cells were stained with anti-GFP-Trap-Alexa Fluor® 647 at the concentrations of 0.003, 0.03, 0.3 and 3 μg/mL. The ρ/η plots were re-calculated using his algorithm. In (B) and (C), preliminary CD86 and pre-TCR data were analysed. The data analysis was undertaken by Dr James McColl, Cambridge University.

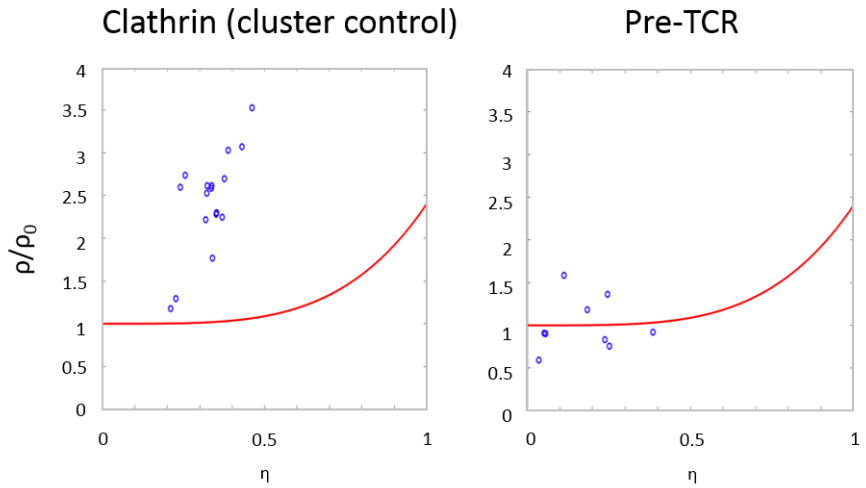

Figure 4.14: Pre-TCR cluster analysis using the method of Baumgart *et al.* [238]. From dSTORM localisation maps, ρ and η values were calculated to generate normalised ρ/η plots plots for (left) clathrin present on DO11.10 cells used as a cluster control stained with fluorescent (Alexa 647 tagged) anti-clathrin heavy chain Fab at concentrations of 1, 2 and 5 μg/mL, and (right) the pre-TCR expressed by DO11.10 cells stained with fluorescent F23.1 Fab at concentrations of 1, 5, 10 and 50 μg/mL. The red line indicates the reference curve for a random distribution. The data analysis was undertaken by Dr James McColl, Cambridge University, using the original code from Baumgart *et al.* [238].

optimised. It is worth noting that it did appear as if T cells exhibited heterogeneity in their TCR organisation even when obtained as resting cells direct from tissue culture. Confirmation that this is a signalling effect could be obtained by examining cells unable to signal, such as T cells lacking Lck or ZAP70. This also pointed to the potential difficulties in investigating the stoichiometry of TCRs with true resting status, and might partly explain the controversies concerning the organisation of TCRs and pre-TCRs (*i.e.* monomers versus clusters) in previous studies that utilised TCCD, DySCo, hsPALM, TEM, FRAP and X-Ray scattering as discussed in Chapter 1.

The HaloTag-based fluorescent labelling system was optimised here for obtaining better signal-to-noise ratios and for better image acquisition for facilitating subsequent analyses, in order to meet the requirements of each super-resolution imaging technique. Among the various ligands available, it was found that the pair of R110Direct and TMRDirect used at a concentration of 12.5 nM gave the best signal-to-noise ratio and the most efficient labelling needed for dSTORM imaging.

However, dSTORM-based imaging and photo-bleaching step analysis utilising HaloTag-fused receptors labelled with TMR revealed that HaloTag Ligands have limitations with respect to their photo-chemistry in certain contexts which prevented the analysis of stoichiometry using photo-bleaching steps. Whereas TMR was claimed to exhibit single exponential decay in another study [333], the photo-bleaching steps in the trials in the present study did not exhibit the necessary simplicity allowing to identify the stoichiometry of receptors, even for monomeric and dimeric controls. Both over-counting of putative monomers (due to under-labelling of dimers) and under-counting of monomers and dimers (due to complex decay kinetics) might each have occurred. More recently, TMR, without any chemical modifications, used as a HaloTag Ligand has been confirmed independently to be ill-fitted by single exponential decay models due to structure-mediated non-radiative decay [327, 328, 334]. Although

the HaloTag-based labelling system in this chapter was unsuitable for generating stoichiometric data using photo-bleaching, the pilot experiments laid the foundations for other imaging work in the laboratory [183].

In a second approach, an attempt was made to use the super-resolution PALM method, which relied on the mEos photoactivatable fluorescent protein. This approach gave very promising data, but pointed to the issue of receptor organisation heterogeneity among resting cells straight from culture. On balance, the TCR behaved more like the monomeric control (CD86) than the dimer control (CD28), however. In this experiment, the apparent clustering of the monomer control might in principle be attributable to "blinking" of the fluorescent protein as proposed by Baumgart *et al.* [238], but this was not directly tested.

To have an expression level-independent investigation, the mEos-fused receptors were then sorted based on their expression levels. It was planned that TCRs would be compared with monomeric or dimeric control receptors such as CD86 and CD28 with correspondingly similar low expression levels on the cell surface. However, at the lower expression levels the signal-to-noise ratios were too low to be confidently able to distinguish fluorescent spots from the background. This may reflect the limited photo-conversion efficiency of current fluorescent dyes and proteins [335, 336].

To overcome the signal to noise issue, an attempt was made to couple PALM and dSTORM. However, it was unfortunate that a promising dye for this experiment, *i.e.* Atto 655, destroyed the activity of the Fab. When Atto 655 was replaced with Alexa Fluor® 647, there became the issue of overlapping of wavelength spectra and the problem of pre-bleaching of the Alexa Fluor® 647, or of pre-activating of mEos before image acquisition. A different antibody allowing Atto 655 labelling might have allowed the application of the dual super-resolution imaging strategy to investigate TCR stoichiometry.

Finally, using dSTORM and the approach to cluster analysis proposed by Baumgart *et al.*, our preliminary data suggested that the pre-TCR is not clustered on transfected DO11.10 cells. The approach of Baumgart *et al.* avoided artefacts such as over-counting of blinking fluorophores from the super-resolution imaging analysis [238, 337]. Although this approach apparently distinguished clusters from non-clusters, it however failed to allow monomers to be distinguished from dimers, or even higher oligomers if they all diffused randomly or shared similar diffusion behaviours. In addition, other possible technical limitations of this approach relates to those membrane proteins diffusing in a cytoskeleton-confined area or those natively expressing at low levels. For example, lower expression levels of CD86 and pre-TCR on the membrane limited the degrees of increase in the mask area (η). Thus, further optimisation and more control experiments would be required to reach a firm conclusion.

Chapter 5

Stoichiometric analysis of the TCR and pre-TCR using single-molecule two-colour co-localisation

I. Introduction

In Chapter 4, initial dSTORM super-resolution data was presented that suggested that the pre-TCR could be randomly organised at the surface of a transfected T-cell hybridoma. In work described in this chapter, attempts were made to complement these findings using single-molecule, two-colour co-localisation tracking to determine the stoichiometries of the TCR and pre-TCR.

The two-colour co-localisation method is based on the principle of DySCo, used previously by this laboratory to quantify the association levels of proteins at low surface-expression levels [236]. The principle is that two proteins labelled with different fluorophores are tracked over multiple time frames using Bayesian-based inference methods. The centroid positions of the fluorophores, with a defined threshold for the fluorescence signal, are first identified. A modified sequential Monte Carlo algorithm and track-before-detection scheme incorporated into the Bayesian-based inference approach then allows fluorophores to be linked in subsequent frames, and single molecules to be tracked [264]. DySCo overcame several previous technical difficulties in tracking fluorophores in two colours with low expression levels or with low mobility [235, 236, 264].

Using DySCo, the false-positive coincidence level could be minimised for random associations of receptors, owing to the low surface densities of the fluorescent proteins.

The randomly associated, or non-associated proteins showed distinct trajectories versus associated proteins, which showed correlated trajectories, allowing constitutive oligomers to be distinguished from freely diffusing monomers (Figure 5.1). The results from DySCo analysis [236] showed that co-association levels exhibited by the TCR were very similar to that of a monomeric control protein, CD86, and very different from that for a dimeric control (CD28). This result complemented work on the TCR using TCCD [3], the method used also to show that the rest of the triggering apparatus of the T cell, *i.e.* MHC molecules, CD4/Lck and CD45, are exclusively monovalent or monomeric [180]. Since pre-TCR surface expression levels in transfected cells (and likely *in vivo*) are very low, the pre-TCR is especially well-suited to DySCo analysis. Since it was first used, an improved form of DySCo, called single-molecule cross-colour coincidence detection (SMCCCD) has been developed [338]. This method continued to utilise comparisons with well-characterised control proteins, but relied on cell fixation to limit artefacts arising from differences in the distribution and diffusion of test proteins versus these controls [338]. Instead of tracking molecules, measures of coincidence (*i.e.* co-localisation) were made. In its first implementation, SMCCCD was used to distinguish between the stoichiometric behaviour of G protein-coupled receptors [338]. In this chapter, SMCCCD is used to probe the organisation of the TCR and pre-TCR.

II. Results

A. Two-colour co-localisation imaging strategy

The in situ stoichiometries of the mouse TCR expressed by DO11.10 cells, the mouse pre-TCR expressed by CRISPR/Cas9-engineered DO11.10 cells, and the native pre-TCR expressed by mouse thymocytes, were analysed using SMCCCD, and

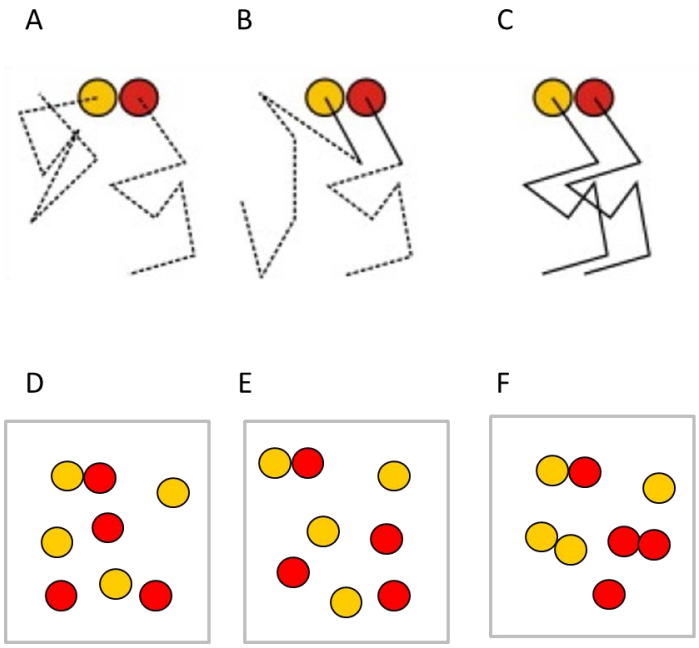

Figure 5.1: The principle of DySCo and SMCCCD. In DySCo, proteins labelled with two fluorophores are tracked over multiple frames and further analysed using a Bayesian-based inference approach. (A) Non-associated, monomeric proteins. (B) Monomers randomly associated with each other over only a short period of time, and not for multiple frames. (C) Co-localisation of associated proteins over time as expected for a dimer. In SMCCCD, protein-of-interest (D) are labelled with two fluorophores and fixed. Coincidence events are measured and compared with the monomeric control proteins (E) and dimeric control proteins (F). Figure (A)-(C) are re-presented from [236].

compared with the stoichiometry of mouse CD86 (as the monomeric control) and mouse CD3ε (as a dimeric control) expressed on the surfaces of DO11.10 cells. Because there was substantial heterogeneity in apparent TCR stoichiometry observable on a cell-to-cell basis using dSTORM (Chapter 4), mature TCRs expressed at several different expression levels on DO11.10 cells were investigated. Anti-receptor Fabs, *i.e.* anti-mouse TCRβ Fab, anti-mouse CD86 Fab and anti-mouse CD3ε Fab, were labelled either with Alexa Fluor® 488 or Alexa Fluor® 647, and the stoichiometry of pre-TCR, CD86, TCR and CD3ε determined by coincidence levels of molecules labelled with the two fluorophore-tagged Fabs. These experiments were done in collaboration with Dr. James McColl and Anna Lippert in Prof. David Klenerman's group at the University of Cambridge. Mouse thymocytes were obtained and sorted with the help of Dr. Consuelo Anzilotti of Prof. Richard Cornall's group (Oxford) and Craig Waugh at the WIMM Flow Cytometry Facility in Oxford.

(a) Hybridoma-expressed pre-TCR and TCR

Since native pre-TCR expression is low on both mouse and human cells [233, 331, 332], DO11.10 cells expressing a low amount of mouse pre-TCR (Figure 4.12) were used. These cells expressed ~20-fold less pre-TCR than the level of mature TCR expressed by the DO11.10 hybridoma. In addition, DO11.10 cells were sorted for comparable levels of CD86. Anti-mouse CD86 Fab and KT3 (anti-mouse CD3ε) Fab were generated from monoclonal antibodies using papain or ficin (Figure 5.2). F23.1 anti-mouse TCRβ Fab had previously been generated by Dr John James. Each Fab was labelled with either Alexa Fluor® 488 or Alexa Fluor® 647. Binding of labelled Fabs to the cognate receptors was tested by FACS before use.

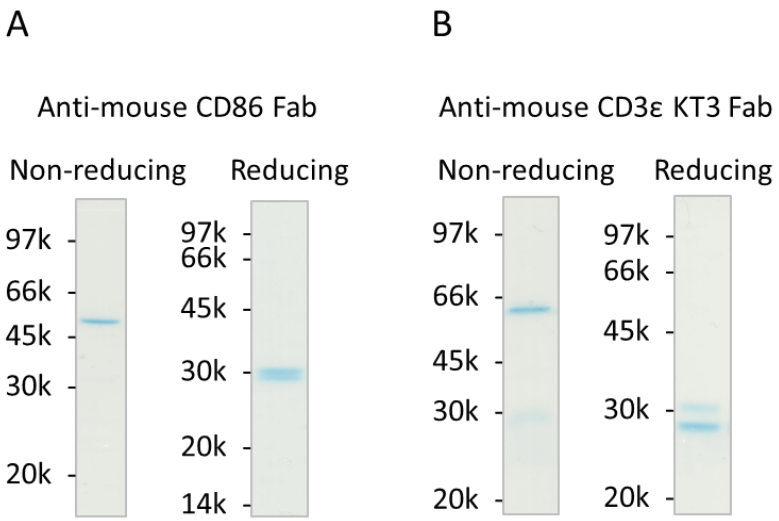

Figure 5.2: SDS-PAGE gel analysis of Fabs. Fabs were digested from the full antibodies using papain or ficin and further purified using a protein-G agarose column and FPLC. (A) Digested anti-mouse CD86 Fab on non-reducing and reducing SDS-PAGE gels. (B) Digested anti-mouse CD3ε KT3 Fab on non-reducing and reducing gels. Molecular-weights of size markers are shown in Daltons. Representative gels are shown.

i. Coincidence analysis

The DO11.10 cells or mouse pre-TCR expressing DO11.10 cells were labelled with Fabs and then fixed with paraformaldehyde and glutaraldehyde before being imaged using TIRF microscopy. The labelled proteins were imaged in fixed cells for 400 frames with an exposure time of 35 ms per frame. Multiple frames were collected to exclude the small fraction of residual mobile proteins that could bias the measurements of coincidence. Fixation generally reduces the movement of most fluorescent objects such that <6% of spots on fixed cells showed enough movement to leave the diffraction-limited starting position within 10 frames. After this, the individual fluorescent puncta were identified using a custom algorithm [339] and were selected using the thresholds for the size, distance and intensity, *i.e.* the maximum size of each fluorescent spot was 5 pixels, the maximum distance between 2 fluorescent spots was 300 pixels, and the minimum and maximum intensities for each fluorophore was 7 and 5000 arbitrary fluorescence units (A.U.; standard deviations above the background), respectively. Overall, more than 97% of fluorescent spots were correctly selected by the custom software (Figure 5.3); representative examples of spot detection are shown in Figure 5.4.

The selected fluorescent spots were then analysed for non-random co-localisation. Coincident events were defined as spatially isolated, diffraction-limited fluorescent puncta within 300 nm of a fluorescent spot detected in the other channel. The distance criterion was based on the positional accuracy for the channel alignment, and the use of 10 frames ensured that the signal/noise ratio was optimised. Initial work showed that the controls in the SMCCCD experiment were 4% and 15%, respectively (Figure 5.5), indicating that the method could easily distinguish between monomeric and dimeric type I membrane proteins. Somewhat unexpectedly, the coincidence level

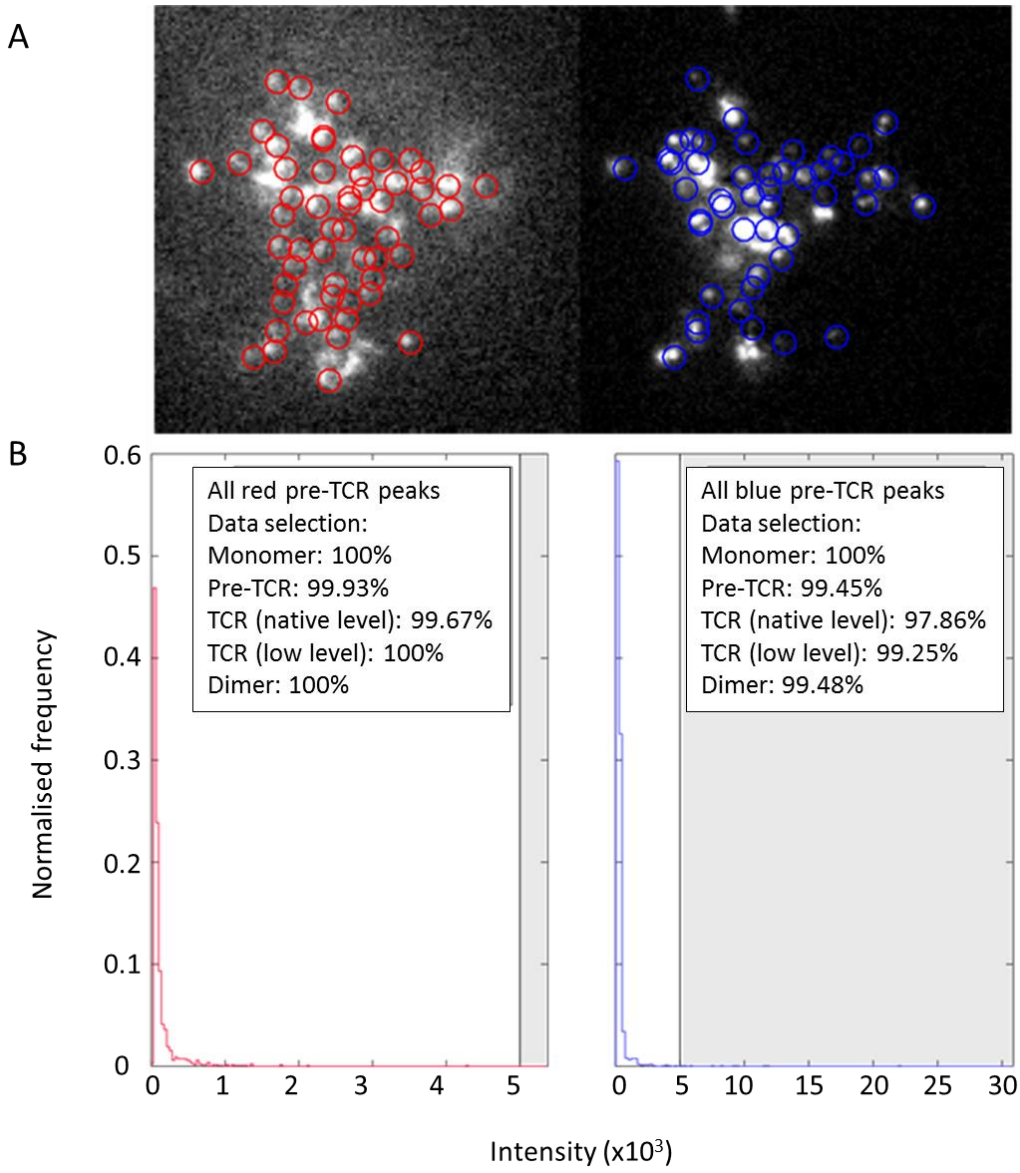

Figure 5.3: Selection of fluorescent spots by the bespoke algorithm [339]. For inclusion in the analysis the maximum size of each fluorescent spot was 5 pixels. The maximum distance between 2 fluorescent spots was 300 pixels, and the minimum intensity for each fluorophore was 7 A.U. The maximum intensity for each fluorophore was set at 5,000 A.U. (A) Representative raw images for data selection. (B) Fraction of all fluorescent spots in raw data in each group selected for SMCCCD analysis. Plots of the intensity variation of selected spots are also shown. Original code developed by Dr James McColl and Anna Lippert.

Figure 5.4: Representative raw and reconstructed co-localisation data. (A) Representative data for mouse CD86 monomeric control using anti-mouse CD86 Fab labelled with either Alexa Fluor® 488 or Alexa Fluor® 647; (B and C) Two examples of data for mouse pre-TCR obtained using F23.1 Fab labelled with either Alexa Fluor® 488 or Alexa Fluor® 647. (D) Representative data for mouse CD3ε dimeric control using KT3 Fab labelled with either Alexa Fluor® 488 or Alexa Fluor® 647. In each panel, the top row shows raw data, and the bottom row shows reconstructed data following spot detection. Scale bar, 1 μm. Data collection in collaboration with Dr James McColl.

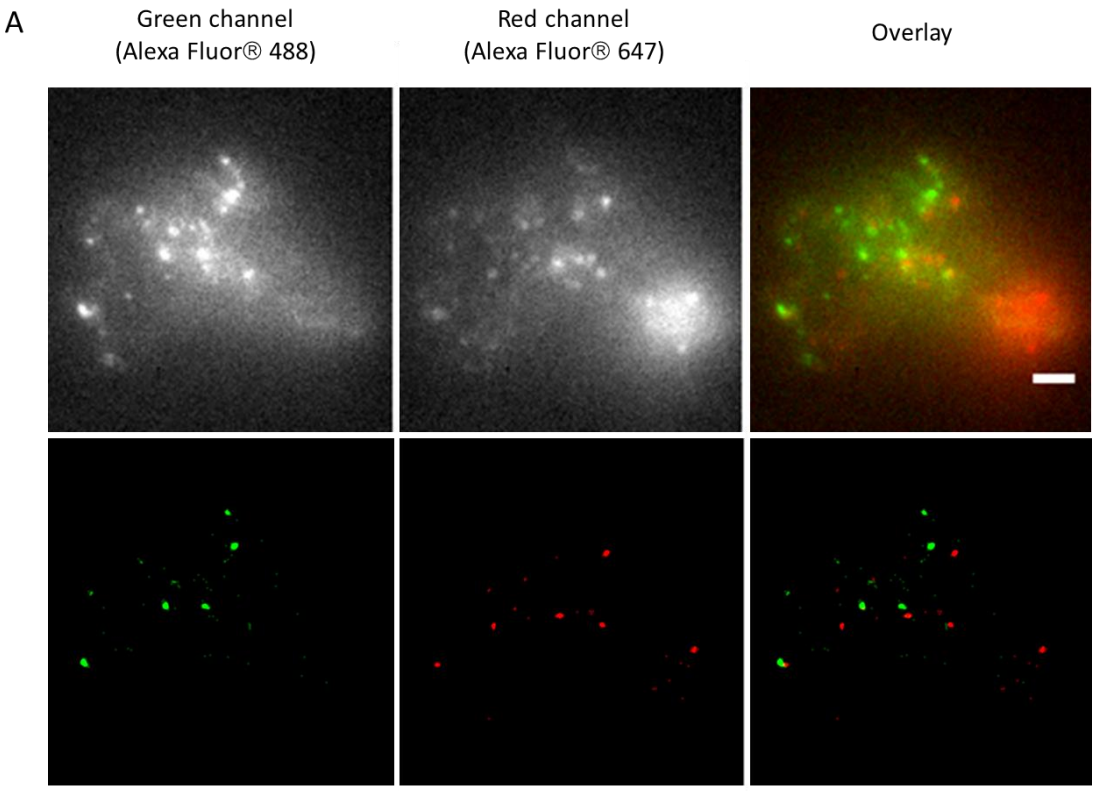
A
Green channel
(Alexa Fluor® 488)
Red channel
(Alexa Fluor® 647)
Overlay

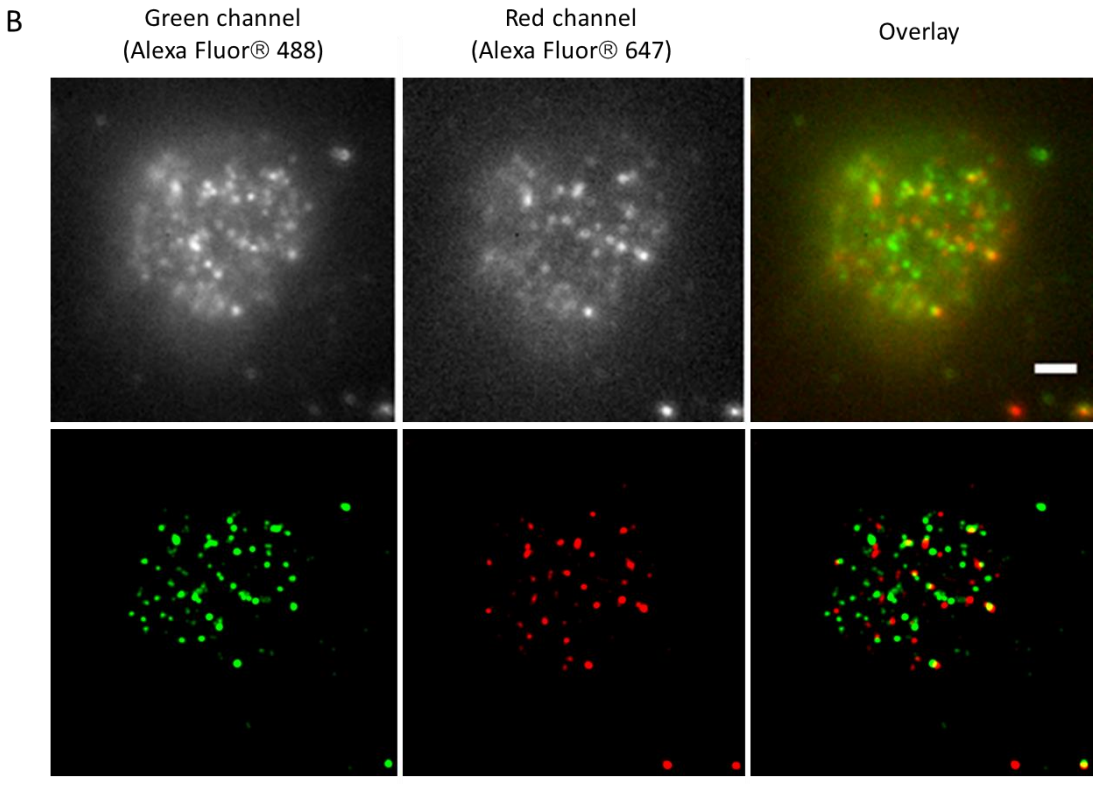
B
Green channel
(Alexa Fluor® 488)
Red channel
(Alexa Fluor® 647)
Overlay

C

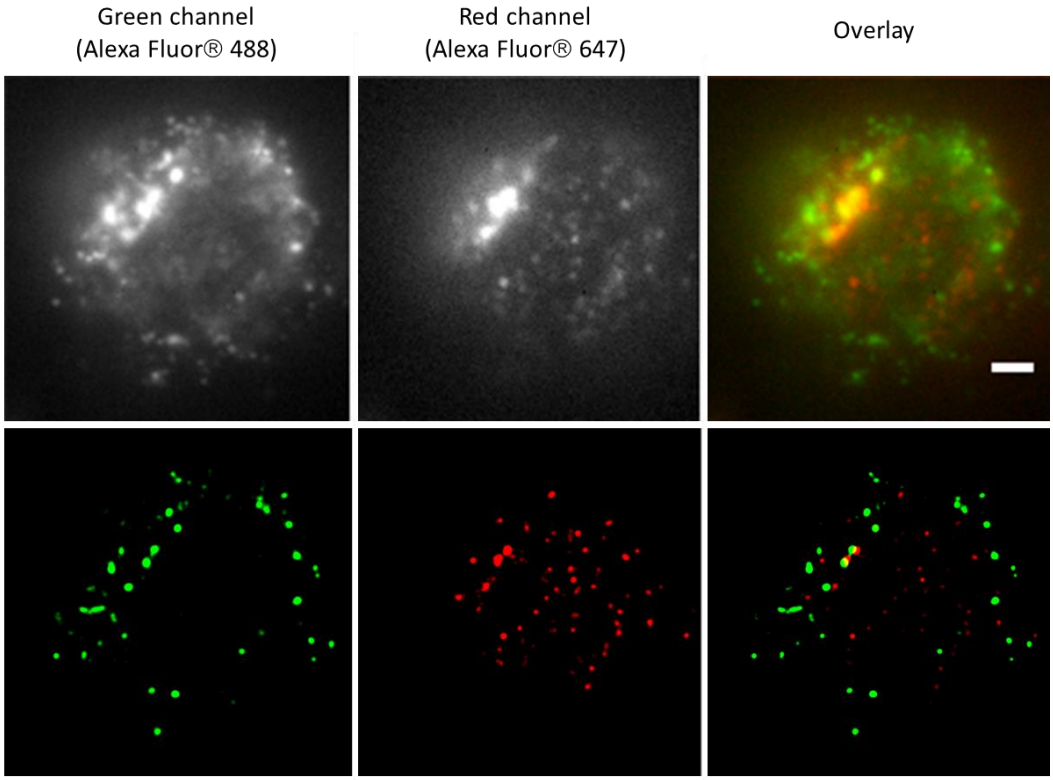
Green channel
(Alexa Fluor® 488)
Red channel
(Alexa Fluor® 647)
Overlay

D

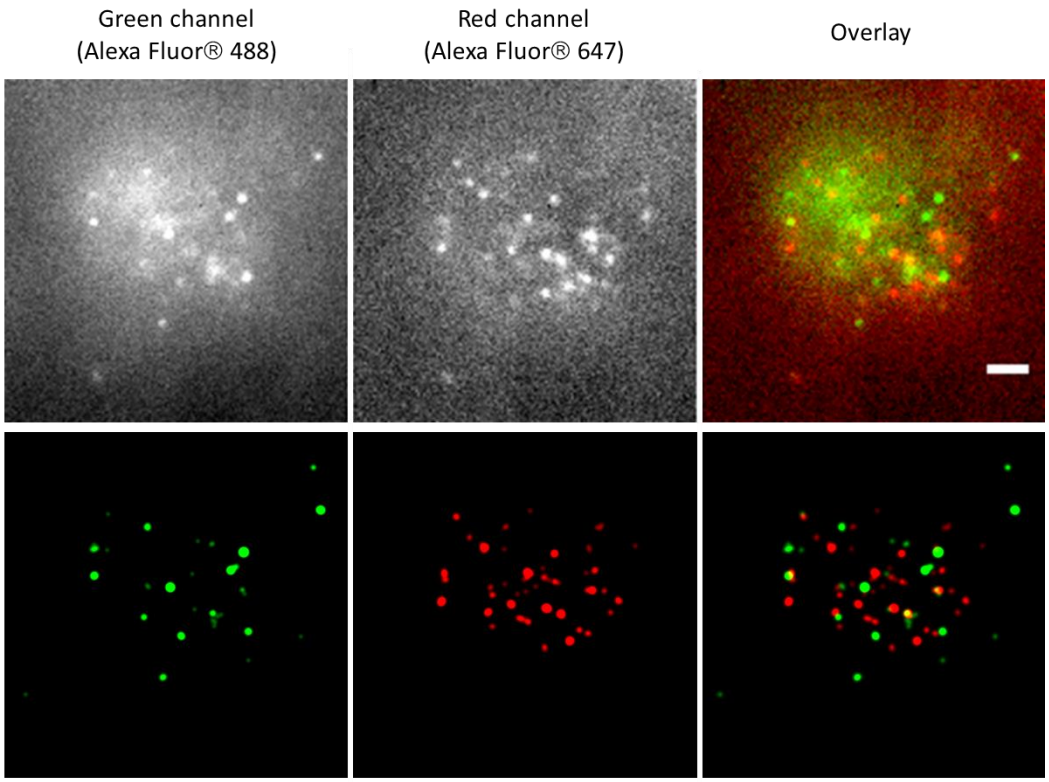
Green channel
(Alexa Fluor® 488)
Red channel
(Alexa Fluor® 647)
Overlay

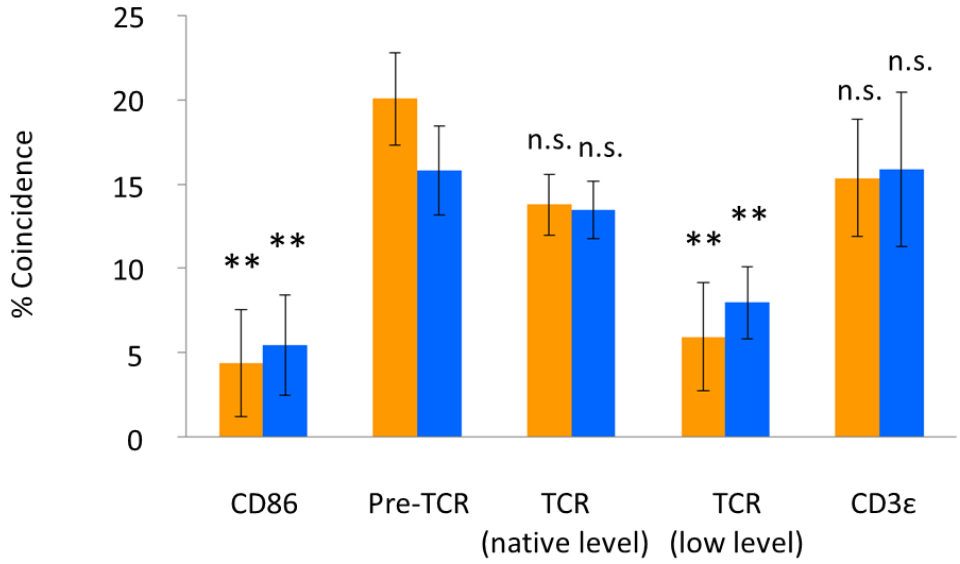

Figure 5.5: Coincidence levels in SMCCCD experiments. Measurements for mouse TCRs (expressed at two different levels) and for pre-TCRs (expressed at low "physiological" levels), versus coincidence levels measured for CD86 monomeric and CD3ε dimeric controls, are shown. Orange, the first experiment; blue, the second experiment. Statistical comparisons of the % coincidence for pre-TCRs versus the other receptors were performed using student's two-tailed t-test. *P*-value is indecated with: **, $p \leq 0.01$; n.s., $p > 0.05$. Error bars show standard error of each mean.

obtained for the mouse pre-TCR was 20%, suggesting that the pre-TCR has a clear tendency to form either dimers or higher-order oligomers in transfected cells. The coincidence level for the pre-TCR was significantly higher than that of the mature TCR expressed at a similar level, and higher than that of the CD86 monomeric control (Figure 5.5).

Interestingly, the coincidence level for the mature mouse TCR at native expression levels was also higher than expected at 14%, very close to that of the dimeric control. In contrast, for mature TCRs expressed at the level of the pre-TCR in these experiments, the coincidence level was comparable to the monomeric control. Importantly, the overall Pearson correlation coefficient (R) between the coincidence levels and the average numbers of spots were 0.68, 0.10, 0.21, 0.34 and 0.16 for CD86, pre-TCR, TCR at native levels, TCR at low levels and CD3ε, respectively. This indicates that for the pre-TCR and TCR, there was no effect of expression level on the amount of coincidence observed.

ii. Intensity analysis

To examine whether the pre-TCR in these experiments was forming a dimer, as would have been predicted based on the crystallographic analysis of the pre-TCR [233], an intensity analysis was undertaken. The fluorescent spots from mouse pre-TCR, monomeric mouse CD86, and dimeric CD3ε were analysed using the same thresholds for size, distance and intensity for fluorescent spot selection as described in II.A.(a).i. in this chapter.

As shown in Figure 5.6, under the same experimental conditions, the average intensity of monomeric mouse CD86 fluorescent spots was ~5,000 A.U. ($\log_{10}$ 5,000=3.70) while that of dimeric mouse CD3ε fluorescent spots was about 20,000 A.U. ($\log_{10}$ 20,000=4.30). For the pre-TCR, the average intensity was about 100,000 A.U.

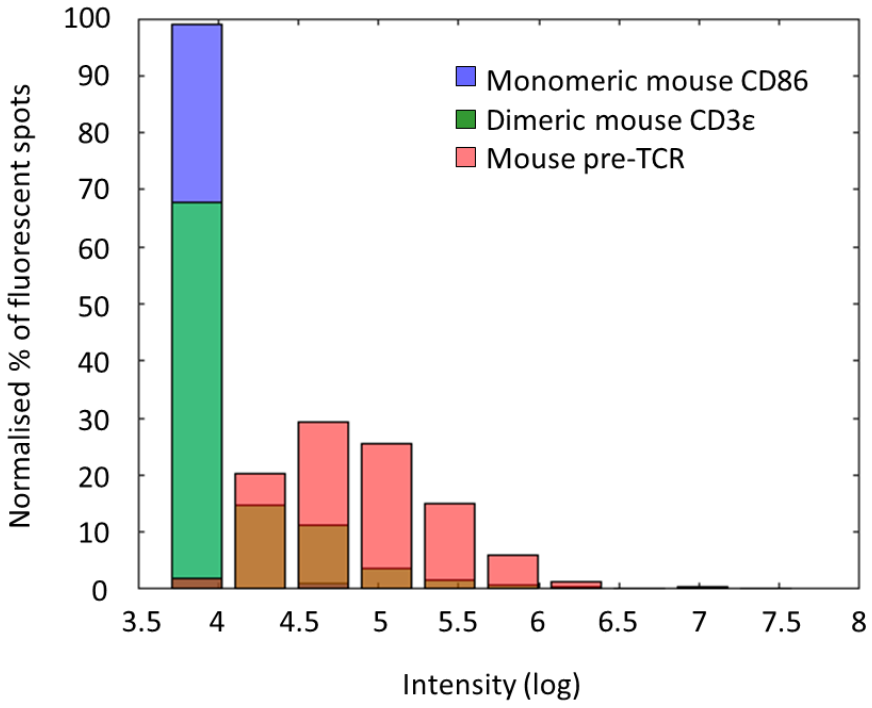

Figure 5.6: Intensity analysis of receptor fluorescence. The blue, green and pink bars show the intensity distributions for monomeric mouse CD86, the CD3ε dimer and the mouse pre-TCR. The brown shading indicates overlap in the distributions of the mouse CD3ε dimer and mouse pre-TCR intensities. For selecting spots for intenisty analysis, the maximum size was five pixels and the maximum distance between two fluorescent spots was 300 pixels. The minimum intensity for each fluorophore was 7 A.U. and maximum intensity for each fluorophore 5,000 A.U. The numbers of spots was normalised to the total number of spots detected for CD86, dimeric mouse CD3ε and mouse pre-TCR, respectively (y-axis). The original code for the analysis was written by Dr James McColl and Anna Lippert.

($\log_{10}$ 100,000=5). These results implied that the pre-TCR is much more likely to form tetramers or even higher-order oligomers, rather than just simple dimers.

(b) Pre-TCR *ex vivo*

i. Cell isolation

An attempt was undertaken to examine the organisation of the pre-TCR on native mouse thymocytes undergoing β-selection. These cells do not express CD4 or CD8 and are therefore termed double negative (DN) cells. The DN cells can be further categorised based on the differential expression of cell surface markers including CD25 and CD44. Thymocytes start to express pre-TCRs from the DN3 stage ($CD4^-CD8^-CD25^+CD44^-$ thymocytes) after TCRβ gene rearrangement, through to the DN4 stage ($CD4^-CD8^-CD25^-CD44^-$ thymocytes). The pre-Tα subunit is then substituted by the mature TCRα subunit [81].

Pre-TCR expressing cells were isolated from the thymi of female C52BL/6 mice at the age of three to four months and selected with cell markers using FACS. To sort the pre-TCR expressing thymocytes at the DN3 and DN4 stages, a hierarchical sorting strategy was used. First, the thymocytes were sorted according to their size and granularity using forward and side scattering, and then negatively selected using DAPI (4',6-diamidino-2-phenylindole) to isolate live cells (Figure 5.7A-C). Following this, DN3- and DN4-stage thymocytes were negatively selected, using anti-CD4 and anti-CD8 antibodies (Figure 5.7D), and the cells were then selected using anti-CD25 and anti-CD44 antibodies (Figure 5.7E). Finally, the DN3 and DN4 thymocytes were sorted for F23.1 anti-TCRβ reactivity (using both Alexa Fluor® 488-labelled F23.1 Fabs and Alexa Fluor® 647-labelled Fabs, allowing subsequent SMCCCD analysis). However, very few DN3 cells were positively stained by the F23.1 Fab. Therefore, the

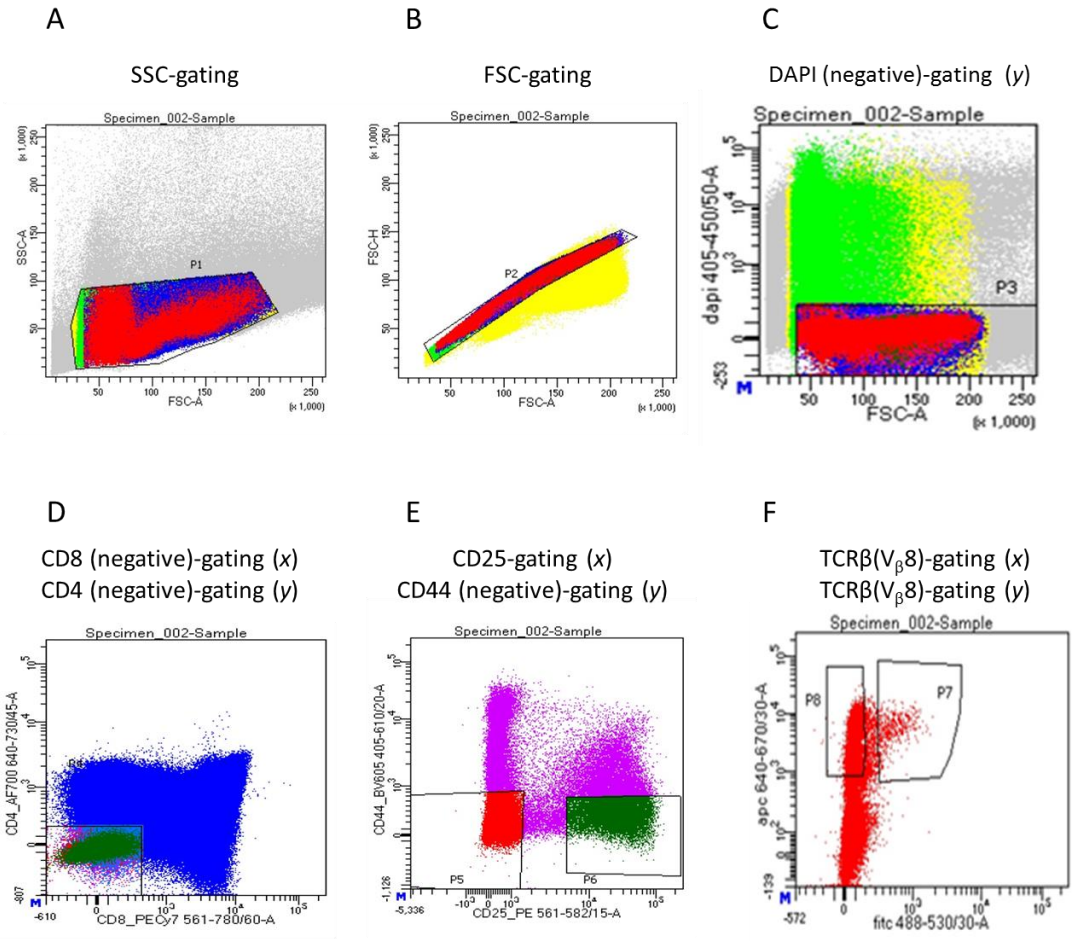

Figure 5.7: Strategy for the FACS-based hierarchical sorting of thymocytes from fresh mouse thymus (mice aged 12 weeks). (A and B) Gating of side-scattered light (SSC) and forward-scattered light (FCS), respectively. (C) Negative gating of DAPI for live healthy thymocytes. (D) Negative gating for CD4 and CD8 to obtain double negative (DN) cells. (E) Negative gating of mouse CD44 for both DN3 and DN4 cells. Further negative gating of mouse CD25 for DN4 cells (left square; Quadrant P5) and positive gating of mouse CD25 for DN3 cells (right square; Quadrant P6). (F) Positive gating from DN4 cells (Quadrant P5) for TCRβ(Vβ8)-specific pre-TCR(Vβ8) expressing DN4 cells. Gating thresholds were set using fluorescence-minus-one (FMO) controls. Mouse thymocytes were obtained and sorted with the help of Dr Consuelo Anzilotti and Craig Waugh.

focus was placed on DN4 cells and those positive for both Alexa Fluor® 488 and Alexa Fluor® 647 (Figure 5.7F; Quadrant P7) were sorted for the SMCCCD analysis. However, dual labelling of Alexa Fluor® 488 and Alexa Fluor® 647 also produced a degree of Förster resonance energy transfer (FRET) from Alexa Fluor® 488 to Alexa Fluor® 647, thus giving rise to the staining shown in Quadrant P8 in Figure 5.7F. The sorted DN4 cells (Figure 5.7F; Quadrant P7) were fixed in PBS with 4% (v/v) paraformaldehyde and 0.2% (v/v) glutaraldehyde overnight before being imaged the following day in Cambridge.

ii. Imaging the thymocytes

Attempts were made to apply the SMCCCD method to the analysis of the pre-TCR expressed natively by thymocytes (Figure 5.8). Two main issues prevented the acquisition of usable data, however. First, the thymocytes were smaller than the mouse cell lines used previously. Although the diameters of the thymocytes (about 1 μm as shown in Figure 5.8) were larger than the diffraction limit (~250 nm), the small size produced relatively few fluorescent spots owing to the very small contact area. The spots that were seen exhibited surprisingly high fluorescence intensities, however (Figure 5.8). Second, the number of sorted DN4 thymocytes from the thymus was extremely low, which also counted against the analysis. Only 2 % of all thymocytes from a thymus were DN4 cells (*i.e.* approximately 54,000 DN4 cells); less than half of these DN4 cells were pre-TCR positive, and only 1 % of the DN4 cells expressed TCRβ ($V_\beta 8$), which was recognised by the F23.1 antibody (approximately 540 cells). In practice, fewer than 100 cells were obtained per sort. Further optimisation of the SMCCCD method would therefore be required for the analysis of the pre-TCR on *ex vivo* thymocytes.

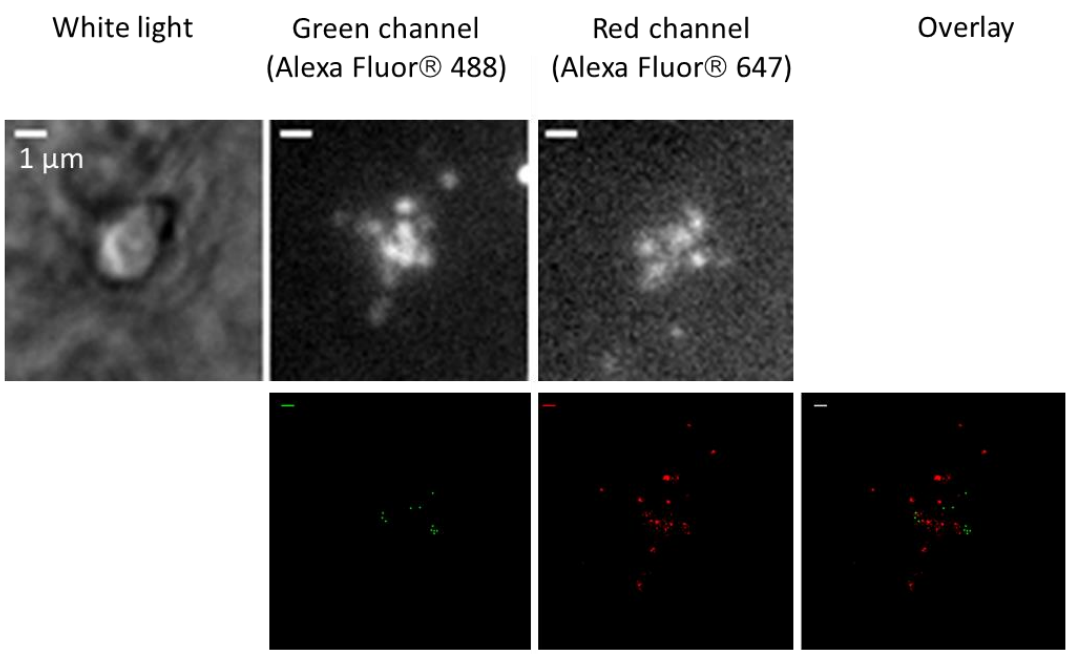

Figure 5.8: Representative raw (top raw) and reconstructed (bottom row) co-localisation images for mouse DN4 thymocytes expressing TCR(Vβ8) using F23.1 Fab labelled with either Alexa Fluor® 488 or Alexa Fluor® 647. Data collection in collaboration with Dr James McColl.

III. Discussion

Single-molecule, two-colour co-localisation imaging techniques generally allow for the investigation of the interaction properties and stoichiometry of receptors at the level of individual proteins. SMCCCD, a DySCo-based two-colour co-localisation method established in the Klenerman laboratory, Cambridge, was found to be well-suited to analyses of the pre-TCR on transfected cells. The co-localisation imaging analysis first confirmed, as had been shown previously [235, 236], that TCRs at low expression levels tended to behave as monomers but at higher expression levels they more often tended to exhibit non-monomeric behaviour comparable to that of control dimers. In marked contrast, pre-TCRs at expression levels, which comparable to the amount of mature TCRs at the lower expression level, formed either dimers or, more likely, high-order oligomers in situ. The co-localisation imaging analysis based on correlation levels was shown to be independent of receptor expression levels according to the Pearson correlation coefficient (R), for all receptors except CD86. This indicates that, in contrast to the results obtained in the dSTORM analysis in Chapter 4, higher levels of expression did not lead to clustering. For the CD86 monomeric control, the modest correlation between expression and coincidence level likely results from corralling effects [180, 236, 340].

Based on intensity analyses that can also be used to obtain stoichiometric information [341], the mouse pre-TCR exhibited greater-than-dimer levels of fluorescence in the mouse cell line. A previous study using a similar intensity analysis also showed that mouse pre-TCRs exhibit higher labelling intensities in comparison to mature TCRs [234]. The intensity analysis allowed different stoichiometries to be distinguished and provided relative stoichiometric information for receptors or proteins. The differences in intensities however did not show a simple linear relationship to the

differences in orders of stoichiometry. This was because intensities also depended on labelling efficiencies and other photo-physical properties such as blinking, although the same experimental conditions and normalisations were carried out among all experiments. Nevertheless, these observations of differences in intensities suggest that the mouse pre-TCR forms higher-order oligomers, contradicting the super-resolution imaging-based findings presented in Chapter 4, in which it was found that pre-TCRs on the same cell lines exhibited comparable behaviour to monomeric controls. The possible reasons for this, and its implications are considered in the General Discussion. It is worth emphasising, however, that the structures that were observed from the these experiments in this chapter seemed to be too large to correspond to the dimers found in the lattice of crystals of the pre-TCR [233].

Ideally, the question of pre-TCR stoichiometry should be settled for the native receptor expressed by thymocytes. In this Chapter, a subpopulation of pre-TCR expressing cells were isolated from the thymi of C52BL/6 using the appropriate antibodies for cell markers and the F23.1 Fabs for anti-TCRβ (Vβ8) reactivity including both Alexa Fluor® 488- and Alexa Fluor® 647-labelled Fabs for cell sorting and subsequent SMCCCD analysis. However, it has not yet been possible to use this technique for the pre-TCR expressed by *ex vivo* thymocytes due to limitations of cell size and the surprisingly high intensities of the fluorescent spots present on the thymocytes. Thymocytes on average tend to be smaller than the cell lines used in this study and their sizes are also very heterogeneous, depending on cell cycle, amino acid intake and activation level [342, 343]. In addition, the analysis of thymocytes here lacked a suitable monomeric receptor as a control and this posed another challenge to investigating the coincidence rates for the pre-TCR *ex vivo*.

Chapter 6

TCR triggering without ligands

I. Introduction

The absence of known ligands for the pre-TCR in the thymus, and the induction of signalling by a receptor that did not seem suited to bind ligands at all (*i.e.* the pre-TCR), is a major puzzle. One possible explanation for this is that the pre-TCR spontaneously dimerises when it successfully expresses on the cell surface, thus generating a signal [233, 234], as in the example of the EGFR, which dimerises upon binding ligand [216, 344]. Another possibility is that the pre-TCR does not dimerise but is nevertheless capable of signalling in the absence of ligands [93, 237].

The strongest argument in favour of the dimerisation-based model is the structure of the pre-TCR complex, which offered evidence of the formation of a dimer in the crystal lattice [233]. To test this proposal, a mutagenesis-based strategy and imaging techniques (Chapters 3, 4 and 5) were used to investigate the stoichiometric requirements for pre-TCR complex assembly and surface expression prior to pre-TCR signalling.

The mutagenesis-based analysis offered clear evidence that pre-TCR dimers are not required to form in order for successful pre-TCR complex assembly and expression on the cell surface. Although head-to-tail autonomous dimerisation of pre-TCRs was proposed to explain pre-TCR signal initiation [233], the results (in Chapter 3) showed that drastic mutations of those residues involved in the 'head-to-tail' dimerisation had no systematic effects on pre-TCR expression. On the contrary, the interface between pre-Tα and the constant region of TCRβ is required to form in order for successful

pre-TCR surface expression. Although he results in Chapter 3 implied that monomeric pre-TCRs were likely to be sufficient for cell surface expression, however, imaging approaches, *i.e.* dSTORM combined with cluster analysis and SMCCCD experiments [238, 338] (discussed in Chapters 4 and 5), on the other hand, were equivocal and revealed that the pre-TCR could have a tendency to form some type of higher oligomer in transfected cell lines. Technical limitations have thus far prevented further application of super-resolution to the stoichiometric analysis of the pre-TCR expressed by thymocytes *ex vivo*, and so the status of the pre-TCR on the cells in which the receptor needs to function is unclear.

Although these approaches seemed to rule-out dimerisation *per se* as an explanation for pre-TCR function but did not come to a firm conclusion about native pre-TCR stoichiometry and signalling initiation by the receptor, attempts were made to determine whether the pre-TCR could be triggered without ligands, and to characterise the associated signalling pathway. This was first investigated by attempting to reprise a published assay wherein the v-ras oncogene had been used. Ras, a small GTPase, is involved in T cell activation and differentiation. When in association with GTP, it is able to activate NFAT and produce IL-2 via the Ras-Raf-MEK-ERK kinase cascade [345-347]. The v-ras oncogene is a constitutively active form of ras, which is insensitive to negative regulation by GTP hydrolysis [347]. The v-ras is used to sensitise a T cell-based system so that weak, ligand-independent pre-TCR signalling could be amplified and detected [237, 348]. However, several attempts failed to detect consistent trends in IL-2 production as a read-out for ligand-independent signalling by the receptor.

In parallel to this, an alternative triggering assay was established in the laboratory (Knox, R. *et al.* unpublished data), which allowed TCR ligand-independent signalling to be detected. The requirements for this signalling could therefore be investigated.

II. Results

A. Published assay for ligand-independent signalling by the pre-TCR

An assay for pre-TCR signalling by a receptor unable to bind ligands was published established by Irving *et al.* in 1998 [237]. Their form of non-ligand binding pre-TCR lacked the pre-Tα and TCRβ extracellular domains. In their assay, the truncated pre-TCR was transfected along with an NFAT-luciferase reporter construct, into TCRβ-deficient cells. In addition, an active form of the v-ras oncogene was expressed in the cells to sensitise the system. Signalling was measured as NFAT-mediated luciferase production. Their results showed that the pre-TCR can initiate signalling without the extracellular domains of both pre-Tα and TCRβ, although signalling from this form of the pre-TCR was somewhat lower than that from the TCR. An asymmetrical form of the pre-TCR (with wild-type pre-Tα and the extracellularly-truncated TCRβ) failed to express on the cell surface and initiate signalling possibly due to improper assembly and/or endoplasmic reticulum retention. However, this work posed a challenge to the notion that there would be a requirement for 'head-to-tail' dimerisation of pre-TCRs in order for signalling initiation [233].

(a) Attempt to recreate the v-ras, ligand-independent triggering system of Irvine *et al.*

i. Transient expression of v-ras

In an approach analogous to that used by Irving *et al.*[237], the system was first sensitised using the activating effects on NFAT and the transient expression of v-ras [349-352]. Spontaneous, apparently ligand-independent signalling initiated by the pre-TCR and TCR was then measured using a luciferase-based IL-2 reporter assay.

IL-2 promoter activity stimulated by ionocycin and PMA was used as a positive control since this efficiently activates protein kinase C (PKC) and triggers signalling in T cells [353]. Cells were infected with the NFAT/IL-2 Renilla luciferase reporter construct using lentivirus (day 0). Three days after infection, v-ras was delivered into the cells, by electroporation as used in Irving's study (day 3) and then IL-2 promoter activity was measured as bioluminescence (day 4). For signalling positive controls, cells were treated with ionomycin and PMA for six hours before IL-2 promoter activity was measured (Figure 6.1). The levels of IL-2 promoter activity triggered by pre-TCR and TCR expression were normalised against basal signalling by native, untransfected E6.1-57 cells, which do not express either the pre-TCR or TCR.

In a first experiment (Figure 6.2) the levels of IL-2 production by pre-TCR and TCR expressing cells, without any v-ras nor stimulation, were generally low, only ~2-fold higher than basal levels. Although receptor expression levels were very different (as shown in Chapter 3, 4 and in previous studies [304, 332]), there were no significant differences between the levels of promoter activity triggered by the pre-TCR and TCR ($p=0.42$). Unexpectedly, instead of sensitising the assay, v-ras either had no effect, or significantly reduced IL-2 promoter activity (Figure 6.2). Ionomycin and PMA also failed to activate each cell line, or even reduced the levels of IL-2 promoter activity (Figure 6.2).

In a second experiment IL-2 promoter activity was monitored at three time points, *i.e.* day 2 (48 hours after infection with the NFAT/IL-2 Renilla luciferase reporter), day 3 (just before v-ras electroporation) and day 4 (24 hours after v-ras electroporation). As shown in Figure 6.3, bioluminescence accumulated over time. The normalised levels of IL-2 promoter activity were highest on day 4, and the levels were comparable with the previous trial. The v-ras in this trial did not affect promoter activity for pre-TCR

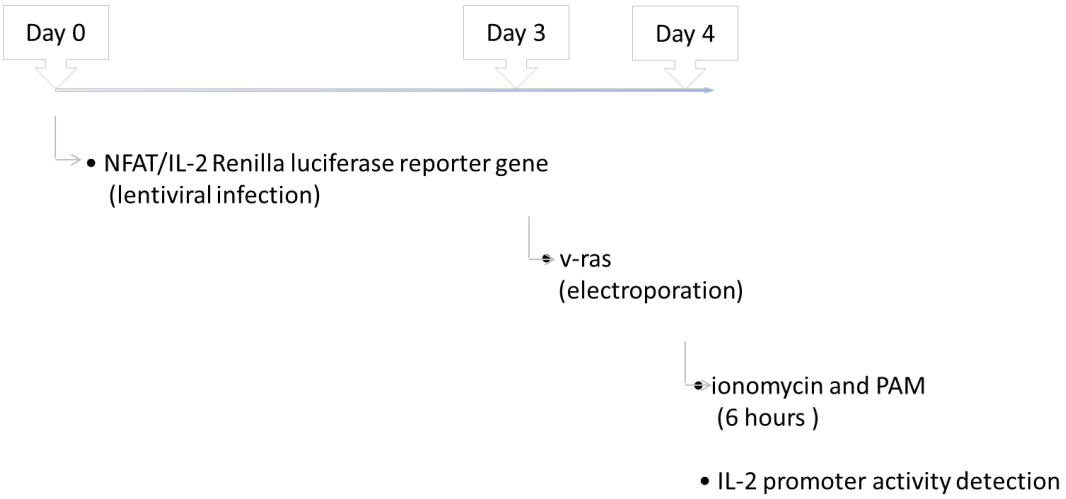

Figure 6.1: The timeline for the v-ras based assay for ligand-independent signalling. Ionomycin and PMA were used as a positive control for signalling.

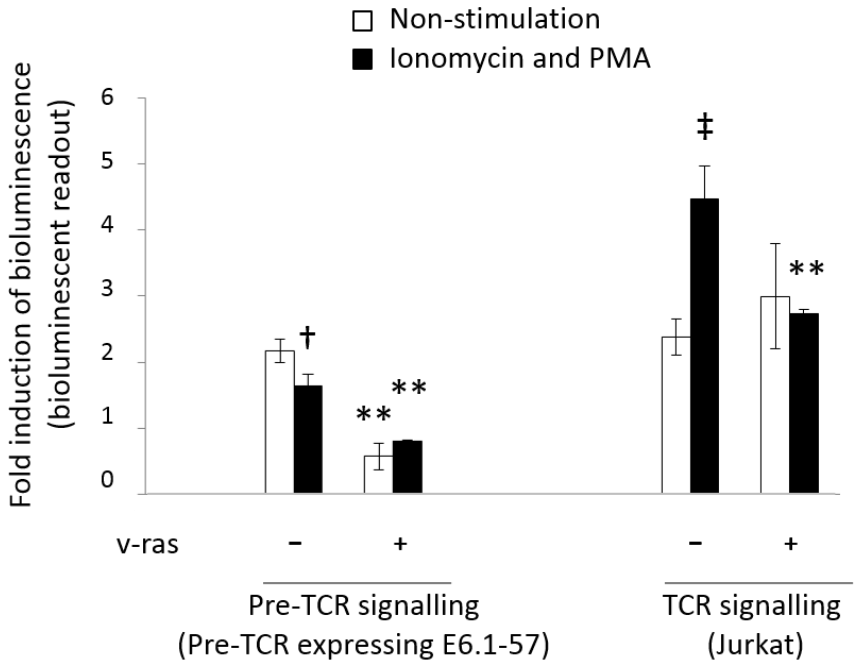

Figure 6.2: Levels of spontaneous IL-2 promoter activity in pre-TCR expressing E6.1-57 cells and in Jurkat cells, normalised against the basal activity for untransfected E6.1-57 cells. Effects of v-ras and stimulation by ionomycin and PMA on promoter activity were tested. IL-2 promoter activity was read out as bioluminescence from an IL-2 reporter construct. Averages and standard deviations for three replicates are shown. *P*-values (comparisons between the respective cell lines with or without v-ras expression) are labelled as: **, $p \leq 0.01$; * , $0.01 < p \leq 0.05$. *P*-values for comparisons between non- and PMA/ionomycin- stimulated cells are labelled as: ‡ , $p \leq 0.01$; † , $0.01 < p \leq 0.05$.

Figure 6.3: Levels of spontaneous IL-2 promoter activity in pre-TCR expressing E6.1-57 cells and in Jurkat cells, normalised against the basal activity for untransfected E6.1-57 cells. IL-2 promoter activity was read out at three time points: (A) day 2 (48 hours after infection with the NFAT/IL-2 Renilla luciferase reporter construct), (B) day 3 (just before v-ras construct electroporation, 72 hours after lentiviral infection with the reporter construct) and (C) day 4 (24 hours after v-ras construct electroporation). Effects of v-ras and stimulation by ionomycin and PMA on promoter activity were also tested. IL-2 promoter activity was read out as bioluminescence from an IL-2 reporter construct. Averages and standard deviations for three replicates are shown. *P*-values (comparisons between the respective cell cell lines with or without v-ras expression) are labelled as: **, $p \leq 0.01$; * , $0.01 < p \leq 0.5$. *P*-values for comparisons between non- and PMA/ionomycin stimulated cells are labelled as: ‡, $p \leq 0.01$; †, $0.01 < p \leq 0.05$.

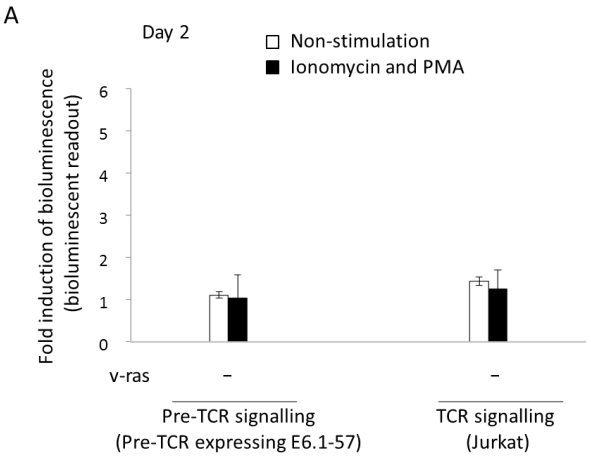
A
Day 2
Non-stimulation
Ionomycin and PMA
Fold induction of bioluminescence
(bioluminescent readout)
0
1
2
3
4
5
6
v-ras
–
–
Pre-TCR signalling
(Pre-TCR expressing E6.1-57)
TCR signalling
(Jurkat)

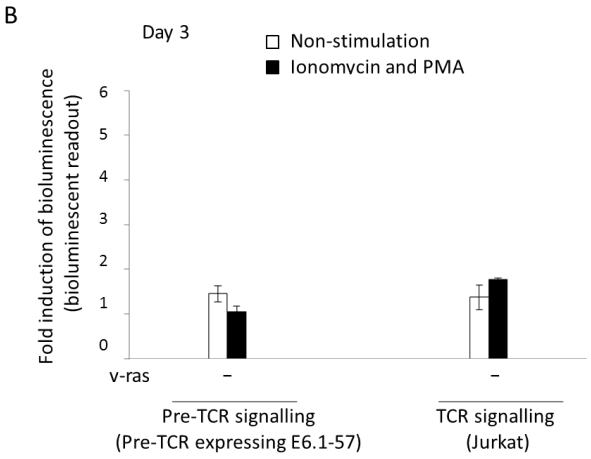
B
Day 3
Non-stimulation
Ionomycin and PMA
Fold induction of bioluminescence
(bioluminescent readout)
0
1
2
3
4
5
6
v-ras
–
–
Pre-TCR signalling
(Pre-TCR expressing E6.1-57)
TCR signalling
(Jurkat)

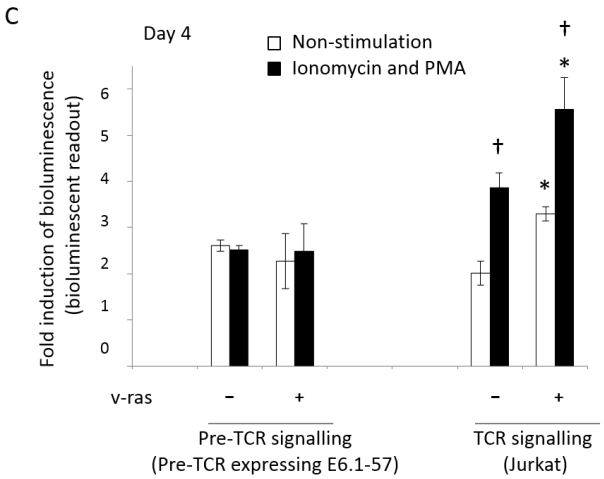
C
Day 4
Non-stimulation
Ionomycin and PMA
Fold induction of bioluminescence
(bioluminescent readout)
0
1
2
3
4
5
6
†
*
†
*
v-ras
–
+
–
+
Pre-TCR signalling
(Pre-TCR expressing E6.1-57)
TCR signalling
(Jurkat)

expressing cells, but it stimulated higher activity in the presence of the TCR on day 4, both in the presence and absence of ionomycin and PMA (Figure 6.3C). In this triali onomycin and PMA also increased IL-2 promoter activity on day 4 (Figure 6.3C). Overall, however, all of the effects, *i.e.* of v-ras and ionomycin and PMA were small.

ii. Effects of v-ras

Possible explanations for the general unresponsiveness of the cells were that the receptor expression was lost or v-ras electroporation was cytotoxic. The surface expression levels of pre-TCR and TCR were determined at three time points, *i.e.* day 2, day 3 and day 4. As shown in Figure 6.4, there was a negligible increase in pre-TCR expression levels over time, and in the Jurkat cells, TCR expression levels remained essentially unchanged. Overall, the transient expression of v-ras in the cells did not change receptor surface expression levels.

The advantage of electroporation of v-ras was that it was only transiently expressed in the cells immediately before IL-2 promoter activity was measured, allowing possible dynamic effects of v-ras on cells and signalling *per se* to be minimised. However, using a combination of lentiviral infection of the NFAT/IL-2 Renilla luciferase reporter gene and electroporation of the v-ras construct within a very short period (three days) could be expected to stress the cells, constraining their responsiveness.

To attempt to prevent these effects, cell lines were first infected with v-ras using lentiviruses and, following stable expression and recovery for one week, the cells were then infected with the NFAT/IL-2 Renilla luciferase reporter construct. The v-ras sequence was cloned into one of two different lentiviral vectors. *i.e.* vectors with a normal promoter (pHR-sin) or with an inducible promoter (pHRI-sin), which gives lower expression. In addition, a GFP sequence was incorporated downstream of an

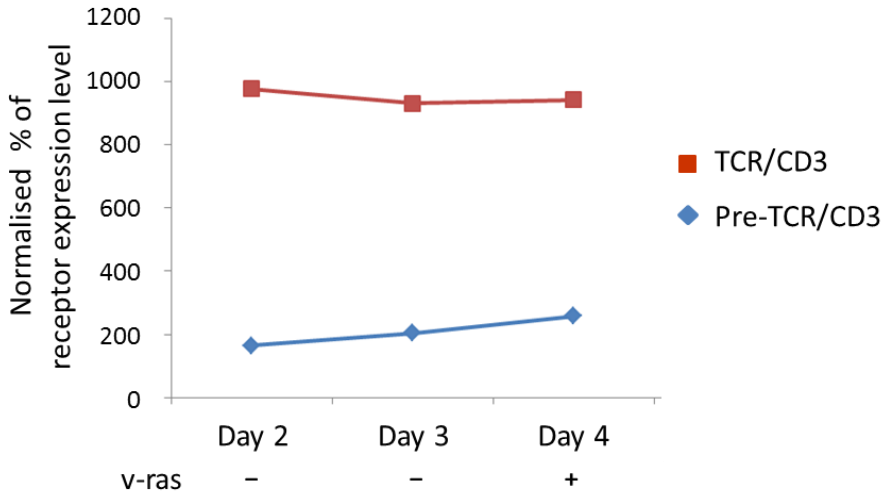

Figure 6.4: Receptor levels following v-ras expression. E6.1-57 cells, pre-TCR expressing E6.1-57 cells, and Jurkat cells were stained with mouse anti-human CD3ε UCHT1 antibody and a secondary anti-mouse IgG conjugated with Alexa Fluor® 647. Receptor levels on the cell surface were measured based on geometric means of fluorescence intensity and normalised against that for E6.1-57 cells.

internal ribosome entry site sequence to test for transfection success. Two cell lines, *i.e.* TCR-negative E6.1-57 cells and Jurkat cells, were then infected with each v-ras expressing lentivirus.

In E6.1-57 cells with no, low, or high levels of v-ras expression, cell growth was unchanged, although variability was high (Figure 6.5A). However, FACS analysis revealed changes in the ratios of v-ras expressing and non-expressing cells over time. A week after lentiviral infection, the GFP-positive, presumably v-ras expressing cells started to decrease, especially the cells with the high levels of GFP expression, *i.e.* cells transfected with the pHR vector (Figure 6.5B). For the Jurkat cells, there was a statistically significant effect of high-level v-ras expression on cell growth ($p=0.006$; Figure 6.5C). Strikingly, FACS analysis showed that very few of the Jurkat cells expressing high levels of GFP, and presumably v-ras, survived (Figure 6.5D). These results indicated that v-ras had adverse effects on cell growth and survival. Based on these observations, it was decided that a v-ras sensitised system would be unsuitable for studying ligand-independent signalling by the pre-TCR.

B. Alternative ligand-independent TCR signalling assay

As discussed above it proved difficult to repeat the findings of Irving *et al.* Therefore, an alternative assay for ligand-independent signalling was established. This assay involved creating a 'close-contact zone' from which bulky phosphatases were excluded by engaging mouse DO11.10 hybridoma cells expressing a truncated form of a rat-mouse chimeric receptor (rmCD28 receptor) with plastic-immobilised rat CD28-specific superagonistic antibody (Figure 6.6). This assay was based on the principles of the kinetic-segregation model for T cell signalling, in which signalling initiation is explained by an imbalance between phosphorylation (by tyrosine kinases) and dephosphorylation (by tyrosine phosphatases generally with bulky extracellular

Figure 6.5: Effects of v-ras on cell proliferation. (A, B) E6.1-57 cells; (C, D) Jurkat cells. In A and C, cell counts at day 4, day 7 and day 9 are shown as fold changes with means and standard deviations. In B and D, relative cell numbers were measured using FACS. Red, mock-infected cells; blue, cells infected with v-ras in the pHRI vector with IRES-GFP (to give low levels of expression); green, cells infected with v-ras in the pHR vector with IRES-GFP (to give high expression). In A and C, statistical comparisons for cells with and without v-ras were performed using student's two-tailed t-test. *P*-value is indicated with: **, $p \leq 0.01$.

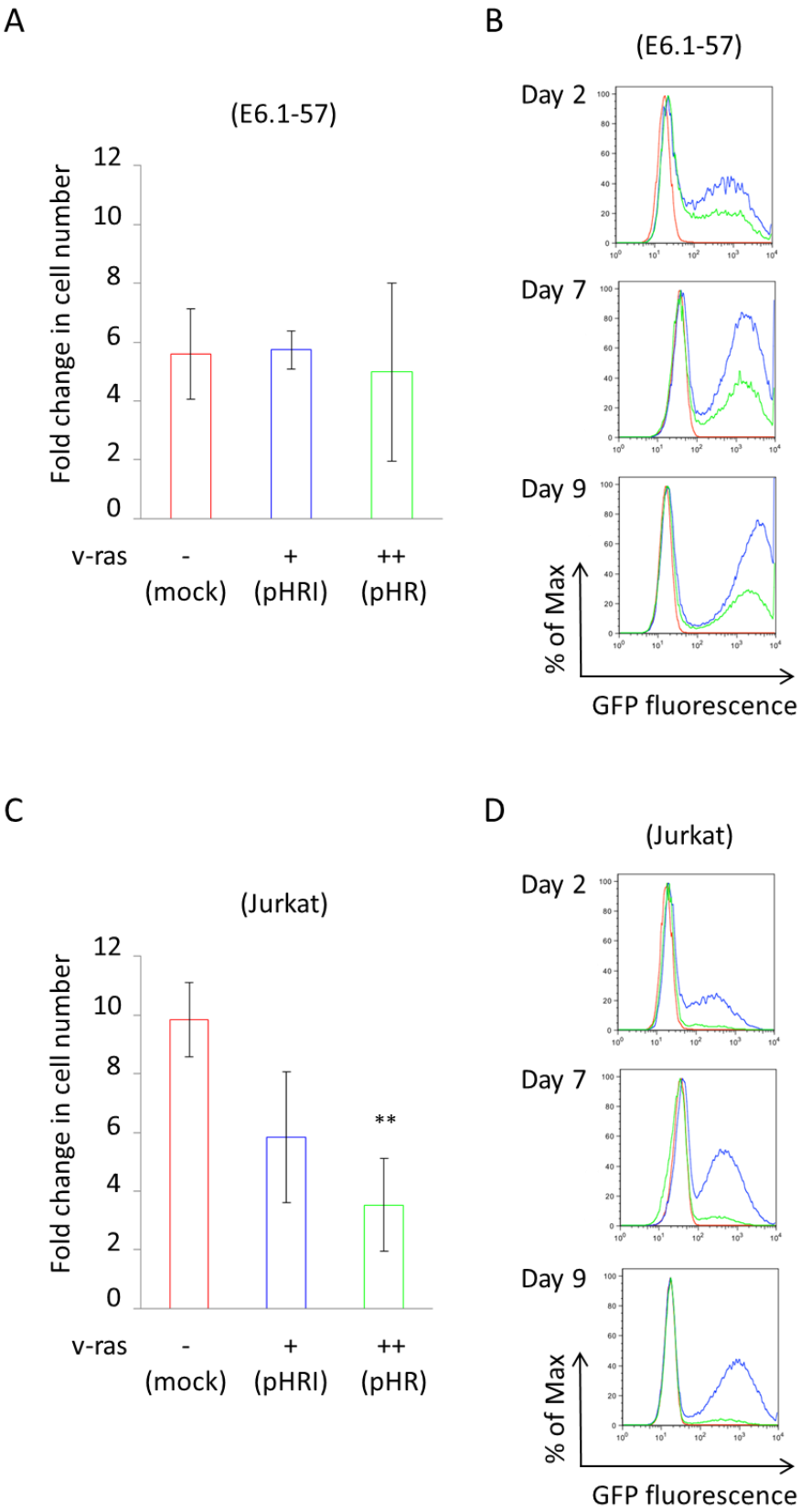
A
(E6.1-57)
Fold change in cell number
12
10
8
6
4
2
0
v-ras
-
+
++
(mock)
(pHRI)
(pHR)
B
(E6.1-57)
Day 2
Day 7
Day 9
% of Max
GFP fluorescence
C
(Jurkat)
Fold change in cell number
12
10
8
6
4
2
0
**
v-ras
-
+
++
(mock)
(pHRI)
(pHR)
D
(Jurkat)
Day 2
Day 7
Day 9
% of Max
GFP fluorescence

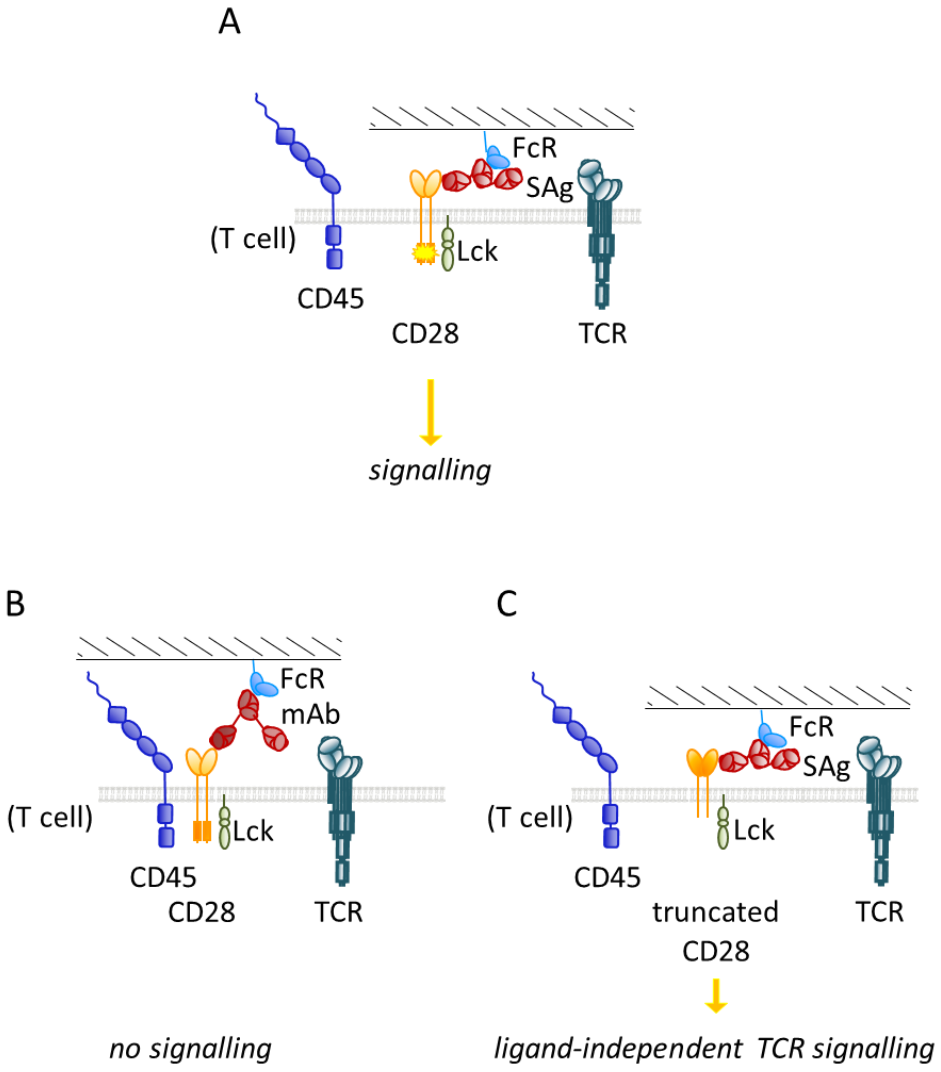

Figure 6.6: The mechanism of ligand-independent TCR signalling induced by superagonistic antibodies as explained by the kinetic-segregation model. (A) Signalling is detected after a "close-contact zone" is created by an immobilised CD28-specific superagonistic antibody binding to the "side" of CD28. Exclusion of the bulky phosphatase CD45 in the close-contact zone favours phosphorylation and signalling. Bystander signalling by the TCR also contributes to the total signalling output. (B) No signalling is detected since phosphorylation is quenched by CD45 in the deeper close-contact zones created by a non-superagonistic (conventional) antibody binding to the "top" of CD28. (C) Ligand-independent TCR signalling only is detected when the close-contact zone is created by the superagonistic antibody binding to a truncated, non-signalling form of CD28. FcR, Fc receptor; SAg, superagonistic antibody; mAb, conventional monoclonal antibody.

domains) created when close-contact zones form [215, 253].

In this alternative assay system, signalling is thought to be induced by "bystander" TCRs that do not engage any ligands because none are present. Instead, it is induced by the immobilised superagonistic antibodies binding the "side" of the receptors on the cell, creating a very close-contact zone that is expected to exclude the phosphatases, favouring receptor phosphorylation (Figure 6.6).

Support for this explanation of signalling was obtained by S. Morgan, R. Knox, M. Aßmann, and A. Lippert. (unpublished data). First, and most importantly, cells lacking TCRs did not produce signals. Second, immobilised non-superagonistic anti-rat CD28-specific antibody JJ319 did not produce IL-2 whereas the superagonistic anti-rat CD28-specific antibody JJ316 did. In comparison with the close-contact zone created by JJ316, JJ319 antibody bound to the 'top' of rmCD28 receptors so that it formed a v-shaped-like complex [354]. This topology was expected to create a deeper contact that would allow phosphatases to more easily diffuse into the close-contact zone where they would block signalling. Third, the amount of IL-2 production was in inverse correlation to the length of the extracellular domain of CD45. Finally, different levels of CD45 exclusion by the JJ316 agonist versus the JJ319 non-agonist were observed using imaging.

This TCR-dependent, ligand-independent system seemed well-suited to study the requirements of TCR signalling without ligands. Because the pre-TCR and TCR share the same signalling elements, *i.e.* the CD3 subunits, the goal was to determine whether signalling without ligands was achieved using the same signalling apparatus as conventionally activated receptors. To test this idea the dependence of this form of TCR signalling on Lck, ZAP70 and TCR was determined using 'knock-down' or 'knock-out' expression approaches. In addition, the pre-TCR was tested for its capability to initiate signalling in this way.

(a) Ligand-independent TCR signalling

In this assay, mouse anti-rat CD28 antibody JJ316 was added to rat/mouse (rm) CD28-expressing DO11.10 mouse T cell hybridoma cells when they were in suspension, and then the cells were added to tissue culture plates adsorbed with donkey anti-mouse antibody (DAM). The rmCD28 was comprised of the rat CD28 extracellular domain, which contains the binding site for the superagonistic anti-rat CD28 antibody JJ316, and the mouse CD28 transmembrane and cytoplasmic domain, which contained the important tyrosine motifs (YMNM and PYAP) needed for recruiting proximal kinases for signalling [131, 191] (Figure 6.7A and C). Other DO11.10 cells were transfected with a truncated form of rmCD28, in which the cytoplasmic domain was removed (Figure 6.7B and D). Thus, ligand-independent signalling by the TCR *per se* could be studied by determining the levels of IL-2 produced by cells expressing the truncated, non-signalling form of rmCD28. Signalling triggered by JJ316 was also compared with that initiated by anti-mouse CD3 KT3 antibody, which was adsorbed directly to the tissue-culture plates.

As shown in Figure 6.8, the parental DO11.10 cells, and DO11.10 cells expressing full-length or truncated rmCD28 all produced similar amounts of IL-2 when triggered by anti-CD3 KT3 antibody, indicating that the TCR signalling machinery of the cell was unperturbed by expression of the rmCD28 constructs. IL-2 production was also induced by triggering with immobilised JJ316 in cells expressing full-length rmCD28, consistent with the antibody being a superagonist. There was no signalling by uninfected DO11.10 cells as expected. Importantly, IL-2 production from DO11.10 cells expressing truncated rmCD28 was approximately half, or more than half, that of cells expressing full-length rmCD28 at an antibody concentration of 10 μg/mL. This observation was equivalent to that made by R. Knox and M. Vuong (Davis laboratory) using the TCR-reconstituted BW5147 T-cell hybridoma cell line, who also found that

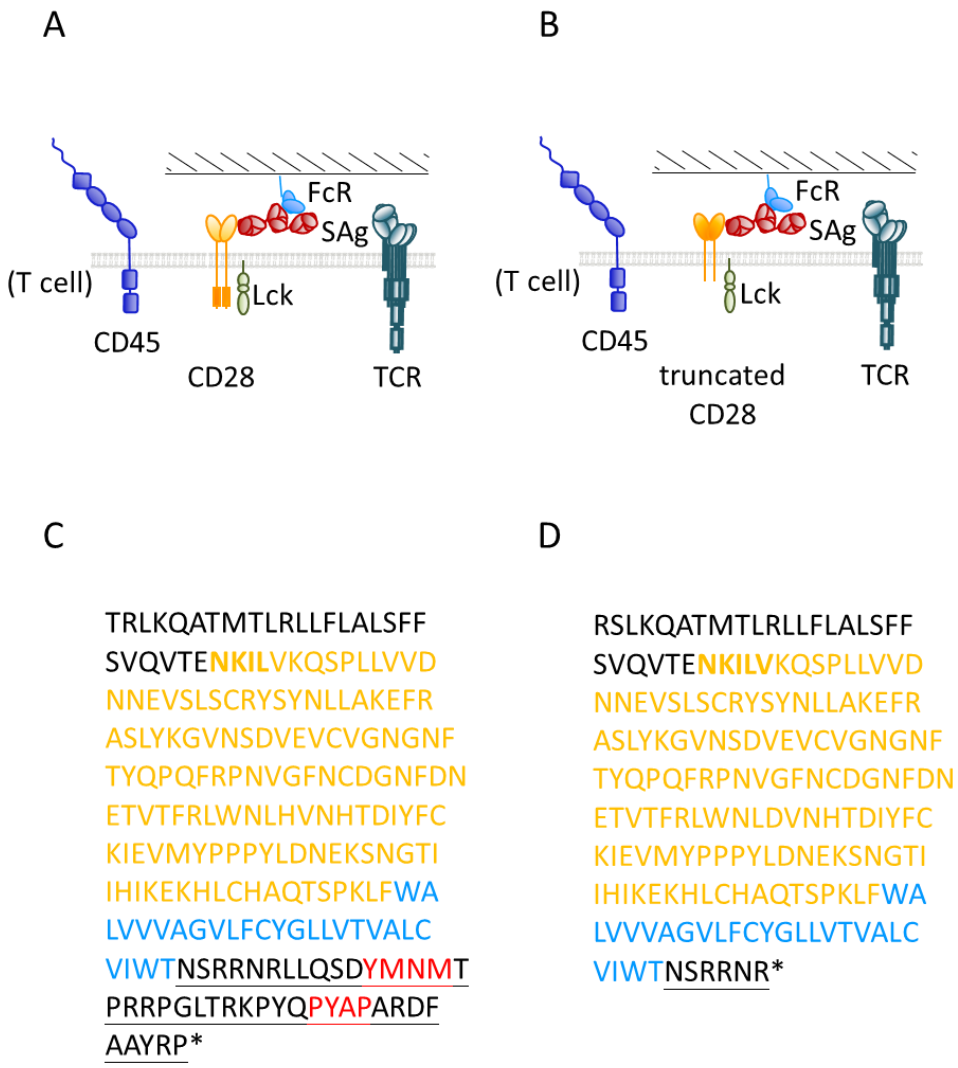

Figure 6.7: The design of the two different forms of rmCD28 expressed in the DO11.10 cells. (A) Full-length rmCD28 with the rat CD28 extracellular domain, the mouse CD28 transmembrane domain and the mouse CD28 cytoplasmic domain. (B) Truncated rmCD28 lacking the majority of the mouse CD28 cytoplasmic domain. In (C) and (D) the amino acid sequences of the constructs are shown. Black, signal peptide, Kozak and cloning sequences; orange, the extracellular domain sequence; blue, the mouse CD28 transmembrane domain; black underlined, mouse CD28 cytoplasmic domain sequences; red underlined, the tyrosine motif sequences for phosphorylation acting as binding sites for proximal signalling mediators. *, stop codon.

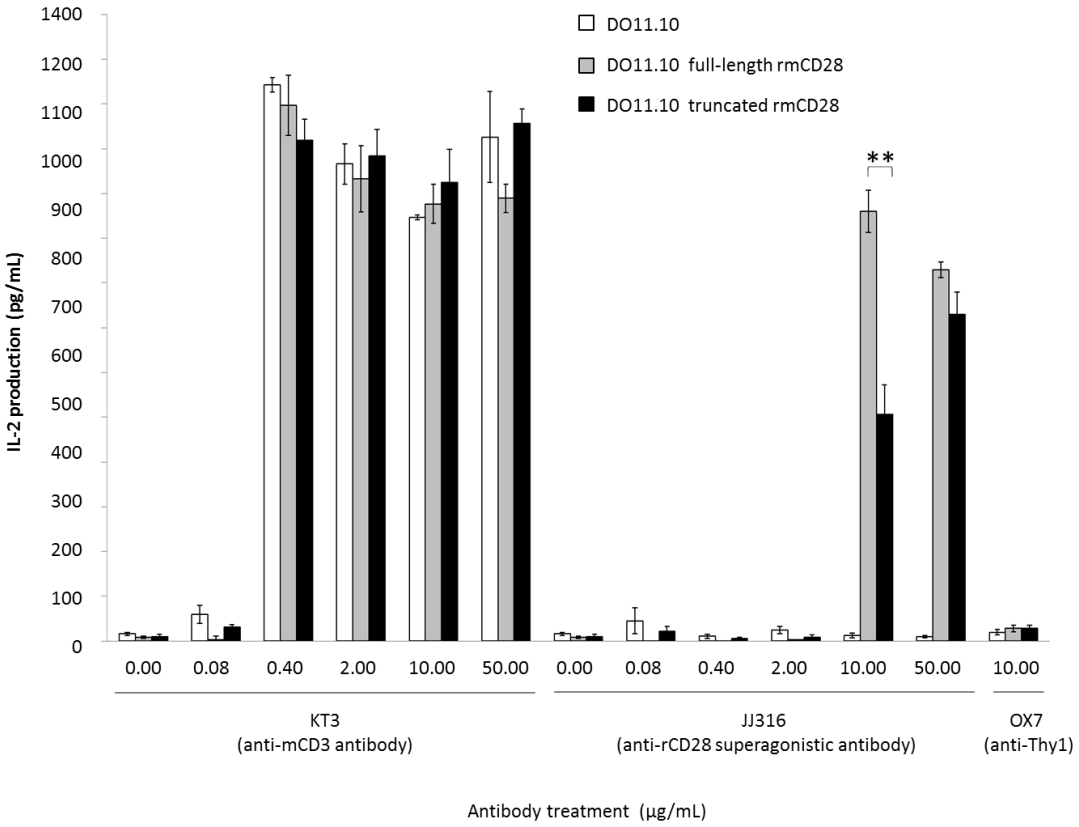

Figure 6.8: The ligand-independent TCR signalling assay. IL-2 production triggered by the anti-mouse CD3 KT3 antibody or the anti-rat CD28 superagonistic JJ316 antibody immobilised at concentrations of 0, 0.08, 0.4, 2, 10 and 50 μg/mL. The anti-Thy1 OX7 antibody at a concentration of 10 μg/mL was used as an isotype control. White bars, IL-2 produced by DO11.10 cells; grey, IL-2 produced by DO11.10 cells expressing full-length rmCD28; black, IL-2 produced by DO11.10 cells expressing rmCD28. Means and standard deviations for three replicates are shown. Statistical comparisons for the full-length rmCD28-expressing DO11.10 cells versus the truncated rmCD28-expressing DO11.10 cells were performed at each concentration of antibody using student's two-tailed t-test. *P*-values are labelled as: **, $p \leq 0.01$.

the levels of IL-2 produced correlated with the levels of TCR/CD3s expression levels restored in these cells. This also implied that the signalling observed following the engagement of truncated, immobilised CD28, is due to ligand-independent signalling by the TCR. In the following experiments the dependence of this type of signalling on Lck, ZAP70 and TCR was determined.

(b) Gene knock-down and knock-out

i. Gene knock-down by shRNA

(i) Design of shRNA sequence

A short hairpin RNA (shRNA) is a short RNA sequence forming a tight hairpin turn that is used for gene "knock-down". Using lentivirus, shRNA is transduced and integrated into the genome. Following transcription, the precursor form of shRNA is processed, exported to the cytosol and then loaded into the RNA-induced silencing complex (RISC). The sense strand is degraded and the anti-sense strand is used as a guide sequence to bind the target gene. The RISC is then able to cleave the target mRNA or suppress translation of the target mRNA, thus knocking down the target gene [355, 356]. Attempts were made first to reduce mouse Lck and Zap70 expression and suitable oligonucleotides were designed using the siRNA Selection Program developed by the Whitehead Institute for Biomedical Research. This yielded shLck (gcatcaagttgaatgtcaa) and shZap70 (gcaatgttctactggtcaa). In addition, a sequence targeting GFP was designed as a non-targeting control. Each of these sequences were cloned into the pHR-sin vector for lentiviral infection.

(ii) Knock-down efficiency

DO11.10 cells were first infected with lentiviruses expressing mouse shLck or shGFP. Intracellular anti-mouse Lck antibody-mediated FACS staining results showed that expression of about 40% of the Lck remained. Therefore, attempts were made, using multiple lentiviral infections, to achieve better knock-down efficiency, leading to a gradual decrease in expression. DO11.10 cells with only 5% of Lck remaining were finally established (Figure 6.9A). In contrast to Lck, however, after four rounds of lentiviral infection with shZap70, about 30% of Zap70 expression persisted (Figure 6.9B).

ii. Gene knock-out by the CRISPR/Cas9 system

(i) Design of CRISPR guide sequence

Owing to the problems reducing Zap70 expression, CRISPR/Cas9 [357, 358] was used in an attempt to thoroughly exclude protein kinase expression in the cells. This system involves CRISPR (clustered regularly interspaced short palindromic repeats), *i.e.* a set of prokaryotic DNA sequences including short palindromic repeats with spacers and cas9, a CRIPSR-associated gene, which generates Cas9 protein that cleaves exogenous DNA sequences. The CRIPSPR-Cas9 system used for these experiments was composed of a lentiCRISPRv2 vector with two cassettes expressing Cas9 and a guide RNA [286]. The guide RNAs comprised 20 base pairs of sequence (targeting the gene of interest) designed by a web tool (crispr.mit.edu) and flanked at the 3'end by a 3 base-pair NGG PAM sequence (in which N represented any base pair). The candidate guide sequence (Table 6.1) were ranked in inverse likelihood of off-targeting binding according to the web tool. In addition to guides targeting Lck and Zap70, others were prepared that targeted mouse TCRα.

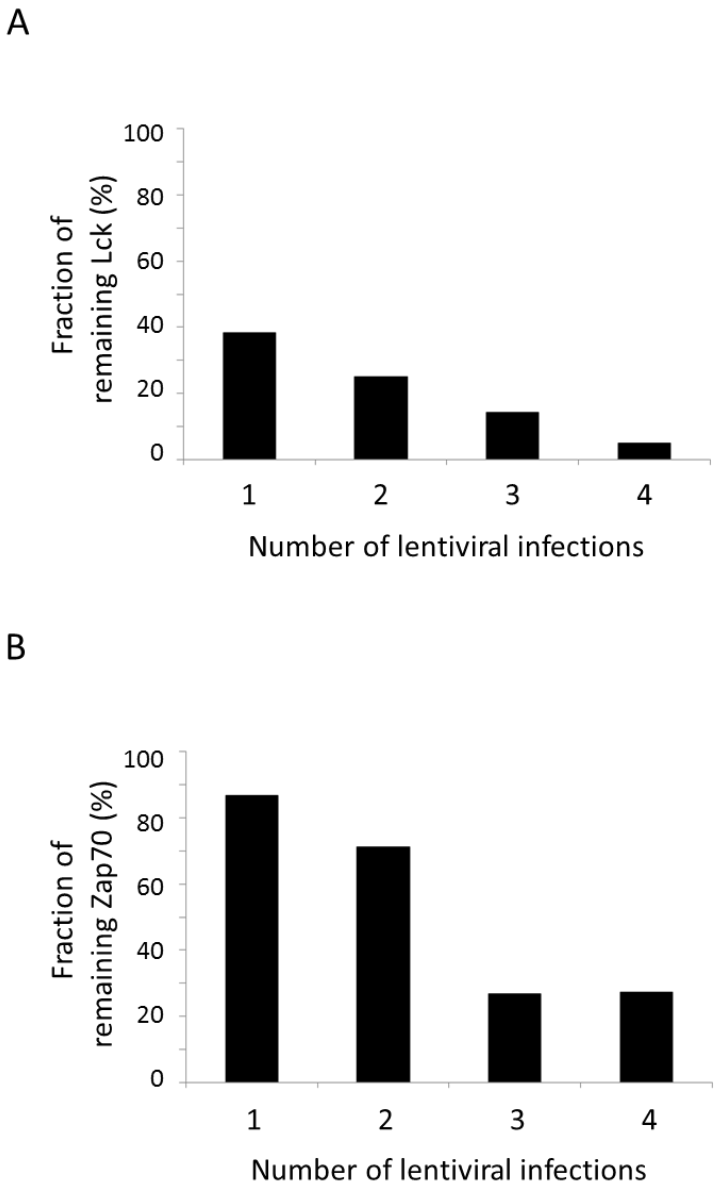

Figure 6.9: The fraction of protein remaining after multiple lentiviral infections with (A) mouse shLck or (B) mouse shZap70. Cells were intracellularly stained with anti-mouse Lck or anti-mouse Zap70 and secondary donkey anti-mouse antibody conjugated with Alexa Fluor® 647. The expression levels are based on the geometric means of fluorescence intensity. Data shown are the percentages of protein remaining in the cells versus the respective non-targeted controls.

Table 6.1: The target guide sequences used for CRISPR/Cas9-mediated gene deletion.

Gene	Target sequences
Lck	atctcgctgcccatccggaa
	gattgcacgatctagtccgc
	tgcagcacccgcggctagtc
	gccttgataggcctttcggt
	Ataccgttccatttcctgaa
Zap70	gccgagcgcaaactctattc
	ctcgtggcggacatcgagct
	gccgatgagccgcacgatgt
	tctggcgcgtaccacttcag
	Tgtgattcgccccgccccat
TCRα	tctaggccttcacctagctg
	ttctaggccttcacctagct
	tcacctagctggggtgagtg
	ggggaaggtcccgctctcct
	gctgagcctggcagagattc

Using ‘maxi-lentiviral’ infections, DO11.10 cells were infected either with the lentiCRISPRv2 vector backbone as a control or simultaneously with the five lentiCRISPRv2 vectors comprised of different guide sequences targeting mouse Lck, Zap70 or TCRα. Puromycin was used for selection of the lentiCRISPRv2 transfected cells. The results in Figure 6.10 showed that CRISPR/Cas9 system reduced the expression of Lck (>90%), Zap70 (>99%) and the TCR (>99%). There was also no evidence of off-targeting effects among the three genes targeted.

C. Dependence of ligand-independent TCR signalling on Lck, Zap70 and TCR

As discussed in II.B.(a), after binding truncated CD28, the superagonistic antibody (JJ316) triggered IL-2 production comparable to that triggered by anti-CD3 KT3 antibody. The dependence of the ligand-independent TCR signalling in the DO11.10 cells, on Lck, Zap70 and TCRα, was investigated by testing the cells in which expression by each of these genes was reduced or eliminated using CRISPR/Cas9. This was undertaken in order to test whether ligand-independent signalling utilised the same proximal tyrosine kinases as those used in conventional T-cell signalling. It was found that IL-2 production triggered by the anti-CD3 KT3 antibody, and by the anti-CD28 antibody superagonist, was greatly impaired in cells lacking Lck (Figure 6.11A), Zap70 (Figure 6.11B) and TCR/CD3 (Figure 6.11C), compared with wild-type DO11.10 cells (Figure 6.11D). Among all the CRISPR/Cas9 DO11.10 treated cells tested, only Lck-depleted DO11.10 cells expressed any IL-2, and only at high KT3 concentrations, *i.e.* 10 and 50 μg/mL (Figure 6.11A). Although the levels of IL-2 production were low (less than 15% of that produced by wild-type cells), they were significantly higher than background, suggesting that the cells were viable and that the signalling machinery of these cells at least, other than lacking Lck, was intact. It was concluded that the proximal tyrosine kinases involved in conventional T-cell signalling

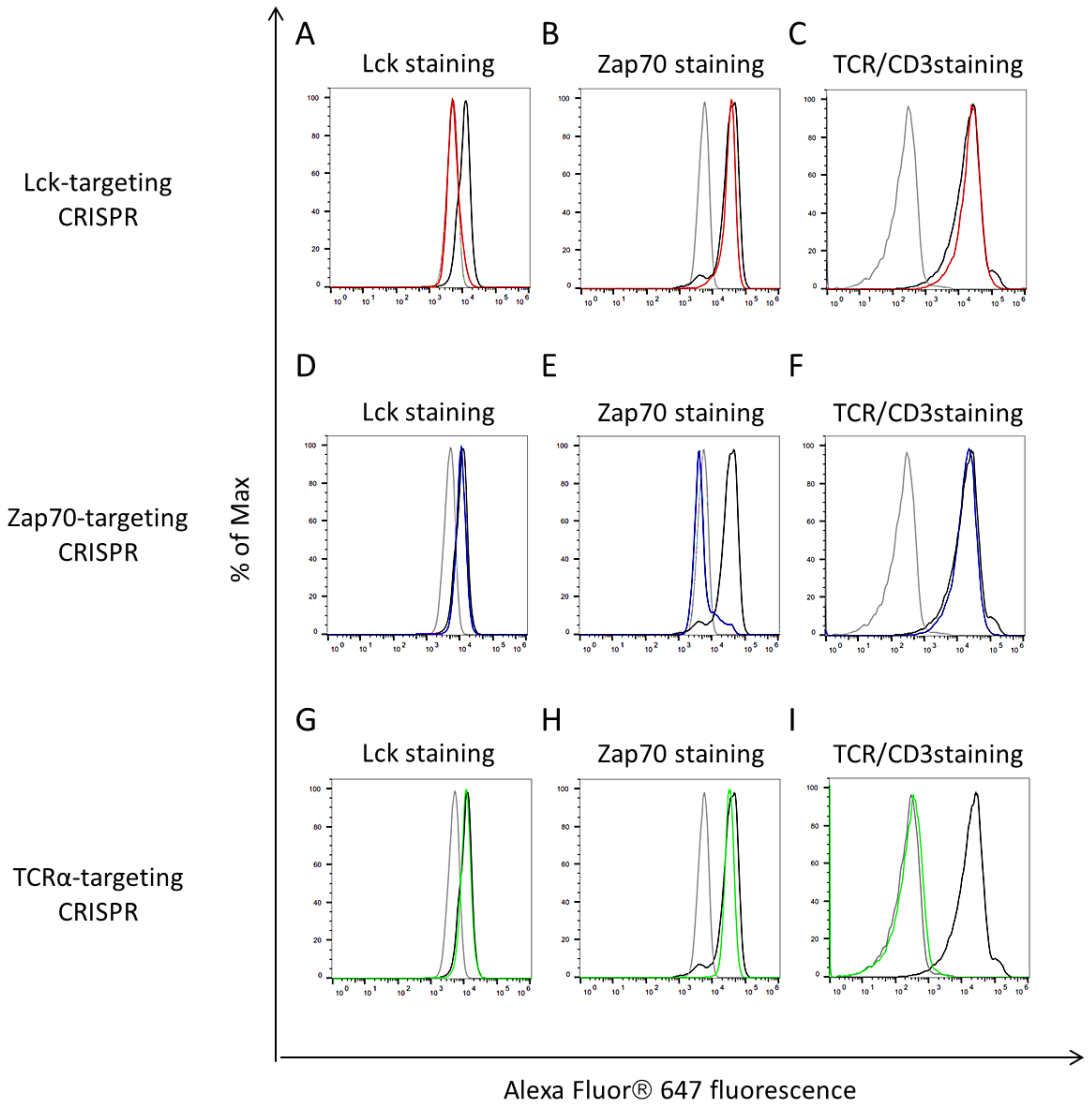

Figure 6.10: CRISPR/Cas9 mediated knock-out of (A-C) Lck, (D-F) Zap70 or (G-I) TCRα. Red, Lck/CRISPR-treated cells (6% Lck remaining); navy, Zap70/CRISPR-treated cells (<1% Zap70 remaining); bright green, TCRα/CRISPR-treated cells (<1% surface TCR expression); black, wild-type DO11.10 cells. These cells were intracellularly stained with anti-mouse Lck and anti-mouse Zap70 antibodies, or with anti-mouse CD3 KT3 antibody, and then with Alexa Fluor®647-tagged secondary antibodies. Grey, wild-type DO11.10 cells stained with the secondary antibody only.

Figure 6.11: The dependence of ligand-independent TCR signalling on conventional signalling pathways in T cells. IL-2 production, triggered by anti-mouse CD3 KT3 antibody or anti-rat CD28 superagonistic JJ316 antibody, by CRISPR/Cas9 treated DO11.10 cells lacking Lck (A), Zap70 (B), and TCRα expression (C), and expressing rmCD28 or truncated rmCD28, compared with wild-type DO11.10 cells (D), is shown. The anti-mouse Thy1 OX7 antibody is used as a negative control. Error bars represent standard deviations for three replicates. Statistical comparisons are made for antibody-induced IL-2 production by cells lacking Lck versus that by non-antibody treated cells lacking Lck in (A), and for induction of IL-2 production by the full-length rmCD28-expressing versus the truncated rmCD28-expressing wild-type DO11.10 cells in (D) at each concentration of antibody using student's two-tailed t-test. *P*-values are labelled as: **, $p \leq 0.01$; *, $0.01 < p \leq 0.05$.

A

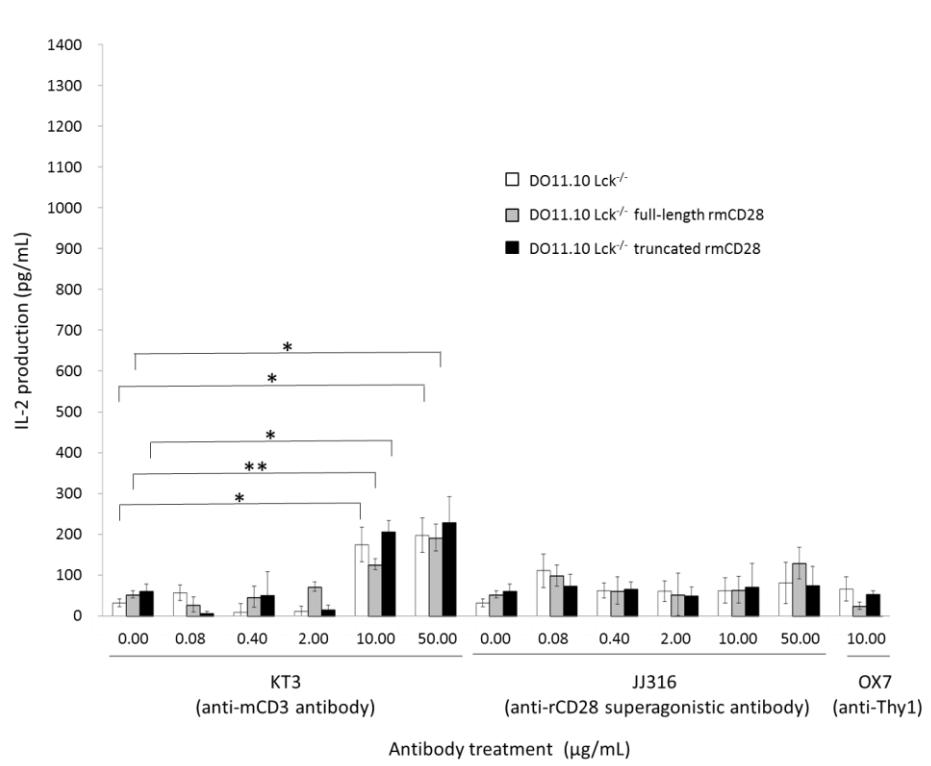
IL-2 production (pg/mL)
1400
1300
1200
1100
1000
900
800
700
600
500
400
300
200
100
0
DO11.10 Lck-/-
DO11.10 Lck-/- full-length rmCD28
DO11.10 Lck-/- truncated rmCD28
*
*
*
**
*
0.00 0.08 0.40 2.00 10.00 50.00 0.00 0.08 0.40 2.00 10.00 50.00 10.00
KT3
(anti-mCD3 antibody)
JJ316
(anti-rCD28 superagonistic antibody)
OX7
(anti-Thy1)
Antibody treatment (μg/mL)

B

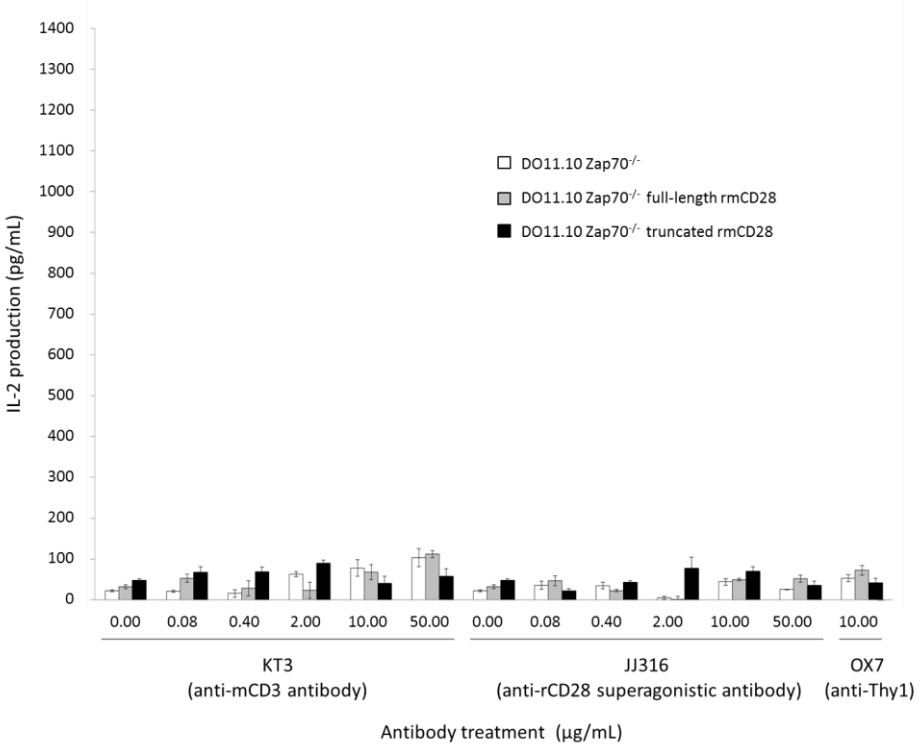
IL-2 production (pg/mL)
1400
1300
1200
1100
1000
900
800
700
600
500
400
300
200
100
0
DO11.10 Zap70-/-
DO11.10 Zap70-/- full-length rmCD28
DO11.10 Zap70-/- truncated rmCD28
0.00 0.08 0.40 2.00 10.00 50.00 0.00 0.08 0.40 2.00 10.00 50.00 10.00
KT3
(anti-mCD3 antibody)
JJ316
(anti-rCD28 superagonistic antibody)
OX7
(anti-Thy1)
Antibody treatment (μg/mL)

C

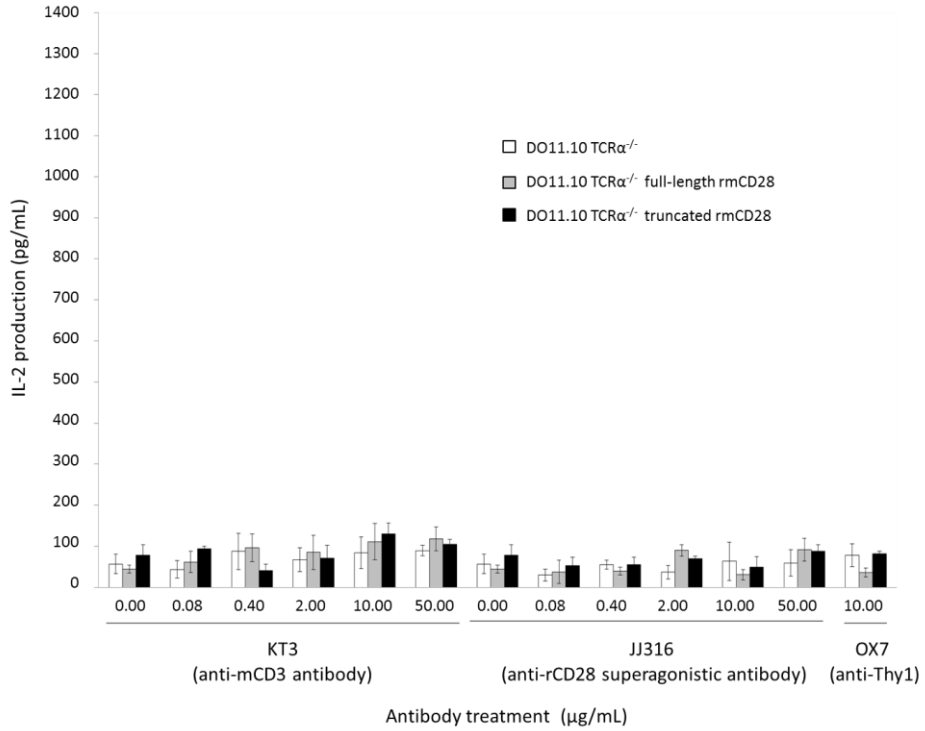
IL-2 production (pg/mL)
1400
1300
1200
1100
1000
900
800
700
600
500
400
300
200
100
0
DO11.10 TCRα-/-
DO11.10 TCRα-/- full-length rmCD28
DO11.10 TCRα-/- truncated rmCD28
0.00 0.08 0.40 2.00 10.00 50.00 0.00 0.08 0.40 2.00 10.00 50.00 10.00
KT3
(anti-mCD3 antibody)
JJ316
(anti-rCD28 superagonistic antibody)
OX7
(anti-Thy1)
Antibody treatment (μg/mL)

D

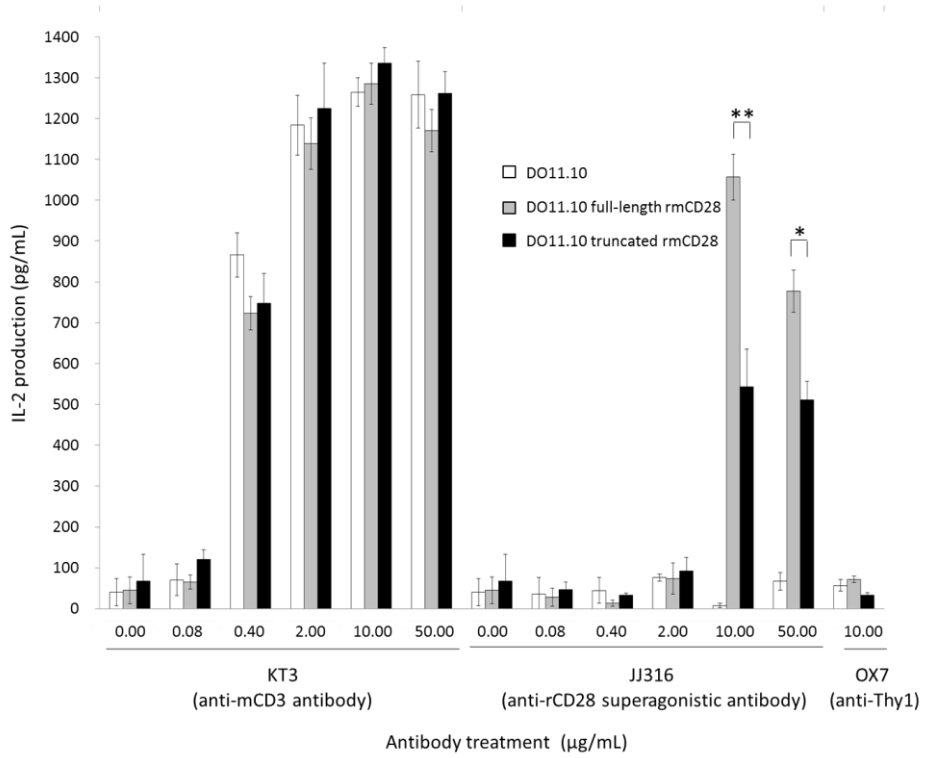
IL-2 production (pg/mL)
1400
1300
1200
1100
1000
900
800
700
600
500
400
300
200
100
0
**
*
DO11.10
DO11.10 full-length rmCD28
DO11.10 truncated rmCD28
0.00 0.08 0.40 2.00 10.00 50.00 0.00 0.08 0.40 2.00 10.00 50.00 10.00
KT3
(anti-mCD3 antibody)
JJ316
(anti-rCD28 superagonistic antibody)
OX7
(anti-Thy1)
Antibody treatment (μg/mL)

were indispensable for ligand-independent TCR signalling.

D. Ligand-independent pre-TCR signalling

Ligand-independent signalling by pre-TCR expressing DO11.10 cells was also investigated. The DO11.10 cells lacking TCRα (Figure 6.11C) were infected with lentiviruses expressing mouse pre-Tα so that these DO11.10 cells expressed pre-TCRs instead of TCRs at the cell surface (Figure 6.12A). However, the levels of IL-2 production from the pre-TCR expressing DO11.10, either induced by KT3 antibody or by superagonistic JJ316 antibody, were very low (Figure 6.12B). These observations suggest that the ligand-independent signalling induced by the contacts formed by the truncated CD28 and superagonistic antibody might be reliant on high levels of TCR expression.

III. Discussion

The results from the mutagenesis and imaging experiments in chapters 3, 4 and 5 did not come to an unequivocal conclusion regarding pre-TCR stoichiometry but argued against a simple, spontaneous dimerisation mechanism. The mutagenesis-based results argued for the assembly of single heterodimers. The question therefore remains of howsignalling by the pre-TCR is initiated.

In this chapter, irrespective of whether signalling is ligand-independent, the possibility was explored that signalling by the pre-TCR is essentially analogous to ligand induced signalling. In a first approach to establishing an assay for studying spontaneous pre-TCR signalling, the published assay for ligand-independent signalling by Irving *et al.* in which v-ras was used to sensitise signalling by the pre-TCR was explored [237]. However, v-ras did not sensitise the assay and instead it was found to

Figure 6.12: Ligand-independent pre-TCR signalling. (A) Surface expression level of the pre-TCR after 'maxi lentiviral' infections of the mouse pre-Tα gene in TCRα-deficient DO11.10 cells. Magenta, pre-TCR expressing DO11.10 cells stained with the rat anti-mouse CD3 KT3 antibody and secondary antibody conjugated with Alexa Fluor® 647; grey, pre-TCR expressing DO11.10 cells stained with the secondary antibody only; black, DO11.10 cells stained with the rat anti-mouse CD3 KT3 antibody and secondary antibody conjugated with Alexa Fluor® 647. (B) IL-2 production, triggered by anti-mouse CD3 KT3 antibody or anti-rat CD28 superagonistic JJ316 antibody, by pre-TCR expressing DO11.10 cells with the full-length rmCD28 or truncated rmCD28, compared with wild-type pre-TCR expressing DO11.10 cells, is shown. The anti-mouse Thy1 OX7 antibody is used as a negative control. Error bars represent standard deviations for three replicates. Statistical comparisons are made for antibody-induced IL-2 production by pre-TCR expressing DO11.10 cells versus that by non-antibody treated pre-TCR expressing DO11.10 cells at each concentration of antibody using student's two-tailed t-test. *P*-values are labelled as: **, $p \leq 0.01$; *, $0.01 < p \leq 0.05$.

A

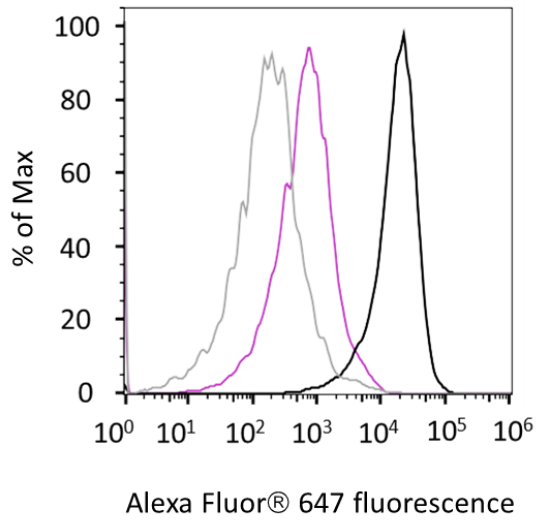
100
80
60
40
20
0
% of Max
10^0 10^1 10^2 10^3 10^4 10^5 10^6
Alexa Fluor® 647 fluorescence

B

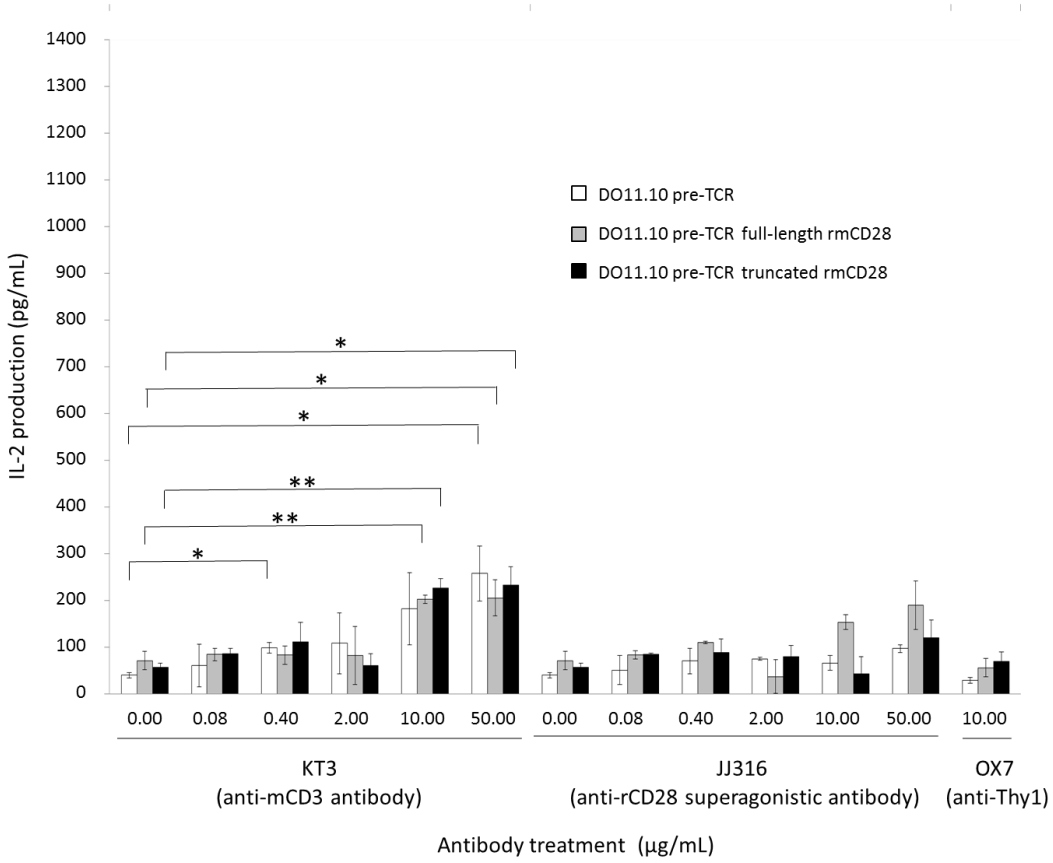
1400
1300
1200
1100
1000
900
800
700
600
500
400
300
200
100
0
IL-2 production (pg/mL)
DO11.10 pre-TCR
DO11.10 pre-TCR full-length rmCD28
DO11.10 pre-TCR truncated rmCD28
*
*
*
**
**
*
0.00 0.08 0.40 2.00 10.00 50.00 0.00 0.08 0.40 2.00 10.00 50.00 10.00
KT3
(anti-mCD3 antibody)
JJ316
(anti-rCD28 superagonistic antibody)
OX7
(anti-Thy1)
Antibody treatment (µg/mL)

alter cell proliferation and the survival of the cells expressing the oncogene. One possibility is that it produced too much signalling, perhaps inducing apoptosis. This was not explored, however.

A second approach to investigating ligand-independent signalling was based on a ligand-independent triggering assay recently established in our group. This assay successfully allowed us to detect strong TCR-dependent signalling in the absence of ligands. Other work in the laboratory strongly suggest that signalling by presumably monovalent TCRs in this assay arises as a result of the exclusion of bulky phosphatases from contact regions created by the binding of a CD28-specific superagonistic antibody to a truncated, non-signalling form of CD28. It is proposed that a similar mechanism of signalling could easily explain signalling by the pre-TCR, with CD28 replaced by small adhesion molecules such as CD2 and its ligands.

The dependence of the TCR and the proximal kinases, Lck and Zap70, in this type of signalling was further investigated by gene editing, with the first attempt by shRNA-mediated knock-down and then the second, successful method being CRISPR/Cas9-mediated gene inactivation. shRNA was first used to knock out Lck and Zap70. The efficiency of gene knock-down by shRNA was not very high and likely individual gene/sequence-dependent. In comparison, CRISPR/Cas9 gene-inactivation gave a relatively high efficiency and no changes in expression levels of the other non-targeted proximal signalling proteins tested, *i.e.* TCR/CD3, Lck or Zap70, was observed.

However, in the course of this study, it was also found out that the viability of cells lacking the kinases very low, with the cells surviving 2-3 weeks. This might due to the 'maxi lentiviral' infection which involved 50 times more virus than is usually used (*i.e.* 10 times more virus for each CRISPR guide; 5 guides for each gene target) or from the fact that these signalling proteins were also involved in other

survival/signalling pathways [359, 360]. A third possibility is that there were some unknown off-target effects of the CRISPR/Cas9 system. A very recent study using whole-genome sequencing revealed unexpectedly high rates of CRISPR off-target mutations including both single-nucleotide variants and small insertions and deletions, some of which were detrimental to key cellular processes [361].

The results in this chapter confirmed, firstly, that signalling could be produced without TCR engagement, since the TCR had to be present on the cell surface. Similar results were observed by R. Knox and M. Vuong using receptor-deficient BW5147 mouse cells reconstituted with the TCR, instead of DO11.10 cells. Secondly, using the CRISPR/Cas9 treated cells, the experiments showed that Lck and Zap70 expression were indispensable for ligand-independent TCR signalling. The levels of IL-2 produced by the pre-TCR in the assay, following reconstitution of the receptor in TCRα-depleted cells, were relatively very low, which was likely due to the low surface expression levels of the pre-TCR, and precluded the analysis of the role of Lck and Zap70 in signalling. Another important caveat of this study is that gene reconstitutions to CRISPR/Cas9 treated cells and signalling competence after gene reconstitutions were not explored. In addition, the ability of the CRISPR/Cas9 treated cells to signal following the gene deletions was not thoroughly tested. Although some degree of signalling was observed in the Lck "deficient" cells induced, for example, by KT3 antibody ($p < 0.01$) suggesting that the cells were signalling competent, ideally it would have been better to have shown, *e.g.* with PMA/ionomycin that the Lck- and ZAP70-deficient cells were otherwise fully signalling competent.

Chapter 7

General discussion

I. Results from this thesis

The pre-TCR shares similarities in structure and signalling components with the TCR but, in contrast to the TCR, there are no known ligands of the pre-TCR. It therefore remains unclear how cells sense the successful surface expression of the pre-TCR containing the pair of an invariant pre-Tα and a gene-rearranged TCRβ, and initiate further development in the thymus. Understanding how signalling is initiated and regulated spatiotemporally will be helped by investigations of receptor stoichiometry. Therefore, in this thesis pre-TCR stoichiometry was investigated using mutagenesis and imaging techniques. Ligand-independent signalling was then investigated in an *in vitro* assay.

Several studies in the field have previously implicated interactions between the extracellular domains of pre-Tα and TCRβ, or the formation of dimeric or oligomeric pre-TCR complexes, in pre-TCR assembly and/or signalling [233, 234]. In this thesis, surface residues in the extracellular domain of pre-Tα were identified [302] and, based on the assumption that the correct assembly of the entire complex is a prerequisite for its expression on the cell surface [78, 79, 252], seventy-four selected residues of pre-Tα were subjected to 'drastic' mutational analysis [252]. The effects of the mutations on pre-TCR surface expression allowed the identification of structural interfaces necessary for assembly to be identified. The analysis showed that, except for the interface that pre-Tα forms with the constant region of TCRβ, no other interface was required for pre-TCR surface expression.

The stoichiometry of the pre-TCR, along with that of the TCR, was further explored using super-resolution imaging techniques and SMCCCD. The imaging results and analyses surprisingly revealed that the pre-TCR, in transfected cells, exhibits a tendency to form dimers, or more likely higher-order of oligomers. Although these results were also inconsistent with the formation of simple pre-TCR dimers, the existence of oligomeric pre-TCRs on the cell surface cannot at present be reconciled with the finding that a single interface was required for pre-TCR expression at the cell surface. There were also technical limitations that emerged in the course of study, which highlighted some of the difficulties in studying receptor stoichiometry generally.

A. Cellular and technical limitations and methdological optimisation

(a) Low expression of the pre-TCR

Native cell surface expression levels of the pre-TCR are generally very low [233, 304, 331, 332], and, in the earliest experiments in this thesis, the pre-TCR at this low level could not be reliably detected using, *e.g.* an anti-HA antibody against the HA-tagged pre-Tα. On the assumption that higher levels of transduction of TCR-deficient E6.1-57 Jurkat cells might lead to higher surface expression, multiple standard lentiviral infections were used, but this failed to increase the pre-TCR surface expression levels. In other experiments, based on the finding that the pre-Tα is retained in the endoplasmic reticulum by its own cytoplasmic domain [304], attempts were made to reduce the effects of this retention, but this was also largely unsuccessful. This suggested that other regulatory mechanisms might play a more important role in restricting expression than the endoplasmic reticulum retention effect, for example, endocytosis or ubiquitin-mediated degradation of the pre-TCR at the cell surface [93, 234, 362]. On the other hand, chimeric pre-Tα with the cytoplasmic domain of mature

TCRα only marginally improved pre-TCR surface expression levels. It is, perhaps, worth noting that in these experiments, the pre-TCR expression levels were determined using the anti-CD3ε UCHT1 antibody, which should have maximised the fluorescence obtainable in the FACS-based analyses of expression.

When it was found that very little could be done to increase the expression of the pre-TCR, it was decided that the effects of the mutations would have to be resolved by the careful inclusion, in the FACS-based analyses, of internal negative controls. By leaving the TCRβ chain in or out of the TCR-deficient Jurkat cell pre-Tα transfections, the ability of pre-Tα mutants to enhance their expression at the cell surface by engaging, and forming complexes with TCRβ could be tested. Although the pre-TCR expression levels were still very low (fluorescence versus background was often, at best, ~2-fold higher than the TCRβ- control for wild-type pre-Tα), very robust and reproducible effects of the mutations could be identified. In this way, the mutation effects of pre-Tα residues on pre-TCR surface expression levels were directly investigated and compared.

(b) Stoichiometric analyses using fluorescence imaging

In other parts of this thesis, several technical limitations prevented the straightforward application of super-resolution imaging techniques to stoichiometric measurements, *i.e.* stoichiometric information could not be directly obtained only from the numbers of fluorescent spots detected when the receptors were tagged with fluorescent proteins or antibodies/Fabs.

i. Photochemistry and over/under-counting biases

Photo-bleaching often results in the number of fluorophores not being correlated with the number of labelled proteins. In the present experiments, photo-bleaching did not

allow the stoichiometry of receptors to be identified, even for clear-cut monomeric and dimeric controls due to the photo-chemical properties of the photoactivatable dyes and fluorescent proteins. In the case of the organic fluorescent dye, HaloTag Ligand TMR, for example, non-single exponential decay resulted in the over-counting of single TMRs in monomers and/or the under-counting of two or more TMRs in dimers or higher-order oligomers.

Under-counting of TMR has been investigated elsewhere. The N,N-dimethyl group of TMR was found to result in irreversible, non-radiative decay [334]. It was proposed that after TMR absorbed a photon leading to the excited state, instead of emission, an energy-favoured 'twisted internal charge transfer (TICT)' state formed by electron transfer from the nitrogen atom to the xanthene ring system. TICT then underwent an irreversible, non-radiative decay to the ground state without emission. This could be avoided by structural modification of TMR, for example, by replacing the N,N-dimethyl group in TMR with a four-membered azetidine ring [334]. Further optimisation of the photo-chemical properties of fluorescent proteins for use in this application would be required before stoichiometry determination will be possible using photo-bleaching steps.

However, the problems relate not only to organic fluorescent dyes. It has been found that mEos and other photoactivatable fluorescent proteins very commonly produce intermittent emission bursts, rather than a single continuous burst, as a result of transient chromophore protonation of Cα atoms [363, 364]. This has commonly led to over-counting results and remains a major obstacle to determining stoichiometries of proteins of interest in fusion with mEos [365]. In one example, the monomeric CD86 fused with mEos appeared to form clusters detected using PALM before post-hoc analysis, due to intermittent mEos emission [366]. Other problems are that only about 40% to 60% of mEos fluorescent protein are effectively activated and detected, and

high background noise or arbitrary detection thresholds can also affect the fraction of mEos fluorescent proteins being detected [335, 336]. These processes then lead to under-counting-biase and therefore monomer-biased results in stoichiometric analysis.

ii. Super resolution imaging-based cluster analysis without counting biases

Now that over/under-counting of blinking fluorophores has become a major issue in super resolution imaging-based cluster analysis, several approaches have emerged to deal with this problem [238, 337]. For example, in order to avoid over-counting of blinking fluorophores, Rollins *et al.* developed a theoretical approach to analyse the behaviour of photoactivatable fluorescent proteins stochastically and attempted to use fluorescence intensities to estimate complex stoichiometry [337]. Another important innovation was proposed by Baumgart *et al.*, who incorporated data obtained with serial dilutions of fluorophore-labelled antibodies into their cluster analyses, thus allowing clustered molecules to be clearly distinguished from randomly organised labelled proteins [238]. Using Baumgart's cluster analysis to avoid counting biases in dSTORM, the organisation of Fcγ receptors has now been reliably analysed [367]. These types of approaches to cluster analysis provide a rigorous basis for fluorophore counting allowing bona fide clusters and non-clusters to be distinguished using dSTORM/PALM imaging data. This leaves only the problem of distinguishing between the physical oligomerisation states of receptors, and the indirect effects of the cytoskeleton, *i.e.* corralling effects [180, 236, 340].

B. Pre-TCR stoichiometry

(a) Only one subunit interface needs to form for pre-TCR complex assembly

In identifying interfaces needed for pre-TCR complex assembly, the criterion used was

that only contiguous interface(s), formed by adjacent residues in the crystal structure, each of whose mutation significantly reduced expression, would be considered. Using this approach, it was found that only mutations of the 'contact' pre-Tα residues identified by Naccess, *i.e.* the residues that are buried by contact with the constant region of TCRβ, reduced expression of the pre-TCR by more than one third versus the level of the wild-type complex. Thus, this mutagenesis approach was shown to be able to identify surfaces that would normally be expected to have to form in order for the pre-TCR complex to assemble. In contrast, there was no contiguous surface populated with residues whose mutation invariably disrupted expression, among the 'dimerising' residues identified and tested by Pang *et al.* [233], or the larger set of residues that are buried according to Naccess, upon formation of the dimer they identified in their crystal lattice. The mutant solvent-exposed residues comprising the 'dimerising' set of amino acids identified by Pang *et al.* were generally dispersed across the surface. However, some of the residues identified by Pang *et al.* as having effects on expression, *i.e.* P44, F58 and W70, were either TCRβ-contacting (F58) as well, or were adjacent to TCRβ-contacting residues (P44 and W70) in the pre-TCR crystal structure. It seems very likely that for these residues the effects of the mutations were due to the disruptive effects on TCRβ association rather than on formation of the 'head-to-tail' dimer *per se*. The dispersed, solvent-exposed residues that did disrupt complex formation, especially given that they included tryptophan and proline residues, might change local stability or folding of either pre-Tα itself, or the complex it forms with TCRβ. The effects of these types of residues are difficult to predict according to this single-residue, mutagenesis-based strategy, but in our experience these residues tend not to form clusters and so are unlikely to be identified incorrectly as interface-forming residues [303, 305, 306, 368]. Nevertheless, given that the TCRβ-contacting surface was robustly identified using this strategy, it does seem as if

the pre-TCR comprises only one interface formed between pre-Tα and TCRβ, and that the dimer proposed by Pang *et al.* either does not form or it is not required to form in order for the pre-TCR to get to the cell surface.

(b) Pre-TCRs may form high-order oligomers but not large clusters

Using dSTORM and Baumgart's cluster analysis [238], pre-TCRs were also found to be non-clustered according to the analysis presented in Chapter 4. On the other hand, the stoichiometric analysis of the pre-TCR using SMCCCD in Chapter 5 suggested that the complex forms higher order oligomers rather than dimers.

The SMCCCD analysis was used in this thesis for the first time to study pre-TCR and mature TCR stoichiometry. Using the co-localisation imaging-based method, mature TCRs at native expression level showed a similar coincidence level to the dimeric control, whereas TCRs at lower expression levels showed coincidence levels that were indistinguishable from that of a monomeric control. The tendency of the mature TCR to exhibit some degree of clustering at higher expression levels was also noted in the PALM measurements of Chapter 4, and attributed to weak spontaneous signalling in cultures of the Jurkat cells. This emphasises the need to be aware of the activation state of the cells being studied. The monomeric stoichiometry of mature TCRs at the lower expression levels echoed the results of a previous study [236], however. In contrast, pre-TCRs at an expression level comparable to the amount of mature TCRs at the lower expression level formed structures not significantly different from dimers in situ according to the co-localisation analysis. Alongside the co-localisation analysis, the intensity analysis was suggestive of the formation of higher-level (non-dimer) pre-TCR oligomers. It needs to be borne in mind that for the most part the stoichiometric data was obtained after transfecting a T-cell hybridoma and only very preliminary data was obtained for *ex vivo* thymocytes. Overall, the

precise organisation of the pre-TCR remains equivocal, and all that can safely be said is that the pre-TCR is unlikely to comprise dimers organised in the way identified by Pang *et al.* If oligomers are required to form, they do not appear to depend on the formation of new interfaces beyond that buried in the single contact of pre-Tα with TCRβ. How these data impact on interpretations of pre-TCR signal initiation, is further discussed in part II below.

C. Ligand-independent signalling uses the conventional T cell signalling pathway

Receptor signalling in the absence of ligands, and the requirements for signal initiation were investigated in a new ligand-independent TCR signalling assay, as presented in Chapter 6. Using this assay, by investigating IL-2 promoter activities, ligand-independent TCR signalling could be detected when contact was mediated between plastic-immobilised CD28-specific superagonistic antibodies and a T cell hybridoma expressing a truncated, signalling-disabled form of CD28. CD28-specific conventional and superagonistic antibodies each bind with different topology to CD28 receptors [354]. Thus, the immobilised superagonistic antibody, which binds to the "side" of CD28 rather than the "top" of CD28 in the manner of conventional antibodies, is assumed to create a 'close-contacts' that excludes bulky phosphatases more efficiently than the conventional antibodies, thus favouring stronger signalling and producing greater IL-2 promotor activity [369, 370]. Ligand-independent TCR triggering was shown to be produced by the CD28-specific superagonistic antibody, JJ316, because signalling was observed for the truncated, non-signalling CD28 receptor, but this signalling stopped when the TCR was deleted from the hybridoma.

Using the CRISPR/Cas9-mediated gene knock-out strategy, ligand-independent signalling by the mature TCR manifested in this assay as IL-2 promoter activation, was shown to be entirely dependent on the proximal signalling mediators Lck and

Zap70. In addition, ligand-independent signalling could also be triggered from pre-TCRs in this assay, although signalling from the pre-TCR-expressing cells was low, probably due to its low surface expression levels as discussed above, and its incapability, as a result, to recruit as many proximal tyrosine kinases for signal initiation as mature TCRs. Consistent with this, in unpublished work, it has been shown by M. Vuong *et al.* (Davis laboratory), that signalling driven by superagonistic antibody binding to truncated CD28-expressing hybridomas is dependent on relatively high levels of TCR expression. The results in Chapter 6 show that signalling in the absence of TCR and pre-TCR ligands involves a similar, or the same mechanism, as conventional *i.e.* ligand-induced mature TCR signalling.

II. Controversies over pre-TCR stoichiometry and signal initiation

In this thesis, the results of stoichiometric measurements of pre-TCRs using different approaches did not come to an unequivocal conclusion. One explanation is that a single pre-TCR is minimally required for pre-TCR complex assembly and for initial expression of the complex on the cell surface, as suggested from the mutagenesis data in Chapter 3. After single pre-TCRs, *i.e.* monomeric ones with respect to pre-Tα expression, reached the cell membrane, they might remain in that state, randomly diffusing on the cell surface before initiating signalling. Chances are also that monomeric pre-TCRs might have a tendency to form higher-order oligomers when encountering pre-TCRs, enhancing their temporal thermodynamic stability, as suggested from the SMCCCD and the intensity analyses in Chapter 5. However, the individual oligomers appeared not to further aggregate nor to form clusters according to the dSTORM and cluster analysis in Chapter 4, using the methods of Baumgart *et al.* [238]. Thus, receptor stoichiometry required for initial cell surface expression does

not necessarily equate with that required for function. In future studies, it will be of interest to further investigate signalling competency of all mutant pre-TCRs made in Chapter 3, using ligand-independent signalling assay, or using animal models. It currently remains unclear how the pre-TCR can initiate signalling in the absence of ligands.

A. Role of the pre-Tα cytoplasmic domain in pre-TCR signalling

Focus has in the past been placed on the cytoplasmic domain of the pre-Tα, in terms of the specific signalling requirements of the pre-TCR. Some studies suggested that the pre-TCR interacts with kinase-rich lipid rafts via palmitoylation of the cysteine in the cytoplasmic domain of pre-Tα. The proline-rich motif in the cytoplasmic domain of pre-Tα was then able to interact with the SH3 domain of intracellular kinases, thus promoting β-selection, self-oligomerisation and, as a result, pre-TCR signalling [273, 274]. However, recent evolutionary analysis *in silico* raises questions about this hypothesis. In Sauropsids and lower Mammalia such as monotremes, marsupials and lagomorphs, the cytoplasmic domains of the pre-Tαs are shorter and lack the proline-rich motifs [276]. Other studies also disproved a requirement for interactions involving the cytoplasmic domain of pre-Tα since it was shown that the pre-TCR could initiate signalling effectively in the absence of the cytoplasmic domains of the pre-Tα [93, 371, 372].

It has also been argued that the cytoplasmic domain of pre-Tα has an important role in restricting expression of the TCR at the cell surface, but in the present experiments it was found that truncating this domain or even swapping it completely with the equivalent region of TCRα had only very marginal effects on expression. One explanation for the low expression of the pre-TCR is simply that it assembles inefficiently, or it is generally somewhat unstable, or it is recognised by chaperones,

rightly or wrongly as being incorrectly assembled. Altogether, the most important region of pre-TCR in terms of signalling seems likely to be the cytoplasmic domains of the CD3 chains, specifically the ITAMs. Especially given that the cytoplasmic domain of the Sauropsid pre-Tα receptors are so short [276], the function of this part of the pre-TCR is a mystery.

B. Role of the pre-Tα extracellular domains in pre-TCR signalling

Autonomous dimerisation or oligomerisation of the pre-TCR via the extracellular domains of pre-Tα and TCRβ has been invoked as an explanation for ligand-independent signal initiation and regulation of the pre-TCR in previous studies [233, 234, 271, 272]. Mutations of these 'dimerising' or 'oligomerising' pre-Tα residues in the extracellular domains were claimed to inhibit signalling and thymocyte development. For example, Yamasaki *et al.* suggested that four charged mouse pre-Tα residues (*i.e.* D22, R24, R102 in the extracellular domain and R117 in the connecting peptide near the transmembrane region) were especially indispensable for pre-TCR autonomous oligomerisation, signalling and continued thymocyte development [234]. The subsequent study using X-ray crystallographic analysis and small-angle X-ray scattering by Pang *et al.*, proposed that an autonomous head-to-tail dimeric structure was formed by human pre-TCRs, which was required for pre-TCR signalling [233]. However, *in silico* gene synteny-based analysis suggested that, like similar claims for the cytoplasmic domain of the receptor, the four charged pre-Tα mouse residues were probably unlikely to have a major role in pre-TCR function because these residues are not conserved among Sauropsids and mammals [276]. In some sauropsidian and mammalian pre-Tαs, these residues were even missing or bore the opposite charges. In addition, Mahtani-Patching *et al.* [93] showed that a truncated form of mouse pre-TCR containing mutant pre-Tα lacking its extracellular domain was capable of

pre-TCR signalling and thymocyte development. In this case, the consequences of expressing a pair of receptor chains (pre-Tα and TCRβ or TCRγ and TCRδ) on the cell surface at the DN stage, for signal initiation and further development was highly dependent on the strength of signal generated. Weaker signalling driven by the pre-TCR resulted in TCRαβ T cell development whereas stronger signalling drove TCRγδ T-lineage development [93]. The work of Mahtani-Patching *et al.* was consistent with a previous study of Irving *et al.*, which showed that the pre-TCR is capable of initiating signalling *in vitro* without the extracellular domains of either pre-Tα and TCRβ - in fact both can be deleted simultaneously [237].

The corresponding residues of the mouse pre-Tα 'dimerising'/'oligomerising' residues in the extracellular domain suggested to be important by Yamasaki *et al.* were D22, K24 and R102 of the human pre-Tα sequence according to gene alignments by Smetly *et al.* [276]. Drastic mutations of these three residues (Chapter 3), which were predicted as solvent-exposed by Naccess analysis, resulted in either no effect (D22R) or only moderate inhibition of surface expression (K24E and R102E). Furthermore, when the non TCRβ-contacting residues that were buried in forming the head-to-tail dimer structure reported by Pang *et al.* were systematically mutated drastically, the mutations with substantial effects on expression did not form a contiguous interface in the crystal structure, in the manner of the TCRβ-contacting residues. These results also suggested that there were no other interfaces that have to form other than that between pre-Tα and the constant region of the TCRβ required for pre-TCR surface expression.

C. Requirement of the pre-TCR *per se* for pre-TCR signalling

The idea that simply the presence, on the cell surface, of successfully-assembled pre-TCRs, each comprising an invariant pre-Tα chain and a rearranged TCRβ chain,

would be enough to initiate pre-TCR signalling is compatible with the kinetic-segregation model of signal initiation [215]. Chang *et al.* [183] have shown that when 'close-contacts' are formed as Jurkat cells interact with model surfaces, CD45 and kinase segregation was observed to occur spontaneously at each local contact site, to the extent that the CD45/Lck ratio decreased from 5:1 in the resting cells to 2.3:1 in the contacts. Chang *et al.* showed that this relatively small change in the balance of phosphorylation and dephosphorylation was sufficient to initiate signalling by the TCR, which was clearly ligand-independent since ligands were absent from the surfaces that they studied. They proposed that the task of ligands in the context of signalling being initiated by phosphatase exclusion alone could be to further heighten signalling, simply by holding receptors in the regions from which the phosphatases are excluded.

The results presented in Chapter 6 are consistent with, and extend this view, because the proximal signalling dependencies of ligand-dependent and -independent signalling appear to be identical. Similarly, in accordance with the results presented in Chapters 4 and 5, irrespective of whether the pre-TCR is an oligomer or forms only monovalent complexes, the work in this thesis and that of Chang *et al.* suggests that the mere presence of the pre-TCR at the cell surface would be sufficient to drive some degree of signalling if phosphatases are excluded at sites of contact between pre-T cells and the thymic cortical epithelium. Importantly, such a mechanism might in fact be tolerant of a range of structures, *i.e.* pre-TCR complexes that can get to the cell surface but vary in stability due to differences in the structures of the nascent TCRβ chains. In further support of this idea, unlike TCR signalling regulated by its engagement with authentic MHC/peptide ligands, pre-TCR signalling is thought to have a relatively low threshold [234, 372]. For example, constant signals delivered through a CD8/CD3ε chimeric protein could produce cellular responses in DN cells, but not in DP or mature T cells [372]. Similarly, TCRα-deficient DN3 thymocytes displayed a

significantly higher level of constitutive ERK activity as compared with DN4 or DP thymocytes [234]. This low-threshold would likely be necessary given the very low levels of expression of the pre-TCR in DN thymocytes [233, 304, 331, 332].

References

1. Akira, S., S. Uematsu, and O. Takeuchi, *Pathogen recognition and innate immunity.* Cell, 2006. **124**(4): p. 783-801.
2. Medzhitov, R., *Recognition of microorganisms and activation of the immune response.* Nature, 2007. **449**(7164): p. 819-26.
3. Iwasaki, A. and R. Medzhitov, *Regulation of adaptive immunity by the innate immune system.* Science, 2010. **327**(5963): p. 291-5.
4. Prabhudas, M., et al., *Standardizing scavenger receptor nomenclature.* J Immunol, 2014. **192**(5): p. 1997-2006.
5. Underhill, D.M. and A. Ozinsky, *Toll-like receptors: key mediators of microbe detection.* Curr Opin Immunol, 2002. **14**(1): p. 103-10.
6. Brown, G.D., *Dectin-1: a signalling non-TLR pattern-recognition receptor.* Nat Rev Immunol, 2006. **6**(1): p. 33-43.
7. Shinkai, K., M. Mohrs, and R.M. Locksley, *Helper T cells regulate type-2 innate immunity in vivo.* Nature, 2002. **420**(6917): p. 825-9.
8. Parkin, J. and B. Cohen, *An overview of the immune system.* Lancet, 2001. **357**(9270): p. 1777-89.
9. Lee, S.H., T. Miyagi, and C.A. Biron, *Keeping NK cells in highly regulated antiviral warfare.* Trends Immunol, 2007. **28**(6): p. 252-9.
10. Smyth, M.J., et al., *New aspects of natural-killer-cell surveillance and therapy of cancer.* Nat Rev Cancer, 2002. **2**(11): p. 850-61.
11. Moretta, A., et al., *Receptors for HLA class-I molecules in human natural killer cells.* Annu Rev Immunol, 1996. **14**: p. 619-48.
12. Raulet, D.H. and N. Guerra, *Oncogenic stress sensed by the immune system: role of natural killer cell receptors.* Nat Rev Immunol, 2009. **9**(8): p. 568-80.
13. Fearon, D.T. and R.M. Locksley, *The instructive role of innate immunity in the acquired immune response.* Science, 1996. **272**(5258): p. 50-3.
14. O'Leary, J.G., et al., *T cell- and B cell-independent adaptive immunity mediated by natural killer cells.* Nat Immunol, 2006. **7**(5): p. 507-16.
15. Sun, J.C., J.N. Beilke, and L.L. Lanier, *Adaptive immune features of natural killer cells.* Nature, 2009. **457**(7229): p. 557-61.
16. Cooper, M.D., R.D. Peterson, and R.A. Good, *Delineation of the Thymic and Bursal Lymphoid Systems in the Chicken.* Nature, 1965. **205**: p. 143-6.
17. Greaves, M.F., I.M. Roitt, and M.E. Rose, *Effect of bursectomy and thymectomy on the responses of chicken peripheral blood lymphocytes to phytohaemagglutinin.* Nature, 1968. **220**(5164): p. 293-5.
18. Min, H., E. Montecino-Rodriguez, and K. Dorshkind, *Effects of aging on early*

B- and T-cell development. Immunol Rev, 2005. **205**: p. 7-17.

19. Lorenz, E., et al., *Modification of irradiation injury in mice and guinea pigs by bone marrow injections.* J Natl Cancer Inst, 1951. **12**(1): p. 197-201.
20. Kondo, M., I.L. Weissman, and K. Akashi, *Identification of clonogenic common lymphoid progenitors in mouse bone marrow.* Cell, 1997. **91**(5): p. 661-72.
21. Schatz, D.G., M.A. Oettinger, and D. Baltimore, *The V(D)J recombination activating gene, RAG-1.* Cell, 1989. **59**(6): p. 1035-48.
22. Oettinger, M.A., et al., *RAG-1 and RAG-2, adjacent genes that synergistically activate V(D)J recombination.* Science, 1990. **248**(4962): p. 1517-23.
23. Isobe, M., et al., *Chromosome localization of the gene for human terminal deoxynucleotidyltransferase to region 10q23-q25.* Proc Natl Acad Sci U S A, 1985. **82**(17): p. 5836-40.
24. Yang-Feng, T.L., et al., *The terminal deoxynucleotidyltransferase gene is located on human chromosome 10 (10q23----q24) and on mouse chromosome 19.* Cytogenet Cell Genet, 1986. **43**(3-4): p. 121-6.
25. Bassing, C.H., W. Swat, and F.W. Alt, *The mechanism and regulation of chromosomal V(D)J recombination.* Cell, 2002. **109 Suppl**: p. S45-55.
26. Wucherpfennig, K.W., et al., *Structural biology of the T-cell receptor: insights into receptor assembly, ligand recognition, and initiation of signaling.* Cold Spring Harb Perspect Biol, 2010. **2**(4): p. a005140.
27. Qadri, A., et al., *Characterization of the interaction of a TCR alpha chain variable domain with MHC II I-A molecules.* Int Immunol, 1999. **11**(6): p. 967-77.
28. Saline, M., et al., *The structure of superantigen complexed with TCR and MHC reveals novel insights into superantigenic T cell activation.* Nat Commun, 2010. **1**: p. 119.
29. Kuo, T.C. and M.S. Schlissel, *Mechanisms controlling expression of the RAG locus during lymphocyte development.* Curr Opin Immunol, 2009. **21**(2): p. 173-8.
30. Hawwari, A. and M.S. Krangel, *Role for rearranged variable gene segments in directing secondary T cell receptor alpha recombination.* Proc Natl Acad Sci U S A, 2007. **104**(3): p. 903-7.
31. Rosenthal, A.S. and E.M. Shevach, *Function of macrophages in antigen recognition by guinea pig T lymphocytes. I. Requirement for histocompatible macrophages and lymphocytes.* J Exp Med, 1973. **138**(5): p. 1194-212.
32. Shevach, E.M. and A.S. Rosenthal, *Function of macrophages in antigen recognition by guinea pig T lymphocytes. II. Role of the macrophage in the regulation of genetic control of the immune response.* J Exp Med, 1973. **138**(5):

p. 1213-29.
33. Zinkernagel, R.M. and P.C. Doherty, *H-2 compatability requirement for T-cell-mediated lysis of target cells infected with lymphocytic choriomeningitis virus. Different cytotoxic T-cell specificities are associated with structures coded for in H-2K or H-2D.* J Exp Med, 1975. **141**(6): p. 1427-36.
34. Piertney, S.B. and M.K. Oliver, *The evolutionary ecology of the major histocompatibility complex.* Heredity (Edinb), 2006. **96**(1): p. 7-21.
35. Zhang, H., et al., *The contribution of major histocompatibility complex contacts to the affinity and kinetics of T cell receptor binding.* Sci Rep, 2016. **6**: p. 35326.
36. Blum, J.S., P.A. Wearsch, and P. Cresswell, *Pathways of antigen processing.* Annu Rev Immunol, 2013. **31**: p. 443-73.
37. Brown, J.H., et al., *Three-dimensional structure of the human class II histocompatibility antigen HLA-DR1.* Nature, 1993. **364**(6432): p. 33-9.
38. Williams, A.P., et al., *Optimization of the MHC class I peptide cargo is dependent on tapasin.* Immunity, 2002. **16**(4): p. 509-20.
39. Cresswell, P., *Assembly, transport, and function of MHC class II molecules.* Annu Rev Immunol, 1994. **12**: p. 259-93.
40. Roche, P.A. and P. Cresswell, *Invariant chain association with HLA-DR molecules inhibits immunogenic peptide binding.* Nature, 1990. **345**(6276): p. 615-8.
41. Townsend, A. and J. Trowsdale, *The transporters associated with antigen presentation.* Semin Cell Biol, 1993. **4**(1): p. 53-61.
42. Nishimura, M.I., et al., *MHC class I-restricted recognition of a melanoma antigen by a human CD4+ tumor infiltrating lymphocyte.* Cancer Res, 1999. **59**(24): p. 6230-8.
43. Arunachalam, B., et al., *Enzymatic reduction of disulfide bonds in lysosomes: characterization of a gamma-interferon-inducible lysosomal thiol reductase (GILT).* Proc Natl Acad Sci U S A, 2000. **97**(2): p. 745-50.
44. Braud, V.M., et al., *HLA-E binds to natural killer cell receptors CD94/NKG2A, B and C.* Nature, 1998. **391**(6669): p. 795-9.
45. Nemazee, D.A. and K. Burki, *Clonal deletion of B lymphocytes in a transgenic mouse bearing anti-MHC class I antibody genes.* Nature, 1989. **337**(6207): p. 562-6.
46. Tiegs, S.L., D.M. Russell, and D. Nemazee, *Receptor editing in self-reactive bone marrow B cells.* J Exp Med, 1993. **177**(4): p. 1009-20.
47. Junt, T., E. Scandella, and B. Ludewig, *Form follows function: lymphoid tissue microarchitecture in antimicrobial immune defence.* Nat Rev Immunol, 2008. **8**(10): p. 764-75.

48. Halin, C., et al., *In vivo imaging of lymphocyte trafficking.* Annu Rev Cell Dev Biol, 2005. **21**: p. 581-603.
49. Seda, V. and M. Mraz, *B-cell receptor signalling and its crosstalk with other pathways in normal and malignant cells.* Eur J Haematol, 2015. **94**(3): p. 193-205.
50. Matsuuchi, L. and M.R. Gold, *New views of BCR structure and organization.* Curr Opin Immunol, 2001. **13**(3): p. 270-7.
51. Andria, M.L., et al., *Genomic organization and chromosomal localization of the TAPA-1 gene.* J Immunol, 1991. **147**(3): p. 1030-6.
52. Otero, D.C., S.A. Omori, and R.C. Rickert, *Cd19-dependent activation of Akt kinase in B-lymphocytes.* J Biol Chem, 2001. **276**(2): p. 1474-8.
53. Clark, E.A., et al., *Activation of human B cells. Comparison of the signal transduced by IL-4 to four different competence signals.* J Immunol, 1989. **143**(12): p. 3873-80.
54. Maddaly, R., et al., *Receptors and signaling mechanisms for B-lymphocyte activation, proliferation and differentiation--insights from both in vivo and in vitro approaches.* FEBS Lett, 2010. **584**(24): p. 4883-94.
55. Stein, K.E., *Thymus-independent and thymus-dependent responses to polysaccharide antigens.* J Infect Dis, 1992. **165 Suppl 1**: p. S49-52.
56. Lesinski, G.B. and M.A. Westerink, *Novel vaccine strategies to T-independent antigens.* J Microbiol Methods, 2001. **47**(2): p. 135-49.
57. El Shikh, M.E., et al., *T-independent antibody responses to T-dependent antigens: a novel follicular dendritic cell-dependent activity.* J Immunol, 2009. **182**(6): p. 3482-91.
58. Aluvihare, V.R., et al., *Acceleration of intracellular targeting of antigen by the B-cell antigen receptor: importance depends on the nature of the antigen-antibody interaction.* EMBO J, 1997. **16**(12): p. 3553-62.
59. Harwood, N.E. and F.D. Batista, *The cytoskeleton coordinates the early events of B-cell activation.* Cold Spring Harb Perspect Biol, 2011. **3**(2).
60. Victora, G.D. and M.C. Nussenzweig, *Germinal centers.* Annu Rev Immunol, 2012. **30**: p. 429-57.
61. Teng, G. and F.N. Papavasiliou, *Immunoglobulin somatic hypermutation.* Annu Rev Genet, 2007. **41**: p. 107-20.
62. Manis, J.P., M. Tian, and F.W. Alt, *Mechanism and control of class-switch recombination.* Trends Immunol, 2002. **23**(1): p. 31-9.
63. Xu, Z., et al., *Immunoglobulin class-switch DNA recombination: induction, targeting and beyond.* Nat Rev Immunol, 2012. **12**(7): p. 517-31.
64. Sanders, V.M., et al., *Characterization of the physical interaction between*

antigen-specific B and T cells. J Immunol, 1986. **137**(8): p. 2395-404.

65. Kurosaki, T., K. Kometani, and W. Ise, *Memory B cells.* Nat Rev Immunol, 2015. **15**(3): p. 149-59.
66. Yoshida, T., et al., *Memory B and memory plasma cells.* Immunol Rev, 2010. **237**(1): p. 117-39.
67. Allison, J.P., B.W. McIntyre, and D. Bloch, *Tumor-specific antigen of murine T-lymphoma defined with monoclonal antibody.* J Immunol, 1982. **129**(5): p. 2293-300.
68. Haskins, K., et al., *The major histocompatibility complex-restricted antigen receptor on T cells. I. Isolation with a monoclonal antibody.* J Exp Med, 1983. **157**(4): p. 1149-69.
69. Hedrick, S.M., et al., *Isolation of cDNA clones encoding T cell-specific membrane-associated proteins.* Nature, 1984. **308**(5955): p. 149-53.
70. Hedrick, S.M., et al., *Sequence relationships between putative T-cell receptor polypeptides and immunoglobulins.* Nature, 1984. **308**(5955): p. 153-8.
71. Chien, Y.H., et al., *Somatic recombination in a murine T-cell receptor gene.* Nature, 1984. **309**(5966): p. 322-6.
72. Yanagi, Y., et al., *A human T cell-specific cDNA clone encodes a protein having extensive homology to immunoglobulin chains.* Nature, 1984. **308**(5955): p. 145-9.
73. Hodges, E., et al., *Diagnostic role of tests for T cell receptor (TCR) genes.* J Clin Pathol, 2003. **56**(1): p. 1-11.
74. Sydora, B.C., et al., *T-cell receptor gamma delta diversity and specificity of intestinal intraepithelial lymphocytes: analysis of IEL-derived hybridomas.* Cell Immunol, 1993. **152**(2): p. 305-22.
75. Garcia, K.C., et al., *An alphabeta T cell receptor structure at 2.5 A and its orientation in the TCR-MHC complex.* Science, 1996. **274**(5285): p. 209-19.
76. Garboczi, D.N., et al., *Structure of the complex between human T-cell receptor, viral peptide and HLA-A2.* Nature, 1996. **384**(6605): p. 134-41.
77. Call, M.E., et al., *The organizing principle in the formation of the T cell receptor-CD3 complex.* Cell, 2002. **111**(7): p. 967-79.
78. Frank, S.J., et al., *Structural mutations of the T cell receptor zeta chain and its role in T cell activation.* Science, 1990. **249**(4965): p. 174-7.
79. Ohashi, P.S., et al., *Reconstitution of an active surface T3/T-cell antigen receptor by DNA transfer.* Nature, 1985. **316**(6029): p. 606-9.
80. Humphrey, M.B., L.L. Lanier, and M.C. Nakamura, *Role of ITAM-containing adapter proteins and their receptors in the immune system and bone.* Immunol Rev, 2005. **208**: p. 50-65.

81. Godfrey, D.I., et al., *A developmental pathway involving four phenotypically and functionally distinct subsets of CD3-CD4-CD8- triple-negative adult mouse thymocytes defined by CD44 and CD25 expression.* J Immunol, 1993. **150**(10): p. 4244-52.
82. Lucas, B., et al., *Control of the thymic medulla and its influence on alphabetaT-cell development.* Immunol Rev, 2016. **271**(1): p. 23-37.
83. Radtke, F., et al., *Notch regulation of lymphocyte development and function.* Nat Immunol, 2004. **5**(3): p. 247-53.
84. Taghon, T., et al., *Developmental and molecular characterization of emerging beta- and gammadelta-selected pre-T cells in the adult mouse thymus.* Immunity, 2006. **24**(1): p. 53-64.
85. Krangel, M.S., *Mechanics of T cell receptor gene rearrangement.* Curr Opin Immunol, 2009. **21**(2): p. 133-9.
86. Mallick, C.A., et al., *Rearrangement and diversity of T cell receptor beta chain genes in thymocytes: a critical role for the beta chain in development.* Cell, 1993. **73**(3): p. 513-9.
87. Fehling, H.J. and H. von Boehmer, *Early alpha beta T cell development in the thymus of normal and genetically altered mice.* Curr Opin Immunol, 1997. **9**(2): p. 263-75.
88. Michie, A.M. and J.C. Zuniga-Pflucker, *Regulation of thymocyte differentiation: pre-TCR signals and beta-selection.* Semin Immunol, 2002. **14**(5): p. 311-23.
89. Gleimer, M. and H. von Boehmer, *Thymocyte selection: chemokine signaling is not only about the destination.* Curr Biol, 2010. **20**(7): p. R316-8.
90. Ciofani, M., et al., *Obligatory role for cooperative signaling by pre-TCR and Notch during thymocyte differentiation.* J Immunol, 2004. **172**(9): p. 5230-9.
91. Plotkin, J., et al., *Critical role for CXCR4 signaling in progenitor localization and T cell differentiation in the postnatal thymus.* J Immunol, 2003. **171**(9): p. 4521-7.
92. von Boehmer, H., *Selection of the T-cell repertoire: receptor-controlled checkpoints in T-cell development.* Adv Immunol, 2004. **84**: p. 201-38.
93. Mahtani-Patching, J., et al., *PreTCR and TCRgammadelta signal initiation in thymocyte progenitors does not require domains implicated in receptor oligomerization.* Sci Signal, 2011. **4**(182): p. ra47.
94. Hayes, S.M., L. Li, and P.E. Love, *TCR signal strength influences alphabeta/gammadelta lineage fate.* Immunity, 2005. **22**(5): p. 583-93.
95. Munoz-Ruiz, M., et al., *TCR signal strength controls thymic differentiation of discrete proinflammatory gammadelta T cell subsets.* Nat Immunol, 2016. **17**(6): p. 721-727.

96. Ciofani, M. and J.C. Zuniga-Pflucker, *Determining gammadelta versus alphass T cell development.* Nat Rev Immunol, 2010. **10**(9): p. 657-63.
97. Huang, C.Y., B.P. Sleckman, and O. Kanagawa, *Revision of T cell receptor {alpha} chain genes is required for normal T lymphocyte development.* Proc Natl Acad Sci U S A, 2005. **102**(40): p. 14356-61.
98. Starr, T.K., S.C. Jameson, and K.A. Hogquist, *Positive and negative selection of T cells.* Annu Rev Immunol, 2003. **21**: p. 139-76.
99. Petrie, H.T., *Role of thymic organ structure and stromal composition in steady-state postnatal T-cell production.* Immunol Rev, 2002. **189**: p. 8-19.
100. Wilkinson, R.W., et al., *Positive selection of thymocytes involves sustained interactions with the thymic microenvironment.* J Immunol, 1995. **155**(11): p. 5234-40.
101. Palmer, E., *Negative selection--clearing out the bad apples from the T-cell repertoire.* Nat Rev Immunol, 2003. **3**(5): p. 383-91.
102. Finkel, T.H., et al., *Apoptosis occurs predominantly in bystander cells and not in productively infected cells of HIV- and SIV-infected lymph nodes.* Nat Med, 1995. **1**(2): p. 129-34.
103. Jekle, A., et al., *In vivo evolution of human immunodeficiency virus type 1 toward increased pathogenicity through CXCR4-mediated killing of uninfected CD4 T cells.* J Virol, 2003. **77**(10): p. 5846-54.
104. Purdy, B.D. and K.I. Plaisance, *Infection with the human immunodeficiency virus: epidemiology, pathogenesis, transmission, diagnosis, and manifestations.* Am J Hosp Pharm, 1989. **46**(6): p. 1185-209.
105. Zhu, J. and W.E. Paul, *CD4 T cells: fates, functions, and faults.* Blood, 2008. **112**(5): p. 1557-69.
106. Mosmann, T.R., et al., *Two types of murine helper T cell clone. I. Definition according to profiles of lymphokine activities and secreted proteins.* J Immunol, 1986. **136**(7): p. 2348-57.
107. Gutcher, I. and B. Becher, *APC-derived cytokines and T cell polarization in autoimmune inflammation.* J Clin Invest, 2007. **117**(5): p. 1119-27.
108. Zhu, J., H. Yamane, and W.E. Paul, *Differentiation of effector CD4 T cell populations (*).* Annu Rev Immunol, 2010. **28**: p. 445-89.
109. Mosmann, T.R. and R.L. Coffman, *TH1 and TH2 cells: different patterns of lymphokine secretion lead to different functional properties.* Annu Rev Immunol, 1989. **7**: p. 145-73.
110. Hsieh, C.S., et al., *Development of TH1 CD4+ T cells through IL-12 produced by Listeria-induced macrophages.* Science, 1993. **260**(5107): p. 547-9.
111. Szabo, S.J., et al., *A novel transcription factor, T-bet, directs Th1 lineage*

commitment. Cell, 2000. **100**(6): p. 655-69.

112. Wan, Y.Y., *GATA3: a master of many trades in immune regulation.* Trends Immunol, 2014. **35**(6): p. 233-42.
113. Le Gros, G., et al., *Generation of interleukin 4 (IL-4)-producing cells in vivo and in vitro: IL-2 and IL-4 are required for in vitro generation of IL-4-producing cells.* J Exp Med, 1990. **172**(3): p. 921-9.
114. Swain, S.L., et al., *IL-4 directs the development of Th2-like helper effectors.* J Immunol, 1990. **145**(11): p. 3796-806.
115. Coffman, R.L., et al., *Antibody to interleukin-5 inhibits helminth-induced eosinophilia in mice.* Science, 1989. **245**(4915): p. 308-10.
116. Kopf, M., et al., *Disruption of the murine IL-4 gene blocks Th2 cytokine responses.* Nature, 1993. **362**(6417): p. 245-8.
117. Wynn, T.A., *IL-13 effector functions.* Annu Rev Immunol, 2003. **21**: p. 425-56.
118. Fiorentino, D.F., M.W. Bond, and T.R. Mosmann, *Two types of mouse T helper cell. IV. Th2 clones secrete a factor that inhibits cytokine production by Th1 clones.* J Exp Med, 1989. **170**(6): p. 2081-95.
119. Romagnani, S., *T-cell subsets (Th1 versus Th2).* Ann Allergy Asthma Immunol, 2000. **85**(1): p. 9-18; quiz 18, 21.
120. Harrington, L.E., et al., *Interleukin 17-producing CD4+ effector T cells develop via a lineage distinct from the T helper type 1 and 2 lineages.* Nat Immunol, 2005. **6**(11): p. 1123-32.
121. Ivanov, II, et al., *The orphan nuclear receptor RORgammat directs the differentiation program of proinflammatory IL-17+ T helper cells.* Cell, 2006. **126**(6): p. 1121-33.
122. Cho, J.S., et al., *IL-17 is essential for host defense against cutaneous Staphylococcus aureus infection in mice.* J Clin Invest, 2010. **120**(5): p. 1762-73.
123. Sutton, C., et al., *A crucial role for interleukin (IL)-1 in the induction of IL-17-producing T cells that mediate autoimmune encephalomyelitis.* J Exp Med, 2006. **203**(7): p. 1685-91.
124. Li, M.O., S. Sanjabi, and R.A. Flavell, *Transforming growth factor-beta controls development, homeostasis, and tolerance of T cells by regulatory T cell-dependent and -independent mechanisms.* Immunity, 2006. **25**(3): p. 455-71.
125. Chen, W., et al., *Conversion of peripheral CD4+CD25- naive T cells to CD4+CD25+ regulatory T cells by TGF-beta induction of transcription factor Foxp3.* J Exp Med, 2003. **198**(12): p. 1875-86.
126. Ruane, D.T. and E.C. Lavelle, *The role of CD103(+) dendritic cells in the*

intestinal mucosal immune system. Front Immunol, 2011. **2**: p. 25.

127. Sun, C.M., et al., *Small intestine lamina propria dendritic cells promote de novo generation of Foxp3 T reg cells via retinoic acid.* J Exp Med, 2007. **204**(8): p. 1775-85.
128. Zhang, N. and M.J. Bevan, *CD8(+) T cells: foot soldiers of the immune system.* Immunity, 2011. **35**(2): p. 161-8.
129. Zinkernagel, R.M. and P.C. Doherty, *Immunological surveillance against altered self components by sensitised T lymphocytes in lymphocytic choriomeningitis.* Nature, 1974. **251**(5475): p. 547-8.
130. Mescher, M.F., et al., *Signals required for programming effector and memory development by CD8+ T cells.* Immunol Rev, 2006. **211**: p. 81-92.
131. Acuto, O. and F. Michel, *CD28-mediated co-stimulation: a quantitative support for TCR signalling.* Nat Rev Immunol, 2003. **3**(12): p. 939-51.
132. Beuneu, H., et al., *Visualizing the functional diversification of CD8+ T cell responses in lymph nodes.* Immunity, 2010. **33**(3): p. 412-23.
133. Peter, M.E. and P.H. Krammer, *Mechanisms of CD95 (APO-1/Fas)-mediated apoptosis.* Curr Opin Immunol, 1998. **10**(5): p. 545-51.
134. Nagata, S. and P. Golstein, *The Fas death factor.* Science, 1995. **267**(5203): p. 1449-56.
135. Allison, T.J., et al., *Structure of a human gammadelta T-cell antigen receptor.* Nature, 2001. **411**(6839): p. 820-4.
136. Das, H., et al., *MICA engagement by human Vgamma2Vdelta2 T cells enhances their antigen-dependent effector function.* Immunity, 2001. **15**(1): p. 83-93.
137. Hockett, R.D., et al., *Human T-cell antigen receptor (TCR) delta-chain locus and elements responsible for its deletion are within the TCR alpha-chain locus.* Proc Natl Acad Sci U S A, 1988. **85**(24): p. 9694-8.
138. Garman, R.D., P.J. Doherty, and D.H. Raulet, *Diversity, rearrangement, and expression of murine T cell gamma genes.* Cell, 1986. **45**(5): p. 733-42.
139. Boucontet, L., et al., *Mechanisms determining cell membrane expression of different gammadelta TCR chain pairings.* Eur J Immunol, 2009. **39**(7): p. 1937-46.
140. Sheridan, B.S., et al., *gammadelta T cells exhibit multifunctional and protective memory in intestinal tissues.* Immunity, 2013. **39**(1): p. 184-95.
141. Kabelitz, D., et al., *A large fraction of human peripheral blood gamma/delta + T cells is activated by Mycobacterium tuberculosis but not by its 65-kD heat shock protein.* J Exp Med, 1990. **171**(3): p. 667-79.
142. Cai, Y., et al., *Pivotal role of dermal IL-17-producing gammadelta T cells in skin inflammation.* Immunity, 2011. **35**(4): p. 596-610.

143. Park, S.G., et al., *T regulatory cells maintain intestinal homeostasis by suppressing gammadelta T cells.* Immunity, 2010. **33**(5): p. 791-803.
144. Petermann, F., et al., *gammadelta T cells enhance autoimmunity by restraining regulatory T cell responses via an interleukin-23-dependent mechanism.* Immunity, 2010. **33**(3): p. 351-63.
145. Holtmeier, W. and D. Kabelitz, *gammadelta T cells link innate and adaptive immune responses.* Chem Immunol Allergy, 2005. **86**: p. 151-83.
146. Kabelitz, D., *gammadelta T-cells: cross-talk between innate and adaptive immunity.* Cell Mol Life Sci, 2011. **68**(14): p. 2331-3.
147. Bonneville, M., R.L. O'Brien, and W.K. Born, *Gammadelta T cell effector functions: a blend of innate programming and acquired plasticity.* Nat Rev Immunol, 2010. **10**(7): p. 467-78.
148. Krammer, P.H., R. Arnold, and I.N. Lavrik, *Life and death in peripheral T cells.* Nat Rev Immunol, 2007. **7**(7): p. 532-42.
149. Zhang, N., et al., *The role of apoptosis in the development and function of T lymphocytes.* Cell Res, 2005. **15**(10): p. 749-69.
150. Weng, N.P., Y. Araki, and K. Subedi, *The molecular basis of the memory T cell response: differential gene expression and its epigenetic regulation.* Nat Rev Immunol, 2012. **12**(4): p. 306-15.
151. Pulendran, B. and R. Ahmed, *Immunological mechanisms of vaccination.* Nat Immunol, 2011. **12**(6): p. 509-17.
152. Pepper, M. and M.K. Jenkins, *Origins of CD4(+) effector and central memory T cells.* Nat Immunol, 2011. **12**(6): p. 467-71.
153. Gattinoni, L., et al., *A human memory T cell subset with stem cell-like properties.* Nat Med, 2011. **17**(10): p. 1290-7.
154. Gattinoni, L., et al., *T memory stem cells in health and disease.* Nat Med, 2017. **23**(1): p. 18-27.
155. Hamann, D., et al., *Phenotypic and functional separation of memory and effector human CD8+ T cells.* J Exp Med, 1997. **186**(9): p. 1407-18.
156. Kambayashi, T., et al., *Memory CD8+ T cells provide an early source of IFN-gamma.* J Immunol, 2003. **170**(5): p. 2399-408.
157. Sakaguchi, S., et al., *FOXP3+ regulatory T cells in the human immune system.* Nat Rev Immunol, 2010. **10**(7): p. 490-500.
158. Bennett, C.L., et al., *The immune dysregulation, polyendocrinopathy, enteropathy, X-linked syndrome (IPEX) is caused by mutations of FOXP3.* Nat Genet, 2001. **27**(1): p. 20-1.
159. Pandiyan, P., et al., *CD4+CD25+Foxp3+ regulatory T cells induce cytokine deprivation-mediated apoptosis of effector CD4+ T cells.* Nat Immunol, 2007.

8(12): p. 1353-62.

160. Sojka, D.K., Y.H. Huang, and D.J. Fowell, *Mechanisms of regulatory T-cell suppression - a diverse arsenal for a moving target.* Immunology, 2008. **124**(1): p. 13-22.
161. Huang, H., et al., *Comparison of induced versus natural regulatory T cells of the same TCR specificity for induction of tolerance to an environmental antigen.* J Immunol, 2013. **191**(3): p. 1136-43.
162. Liu, Z.M., et al., *The role of all-trans retinoic acid in the biology of Foxp3+ regulatory T cells.* Cell Mol Immunol, 2015. **12**(5): p. 553-7.
163. Lee, W. and G.R. Lee, *Transcriptional regulation and development of regulatory T cells.* Exp Mol Med, 2018. **50**(3): p. e456.
164. Kawano, T., et al., *CD1d-restricted and TCR-mediated activation of valpha14 NKT cells by glycosylceramides.* Science, 1997. **278**(5343): p. 1626-9.
165. Brennan, P.J., M. Brigl, and M.B. Brenner, *Invariant natural killer T cells: an innate activation scheme linked to diverse effector functions.* Nat Rev Immunol, 2013. **13**(2): p. 101-17.
166. Bendelac, A., P.B. Savage, and L. Teyton, *The biology of NKT cells.* Annu Rev Immunol, 2007. **25**: p. 297-336.
167. Bendelac, A., et al., *CD1 recognition by mouse NK1+ T lymphocytes.* Science, 1995. **268**(5212): p. 863-5.
168. Bendelac, A., *Positive selection of mouse NK1+ T cells by CD1-expressing cortical thymocytes.* J Exp Med, 1995. **182**(6): p. 2091-6.
169. Reth, M., *Antigen receptor tail clue.* Nature, 1989. **338**(6214): p. 383-4.
170. Mukhopadhyay, H., et al., *Multisite Phosphorylation Modulates the T Cell Receptor zeta-Chain Potency but not the Switchlike Response.* Biophys J, 2016. **110**(8): p. 1896-906.
171. Straus, D.B. and A. Weiss, *Genetic evidence for the involvement of the lck tyrosine kinase in signal transduction through the T cell antigen receptor.* Cell, 1992. **70**(4): p. 585-93.
172. van Oers, N.S., N. Killeen, and A. Weiss, *Lck regulates the tyrosine phosphorylation of the T cell receptor subunits and ZAP-70 in murine thymocytes.* J Exp Med, 1996. **183**(3): p. 1053-62.
173. Smith-Garvin, J.E., G.A. Koretzky, and M.S. Jordan, *T cell activation.* Annu Rev Immunol, 2009. **27**: p. 591-619.
174. Parsons, S.J. and J.T. Parsons, *Src family kinases, key regulators of signal transduction.* Oncogene, 2004. **23**(48): p. 7906-9.
175. Boggon, T.J. and M.J. Eck, *Structure and regulation of Src family kinases.* Oncogene, 2004. **23**(48): p. 7918-27.

176. Xu, W., et al., *Crystal structures of c-Src reveal features of its autoinhibitory mechanism.* Mol Cell, 1999. **3**(5): p. 629-38.
177. Sicheri, F., I. Moarefi, and J. Kuriyan, *Crystal structure of the Src family tyrosine kinase Hck.* Nature, 1997. **385**(6617): p. 602-9.
178. Yamaguchi, H. and W.A. Hendrickson, *Structural basis for activation of human lymphocyte kinase Lck upon tyrosine phosphorylation.* Nature, 1996. **384**(6608): p. 484-9.
179. Fernandes, R.A., et al., *On the Control of TCR Phosphorylation.* Front Immunol, 2012. **3**: p. 92.
180. James, J.R., et al., *The T cell receptor triggering apparatus is composed of monovalent or monomeric proteins.* J Biol Chem, 2011. **286**(37): p. 31993-2001.
181. Eswaran, J., et al., *The crystal structure of human receptor protein tyrosine phosphatase kappa phosphatase domain 1.* Protein Sci, 2006. **15**(6): p. 1500-5.
182. Trowbridge, I.S. and M.L. Thomas, *CD45: an emerging role as a protein tyrosine phosphatase required for lymphocyte activation and development.* Annu Rev Immunol, 1994. **12**: p. 85-116.
183. Chang, V.T., et al., *Initiation of T cell signaling by CD45 segregation at 'close contacts'.* Nat Immunol, 2016. **17**(5): p. 574-582.
184. Cordoba, S.P., et al., *The large ectodomains of CD45 and CD148 regulate their segregation from and inhibition of ligated T-cell receptor.* Blood, 2013. **121**(21): p. 4295-302.
185. Choudhuri, K., et al., *T-cell receptor triggering is critically dependent on the dimensions of its peptide-MHC ligand.* Nature, 2005. **436**(7050): p. 578-82.
186. Chan, A.C., et al., *ZAP-70: a 70 kd protein-tyrosine kinase that associates with the TCR zeta chain.* Cell, 1992. **71**(4): p. 649-62.
187. Sommers, C.L., L.E. Samelson, and P.E. Love, *LAT: a T lymphocyte adapter protein that couples the antigen receptor to downstream signaling pathways.* Bioessays, 2004. **26**(1): p. 61-7.
188. Acuto, O., V. Di Bartolo, and F. Michel, *Tailoring T-cell receptor signals by proximal negative feedback mechanisms.* Nat Rev Immunol, 2008. **8**(9): p. 699-712.
189. Jenkins, M.K., et al., *CD28 delivers a costimulatory signal involved in antigen-specific IL-2 production by human T cells.* J Immunol, 1991. **147**(8): p. 2461-6.
190. LaSalle, J.M. and D.A. Hafler, *T cell anergy.* FASEB J, 1994. **8**(9): p. 601-8.
191. Dobbins, J., et al., *Binding of the cytoplasmic domain of CD28 to the plasma membrane inhibits Lck recruitment and signaling.* Sci Signal, 2016. **9**(438): p.

ra75.
192. Fife, B.T. and J.A. Bluestone, *Control of peripheral T-cell tolerance and autoimmunity via the CTLA-4 and PD-1 pathways.* Immunol Rev, 2008. **224**: p. 166-82.
193. Krummel, M.F. and J.P. Allison, *CD28 and CTLA-4 have opposing effects on the response of T cells to stimulation.* J Exp Med, 1995. **182**(2): p. 459-65.
194. Valk, E., C.E. Rudd, and H. Schneider, *CTLA-4 trafficking and surface expression.* Trends Immunol, 2008. **29**(6): p. 272-9.
195. Collins, A.V., et al., *The interaction properties of costimulatory molecules revisited.* Immunity, 2002. **17**(2): p. 201-10.
196. Salomon, B. and J.A. Bluestone, *Complexities of CD28/B7: CTLA-4 costimulatory pathways in autoimmunity and transplantation.* Annu Rev Immunol, 2001. **19**: p. 225-52.
197. Paul, W.E. and R.A. Seder, *Lymphocyte responses and cytokines.* Cell, 1994. **76**(2): p. 241-51.
198. Monks, C.R., et al., *Three-dimensional segregation of supramolecular activation clusters in T cells.* Nature, 1998. **395**(6697): p. 82-6.
199. van Der Merwe, P.A. and S.J. Davis, *Immunology. The immunological synapse--a multitasking system.* Science, 2002. **295**(5559): p. 1479-80.
200. Lee, K.H., et al., *T cell receptor signaling precedes immunological synapse formation.* Science, 2002. **295**(5559): p. 1539-42.
201. Springer, T.A., *Adhesion receptors of the immune system.* Nature, 1990. **346**(6283): p. 425-34.
202. Pasquier, B., et al., *Defective NKT cell development in mice and humans lacking the adapter SAP, the X-linked lymphoproliferative syndrome gene product.* J Exp Med, 2005. **201**(5): p. 695-701.
203. Peterson, E.J., et al., *Coupling of the TCR to integrin activation by Slap-130/Fyb.* Science, 2001. **293**(5538): p. 2263-5.
204. Delon, J., K. Kaibuchi, and R.N. Germain, *Exclusion of CD43 from the immunological synapse is mediated by phosphorylation-regulated relocation of the cytoskeletal adaptor moesin.* Immunity, 2001. **15**(5): p. 691-701.
205. Freiberg, B.A., et al., *Staging and resetting T cell activation in SMACs.* Nat Immunol, 2002. **3**(10): p. 911-7.
206. Grakoui, A., et al., *The immunological synapse: a molecular machine controlling T cell activation.* Science, 1999. **285**(5425): p. 221-7.
207. Dustin, M.L., *The immunological synapse.* Cancer Immunol Res, 2014. **2**(11): p. 1023-33.
208. Dustin, M.L., et al., *A novel adaptor protein orchestrates receptor patterning*

and cytoskeletal polarity in T-cell contacts. Cell, 1998. **94**(5): p. 667-77.

209. Davis, S.J. and P.A. van der Merwe, *The immunological synapse: required for T cell receptor signalling or directing T cell effector function?* Curr Biol, 2001. **11**(8): p. R289-91.
210. Purbhoo, M.A., et al., *T cell killing does not require the formation of a stable mature immunological synapse.* Nat Immunol, 2004. **5**(5): p. 524-30.
211. Yokosuka, T., et al., *Newly generated T cell receptor microclusters initiate and sustain T cell activation by recruitment of Zap70 and SLP-76.* Nat Immunol, 2005. **6**(12): p. 1253-62.
212. Varma, R., et al., *T cell receptor-proximal signals are sustained in peripheral microclusters and terminated in the central supramolecular activation cluster.* Immunity, 2006. **25**(1): p. 117-27.
213. Stinchcombe, J.C., et al., *The immunological synapse of CTL contains a secretory domain and membrane bridges.* Immunity, 2001. **15**(5): p. 751-61.
214. van der Merwe, P.A. and O. Dushek, *Mechanisms for T cell receptor triggering.* Nat Rev Immunol, 2011. **11**(1): p. 47-55.
215. Davis, S.J. and P.A. van der Merwe, *The kinetic-segregation model: TCR triggering and beyond.* Nat Immunol, 2006. **7**(8): p. 803-9.
216. Tao, R.H. and I.N. Maruyama, *All EGF(ErbB) receptors have preformed homo- and heterodimeric structures in living cells.* J Cell Sci, 2008. **121**(Pt 19): p. 3207-17.
217. Downward, J., P. Parker, and M.D. Waterfield, *Autophosphorylation sites on the epidermal growth factor receptor.* Nature, 1984. **311**(5985): p. 483-5.
218. Cooper, J.A. and H. Qian, *A mechanism for SRC kinase-dependent signaling by noncatalytic receptors.* Biochemistry, 2008. **47**(21): p. 5681-5688.
219. Boniface, J.J., et al., *Initiation of signal transduction through the T cell receptor requires the multivalent engagement of peptide/MHC ligands [corrected]*. Immunity, 1998. **9**(4): p. 459-66.
220. Meuer, S.C., et al., *Antigen-like effects of monoclonal antibodies directed at receptors on human T cell clones.* J Exp Med, 1983. **158**(3): p. 988-93.
221. Trautmann, A. and C. Randriamampita, *Initiation of TCR signalling revisited.* Trends Immunol, 2003. **24**(8): p. 425-8.
222. Locksley, R.M., et al., *Helper T cells without CD4: control of leishmaniasis in CD4-deficient mice.* Science, 1993. **261**(5127): p. 1448-51.
223. Schilham, M.W., et al., *Alloreactive cytotoxic T cells can develop and function in mice lacking both CD4 and CD8.* Eur J Immunol, 1993. **23**(6): p. 1299-304.
224. Van Laethem, F., et al., *Deletion of CD4 and CD8 coreceptors permits generation of alphabetaT cells that recognize antigens independently of the*

MHC. Immunity, 2007. **27**(5): p. 735-50.
225. Sykulev, Y., et al., *Evidence that a single peptide-MHC complex on a target cell can elicit a cytolytic T cell response.* Immunity, 1996. **4**(6): p. 565-71.
226. Irvine, D.J., et al., *Direct observation of ligand recognition by T cells.* Nature, 2002. **419**(6909): p. 845-9.
227. Delon, J., et al., *CD8 expression allows T cell signaling by monomeric peptide-MHC complexes.* Immunity, 1998. **9**(4): p. 467-73.
228. Jonsson, P., et al., *Remarkably low affinity of CD4/peptide-major histocompatibility complex class II protein interactions.* Proc Natl Acad Sci U S A, 2016. **113**(20): p. 5682-7.
229. Jiang, N., et al., *Two-stage cooperative T cell receptor-peptide major histocompatibility complex-CD8 trimolecular interactions amplify antigen discrimination.* Immunity, 2011. **34**(1): p. 13-23.
230. Choudhuri, K. and P.A. van der Merwe, *Molecular mechanisms involved in T cell receptor triggering.* Semin Immunol, 2007. **19**(4): p. 255-61.
231. Lillemeier, B.F., et al., *TCR and Lat are expressed on separate protein islands on T cell membranes and concatenate during activation.* Nat Immunol, 2010. **11**(1): p. 90-6.
232. Rossy, J., et al., *Conformational states of the kinase Lck regulate clustering in early T cell signaling.* Nat Immunol, 2013. **14**(1): p. 82-9.
233. Pang, S.S., et al., *The structural basis for autonomous dimerization of the pre-T-cell antigen receptor.* Nature, 2010. **467**(7317): p. 844-8.
234. Yamasaki, S., et al., *Mechanistic basis of pre-T cell receptor-mediated autonomous signaling critical for thymocyte development.* Nat Immunol, 2006. **7**(1): p. 67-75.
235. James, J.R., et al., *Single-molecule level analysis of the subunit composition of the T cell receptor on live T cells.* Proc Natl Acad Sci U S A, 2007. **104**(45): p. 17662-7.
236. Dunne, P.D., et al., *DySCo: quantitating associations of membrane proteins using two-color single-molecule tracking.* Biophys J, 2009. **97**(4): p. L5-7.
237. Irving, B.A., F.W. Alt, and N. Killeen, *Thymocyte development in the absence of pre-T cell receptor extracellular immunoglobulin domains.* Science, 1998. **280**(5365): p. 905-8.
238. Baumgart, F., et al., *Varying label density allows artifact-free analysis of membrane-protein nanoclusters.* Nat Methods, 2016. **13**(8): p. 661-4.
239. Janeway, C.A., Jr., *Ligands for the T-cell receptor: hard times for avidity models.* Immunol Today, 1995. **16**(5): p. 223-5.
240. Ding, Y.H., et al., *Four A6-TCR/peptide/HLA-A2 structures that generate very*

different T cell signals are nearly identical. Immunity, 1999. **11**(1): p. 45-56.

241. Kjer-Nielsen, L., et al., *A structural basis for the selection of dominant alphabeta T cell receptors in antiviral immunity.* Immunity, 2003. **18**(1): p. 53-64.
242. Beddoe, T., et al., *Antigen ligation triggers a conformational change within the constant domain of the alphabeta T cell receptor.* Immunity, 2009. **30**(6): p. 777-88.
243. Gil, D., et al., *Recruitment of Nck by CD3 epsilon reveals a ligand-induced conformational change essential for T cell receptor signaling and synapse formation.* Cell, 2002. **109**(7): p. 901-12.
244. Gil, D., et al., *T cell receptor engagement by peptide-MHC ligands induces a conformational change in the CD3 complex of thymocytes.* J Exp Med, 2005. **201**(4): p. 517-22.
245. Szymczak, A.L., et al., *The CD3epsilon proline-rich sequence, and its interaction with Nck, is not required for T cell development and function.* J Immunol, 2005. **175**(1): p. 270-5.
246. Xu, C., et al., *Regulation of T cell receptor activation by dynamic membrane binding of the CD3epsilon cytoplasmic tyrosine-based motif.* Cell, 2008. **135**(4): p. 702-13.
247. Kuhns, M.S. and M.M. Davis, *The safety on the TCR trigger.* Cell, 2008. **135**(4): p. 594-6.
248. Secrist, J.P., et al., *Stimulatory effects of the protein tyrosine phosphatase inhibitor, pervanadate, on T-cell activation events.* J Biol Chem, 1993. **268**(8): p. 5886-93.
249. Imbert, V., et al., *Induction of tyrosine phosphorylation and T-cell activation by vanadate peroxide, an inhibitor of protein tyrosine phosphatases.* Biochem J, 1994. **297 (Pt 1)**: p. 163-73.
250. Kuhns, M.S., M.M. Davis, and K.C. Garcia, *Deconstructing the form and function of the TCR/CD3 complex.* Immunity, 2006. **24**(2): p. 133-9.
251. Kuhns, M.S. and M.M. Davis, *Disruption of extracellular interactions impairs T cell receptor-CD3 complex stability and signaling.* Immunity, 2007. **26**(3): p. 357-69.
252. Fernandes, R.A., et al., *T cell receptors are structures capable of initiating signaling in the absence of large conformational rearrangements.* J Biol Chem, 2012. **287**(16): p. 13324-35.
253. Davis, S.J. and P.A. van der Merwe, *The structure and ligand interactions of CD2: implications for T-cell function.* Immunol Today, 1996. **17**(4): p. 177-87.
254. Lin, J. and A. Weiss, *The tyrosine phosphatase CD148 is excluded from the*

immunologic synapse and down-regulates prolonged T cell signaling. J Cell Biol, 2003. **162**(4): p. 673-82.

255. Anton van der Merwe, P., et al., *Cytoskeletal polarization and redistribution of cell-surface molecules during T cell antigen recognition.* Semin Immunol, 2000. **12**(1): p. 5-21.
256. Davis, S.J. and P.A. van der Merwe, *CD2: an exception to the immunoglobulin superfamily concept?* Science, 1996. **273**(5279): p. 1241-2.
257. Mustelin, T., K.M. Coggeshall, and A. Altman, *Rapid activation of the T-cell tyrosine protein kinase pp56lck by the CD45 phosphotyrosine phosphatase.* Proc Natl Acad Sci U S A, 1989. **86**(16): p. 6302-6.
258. Choudhuri, K., et al., *Peptide-major histocompatibility complex dimensions control proximal kinase-phosphatase balance during T cell activation.* J Biol Chem, 2009. **284**(38): p. 26096-105.
259. Eigen, M. and R. Rigler, *Sorting single molecules: application to diagnostics and evolutionary biotechnology.* Proc Natl Acad Sci U S A, 1994. **91**(13): p. 5740-7.
260. Hassler, K., et al., *Total internal reflection fluorescence correlation spectroscopy (TIR-FCS) with low background and high count-rate per molecule.* Opt Express, 2005. **13**(19): p. 7415-23.
261. Li, H., et al., *Ultrasensitive coincidence fluorescence detection of single DNA molecules.* Anal Chem, 2003. **75**(7): p. 1664-70.
262. Axelrod, D., *Cell-substrate contacts illuminated by total internal reflection fluorescence.* J Cell Biol, 1981. **89**(1): p. 141-5.
263. Ambrose, E.J., *A surface contact microscope for the study of cell movements.* Nature, 1956. **178**(4543): p. 1194.
264. Yoon, J.W., et al., *Bayesian inference for improved single molecule fluorescence tracking.* Biophys J, 2008. **94**(12): p. 4932-47.
265. Betzig, E., et al., *Imaging intracellular fluorescent proteins at nanometer resolution.* Science, 2006. **313**(5793): p. 1642-5.
266. Rust, M.J., M. Bates, and X. Zhuang, *Sub-diffraction-limit imaging by stochastic optical reconstruction microscopy (STORM).* Nat Methods, 2006. **3**(10): p. 793-5.
267. Small, A. and S. Stahlheber, *Fluorophore localization algorithms for super-resolution microscopy.* Nat Methods, 2014. **11**(3): p. 267-79.
268. Shroff, H., et al., *Live-cell photoactivated localization microscopy of nanoscale adhesion dynamics.* Nat Methods, 2008. **5**(5): p. 417-23.
269. Lillemeier, B.F., et al., *Plasma membrane-associated proteins are clustered into islands attached to the cytoskeleton.* Proc Natl Acad Sci U S A, 2006. **103**(50):

p. 18992-7.
270. Groves, J.T., R. Parthasarathy, and M.B. Forstner, *Fluorescence imaging of membrane dynamics.* Annu Rev Biomed Eng, 2008. **10**: p. 311-38.
271. Yamasaki, S. and T. Saito, *Molecular basis for pre-TCR-mediated autonomous signaling.* Trends Immunol, 2007. **28**(1): p. 39-43.
272. Ishikawa, E., et al., *Germ-line elimination of electric charge on pre-T-cell receptor (TCR) impairs autonomous signaling for beta-selection and TCR repertoire formation.* Proc Natl Acad Sci U S A, 2010. **107**(46): p. 19979-84.
273. Aifantis, I., et al., *A critical role for the cytoplasmic tail of pTalpha in T lymphocyte development.* Nat Immunol, 2002. **3**(5): p. 483-8.
274. Navarro, M.N., et al., *Identification of CMS as a cytosolic adaptor of the human pTalpha chain involved in pre-TCR function.* Blood, 2007. **110**(13): p. 4331-40.
275. Mallis, R.J., et al., *Pre-TCR ligand binding impacts thymocyte development before alphabetaTCR expression.* Proc Natl Acad Sci U S A, 2015. **112**(27): p. 8373-8.
276. Smelty, P., et al., *Identification of the pre-T-cell receptor alpha chain in nonmammalian vertebrates challenges the structure-function of the molecule.* Proc Natl Acad Sci U S A, 2010. **107**(46): p. 19991-6.
277. Mallis, R.J., et al., *NMR-directed design of pre-TCRbeta and pMHC molecules implies a distinct geometry for pre-TCR relative to alphabetaTCR recognition of pMHC.* J Biol Chem, 2018. **293**(3): p. 754-766.
278. Das, D.K., et al., *Pre-T Cell Receptors (Pre-TCRs) Leverage Vbeta Complementarity Determining Regions (CDRs) and Hydrophobic Patch in Mechanosensing Thymic Self-ligands.* J Biol Chem, 2016. **291**(49): p. 25292-25305.
279. Takahashi, H., et al., *A novel NMR method for determining the interfaces of large protein-protein complexes.* Nat Struct Biol, 2000. **7**(3): p. 220-3.
280. Chen, W., et al., *Monitoring receptor-ligand interactions between surfaces by thermal fluctuations.* Biophys J, 2008. **94**(2): p. 694-701.
281. Ladi, E., et al., *Thymic microenvironments for T cell differentiation and selection.* Nat Immunol, 2006. **7**(4): p. 338-43.
282. Kurd, N. and E.A. Robey, *T-cell selection in the thymus: a spatial and temporal perspective.* Immunol Rev, 2016. **271**(1): p. 114-26.
283. Munoz-Ruiz, M., et al., *Thymic Determinants of gammadelta T Cell Differentiation.* Trends Immunol, 2017. **38**(5): p. 336-344.
284. Zhang, F., Y. Wen, and X. Guo, *CRISPR/Cas9 for genome editing: progress, implications and challenges.* Hum Mol Genet, 2014. **23**(R1): p. R40-6.
285. Demaison, C., et al., *High-level transduction and gene expression in*

hematopoietic repopulating cells using a human immunodeficiency [correction of imunodeficiency] virus type 1-based lentiviral vector containing an internal spleen focus forming virus promoter. Hum Gene Ther, 2002. **13**(7): p. 803-13.

286. Sanjana, N.E., O. Shalem, and F. Zhang, *Improved vectors and genome-wide libraries for CRISPR screening.* Nat Methods, 2014. **11**(8): p. 783-4.
287. Pei, Y. and T. Tuschl, *On the art of identifying effective and specific siRNAs.* Nat Methods, 2006. **3**(9): p. 670-6.
288. Reynolds, A., et al., *Rational siRNA design for RNA interference.* Nat Biotechnol, 2004. **22**(3): p. 326-30.
289. Matveeva, O., et al., *Comparison of approaches for rational siRNA design leading to a new efficient and transparent method.* Nucleic Acids Res, 2007. **35**(8): p. e63.
290. Schneider, U., H.U. Schwenk, and G. Bornkamm, *Characterization of EBV-genome negative "null" and "T" cell lines derived from children with acute lymphoblastic leukemia and leukemic transformed non-Hodgkin lymphoma.* Int J Cancer, 1977. **19**(5): p. 621-6.
291. Graham, F.L., et al., *Characteristics of a human cell line transformed by DNA from human adenovirus type 5.* J Gen Virol, 1977. **36**(1): p. 59-74.
292. DuBridge, R.B., et al., *Analysis of mutation in human cells by using an Epstein-Barr virus shuttle system.* Mol Cell Biol, 1987. **7**(1): p. 379-87.
293. Rawlings, N.D. and A.J. Barrett, *Families of cysteine peptidases.* Methods Enzymol, 1994. **244**: p. 461-86.
294. Rousseaux, J., R. Rousseaux-Prevost, and H. Bazin, *Optimal conditions for the preparation of Fab and F(ab')2 fragments from monoclonal IgG of different rat IgG subclasses.* J Immunol Methods, 1983. **64**(1-2): p. 141-6.
295. Coulter, A. and R. Harris, *Simplified preparation of rabbit Fab fragments.* J Immunol Methods, 1983. **59**(2): p. 199-203.
296. Mage, M.G., *Preparation of Fab fragments from IgGs of different animal species.* Methods Enzymol, 1980. **70**(A): p. 142-50.
297. Mariani, M., et al., *A new enzymatic method to obtain high-yield F(ab)2 suitable for clinical use from mouse IgGl.* Mol Immunol, 1991. **28**(1-2): p. 69-77.
298. Milenic, D.E., J.M. Esteban, and D. Colcher, *Comparison of methods for the generation of immunoreactive fragments of a monoclonal antibody (B72.3) reactive with human carcinomas.* J Immunol Methods, 1989. **120**(1): p. 71-83.
299. Hayashi-Takanaka, Y., et al., *Evaluation of chemical fluorescent dyes as a protein conjugation partner for live cell imaging.* PLoS One, 2014. **9**(9): p. e106271.

300. Evans, E.J., et al., *Crystal structure and binding properties of the CD2 and CD244 (2B4)-binding protein, CD48.* J Biol Chem, 2006. **281**(39): p. 29309-20.
301. Davis, S.J., et al., *The role of charged residues mediating low affinity protein-protein recognition at the cell surface by CD2.* Proc Natl Acad Sci U S A, 1998. **95**(10): p. 5490-4.
302. Lee, B. and F.M. Richards, *The interpretation of protein structures: estimation of static accessibility.* J Mol Biol, 1971. **55**(3): p. 379-400.
303. Creighton, T.E., *Proteins : structures and molecular properties*. 2013, New York: Freeman.
304. Carrasco, Y.R., et al., *An endoplasmic reticulum retention function for the cytoplasmic tail of the human pre-T cell receptor (TCR) alpha chain: potential role in the regulation of cell surface pre-TCR expression levels.* J Exp Med, 2001. **193**(9): p. 1045-58.
305. Rasmussen, A., et al., *The role of tryptophan residues in the function and stability of the mechanosensitive channel MscS from Escherichia coli.* Biochemistry, 2007. **46**(38): p. 10899-908.
306. Maenaka, K., et al., *Functional and structural role of a tryptophan generally observed in protein-carbohydrate interaction. TRP-62 of hen egg white lysozyme.* J Biol Chem, 1994. **269**(10): p. 7070-5.
307. Sanan, D.A. and R.G. Anderson, *Simultaneous visualization of LDL receptor distribution and clathrin lattices on membranes torn from the upper surface of cultured cells.* J Histochem Cytochem, 1991. **39**(8): p. 1017-24.
308. Kumar, R., et al., *Increased sensitivity of antigen-experienced T cells through the enrichment of oligomeric T cell receptor complexes.* Immunity, 2011. **35**(3): p. 375-87.
309. Abbe, E., *On the estimation of aperture in the microscope*. 1881, Lond.
310. Hell, S.W., *Far-field optical nanoscopy.* Science, 2007. **316**(5828): p. 1153-8.
311. Hell, S.W. and J. Wichmann, *Breaking the diffraction resolution limit by stimulated emission: stimulated-emission-depletion fluorescence microscopy.* Opt Lett, 1994. **19**(11): p. 780-2.
312. https://www.activemotif.com/catalog/627/sted-microscopy-products.
313. Heilemann, M., et al., *Super-resolution imaging with small organic fluorophores.* Angew Chem Int Ed Engl, 2009. **48**(37): p. 6903-8.
314. van de Linde, S., et al., *Multicolor photoswitching microscopy for subdiffraction-resolution fluorescence imaging.* Photochem Photobiol Sci, 2009. **8**(4): p. 465-9.
315. Los, G.V., et al., *HaloTag: a novel protein labeling technology for cell imaging and protein analysis.* ACS Chem Biol, 2008. **3**(6): p. 373-82.

316. Wiedenmann, J., et al., *EosFP, a fluorescent marker protein with UV-inducible green-to-red fluorescence conversion.* Proc Natl Acad Sci U S A, 2004. **101**(45): p. 15905-10.
317. Nienhaus, K., et al., *Structural basis for photo-induced protein cleavage and green-to-red conversion of fluorescent protein EosFP.* Proc Natl Acad Sci U S A, 2005. **102**(26): p. 9156-9.
318. McKinney, S.A., et al., *A bright and photostable photoconvertible fluorescent protein.* Nat Methods, 2009. **6**(2): p. 131-3.
319. Zhang, M., et al., *Rational design of true monomeric and bright photoactivatable fluorescent proteins.* Nat Methods, 2012. **9**(7): p. 727-9.
320. Lippincott-Schwartz, J. and G.H. Patterson, *Photoactivatable fluorescent proteins for diffraction-limited and super-resolution imaging.* Trends Cell Biol, 2009. **19**(11): p. 555-65.
321. Steinhauer, C., et al., *Superresolution microscopy on the basis of engineered dark states.* J Am Chem Soc, 2008. **130**(50): p. 16840-1.
322. Dempsey, G.T., et al., *Evaluation of fluorophores for optimal performance in localization-based super-resolution imaging.* Nat Methods, 2011. **8**(12): p. 1027-36.
323. Bowers-Komro, D.M. and D.B. McCormick, *Characterization of ascorbic acid uptake by isolated rat kidney cells.* J Nutr, 1991. **121**(1): p. 57-64.
324. Noh, K., et al., *Mega-dose Vitamin C modulates T cell functions in Balb/c mice only when administered during T cell activation.* Immunol Lett, 2005. **98**(1): p. 63-72.
325. Grant, M.M., et al., *Dose-dependent modulation of the T cell proteome by ascorbic acid.* Br J Nutr, 2007. **97**(1): p. 19-26.
326. Hsuan, J. and S. Cockcroft, *The PITP family of phosphatidylinositol transfer proteins.* Genome Biol, 2001. **2**(9): p. REVIEWS3011.
327. Belov, V.N., et al., *Rhodamines NN: a novel class of caged fluorescent dyes.* Angew Chem Int Ed Engl, 2010. **49**(20): p. 3520-3.
328. Lukinavicius, G., et al., *A near-infrared fluorophore for live-cell super-resolution microscopy of cellular proteins.* Nat Chem, 2013. **5**(2): p. 132-9.
329. Turkowyd, B., D. Virant, and U. Endesfelder, *From single molecules to life: microscopy at the nanoscale.* Anal Bioanal Chem, 2016. **408**(25): p. 6885-911.
330. Endesfelder, U., et al., *Chemically induced photoswitching of fluorescent probes--a general concept for super-resolution microscopy.* Molecules, 2011. **16**(4): p. 3106-18.
331. von Boehmer, H., *Unique features of the pre-T-cell receptor alpha-chain: not*

just a surrogate. Nat Rev Immunol, 2005. **5**(7): p. 571-7.
332. Trigueros, C., et al., *Identification of a late stage of small noncycling pTalpha-pre-T cells as immediate precursors of T cell receptor alpha/beta+ thymocytes.* J Exp Med, 1998. **188**(8): p. 1401-12.
333. Morisaki, T. and J.G. McNally, *Photoswitching-free FRAP analysis with a genetically encoded fluorescent tag.* PLoS One, 2014. **9**(9): p. e107730.
334. Grimm, J.B., et al., *A general method to improve fluorophores for live-cell and single-molecule microscopy.* Nat Methods, 2015. **12**(3): p. 244-50, 3 p following 250.
335. Durisic, N., et al., *Single-molecule evaluation of fluorescent protein photoactivation efficiency using an in vivo nanotemplate.* Nat Methods, 2014. **11**(2): p. 156-62.
336. Shivanandan, A., et al., *Challenges in quantitative single molecule localization microscopy.* FEBS Lett, 2014. **588**(19): p. 3595-602.
337. Rollins, G.C., et al., *Stochastic approach to the molecular counting problem in superresolution microscopy.* Proc Natl Acad Sci U S A, 2015. **112**(2): p. E110-8.
338. Latty, S.L., et al., *Referenced Single-Molecule Measurements Differentiate between GPCR Oligomerization States.* Biophys J, 2015. **109**(9): p. 1798-806.
339. Weimann, L., et al., *A quantitative comparison of single-dye tracking analysis tools using Monte Carlo simulations.* PLoS One, 2013. **8**(5): p. e64287.
340. Goiko, M., J.R. de Bruyn, and B. Heit, *Short-Lived Cages Restrict Protein Diffusion in the Plasma Membrane.* Sci Rep, 2016. **6**: p. 34987.
341. Leake, M.C., et al., *Variable stoichiometry of the TatA component of the twin-arginine protein transport system observed by in vivo single-molecule imaging.* Proc Natl Acad Sci U S A, 2008. **105**(40): p. 15376-81.
342. Kelly, A.P., et al., *Notch-induced T cell development requires phosphoinositide-dependent kinase 1.* EMBO J, 2007. **26**(14): p. 3441-50.
343. Okamura, S., et al., *Heterogeneity of human thymocytes and a malignant T-lymphoblast cell line, MOLT-3.* Cancer Res, 1981. **41**(5): p. 1664-8.
344. Yarden, Y. and J. Schlessinger, *Epidermal growth factor induces rapid, reversible aggregation of the purified epidermal growth factor receptor.* Biochemistry, 1987. **26**(5): p. 1443-51.
345. Satoh, T., M. Nakafuku, and Y. Kaziro, *Function of Ras as a molecular switch in signal transduction.* J Biol Chem, 1992. **267**(34): p. 24149-52.
346. Rayter, S.I., et al., *p21ras mediates control of IL-2 gene promoter function in T cell activation.* EMBO J, 1992. **11**(12): p. 4549-56.
347. Baldari, C.T., G. Macchia, and J.L. Telford, *Interleukin-2 promoter activation in*

T-cells expressing activated Ha-ras. J Biol Chem, 1992. **267**(7): p. 4289-91.

348. Gupta, S., *Mechanisms of lymphocyte activation and immune regulation V : molecular basis of signal transduction*. 1994, New York ; London: Plenum. ix, 264 p.
349. Turner, H. and D.A. Cantrell, *Distinct Ras effector pathways are involved in Fc epsilon R1 regulation of the transcriptional activity of Elk-1 and NFAT in mast cells.* J Exp Med, 1997. **185**(1): p. 43-53.
350. Izquierdo, M., et al., *p21ras couples the T cell antigen receptor to extracellular signal-regulated kinase 2 in T lymphocytes.* J Exp Med, 1993. **178**(4): p. 1199-208.
351. Woodrow, M., N.A. Clipstone, and D. Cantrell, *p21ras and calcineurin synergize to regulate the nuclear factor of activated T cells.* J Exp Med, 1993. **178**(5): p. 1517-22.
352. Genot, E., et al., *Multiple p21ras effector pathways regulate nuclear factor of activated T cells.* EMBO J, 1996. **15**(15): p. 3923-33.
353. Chatila, T., et al., *Mechanisms of T cell activation by the calcium ionophore ionomycin.* J Immunol, 1989. **143**(4): p. 1283-9.
354. Evans, E.J., et al., *Crystal structure of a soluble CD28-Fab complex.* Nat Immunol, 2005. **6**(3): p. 271-9.
355. Paddison, P.J., et al., *Short hairpin RNAs (shRNAs) induce sequence-specific silencing in mammalian cells.* Genes Dev, 2002. **16**(8): p. 948-58.
356. Brummelkamp, T.R., R. Bernards, and R. Agami, *A system for stable expression of short interfering RNAs in mammalian cells.* Science, 2002. **296**(5567): p. 550-3.
357. Shalem, O., et al., *Genome-scale CRISPR-Cas9 knockout screening in human cells.* Science, 2014. **343**(6166): p. 84-7.
358. Platt, R.J., et al., *CRISPR-Cas9 knockin mice for genome editing and cancer modeling.* Cell, 2014. **159**(2): p. 440-55.
359. Schim van der Loeff, I., et al., *Zap70 is essential for long-term survival of naive CD8 T cells.* J Immunol, 2014. **193**(6): p. 2873-80.
360. Palacios, E.H. and A. Weiss, *Function of the Src-family kinases, Lck and Fyn, in T-cell development and activation.* Oncogene, 2004. **23**(48): p. 7990-8000.
361. Schaefer, K.A., et al., *Unexpected mutations after CRISPR-Cas9 editing in vivo.* Nat Methods, 2017. **14**(6): p. 547-548.
362. Panigada, M., et al., *Constitutive endocytosis and degradation of the pre-T cell receptor.* J Exp Med, 2002. **195**(12): p. 1585-97.
363. Roy, A., et al., *The nature of transient dark states in a photoactivatable fluorescent protein.* J Am Chem Soc, 2011. **133**(46): p. 18586-9.

364. Adam, V., et al., *Phototransformable fluorescent proteins: Future challenges.* Curr Opin Chem Biol, 2014. **20**: p. 92-102.
365. Uno, S.N., et al., *A guide to use photocontrollable fluorescent proteins and synthetic smart fluorophores for nanoscopy.* Microscopy (Oxf), 2015. **64**(4): p. 263-77.
366. Fricke, F., et al., *One, two or three? Probing the stoichiometry of membrane proteins by single-molecule localization microscopy.* Sci Rep, 2015. **5**: p. 14072.
367. Lopes, F.B., et al., *Membrane nanoclusters of FcgammaRI segregate from inhibitory SIRPalpha upon activation of human macrophages.* J Cell Biol, 2017. **216**(4): p. 1123-1141.
368. Richman, S.A., et al., *Structural features of T cell receptor variable regions that enhance domain stability and enable expression as single-chain ValphaVbeta fragments.* Mol Immunol, 2009. **46**(5): p. 902-16.
369. Tacke, M., et al., *CD28-mediated induction of proliferation in resting T cells in vitro and in vivo without engagement of the T cell receptor: evidence for functionally distinct forms of CD28.* Eur J Immunol, 1997. **27**(1): p. 239-47.
370. Luhder, F., et al., *Topological requirements and signaling properties of T cell-activating, anti-CD28 antibody superagonists.* J Exp Med, 2003. **197**(8): p. 955-66.
371. Gibbons, D., et al., *The biological activity of natural and mutant pTalpha alleles.* J Exp Med, 2001. **194**(5): p. 695-703.
372. Haks, M.C., et al., *Low activation threshold as a mechanism for ligand-independent signaling in pre-T cells.* J Immunol, 2003. **170**(6): p. 2853-61.